LIBRARY OF THE UNIVERSITY OF ADELAIDE
9 · 7 · 69

REACTION RATES IN THE FLUIDIZED STATE
(BARIUM SULPHATE REDUCTION)

by

C.J. Hamdorf, B.E. (Hons.)

A THESIS
Submitted for the Degree of
Doctor of Philosophy
in the
Faculty of Engineering
of the
University of Adelaide

June
1956

ACKNOWLEDGEMENTS

The author wishes to express his gratitude to Professor E.C.R. Spooner for his continuous interest in this project and to acknowledge the guidance and encouragement of Dr. R.V. Culver who supervised the work.

He is grateful to Consolidated Zinc Pty. Ltd. for financial support in the form of a Metallurgical Research Scholarship.

The author is indebted to the Departmental workshop staff for their co-operation in the manufacture of equipment and also to Dr. R.W.F. Tait of this Department for reading the manuscript.

TABLE OF CONTENTS

Section	Item.	Page
1	INTRODUCTION	1
2	LITERATURE REVIEW	3
2:1	Data available on the reduction of barium sulphate	4
2:2	Experimental determination of equilibrium constants	6
2:2:1	Static methods for determining equilibrium constants	6
2:2:2	Dynamic methods for determining equilibrium constants	10
2:3	Theory of heterogeneous reaction rates	12
2:3:1	Nernst theory	12
2:3:2	Diagnosis of reaction type	14
2:3:3	Use of experimental data for predicting reaction rates	20
2:4	Experimental determination of reaction rates	24
2:4:1	Static methods	24
2:4:2	Dynamic methods	25
2:5	Data available on reaction kinetics in fluidized beds	26
2:6	Design and operation of fluidized beds	28
2:6:1	Effect of mass velocity on bed properties	29
2:6:2	Solid and gas mixing in fluidized beds	35
2:6:3	Effect of the physical properties of the solids	38
2:6:4	Mass transfer and heat transfer in fluidized beds	40
2:6:5	General design information	41
2:7	Conclusions and resulting proposals for experimental work	44

Table of contents (cont.)

Section	Item	Page
3	DETERMINATION OF EQUILIBRIUM CONSTANTS	47
3:1	Experimental procedure	47
3:1:1	Apparatus	48
3:1:2	Experimental technique	53
3:1:3	Treatment of results	54
3:1:4	Preparation of samples	55
3:2	Results	58
3:2:1	X-ray analyses	58
3:2:2	Equilibrium data	59
3:3	Discussion of results	61
3:3:1	Series A and B samples	61
3:3:2	Series C and D samples	63
3:3:3	Thermodynamic calculations	66
3:4	Conclusions	69
4	DETERMINATION OF REACTION RATES - FIXED BEDS	70
4:1	Experimental procedure (Preliminary stage)	71
4:1:1	Apparatus	73
4:1:2	Experimental technique	77
4:1:3	Raw materials	78
4:1:4	Treatment of results	79
4:2	Discussion of results (Preliminary stage)	80
4:2:1	Effect of gaseous diffusion	85
4:2:2	Inconsistency of results	85
4:2:3	Conclusions	88
4:3	Experimental procedure (Final stage)	88
4:3:1	Apparatus	90
4:3:2	Experimental technique	92
4:3:3	Preparation of samples	92
4:3:4	Treatment of results	93
4:4	Discussion of results (Final stage)	93
4:4:1	Effect of specific surface	94
4:4:2	Effect of changes in hydrogen partial pressure	95

Table of contents (cont.)

Section	Item	Page
4:4:3	Temperature dependence of reaction rate	101
4:4:4	Effect of silica and iron impurities	101
4:4:5	Effect of heating barytes above the transformation temperature	104
4:4:6	Correlation of results	106
4:4:7	Reaction mechanism	114
4:5	Conclusions	123
5	PREDICTION OF RATES FOR FLUIDIZED BEDS	125
5:1	Prediction of rates at 1100°C	127
5:1:1	Initial bed weight of 1500g	127
5:1:2	Initial bed weight of 750g	133
5:2	Prediction of rates at 1000°C	134
5:2:1	Initial bed weight of 1500g	134
5:2:2	Initial bed weight of 750g	139
5:3	Prediction of rates at 900°C	139
6	DETERMINATION OF REACTION RATES - FLUIDIZED BEDS	141
6:1	Experimental procedure (Preliminary stage)	142
6:1:1	Apparatus	142
6:1:2	Experimental technique	148
6:1:3	Raw materials	149
6:1:4	Treatment of results	150
6:2	Discussion of results (Preliminary stage)	150
6:2:1	Fluidization in perspex model	151
6:2:2	Comparison of measured and predicted rates of reaction	152
6:2:3	Factors producing inconsistency in experimental results	156
6:2:4	Conclusions	158

Table of contents (cont.)

Section	Item	Page
6:3	Experimental procedure (Final stage)	158
6:3:1	Apparatus	160
6:3:2	Experimental technique	161
6:3:3	Treatment of results	161
6:4	Discussion of results (Final stage)	161
6:4:1	Comparison of measured and predicted rates at 1100°C	162
6:4:2	Effect of variation in bed depth and gas flow rate on the rate of reaction obtained in fluidized beds at 1000°C and 900°C	168
6:4:3	Effect of hydrogen sulphide on the reaction rate at 1000°C	173
6:5	Conclusions	178
7	SUMMARY AND CONCLUSIONS	180
8	RECOMMENDATIONS FOR FUTURE WORK	184
APPENDICES		
A	Thermodynamic investigation of the reduction of barium sulphate by hydrogen	186
B	Data from the equilibrium determinations	190
C	Rate data obtained from fixed beds	194

Table of contents (cont.)

Section	Item.	Page
D	Rate data obtained from fluidized beds	224
E	Design calculations for the fluidizing unit	242
E:1	Basic specifications for experimental unit	243
E:1:1	Bed diameter and height	243
E:1:2	Maximum particle diameter	243
E:1:3	Furnace requirements	244
E:1:4	Rate measurements and flow sheet	244
E:2	Selection of operating velocity and heating furnaces	245
E:2:1	Minimum gas velocity for fluidization	245
E:2:2	Furnaces and maximum gas rate	248
E:3	Reactor	250
E:4	Gas cooler - atmospheric	250
E:4:1	Pure hydrogen	252
E:4:2	Pure steam	257
E:5	Dust removal	259
E:5:1	Largest dust particle	260
E:5:2	Dust trap	262
E:5:3	Cyclone	264
E:6	Design of a cooler-condenser	267
E:6:1	Diameter of water jacket	267
E:6:2	Area of cooler-condenser for water-hydrogen mixture	268
E:6:3	Area of cooler-condenser for pure hydrogen	276
E:6:4	Area of cooler-condenser for pure steam	277
E:6:5	Length of cooler-condenser	280
E:6:6	Pressure drop across the cooler-condenser	280
E:7	Silica gel gas drier	282

Table of Contents (cont.)

Section	Item	Page
E:8	Selection of gas circulating fan	288
E:9	Hydrogen consumption and storage	289
E:10	General layout of the fluidizer	290
E:11	Instrumentation	290
E:12	Operating notes	292
F	Comparison between the design and actual performances of the fluidizer	293
F:1	Gas preheater	294
F:2	Reactor	295
F:3	Gas cooler	298
F:4	Dust removal	298
F:5	Cooler-condenser	298
F:6	Silica gel gas drier	299
G	Rate data for $\pm$14-10# barytes reduced at 1100°C and 900°C	300
G:1	At 1100°C	301
G:2	At 900°C	302
H	Electrical circuits	304
H:1	Photo-cell relay temperature controller	305
H:2	Cycling unit	309
BIBLIOGRAPHY		311

LIST OF FIGURES

Fig.	Title	Page
1	Feeders for adding solids to fluid streams	42
2	Apparatus for equilibrium determinations: schematic diagram	49
3	Experimental data for Sample C10	56
4	Plot of experimental equilibrium data	60
5	Sigma plot prepared from the correlation in Fig. 4, page 60.	68
6	Line diagram of the reaction rate apparatus	74
7	Photograph of the reaction rate apparatus	75
8	Rate curves for 800°C and 900°C	81
9	Rate data for 1000°C	82
10	Rate data at 1100°C	83
11	Diagrammatic representation of the reduction of barytes	84
12	Temperature dependence of the reaction rate	86
13	Effect of variation in hydrogen partial pressure on the reaction rate at 1000°C (Nitrogen dilution)	96
14	Effect of variation in hydrogen partial pressure on the reaction rate at 1100°C (Nitrogen dilution)	97
15	Effect of variation in hydrogen partial pressure on the reaction rate at 1000°C (Water dilution)	99
16	Effect of variation in hydrogen partial pressure on the reaction rate at 1100°C (Water dilution)	100
17	Variation in temperature dependence as the reaction proceeds	102

List of Figures (cont.)

Fig.	Title	Page
18	First order plot for data at 1000°C	107
19	First order plot for data at 1100°C	108
20	Correlation of results for Samples F, H, and I, at 1100°C	109
21	Variation of K with the percentage impurity in the barytes	111
22	Variation of the rate per unit area of interface as the reaction proceeds	119
23	Predicted rate vs time curves for fluidized and fixed beds of +14-10# barytes reduced at 1100°C	130
24	Predicted rate vs time curves for +14-10# barytes reduced in fixed and fluidized beds at 1000°C and 900°C	137
25	Schematic flow sheet for fluidizing apparatus	143
26	Arrangement drawing of fluidizer	145
27	Photograph of fluidizer	146
28	Detail of fluidizing reactor showing thermocouple sheaths	147
29	Rate data for fixed beds at 1000°C	153
30	Rate data for fluidized beds at 1000°C	154
31	Photograph of the top of the reactor showing the cooling spray in position	160
32	Comparison of measured and predicted rates of reaction for a 1500g fixed bed at 1100°C	163
33	Comparison of measured and predicted rates of reaction for a 1500g bed fluidized with hydrogen at 1100°C	165

List of Figures (cont.)

Fig.	Title	Page
34	Comparison of measured and predicted rates of reaction for a 1500g bed fluidized with a hydrogen-nitrogen mixture at 1100°C	166
35	Comparison of measured and predicted rates of reaction for a 750g bed fluidized with hydrogen at 1100°C	167
36	Effects of variations in the initial bed weights and hydrogen flow rate on the rate of reaction at 1000°C	169
37	Effect of variation in the initial bed weight on the rate of reaction at 900°C	170
38	Variation of water vapour partial pressure in the continuous phase of a fluidized bed with distance from the gas inlet	172
39	Effect of hydrogen sulphide on the rate of reaction at 1000°C	175
40	Rate data for a fluidized bed of +65-48# barytes	177
41	Block flow sheet for fluidizing apparatus	246
42	Detail of reactor-preheater tube	251
43	Detail of gas cooler and dust trap	263
44	Detail of cyclone	266
45	Detail of cooler-condenser tube showing water jacket seals	281
46	Detail of silica gel gas drier	287
47	Furnace control circuit	291
48	Circuit diagram for photo-cell temperature controller	306
49	Circuit diagram for cycling unit	308

LIST OF TABLES

Table	Title	Page
I	Temperature of reduction and composition of reaction masses	64
II	Gas flow rates used in the determination of equilibrium constants	65
III	Log sheet for a typical rate determination	79
IV	Effect of specific surface and particle size on the initial reaction rate for Sample F	95
V	Effect of impurities on the initial reaction rate	103
VI	Effect on the reaction rate at 1100°C of heating samples above 1150°C	109
VII	Values of K_1 and K_2 for various spherical samples	113
VIII	Rate data for a +14-10# sample of barytes reduced in a differential bed at 1100°C	127
IX	Rate data for Run No. E52 (+14-10#) obtained at 1000°C in a differential bed	135
X	Specific heats as functions of temperature	189
XI	Standard heats of formation and molal entropies	189
XII	Values of the ratio $(H_2O/H_2)_{equilibrium}$ for Series C and D samples	191
XIII	Rate data - fixed beds	195
XIV	Sample assays	223
XV	Rate data - fluidized beds	225
XVI	Comparison of calculated and measured values of V_{mf} for barytes beds fluidized with air at room temperatures	297

THE UNIVERSITY OF ADELAIDE

1. INTRODUCTION

Since the beginning of this century, with the pre-eminence of flotation processes in ore concentration, the trend in extractive metallurgy has been towards the treatment of materials in the fine particle state. Many of the reactions utilized in extraction processes require contacting of these fine powders with a reactant gas and, consequently, the use of fluidization techniques is assuming growing importance in this field.

Although there has been much published research on heat and mass transfer in fluidized beds only a few investigators have studied the effects of bed variables on reaction kinetics, and, since kinetic considerations are of primary importance in the design of a fluidized reactor, this field has been chosen for the present investigation. A comparison has been made between the rates of reaction measured in a fluidized reactor and those predicted for identical conditions, using kinetic data obtained from a small fixed bed reactor, the objective being to elucidate the problems associated with such rate predictions; a necessary step in simplifying the application of the fluidization technique to gas-solid reactions.

The reduction of barytes by hydrogen to give barium sulphide was chosen as the medium for the investigation because,

(1) there was an apparent absence of complicating side reactions,

(2) the barytes deposits of South Australia represent a

relatively untouched source of raw material, and

(3) it was felt that reduction of barytes in a fluidized reactor might offer possibilities for economic production of barium sulphide on a small scale.

However, the approach adopted was such that any other similar gas-solid reaction could have been treated in the same way, thus this method of predicting rates should have general application.

A literature search revealed that there had been little work published on the reduction of barium sulphate by hydrogen so that the programme of experimental work involved determination of,

(1) equilibrium data for the reduction,

(2) rates of reduction in fixed beds, and

(3) rates of reduction in fluidized beds.

The thesis commences with a review of the literature covering these topics and then each phase of the experimental work is discussed in turn. A summary of the project and the findings of the experimental work are given in Section 7, while Section 8 contains recommendations for future investigation in the field.

2. LITERATURE REVIEW

As far as possible, this review has been restricted to those works which contain the information needed to understand the problems likely to be met in an investigation of this type. However, in those cases where there was a dearth of published research, e.g. regarding the reaction of barium sulphate with reducing gases, an exhaustive literature search was made to ensure that no relevant information was omitted.

The review commences with an outline of the published information pertaining to the reduction of barium sulphate and this is followed by a discussion of the experimental methods available for determining equilibrium constants in gas-solid systems. A short resume of the basic theory of heterogeneous reaction rates precedes the section on experimental determination of reaction rates to show how the problem must be tackled if it is proposed to use the reaction rate, measured in a static system (fixed bed), to predict the reaction rate which may be expected in a dynamic system (fluidized bed). A survey is then made of those references which present the results of kinetic studies where a fluidized bed was used as the reaction medium. The last section of the review summarises the literature dealing with the design and operation of small fluidizing units.

2:1 Data available on the reduction of barium sulphate

There was very little published work available on the reduction of barium sulphate by gaseous media and much of this was only of a descriptive nature.

Okuno[1] has investigated the reduction of barium sulphate by carbon monoxide but only considered the reaction,

$$BaSO_4 + 4CO = BaS + 4CO_2 \quad \ldots\ldots\ldots\ldots (1)$$

at equilibrium. The experimental values of the ratio p_{CO_2}/p_{CO} were higher than the calculated values and considerable quantities of sulphur were found on the cold portions of the reaction tube. This seems to indicate that the reaction,

$$BaSO_4 + CO_2 = BaCO_3 + SO_2 \quad \ldots\ldots\ldots\ldots (2)$$

with the subsequent reduction of the SO_2 to elemental sulphur, should have been taken into account. The effect of the concentration of carbon monoxide, in the inlet gas, on the reaction rate was also determined at a number of temperatures, using a flow type of apparatus. It was found that the rate of reaction increased with temperature and with carbon monoxide concentration.

Welles[2] carried out tests to determine the relative rates of reduction of barium sulphate by hydrogen and by carbon monoxide. He found that reduction by carbon monoxide was the more rapid but that, below 600°C, the reaction rates were very slow in each case. Welles also reported small quantities of hydrogen sulphide in the exit gases when hydrogen was used as the reducing agent.

At 1000°C it was found that the reduction product contained 6% of barium oxide; in none of the tests carried out did the exit gases approach equilibrium with the solid.

Neric[3] reduced barium sulphate in a stream of methane and found that a small quantity of hydrogen sulphide was evolved. The product obtained was almost free from sulphite when the reduction was carried out at temperatures below 1000°C.

Chaborski and Pirtea[4] investigated the reduction of barium sulphate by hydrogen and by ammonia and reported that ammonia appeared to be a more active reducing agent than hydrogen.

The limited published data seemed to indicate that the reduction of barium sulphate by hydrogen was not complicated by extensive side reactions and this contention is supported by the results of the thermodynamic calculations for the $BaSO_4$-H_2 system (see Appendix A) which indicate that, below 1100°C, reduction by hydrogen proceeds by only two paths, viz. direct formation of barium sulphide or formation of barium sulphite followed by further reduction to barium sulphide. <u>The reduction of barium sulphate by hydrogen was, therefore, chosen as the reaction upon which the project should be based.</u>

It can be seen that there had been no work of a quantitative nature carried out on this reaction. Experimental values of the equilibrium constant had not been obtained and the work on reaction

rates, at best, only gave an indication of the relative rates to be expected using different reducing gases. It was necessary, therefore, to determine these facts by experiment.

2:2 Experimental determination of equilibrium constants

The values of the equilibrium constant calculated from the thermodynamic data were only an estimate of the true values since the accuracy of some of the specific heat and free energy data was comparatively poor (see Appendix A). It was necessary, therefore, to obtain experimental values of the equilibrium constant to establish definitely that the equation for the reduction of barium sulphate by hydrogen was,

$$BaSO_4 + 4H_2 = BaS + 4H_2O \quad \ldots\ldots\ldots\ldots (3)$$

Further, since the driving force of a reaction may be defined as the magnitude of the displacement from equilibrium, it was also possible that accurate equilibrium data might be required to build up the equations correlating the rates of reaction obtained in the later phases of the project.

A survey of the literature showed that the experimental techniques used for measuring equilibrium constants in reduction systems could be divided into two classes, static methods and dynamic methods.

2:2:1 Static methods for determining equilibrium constants

The static method is the simplest approach to the problem of measuring equilibrium constants and hence was widely used by early

workers. The general procedure is that due to Deville and later improved by Eastman and Evans[5] who used it to study the reduction of iron oxides by hydrogen. Water vapour from an external, temperature controlled, water reservoir was admitted to an evacuated reaction chamber containing the reaction mass, also at a constant, known temperature. At equilibrium, the partial pressure of water vapour in the system must be equal to the vapour pressure of the water in the reservoir and, therefore, the hydrogen partial pressure can be obtained by measuring the total pressure in the apparatus. The static method suffers from two serious disadvantages, viz. evolution of occluded gases and thermal diffusion errors.

(1) Errors due to evolution of occluded gases

When the hydrogen partial pressure is a small fraction of the water vapour pressure then equilibrium constants obtained by the static method may be in serious error. Emmett and Shultz[6] found that the H_2O/H_2 ratio for the system cobalt-oxygen-hydrogen is approximately 60 at 500°C while previous workers using the static method obtained a value of approximately 15. The work of Emmett and Shultz appears to be reliable since they calculate constants from thermodynamic data and obtain good agreement with the experimental values which they secured using a flow type of apparatus. They maintain that the errors in the results of the earlier workers were due to the evolution of occluded gas from the walls of the apparatus after the water vapour had been admitted

to the reaction chamber. This is quite possible since, with a water vapour pressure of the order of 25 mm of mercury, the hydrogen pressure for this system will be less than 0.5 mm of mercury. Considerable errors could, therefore, be introduced by the evolution of a small quantity of occluded gas.

It seems probable, however, that greater accuracy could have been obtained by using water vapour pressures of the order of 250 mm of mercury even though under these conditions, the temperature coefficient of the water vapour pressure would be comparatively large, necessitating rigid control of the temperature in the water reservoir.

(2) Errors due to thermal diffusion

It is well known that, if a mixture of two gases is subjected to a temperature gradient, there will be a tendency for the heavy molecules to collect in the cold region while light molecules concentrate in the hot region. This means that the water vapour pressure in the reaction chamber of the static type of apparatus referred to above will be less than the water vapour pressure in the water reservoir, even though the total pressure at the two points is identical, i.e. the actual H_2O/H_2 ratio in the reaction chamber will be smaller than the measured H_2O/H_2 ratio. Unless corrections are applied, the errors due to this source may be of the order of 40%, as Emmett and Shultz[7] found when comparing static and dynamic methods of determining equilibria in the iron-oxygen-

hydrogen system.

This error can be minimised by circulating the gaseous phase through the reaction chamber and water reservoir in series as Emmett and Shultz[7] did. In this case precautions must be taken where the flowing gas passes through a temperature gradient otherwise a concentration gradient may still exist. The measures which must be taken to minimise this effect will be discussed in the next section.

Alternatively, equations have been developed by Gillespie[8] and by Whalley[9] which make it possible to calculate the composition of the gaseous phase in the reactor if the composition in the water reservoir and the respective temperatures are known. These equations have been derived from the elementary kinetic theory of gases and hence the calculated concentration gradients are not exact; it has been found by experiment that the gradients predicted are nearly always greater than those found in actual practice. Whalley states that the discrepancy between predicted and actual gradients should not be greater than 20% and is usually considerably less. Even though these corrections are not exact Kubaschewski and Evans[10] say that the static method for determining equilibrium constants can be as useful as the dynamic method if both techniques are practicable.

2:2:2 Dynamic methods for determining equilibrium constants

Equilibria involving reduction by hydrogen or carbon monoxide have been studied by a number of workers[6)7)11)12)13)14)] using modifications of the dynamic method. Fundamentally, this consists of passing a steady stream of gas, of known composition, over the solid phases involved in the reaction at such a rate that the exit gases are in equilibrium with the solid. The exit gases are then analysed and, since the temperature of the solid is known, the equilibrium constant for the reaction is obtained directly from the composition of the exit gas.

Rosenqvist[15)] points out that there are two important factors which must be considered in the design of the apparatus and the selection of gas flow rates, viz. the effects of thermal diffusion and of incomplete equilibria.

(1) Effects of thermal diffusion

Thermal diffusion tends to cause migration of the heavy molecules in a gaseous mixture to cold regions and of light molecules to hot regions, however, according to Emmett and Shultz[7)] this segregation can be minimised by causing the gas to flow through the temperature gradient at a sufficiently high velocity. Whalley[9)] has derived an equation from which, for a tube of given diameter in a known temperature gradient, an estimate can be made of the minimum gas velocity needed to reduce the effect of thermal diffusion to

negligible proportions. In a reaction involving hydrogen as the reducing agent thermal diffusion would cause an increase in the measured value of the H_2O/H_2 ratio as the flow rate is decreased since the gas composition is measured in the cold part of the apparatus where the heavy water molecules would tend to collect.

It is interesting to note that the experimental techniques adopted by Pease and Cook[12] included capillary tubing to transport the gases to and from the hot reaction chamber although the importance of thermal diffusion was not discussed by Emmett and Shultz[7] until six years later.

(2) Effect of incomplete equilibrium

Kitchener and Ignatowicz[11] specify that the exit gas must be in thermal and chemical equilibrium with the solid if accurate results are to be obtained. This condition is usually satisfied by using a long, porous bed of solid of such a width that the gas velocity through the bed is very slow, the bed being maintained at a constant temperature along its length to eliminate any thermal diffusion effects.

It is possible that, for a slow reaction, thermal equilibrium could be attained before chemical equilibrium if the inlet gas composition differed greatly from the equilibrium composition. It is possible, therefore, for a given flow rate, to have chemical equilibrium between solid and gas when the inlet gas composition

is near the equilibrium value even though chemical equilibrium may not be remotely approached when the inlet gas composition differs greatly from the equilibrium value. This type of behaviour was used by Pease and Cook[12] to obtain an equilibrium constant for a slow reaction. The composition of the inlet gas was made to approach equilibrium from both sides and the composition of the exit gases for each run was determined. When the inlet and exit gases had the same composition this was taken as the equilibrium value.

2:3 Theory of heterogeneous reaction rates

Langmuir[16] showed, from a consideration of the phase rule, that a reaction between two phases can take place only at the interface between those two phases, unless solid solutions are formed. If solid solutions are formed, however, the reaction zone will be a narrow band of finite thickness instead of a sharp line. This is a more complicated case than where the solid phases are not mutually soluble.

Heterogeneous reactions must, therefore, involve at least three steps,

(1) transport of the reactants to the interface;

(2) reaction at the interface, and

(3) recession of the products from the interface.

2:3:1 The Nernst Theory

Bircumshaw and Riddiford[17] review the theories which have

been evolved to explain the rates of heterogeneous reactions. Nernst, a pioneer in this field, postulated that the chemical processes at the interface are always much more rapid than one or other of the transport steps. This means that equilibrium should be established instantaneously at the interface and the reactants then diffuse to the interface under the influence of the concentration gradient set up between the bulk of the fluid phase and the interface. Nernst also assumed that,

(1) in an agitated fluid-solid system the concentration gradient is limited to a thin film of fluid adhering to the solid,

(2) within this layer the concentration varies linearly with distance, and

(3) the thickness of this layer is a function only of the flow rate and the geometry of the system and is independent of viscosity and temperature.

Bircumshaw and Riddiford point out that none of Nernst's assumptions is entirely correct since there are chemically controlled reactions where the transport processes are more rapid than the chemical process at the interface, e.g. dissolution of glass in alkali; dissolution of metallic tin, cadmium, and aluminium in hydrochloric acid; oxidation of carbon with air at low temperatures. There is considerable evidence in the case of liquids at least, that fluid

motion in all directions persists down to the solid surface and consequently the assumption that the concentration gradient is linear must also be an approximation. It has also been shown that the thickness of the Nernst "layer" varies with temperature. However, while the static film theory of Nernst is clearly only an approximation because of the complex conditions which exist near an irregular solid surface in a flowing fluid, the concept does appear to be useful for comparing the kinetics of different reactions under fixed conditions of flow and temperature.

Van Name and Hill[18] were the first to suggest a classification of reactions on the basis of the rate determining step and they recognized three different types of reactions,

(1) transport or diffusion controlled,

(2) chemical or activation controlled, and

(3) intermediate type, i.e. where both rates are of the same order of magnitude.

2:3:2 Diagnosis of reaction type.

It is apparent from Section 2:3:1 that the effect on the observed reaction rate of changing a system variable, e.g. temperature, flow rate, or solid properties, will depend on which step is controlling. Each type of reaction will be discussed in turn.

(1) Characteristics of transport controlled reactions

Consider a reaction of the type,

$$aA_{(solid)} + bB_{(fluid)} = cC_{(solid)} + dD_{(fluid)} \quad \ldots\ldots(4)$$

According to Parravano[19], when the ratio

Q = (specific volume of product)/(specific volume of reactant)

approaches unity, the rate of diffusion of the fluid phase reactants and products through the solid product layer will be the controlling step in the reaction. If, however, Q varies from unity it is probable that the solid product film will buckle or crack and expose the solid reactant to the other reactant phase, i.e., the only effect will be to reduce the area of the interface available for reaction. Bircumshaw and Everdell[20] have examined reactions controlled by the rate of solid diffusion and they conclude that an alteration of Reynolds Number for the system will not affect the observed reaction rate if the temperature is held constant. Further, the reaction rate will be independent of the apparent area of the solid and will obey the well known parabolic law,

$$dx/dt = k/x \quad \ldots\ldots\ldots\ldots\ldots\ldots\ldots\ldots \quad (a)$$

where x = the fraction of reactant consumed at a time t

k = the specific rate constant.

Since diffusion of fluids through solids generally satisfies an equation of the type,

$$D = Ae^{-E/RT} \quad \ldots\ldots\ldots\ldots\ldots\ldots\ldots\ldots (b)$$

where D = the diffusion rate

A = a constant

E = the activation energy for the process

R = the gas constant

T = absolute temperature

it follows that the observed reaction rate will vary exponentially with temperature.

In the case where the solid product layer distorts and exposes the underlying reactant the reaction could still be transport controlled by the rate of diffusion through the adhering fluid film. Zimmerman[21] has discussed this class of reaction and she states that alteration of any variable which affects the value of Reynolds Number for the fluid phase will influence the observed reaction rate; in general, an increase in Reynolds Number will cause an increase in the reaction rate. Further, the temperature coefficient of the observed reaction rate will be approximately that for gaseous diffusion and the rate of reaction will depend on the apparent area of the solid reactant. In addition, the rate of reaction will be affected by any alteration of the diffusivity of the reactants and the reaction rate will also obey the equation for a first order reaction.

(2) Characteristics of activation controlled reactions

Zimmerman[21] makes the following points regarding activation or chemically controlled reactions.

(a) The observed rate is independent of Reynolds Number at constant temperature.

(b) The rate of reaction varies exponentially with temperature,

i.e. the rate constant obeys a relationship of the type,

$$k = Ae^{-E/RT} \quad \text{(Arrhenius Equation)} \ldots\ldots\ldots (c)$$

where k = the rate constant

A = a constant

E = the energy of activation

R = the gas constant

T = the absolute temperature.

(c) The rate of reaction is independent of changes in the diffusivity of the reactants or products.

(d) The reaction rate depends on the area of the interface between the two phases so that the rate may be sensitive to variations in the method of surface preparation.

(e) The order of reaction may be zero, first, second, or third, or some intermediate value.

Both Hougen and Watson[22] and Corrigan[23] have developed equations which will permit a diagnosis to be made of the mechanism by which a chemically controlled reaction proceeds. Reaction rates are obtained over a wide range of gaseous reactant and product concentrations; the resulting curves of reaction rate vs concentration are compared with theoretical curves, calculated assuming a number of possible mechanisms, and the unfeasible mechanisms are then eliminated.

(3) Characteristics of intermediate type reactions

According to the classification proposed by Van Name and Hill[18] this group includes all reactions which do not distinctly fall into either of the above categories.

Olson, Schuler, and Smith[24], studying the catalytic oxidation of sulphur dioxide, found that the effect of variation in gas flow rate on the measured rate of reaction was more pronounced at high temperatures than at low temperatures and that the measured rate of reaction, at high temperatures, approached a constant value as the gas flow rate was increased. This same phenomenon was noted by Tu, Davis, and Hottel[25] while studying the oxidation of carbon in air and they concluded that the diffusion rate approached a large constant value as the Reynolds Number for the system increased.

If the surface reaction is of the first order then, from a consideration of the Nernst Theory, it can be shown[26)27)] that the reciprocal of the characteristic time of reaction is equal to the sum of the characteristic times of diffusion and activation. That is,

$$1/k_{ob.} = 1/k_r + 1/k_d \quad \text{.....(d)}$$

Where $k_{ob.}$ = the value of the rate constant obtained by experiment

$k_r = Ae^{-E/RT}$ (Arrhenius Equation)

$1/k_d = 1/k_{d_A} + 1/k_{d_B}K$

K = the equilibrium constant for the reaction

The constants k_{d_A} and k_{d_B} are defined by the equations,

$$- d(c_A)/dt = k_{d_A}(p_A - p_{i_A}) \quad \text{.....(e)}$$

$$- d(c_B)/dt = k_{d_B}(p_B - p_{i_B}) \quad \text{.....(f)}$$

Where p_A and p_B are the partial pressures of components A and B in the body of the flowing gas and p_{i_A} and p_{i_B} are the corresponding pressures at the solid surface. Of course these equations are subject to all the limitations of the Nernst "static film" theory (see Section 2:3:1) but they do serve to correlate data in simple fashion and they are particularly useful where the value of k_d for the system being studied is known from previous experiments.

Riddiford[26] discusses the temperature coefficient of the observed rate of intermediate type heterogeneous reactions but the relations which he derived hold only for solid-liquid systems where k_d varies exponentially with temperature. However, since k_d for gaseous systems is relatively insensitive to temperature change, while k_r varies exponentially with temperature, it is clear that a gas-solid reaction might be chemically controlled at low temperatures and change through an intermediate type reaction to a transport controlled reaction as the temperature rises. The investigations of Tu, Davis, and Hottel[25] on carbon oxidation and of Olson, Schuler, and Smith[24] into the catalytic oxidation of sulphur di-

oxide are good examples of such changes in control.

2:3:3 Use of experimental data for predicting reaction rates

The problem of predicting the rates, for a given system, of the intermediate type of reaction where chemical and diffusion rates are of the same order, has received some attention from workers in the chemical engineering field. Hougen and Watson[28] and Hurt[29] were the first to suggest that the observed reaction rate should be separated into its component parts to obtain the chemical rate devoid of any diffusion effects. The chemical rate is unique for a given reaction at a set temperature and does not depend on the other properties of the system (see Section 2:3:2); when the chemical rate has been obtained it can be combined with the known mass transfer data for a new system to derive an overall rate of reaction.

There are two different approaches to the problem of eliminating the mass transfer component from the observed rate of reaction, viz. recourse to known mass transfer data or extrapolation of the measured rate to infinite gas velocity.

Hougen and Watson[28], Hurt[29], and Wilhelm[27] all used published correlations of mass transfer data. Their approach to the problem may be illustrated by considering the reaction,

$$\text{Solid}_{(1)} + A_{(gas)} = \text{Solid}_{(2)} + B_{(gas)} \quad \ldots\ldots(5)$$

The rate of mass transfer of component A from the body of the gas

to the interface will be defined by the equation[28],

$$r_{dA} = k_{gA} (p_A - p_{iA}) \quad \ldots\ldots\ldots\ldots\ldots\ldots (g)$$

Where r_d = the transfer rate

k_g = the gas phase transfer coefficient

p_A = the partial pressure of component A in the body of the gas

p_{i_A} = the partial pressure of component A at the interface.

For a first order reaction the chemical rate is given by the equation[28],

$$r_r = k_r(p_{i_A} - p^*_{i_A}) \quad \ldots\ldots\ldots\ldots\ldots\ldots (h)$$

Where r_r = the chemical reaction rate

k_r = the chemical rate constant

$p^*_{i_A} = p_{i_B}/K$

K = the equilibrium constant for the reaction

The rate of diffusion of product B away from the interface will be given by the equation[28],

$$r_{d_B} = k_{g_B}(p_{i_B} - p_B) \quad \ldots\ldots\ldots\ldots\ldots\ldots (i)$$

At steady state,

$$r_{ob.} = r_{d_A} = r_r = r_{d_B}$$

but, $r_{ob.}$ = the observed rate of reaction

$$= k_{ob.}(p_A - p^*_A)$$

and, $$p^*_A = p^*_B/K$$

therefore, $1/k_{ob.} = 1/k_{g_A} + 1/k_r + 1/k_{g_B} K$ .....(j)

It can be seen that if k_g values for reactant and product are available the rate of the chemical process can be determined directly. Mass transfer data are presented either as a correlation of gas phase transfer coefficients (k_g) or as heights of the transfer unit (H.T.U. values). Hurt[29] and Wilhelm[27] developed methods similar to that given above but they utilized correlations of H.T.U. values.

Olsen, Schuler, and Smith[24] obtained experimental values of the reaction rate (r), over a range of mass velocities (G), for the catalysed oxidation of sulphur dioxide. A plot was then prepared of 1/r vs 1/G at constant temperature and the curve was extrapolated to an infinite mass velocity. The value of r so obtained was assumed to approximate the case of reaction without diffusion. This method has the disadvantage that the reaction must be studied over a wide range of mass velocities if the extrapolation is to be accurate.

In either of these cases the chemical rate obtained must be recombined with the mass transfer data for the new system to predict the rate at which the reaction will proceed. This is achieved by reversing the procedure given above for separating diffusion and chemical rates.

To date this approach to the design of reactors has been applied to only a few problems. Some success has been achieved[24)27)28)29)] in designing reactors for gaseous reactions which are catalysed by

a solid surface, particularly for the case of the catalytic oxidation of sulphur dioxide. One of the most comprehensive publications on this subject is due to Olson, Schuler, and Smith[24] who used the methods of Hurt[29] and Hougen and Watson[28] for the design of a sulphur dioxide converter. They found that the method developed by Hougen and Watson was the most satisfactory since it allowed for retardation of the reaction rate by the products of reaction.

The prediction of rates for reactions which are purely transport controlled has received little attention, probably because the calculations are quite straightforward. Should the reaction be controlled by diffusion through the gas phase it is only necessary to have access to mass transfer data for the new system in order that the rate of reaction may be predicted. The calculations involved are covered by any text or handbook on mass transfer, e.g. Perry[30].

Johnstone and co-workers[31][32] have considered the problem of predicting the rates at which chemically or activation controlled reactions will proceed in fluidized beds. The oxidation of ammonia[31] and the decomposition of nitrous oxide on solid catalysts[32] were the reactions which were used to study the problems involved. They pointed out that the major difficulty is encountered in calculating the component partial pressures in the gas phase of the bed and they recommended that use should be made of the "two phase" theory of fluidization which was developed by Toomey and Johnstone[33]

(see Section 2:6:2 below).

2:4 Experimental determination of reaction rates

Attention has been confined to a survey of methods for measuring heterogeneous reaction rates in fixed beds and, in particular, to the work of those investigators who studied reactions involving the reducing gases, hydrogen and carbon monoxide.

As was the case for the determination of equilibrium constants, the techniques of the various workers can be divided into two main classes, viz. static methods and dynamic methods.

2:4:1 Static methods

Taylor and Starkweather[34] describe a constant pressure apparatus in which the sample of solid being studied is heated under vacuum to remove adsorbed gases and the reactant gas then admitted at atmospheric pressure. The pressure in the reactor is maintained at one atmosphere and the course of the reaction is followed by measuring the volume of reactant consumed at a given time. If the products of reaction include gases some means must be provided to remove them or keep them at a constant concentration. This system was used by Taylor and Starkweather to study the reduction of metal oxides by hydrogen.

A similar technique, utilizing a constant volume apparatus was originated by Parravano[19]. In this case a given volume of reducing gas is admitted to the apparatus after the solid has been

freed from adsorbed gases and the course of the reaction followed by measuring the pressure in the system at given time intervals. Some means must also be provided for removing the product gases.

Parravano used this method to study the reduction of nickel oxide by hydrogen and his apparatus included a pump for circulating the gas through the oxide bed. The gas was pumped at such a velocity that small changes in the pumping rate had no effect on the rate of reaction.

2:4:2 Dynamic methods

Basically the technique is to pass gas of known composition through the bed of solid reactant and to follow the progress of the reaction by measuring the composition of the exit gases. The rate of reaction vs time curve is then found by differentiating the composition vs time curve.

This is by far the most common approach to the problem and has been used by a number of investigators.

(1) Benton and Emmett[35] and Pease and Taylor[36] studied the reduction of nickel and copper oxides by hydrogen.

(2) Wetherill and Furnas[37] and Woods[38] considered the reduction of iron oxides.

(3) The combustion of carbon in air was studied by Tu, Davis, and Hottel[25].

(4) Gadsby and coworkers[39][40] investigated the steam carbon reaction.

(5) Olson, Schuler, and Smith[24] used a flow apparatus to study the catalytic oxidation of sulphur dioxide.

2:5 Data available on reaction kinetics in fluidized beds

Little information has been published on reaction kinetics in fluidized beds. Eliminating purely descriptive articles the only relevant works appear to be those listed below.

(1) Kivnick and Hixson[41] studied the reduction of nickel oxide by hydrogen and they found that the reaction appeared to be diffusion controlled above 600°F. An attempt was made to calculate the value of the chemical rate constant (k_r) using the available mass transfer data (k_g) but it was found that the calculated mass transfer rate was far greater than the observed rate, even though the reaction appeared to be diffusion controlled. They suggest that the area to be used in calculating the mass transfer rate may not be the total surface area of the solid particles but rather, the area of the solids in turbulent flow, i.e. at the edges of the bubbles.

(2) Lewis, Gilliland, and Sweeney[42] studied the gasification of carbon using metal oxides as the oxygen carrier. It was found that the reaction mechanism could be expressed by the equations,

$$C + CO_2 = 2CO \quad \text{.....(6)}$$

$$CO + MO = M + CO_2 \quad \text{.....(7)}$$

and that reaction (6) appeared to be the rate controlling step. The reaction was chemically controlled at the temperature (900°C) and flow rates studied. The results obtained did not agree with those of Gadsby and co workers[39)40)] who studied reaction (6) in a packed bed but the authors explain this by assuming that some of the gas is by-passed through the bed as bubbles and therefore has a different composition to the gas in the rest of the bed.

(3) The gasification of carbon by carbon dioxide has been investigated by Lewis, Gilliland, and McBride[43)]. The temperature range studied was from 1475°F to 2000°F but the reaction appeared to be chemically controlled in this region.

(4) Lewis, Gilliland, and Reed[44)] have reported an investigation into the reaction of methane with copper oxide. They operated their reactor in the temperature range of 1500°F to 2000°F and found that the chemical reaction was the controlling step.

(5) Gilliland and Mason[45)] reported that, for identical space velocities, a fluidized bed gives a lower conversion for first and second order homogeneous gas phase reactions than does a fixed bed. This was attributed to gas mixing and by-passing in the fluidized bed.

(6) The low temperature, catalysed oxidation of ammonia, a zero order reaction, in a fluidized bed was studied by Johnstone,

Batchelor, and Shen[31]. They found that the rate of reaction was higher for a fluidized bed than for the corresponding fixed bed and showed that this effect is due to by-passing of gas, as bubbles, through the fluidized beds.

2:6 Design and operation of fluidized beds

The object of this section of the review is to survey the literature dealing with fluidized reactors so that a laboratory scale reactor suitable for reducing barytes with hydrogen may be designed.

If a satisfactory basis is to be established for the comparison of static and dynamic test data it is necessary that the dispersed solid contained in the reactor be held in contact with the gas for a determinable period of time; accordingly the dense phase system, in which the bed has a well defined upper surface, has been selected as the most suitable for the present investigation. For this reason, articles on dilute phase fluidization where the solids are uniformly distributed throughout the reactor have not been reported. The survey has been further restricted to those articles dealing with fluidization of solids with gases only except where indicated in the discussion on bed expansion.

Sections 2:6:1 to 2:6:4, inclusive, deal with those aspects of reactor design - mass velocity, mixing, solids and properties, and mass and heat transfer - which can, in some measure, be based on theories developed from the results of controlled experiments. Section 2:6:5, on the other hand, refers to those features of design, e.g. feeding devices, which are necessarily based on practical

experience.

2:6:1 Effect of mass velocity on bed properties

Consider a packed bed of solid particles to which a gas stream is introduced from the bottom at an increasing rate. The pressure drop, at first, increases without bed expansion, i.e. the fractional void volume remains unchanged. When the flow rate becomes large enough to cause a pressure gradient across the bed equal to the buoyant weight of the solids per unit volume, the point of incipient fluidization is reached and any further increase in flow rate will cause the bed to expand while the pressure drop remains substantially constant. On increasing the gas flow above that for incipient fluidization, gas bubbles appear, and the bed becomes fully fluidized as the solids circulate and mix; continued increase in the flow rate causes the passage of larger bubbles with increasing frequency. A fluidized bed is not, therefore, homogeneous with regard to the concentration of solids and may be considered as consisting of two phases; the bubbles constituting a dilute or discontinuous phase; the remainder of the bed constituting a dense or continuous phase. The relative proportions of these phases vary with the gas flow rate.

(1) Critical gas velocity

The variation of pressure drop with gas velocity in a fixed bed has been extensively studied and one of the most widely used

correlations was that developed by Carman[46],

$$f = \frac{\Delta p}{L} \quad \frac{d}{2G^2} \quad \frac{\epsilon^3}{(1-\epsilon)^2} \quad \frac{1}{\beta} \quad \ldots\ldots(k)$$

where f = the friction coefficient

Δp = the pressure drop

L = the bed depth

d = particle diameter

G = the mass flow based on the superficial area of the bed

ϵ = the void fraction

β = the particle shape factor.

This equation has been applied at the point of incipient fluidization by several investigators[47)48)49)50)] to give a relationship of the form,

$$G_o = K \frac{\epsilon_o^3}{(1-\epsilon_o)} \quad \frac{d^2}{\beta} \quad \frac{(\rho_s - \rho)\, g}{\eta} \quad \ldots(m)$$

where G_o = the mass velocity at the onset of fluidization

K = a constant

ρ = the density of the fluid

ρ_s = the density of the solid particles

g = the gravitational constant

η = the viscosity of the fluid

Various investigators have obtained slightly different values for the constant K in equation (m), viz.,

Leva[47]	K = 0.005
Miller and Logwinuck[48]	K = 0.006
Van Heerden[49]	K = 0.0065
Cathala[50]	K = 0.0055 (from theoretical calculations)

Only van Heerden and his coworkers[49] have successfully extended this equation to predict the onset of fluidization in beds containing solids of various sizes. They define an effective diameter equal to the diameter of a sphere which would give the same number of particles per unit volume of packed bed as the material under consideration (both counted at maximum porosity).

All investigators agree that the correct value of ϵ_0 for a bed should be obtained by fluidizing the material and slowly reducing the gas flow rate until the bed is quiescent when the void fraction can be measured at the loosest stable packing. Both Leva[47] and van Heerden[49] point out, however, that there is little error involved if the material is simply poured into a measuring vessel and the bed porosity determined directly. This method has the advantage of simplicity and Leva found that porosities measured in this way are only about 5% lower than those obtained by fluidization.

(2) Pressure drop

At the point of incipient fluidization the pressure drop across the bed is given by the equation,

$$\Delta p/L = (\rho_s - \rho)(1 - \epsilon_0)g \quad \ldots\ldots\ldots\ldots\ldots\ldots (n)$$

and, as the flow of gas is further increased, the pressure drop increases only slightly above this value. Leva[47] was the first to attach any significance to the increase in pressure drop above that necessary to support the weight of the bed. He postulated that the excess pressure drop provided the energy necessary to agitate the solid particles in the bed and introduced the concept of fluidization efficiency as a measure of the degree of bed agitation. The fluidization efficiency (E) was defined by the equation,

$$(G_f - G_e)/G_e = E \quad \ldots\ldots\ldots\ldots\ldots\ldots\ldots\ldots (o)$$

Where G_f = the mass flow for fluidization

G_e = the mass flow to expand the bed (calculated from (m))

Leva[52] also studied the effects of change in fluidization efficiency on the linear velocity of the solid particles in the bed and on the heat transfer coefficients from bed to wall. He found that both increased as the fluidization efficiency increased and that both could be satisfactorily correlated in terms of fluidization efficiency. Toomey and Johnstone[33] reached much the same conclusions but they considered that the excess pressure drop was used entirely in giving

rotational energy to the particles in the bed. They also found that the increase in pressure drop, over that at incipient fluidization, increased with bed depth and with the square root of the particle size of the solids in the bed. They put forward a relationship which satisfactorily correlated their results.

(3) Bed expansion

Knowledge of the increase in bed volume caused by a given flow rate is important in design work since the size of the bed will be an important factor in determining the height of the reactor to be used. Unfortunately, there is a difference of opinion among the various investigators as to the form of the relationship between bed height (L) and superficial gas velocity (v).

Leva[47] found that a plot of Lv against log $\frac{\epsilon^3}{(1-\epsilon)^2}$ gave straight lines for air fluidization but that the slope of the straight lines was a function of the particle size. Leva gives experimental values for these slopes but does not suggest any correlation.

Lewis, Gilliland, and Bauer[52] found that a plot of log ϵ against log v gave parallel straight lines which could be extrapolated to the free falling velocity of the particles. The slope of the lines for air fluidization of glass beads was 4.5. Unfortunately, this relationship gave the best correlation for slugging or "bumping" conditions but showed marked variation from the experimental results

obtained with fine particles giving good fluidization. Jottrand[53] also used this method for correlating the results obtained with a sand bed fluidized by water. He obtained excellent correlations on lines having a slope of 5.6.

Cathala[50] gives a graphical method for extending results obtained at room temperature with air as the fluidizing medium to any other gas at a different temperature. He assumes a relationship similar to that proposed by Leva[47] but quotes no experimental evidence to support his method.

Shuster and Kisliak[54] studied the effect of bed expansion on fluidization quality by using a pressure gauge with a high speed of response to record the variations in the pressure drop across the bed. When slugging occurs in the bed the particles are lifted by gas bubbles which increase in size as they rise until they may cover the entire cross section of the bed. With good quality fluidization, however, the gas rises more or less uniformly through the bed and the particles, distributed rather evenly in the fluid stream are free to circulate at random. Shuster and Kisliak found that slugging conditions gave large violent fluctuations in the pressure drop across the bed while good quality fluidization corresponded to small rapid variations in the pressure drop. The tests showed that the fluidization quality improved as the bed expanded.

2:6:2 Solid and gas mixing in fluidized beds

Gilliland and Mason[55] and Leva[51] carried out a series of experiments to determine the degree of solid mixing in laboratory scale units and came to the conclusion that mixing was very rapid and practically complete. Their conclusions were confirmed by Thompson[56] who reported on a 16 foot diameter commercial unit used for roasting sulphide ores. Although cold slurry (75% solids) was fed at a single point, with a rate of approximately 100 pounds per minute, into a bed at 900°C the maximum temperature variation, indicated by traverses of the bed, was less than 10°C. (It is generally accepted that such rapid heat transfer within the bed is due to the high degree of solid mixing.) Sittig[57] points out that complete mixing can be a disadvantage in a process where it is desired to produce a solid product which has completely reacted since a large bed volume may be required to reduce the chances of partly reacted solids being discharged from the system. Alternatively, a multibed system may be adopted to avoid short circuiting of unreacted feed from inlet to outlet. Such a multibed system has been utilized in the Dorr process for calcining limestone[58].

The experimental evidence concerning gas mixing in a fluidized bed is rather conflicting. Gilliland and Mason[45)55] carried out tests with tracer gases and found that, as L/D for the bed decreased, the residence time curves for the tracer gas approached the theoretical curve for the case where there was complete mixing in

the gas phase. However, they also showed that there was little back mixing of gas in the bed so that the residence time effect must have been produced through the by-passing of considerable quantities of gas through the bed. They calculated that some of the gas must have passed through the bed with a velocity of up to ten times the average gas velocity. As L/D for the bed increased the gas flow pattern tended towards the piston type flow obtained in open pipes. The work with tracer gases was confirmed by carrying out homogeneous, gas phase reactions in a fluidized bed reactor. Gilliland and Mason worked with 4 inch and 1 inch diameter beds.

Johnstone and his coworkers[31)32)33)] have shown that all the gas in excess of the quantity corresponding to the point of incipient fluidization is by-passed through the bed as bubbles. They visualize a fluidized bed as consisting of two parts, a discontinuous phase comprising the bubbles passing up through the bed, and a continuous phase, which has a porosity equal to that which the bed had at the point of incipient fluidization. They state that the discontinuous phase has little contact with the particles in the bed while in the continuous phase the gas and solids are in intimate contact. Johnstone did not, however, give any information on gas back mixing in the continuous phase of the fluidized beds which were used. All the work was carried out on 3 inch diameter beds.

Danckwerts, Jenkins, and Place[59] carried out experiments on a 40 foot diameter catalyst regenerator with a bed having an L/D ratio equal to 0.5 using a tracer gas technique similar to that developed by Gilliland and Mason[55]. They found that the residence time curve corresponded fairly closely to that for piston type flow through the bed. Askins, Hinds, and Kunreuther[60] measured the gas composition at various points in the bed of a similar catalyst regenerator under the same operating conditions but found that the gas composition was practically constant. Danckwerts points out, however, that the sampling method adopted by Askins, Hinds, and Kunreuther would allow a large part of the gas sample to be drawn from the continuous phase of the bed where the gas composition might be substantially constant, although, he admits that this does not entirely explain the difference in the two sets of results.

The work of Gilliland and Mason[55] on back mixing has been partly confirmed by Heertjes, deBoer, and van Dorssor[61] who carried out drying experiments with a bed of silica gel which had a high L/D ratio. The results indicated that there was a piston type flow pattern in the bed. They also found that practically all the heat and mass transfer occurred in a narrow layer of the bed just above the supporting sieve. The height of this layer was approximately equal to the diameter of the bed and was not affected by the height of the bed proper.

2:6:3 Effect of the physical properties of the solids

(1) Fluidization quality

Sittig[57], in a review of fluidization techniques, emphasises that the size distribution of the solids in a fluidized bed has a very great influence on the quality of the fluidization obtained. A mixture of coarse and fine sizes gives the best results; fine material tends to channel while coarse material gives slugging fluidization. Sittig recommends adding inert fines to heavy material of large size to improve the quality of fluidization obtained. He states that the maximum permissible particle size is in the region of 0.125 in. to 0.06 in. diameter; the maximum permissible size decreases as the particle density increases.

It is interesting to note that all investigators who have worked on laboratory scale units, with the exception of van Heerden[49] have used beds consisting of closely sized material. It appears that the simplification of using a bed having uniform properties compensates for any consequent loss in fluidization quality.

(2) Elutriation rates

In a bed consisting of a mixture of coarse and fine material the fluidizing velocity will usually exceed the terminal (free settling) velocities of the finer particles, however, both Osberg and Charlesworth[62] and Leva[63] point out that the bed can retain such fine material for a considerable time even though the superficial gas velocity may be much larger than the terminal velocities of the fine

particles. Leva found that the rate of removal of very fine dust from a catalyst bed followed a first order rate law. He deduced, from his results, that the rate constant was independent of the dust diameter and varied as the fourth power of the superficial velocity. Osberg and Charlesworth[62] also found that the rate of elutriation of dust from a bed of scotchlite glass beads followed a first order equation. They studied the effects of superficial velocity, gas properties, and bed properties, on the rate constant and found that,

$$k \propto (v_f - v_{mf})^n \quad \ldots\ldots\ldots\ldots\ldots\ldots\ldots\ldots (p)$$

where k = the rate constant

v_f = the superficial gas velocity

v_{mf} = the superficial gas velocity at the point of incipient fluidization

n = a constant depending on gas density and viscosity.

They noted that there was a marked segregation of dust in the top section of the bed where the dust concentration was up to twice the average concentration in the bed.

(3) Attrition rates

Hall and Crumley[64] examined the break down of Fischer-Tropsch catalysts in fluidized beds and came to the conclusion that chemical attack caused most of the breakdown while attrition, brought about by bed turbulence, was practically negligible. Evans and Kepper[65]

report on pilot plant installations for calcining limestone and roasting sulphide ores and agree that the attrition rate is insignificant. They attribute this to the gas "cushion" which surrounds the particles in the bed and prevents jostling.

2:6:4 Mass transfer and heat transfer in fluidized beds

Chu, Kalil, and Wetteroth[66] combine their own data on transfer of naphthalene to air with the data of previous investigators in the form of a j_d plot to produce the most comprehensive correlation which has been published to date. It must be pointed out, however, that this work has all been carried out at room temperatures with extremely low rates of mass transfer and caution should be exercised in applying the data for other conditions. For example, Kivnick and Hixson[41] found that the mass transfer rate to the reaction zone of a nickel oxide particle which was being reduced by hydrogen in a fluidized bed at 400°C was considerably less than the rate predicted from the j_d correlations. However, Shen and Johnstone[32] point out that, in a case such as this, where there is a rapid reaction involving solid and gas, it is the mass transfer rate between continuous and discontinuous phases which controls the velocity of reaction. They calculate mass transfer coefficients, between each phase, for the N_2O-N_2-O_2 system using deep beds of fluidized alumina catalyst.

Leva and Grummer[51] have summarised most of the work which has been published on heat transfer between fluidized bed and

confining surface. Since the appearance of their survey additional data have been published by Dow and Jakob[67] and Bartholomew and Katz[68]. The latest contribution by van Heerden, Nobel, and van Krevelen[69] stresses the complexity of the problem and points out the poor agreement between the various sets of data. It appears that the rate of heat transfer is very sensitive to the mode of solids circulation within the bed which, in turn, depends on the details of construction of the fluidizing unit.

The limited data on gas-solid heat transfer rates have been summarised by Wamsley and Johanson[70] who obtained rates by investigating unsteady state heating of solids in a fluidized bed. They found that their results were much lower than those previously reported and put forward a new correlation based on the two phase concept of fluidization developed by Toomey and Johnstone[33] wherein any gas flow in excess of that at incipient fluidization is assumed to pass through the bed as bubbles. Wamsley and Johanson postulate that the gas which is by-passed through the bed in bubbles takes no part in gas-solid heat transfer.

2:6:5 General design information

This section deals with those features of design which are necessarily based on practical experience. The available information on these topics is unfortunately somewhat scanty.

(1) Solids feeding

The problem is to introduce the powdered solid from a relatively low pressure zone (a hopper) to a relatively high pressure

zone (a reactor or flowing gas stream) at a controlled rate. The usual types of feeder are depicted in Fig. 1 (after Sittig[57]). Gregory[71] emphasises that neither the star feeder, slide valve, nor screw conveyor, can add extra pressure and use must be made of the effective head of the solid in a stand pipe to overcome the pressure difference across the feeder. The star feeder or slide valve may be replaced, for freely flowing powders, by the non-mechanical

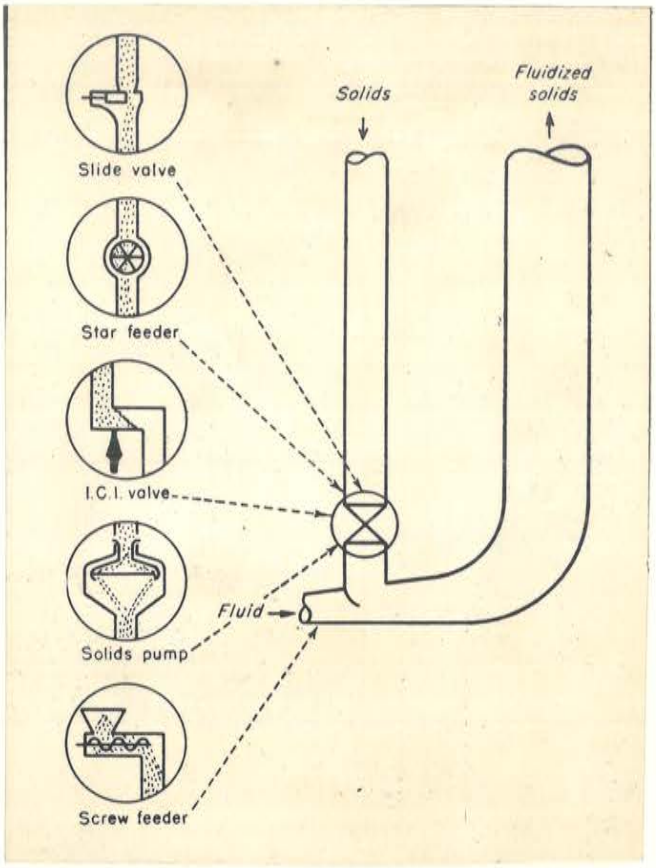

Fig. 1. Feeders used for adding solids to the fluid stream.

I.C.I. valve which utilizes the natural angle of repose of the non-fluidized solid to halt flow when desired. Aeration gas injected at the point indicated by the arrow (see Fig. 1) disturbs the angle of repose and the flow of solids is resumed. It is claimed[57] that the solids pump - a centrifugal pump operating on powdered solid - can be used for a pressure differential of 10 to 100 pounds per square inch and that erosion of the pump components is not a serious problem. It appears, however, that this device only operates successfully on fine solids such as catalyst powders.

(2) Gas distribution

Sittig[57] and Gregory[71] agree that the gas may be distributed to the bottom of the bed by any of the three systems (a) conical bottom, (b) packed bed, or (c) grid. Investigators working on laboratory scale units at room temperatures almost exclusively use a grid of metal cloth or plastic gauze while the tendency at high temperatures is towards a grid of stainless steel gauze or to a 60° conical bottom. The number of investigators who have worked at elevated temperatures is small but Kivnick and Hixson[41] and Lewis[42] used stainless steel cloth while earlier workers[43][44] relied on the conical bottom of the reactor for good gas distribution. It is generally agreed[57][71] that a grid gives a much more uniform gas distribution than a cone.

(3) Solids separation from the gas

Both Sittig[57] and Gregory[71] review methods available for the removal of solids from the effluent gases of fluidized reactors.

They recommend porous ceramic filters or a combination of cyclones, and bag filters, for pilot plant installations. The design of filters and cyclones is reviewed by Lapple[72] while Stairmand[73] presents the design and test results for a small laboratory cyclone.

(4) Materials of construction

It appears that any material which will withstand the combined effects of temperature and reaction atmosphere can be used to build the body of the reactor. Both Thompson[56] and Kepper[65] agree that abrasion of the walls of the reactor is practically negligible and that even soft refractory materials can be used quite successfully. It appears that the walls are protected from abrasion by a thin film of gas. On the other hand, according to Sittig[57], abrasion can be severe in gas exit lines and dust collection equipment. He recommends a silicon-killed carbon steel for the construction of these components since this material stands erosion better than stainless alloys. It is also common practice to build wear plates into cyclones to simplify maintenance due to erosion.

2:7 Conclusions and resulting proposals for experimental work

The survey of existing work on barium sulphate reduction indicated that this reaction would meet the needs of the project for a process uncomplicated by additional side reactions. It was also apparent that no quantitative data were available concerning the reduction process so it was necessary to obtain experimental values

of the equilibrium constant to check the thermodynamic data (see Appendix A) and confirm that reduction proceeded according to the equation,

$$BaSO_4 + 4H_2 = BaS + 4H_2O \quad \text{.....(3)}$$

before undertaking a kinetic study of the process. Since the thermodynamic calculations (see Appendix A) indicated that the H_2O/H_2 ratio, at equilibrium, was approximately 30, the dynamic method of determining equilibrium constants was the logical choice for this work; a value of 30 is outside the range of the static type of apparatus.

The next step in the experimental programme was to study the kinetics of the reduction, in a fixed bed, with the objective of obtaining data which would permit the rate of reaction in a fluidized bed to be predicted. A survey of the experimental techniques used to study reaction rates showed that the static methods for determining kinetic data are only suitable where comparative results are required, e.g. to demonstrate the relative effects of solid impurities on the reaction rate. A dynamic type of apparatus was, therefore, essential in this case.

On completion of the work with fixed beds it was proposed to measure rates of reaction in a fluidized bed and compare the predicted and measured rates to find out if the method of rate prediction was valid. Reviewing the published information which could be used to design a small fluidized reactor brought forth the

following important points.

(1) The minimum gas velocity needed to produce fluidization can be calculated, with fair accuracy, using the method developed by van Heerden, Nobel, and van Krevelen[49].

(2) There is little or no back mixing in the gas phase of a fluidized bed but considerable quantities of gas are by-passed through the bed in bubbles.

(3) There are no reliable mass transfer data which can be used where a rapid gas-solid reaction is proceeding in the bed.

However, in spite of some deficiencies in the published data, there appeared to be sufficient information available to enable a small fluidized reactor, suitable for reducing barium sulphate with hydrogen, to be designed and operated successfully.

The proposed experimental programme can, therefore, be set out as follows.

(1) Measurement of equilibrium constants for the reduction.

(2) Determination of kinetic data in fixed beds.

(3) Determination of kinetic data in fluidized beds.

3. DETERMINATION OF EQUILIBRIUM CONSTANTS

It will be recalled that the aim of this project was to compare the rate of reaction obtained in a fluidized reactor with the rate predicted using the kinetic data resulting from bench-scale work on a small fixed bed. The reduction of barium sulphate by hydrogen was chosen as the reaction most suitable for investigation on the basis of both theoretical and practical considerations (see Section 1), particularly, since a thermodynamic study (see Appendix A) revealed that reduction by hydrogen would probably proceed via the single reaction,

$$BaSO_4 + 4H_2 = BaS + 4H_2O \quad \ldots\ldots\ldots\ldots (3)$$

Unfortunately, it was found during the course of the thermodynamic analysis, that the specific heat equation and standard entropy for barium sulphide were not available. It was necessary, therefore, before proceeding to a kinetic study of the reduction process, to obtain experimental figures for the equilibrium constant in order to confirm the conclusions drawn from the thermodynamic investigation.

3:1 Experimental procedure

The literature survey indicated that a dynamic or flow type of apparatus, similar to that used by Kitchener and Ignatowicz[11] and others[13], was essential for this work.

3:1:1 Apparatus

A diagram of the set-up used is shown in Fig. 2. A mixture of hydrogen and steam of known composition was passed, at constant temperature, over a solid reaction mass composed of barium sulphate and barium sulphide, and the composition of the exit gas measured. Stepwise variations were made to the composition of the gas and the equilibrium composition obtained at the point where there was no change in composition between inlet and outlet gases.

As can be seen from Fig. 2, steam was generated in an electrically heated boiler and escaped continuously through a safety valve at the top of the unit. The steam pressure in the boiler, for a valve of given weight, remained at constant within quite small limits; the weight of the safety valve was varied by placing lead shot in it. In practice, fine control of the steam flow rate was achieved by altering the setting of the needle valve while large changes were produced by altering the weight of the safety valve. Tests showed that, for a given valve setting and steam pressure, the steam flow rate remained constant to $\pm$ 2%. Since the steam escaping through the safety valve was condensed and returned to the boiler it was only necessary to add sufficient distilled water to the boiler to make up for the water being delivered to the reactor. This generally amounted to about 1 cm^3 per hour.

The principal features of the hydrogen feeder are also shown in Fig. 2. Hydrogen was fed to the reactor by displacing it from

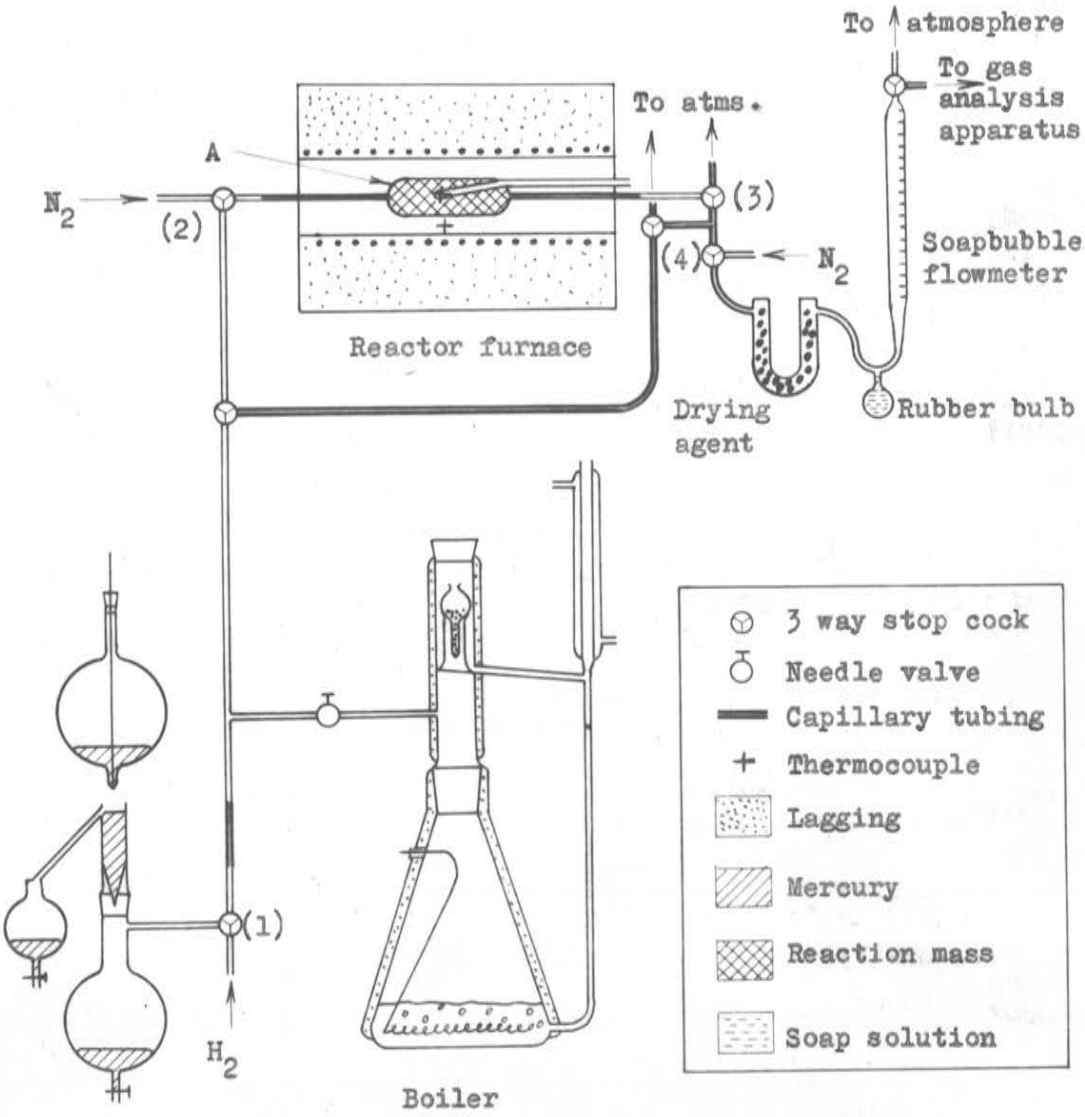

Fig. 2. Apparatus for equilibrium determinations : schematic diagram

the lower bulb of the feeder by a stream of mercury which flowed in at a constant rate. This mercury was supplied from a constant head tank which discharged into the lower bulb through a fixed jet at a rate of approximately 1 cm^3 per min. The rate at which mercury was fed from the upper reservoir to the constant head tank was controlled manually and was always set so that there was a steady overflow from the tank.

In operation, the bottom bulb of the feeder was filled with commercial hydrogen (99.7% pure), from a cylinder fitted with a reducing valve, by downward displacement of the air through the bottom tap. This tap was then closed and the three way tap (1) set to allow hydrogen to pass from the feeder into the reactor. Mercury was immediately allowed to enter from the constant head tank and a stopclock simultaneously started. At the end of a run the mercury in the bottom bulb was run out into a measuring vessel to determine its volume and from this figure, and from the stopclock reading, the average mercury rate was calculated. It was assumed that the average mercury rate and the average hydrogen rate were identical; a number of tests showed that the rate at which hydrogen entered the apparatus never diverged more than $\pm$ 3% from the average mercury rate.

It was found that, if clean mercury was used, the major factor causing variation of the mercury rate was variation of the ambient temperature during a run since the viscosity of mercury is quite

sensitive to changes in temperature. However, the difficulties of providing a constant temperature jacket for this part of the apparatus were not justified by the small gain in accuracy.

Some trouble was also encountered in the early stages of operation due to surging of the pressure in the gas space of the hydrogen feeder. The pressure changes were very small but the consequent variation in hydrogen rate was quite considerable. This difficulty was overcome by placing a length of fine capillary in the hydrogen outlet line; it was found that the small added resistance to flow made the system much more stable.

All lines carrying steam were wound with heating elements to prevent condensation. Some difficulty was encountered with stop cock lubricants under these high temperature conditions but Dow Corning silicone high vacuum grease gave satisfactory results.

The fused silica reactor bulb (A) was heated by a nichrome wound furnace controlled by a Kent Multelec on-off temperature controller using a bare chromel-alumel thermocouple, placed close to the furnace winding, as the control element. It was found that the temperature of the reaction mass could be held constant to within $\pm 2^{\circ}C$ over long periods. Silica capillary tubes having a bore of 2 mm were used to pass gas through the temperature gradients encountered entering and leaving the reactor bulb; calculations using the equations developed by Gillespie[8] and Whalley[9] showed that thermal diffusion effects for such tubes would be negligible if the gas flow

rate was greater than 10 cm^3 per min. The silica capillaries were joined to the rest of the apparatus by graded Pyrex/silica seals.

The drying tube, containing silica gel, was fitted to the rest of the apparatus by a standard ground glass joint so that it could be easily detached for weighing. There was sometimes a little hydrogen sulphide in the exit gases from the reactor so it was usual to place a pellet of potassium hydroxide at the entrance to the drying tube to absorb the hydrogen sulphide as potassium sulphide. This was necessary because any unabsorbed hydrogen sulphide in the exit gas would be analysed as hydrogen in the gas analysis apparatus. The weight changes usually encountered were of the order of 0.5g and it was considered that the weight of water collected could be determined with an accuracy of $\pm$ 0.1%. This meant that the errors in weighing constituted a negligible part of the total error encountered in measuring the ratio $(H_2O/H_2)_{exit}$.

The soap bubble flowmeter (see fig. 2) was constructed after the description given by Barr[74] who states that it should provide a very accurate means of measuring small gas flow rates. It was, however, found impossible to obtain an accurate measure of the hydrogen rate leaving the reactor with this type of flowmeter because the volume of gas behind the bubbles was very sensitive to changes in the temperature of the drying tube; this varied widely as the steam condensed. Since it was found impractical to jacket the drying tube to eliminate these

errors the soap bubble flowmeter was only used as a storage space for the hydrogen before it was transferred to the gas analysis apparatus. It also provided a rough check on the results given by the gas analyses.

Hydrogen determinations were carried out in the well known "Bone and Newitt" type of gas analysis apparatus using a constant pressure technique. Copper oxide needles heated to 400°C were used to oxidise the hydrogen. It was considered that a hydrogen volume of the order of 20 cm^3 could be measured with an accuracy exceeding $\pm 2\%$. This was the major error encountered in measuring the ratio $(H_2O/H_2)_{exit}$.

The temperature at the centre of the reaction mass was measured by a standardized chromel-alumel thermocouple placed inside a silica sheath sealed into the reactor bulb (A) (see Fig. 2). A Cambridge Portable Potentiometer was used to measure the E.M.F. generated by the thermocouple.

3:1:2 Experimental technique

The usual practice was to set the boiler pressure to give a steam rate of the required order and then put the hydrogen feeder into operation. As soon as the boiler pressure reached its set value, stop cocks (2) and (3) were turned so that steam, and subsequently, the steam hydrogen mixture passed through the reactor to atmosphere. The drying tube was then weighed and placed in position and all the apparatus beyond valve (4) flushed out with nitrogen. The nitrogen used for this operation and all other cases where an inert gas was

required was of commercial quality.

After the gases from the reactor had been passing to the atmosphere for half an hour and conditions had reached a steady state, a number of soap bubbles was formed at the base of the flowmeter; stop cocks (3) and (4) were then manipulated so that the reactor exit gases passed to the analysis train. A stopclock was started simultaneously. When the reactor gas had been passing through the analysis train for twenty minutes, valve (3) was turned to atmosphere and valve (4) manipulated so that the contents of the analysis train were swept over to the gas analysis apparatus by about 200 cm^3 of nitrogen. The drying tube was then detached and weighed to determine the quantity of water condensed. The quantity of hydrogen collected was measured in the gas analysis apparatus. It was then possible to calculate the ratio $(H_2O/H_2)_{exit}$ from these figures.

The rate at which hydrogen entered the reactor was known from the rate at which mercury was admitted to the displacement vessel and it was assumed*, for the purposes of calculation, that there was no change in the quantities of steam entering and leaving the reactor; hence it was possible to calculate $(H_2O/H_2)_{inlet}$.

3:1:3 Treatment of results

The equilibrium value of the steam/hydrogen ratio at any temperature was determined by stepwise increases in the ratio $(H_2O/H_2)_{inlet}$ until the equilibrium value was exceeded. When the inlet ratio was

* This was quite justified since the change in the hydrogen rate never exceeded 0.1 cm^3 per min. which was equivalent to a change of 0.3% in the steam rate.

equal to the equilibrium ratio there was no change between inlet and exit values; for all other values there was a change in the direction of equilibrium. Therefore, a plot of the percentage change in the H_2O/H_2 ratio, from inlet to exit, against the exit value gave $(H_2O/H_2)_{equilibrium}$ as the intercept on the $(H_2O/H_2)_{exit}$ axis. Such a plot is shown in Fig. 3. For temperatures where the reaction rate was sufficiently rapid, e.g. 1000°C, the value of the ratio $(H_2O/H_2)_{equilibrium}$ could often be determined by inspection of the experimental data, eliminating the necessity to plot the points and draw a curve.

3:1:4 Preparation of samples

(1) Series A samples

The raw material for these tests was produced by sintering precipitated barium sulphate (prepared for use in medical radiography) at approximately 1000°C. The sinter was then crushed and screened to give a product within the size range +35-20# (Tyler). The barium sulphate had the analysis,

Fe	2%
Acid sol. barium	0.06%
Sulphide	nil
Sulphite and thiosulphite	trace
Heavy metals	nil

This material was chosen because it had a composition similar to that of the mineral barytes which was to be used in the work on

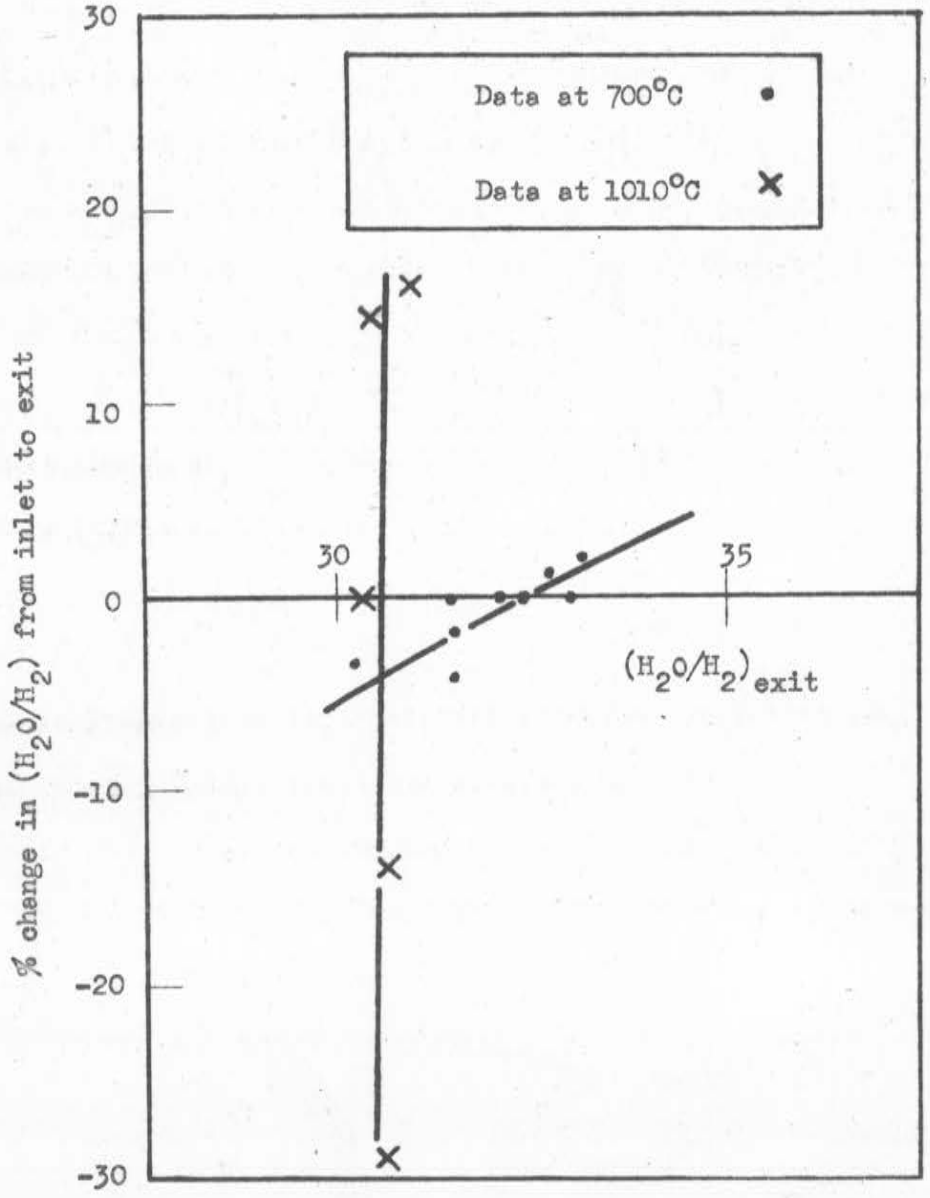

Fig. 3. Experimental data for Sample C10

reaction rates. It was felt desirable that both parts of the investigation should have something of the same background.

Series A samples were produced by reducing the sized sinter with hydrogen at various temperatures.

(2) Series B samples

Material consisting mainly of barium sulphide was produced by acting upon anhydrous barium hydroxide - obtained by heating A.R. $Ba(OH)_2.8H_2O$ crystals to 300°C under reduced pressure - with hydrogen sulphide gas at elevated temperatures.

Series B samples were made up by mixing equal weights of sulphide/hydroxide material and sized and sintered barium sulphate of Series A.

(3) Series C samples

Precipitated barium sulphate having a low iron content (Fe = 0.001%) was produced by neutralizing A.R. barium hydroxide with A.R. sulphuric acid. This product was sintered and sized in the way described in (1), above. Series C samples were then produced by reducing this sized sinter with hydrogen.

(4) Series D samples

Barium sulphide/hydroxide material produced for Series B was mixed with an equal weight of the sized and sintered barium sulphate of Series C to give samples which were designated as Series D.

3:2 Results

The results obtained with Series A and B samples showed a distressing tendency to vary from sample to sample, for temperatures below 900°C. Experimental values of the equilibrium constant have, therefore, not been reported for these samples. It was found that elemental sulphur was evolved from Series A and B samples on heating in a stream of nitrogen at temperatures above 850°C. Series C and D samples did not exhibit this phenomenon and also yielded consistent values for the equilibrium constant. A comparison of the results for Series A and Series C samples showed that the values of $(H_2O/H_2)_{equilibrium}$ obtained for the former were too high.

It was ascertained that evolution of sulphur did not result in any change in the percentage of acid soluble barium in the reaction mass. Series A samples reduced at 600°C lost sulphur stoicheiometrically equivalent to 10% of the barium in the barium sulphide layer during reduction. On heating at 900°C, a further 3-5% of the sulphur equivalent was lost. The assay methods used for this work were based on those described by Terres and Bruckner[75].

3:2:1 Xray analyses

A number of samples from Series A, B, and C were submitted for examination* by Xray analysis. The Xray patterns revealed that, in the case of Series A and C samples, reduction by hydrogen produced a mixture of barium sulphate and sulphide. Neither barium sulphite

* By courtesy of Dr. K. Norrish, Soils Division, C.S.I.R.O.

nor barium oxide were detected in the reduction product. Examination of the Xray diffraction patterns also revealed that neither the barium sulphate nor the barium sulphide were participating in the formation of solid solutions. The Xray patterns obtained from the barium sulphide/hydroxide material used to make up Series B samples showed that the specimens examined contained barium sulphide together with a quantity of some other compound for which no tabulated Xray pattern was available. This was probably barium hydroxy hydrosulphide, Ba(SH)(OH).

3:2:2 Equilibrium data

Tabulated values of the $(H_2O/H_2)_{equilibrium}$ ratio are presented in Appendix B together with details of the gas flowrates used, reduction temperatures, and compositions of the reaction masses. For the reaction,

$$BaSO_4 + 4H_2 = BaS + 4H_2O \quad \ldots\ldots\ldots\ldots (3)$$

$K_p = (H_2O/H_2)^4$. The results of the equilibrium determinations are, therefore, shown in Fig. 4 as a plot of log K_p against the reciprocal of the absolute temperature. Examination of Fig. 3, page 56, shows that the plot of percentage change, from inlet to outlet, against $(H_2O/H_2)_{exit}$ crosses the axis at a very acute angle at low temperatures and consequently the accuracy of equilibrium values determined below 800°C is difficult to assess. The limited number of tests carried out at 700°C has been summarised on Fig. 4 and an approximate indication given of the likely error involved. The highest temperature

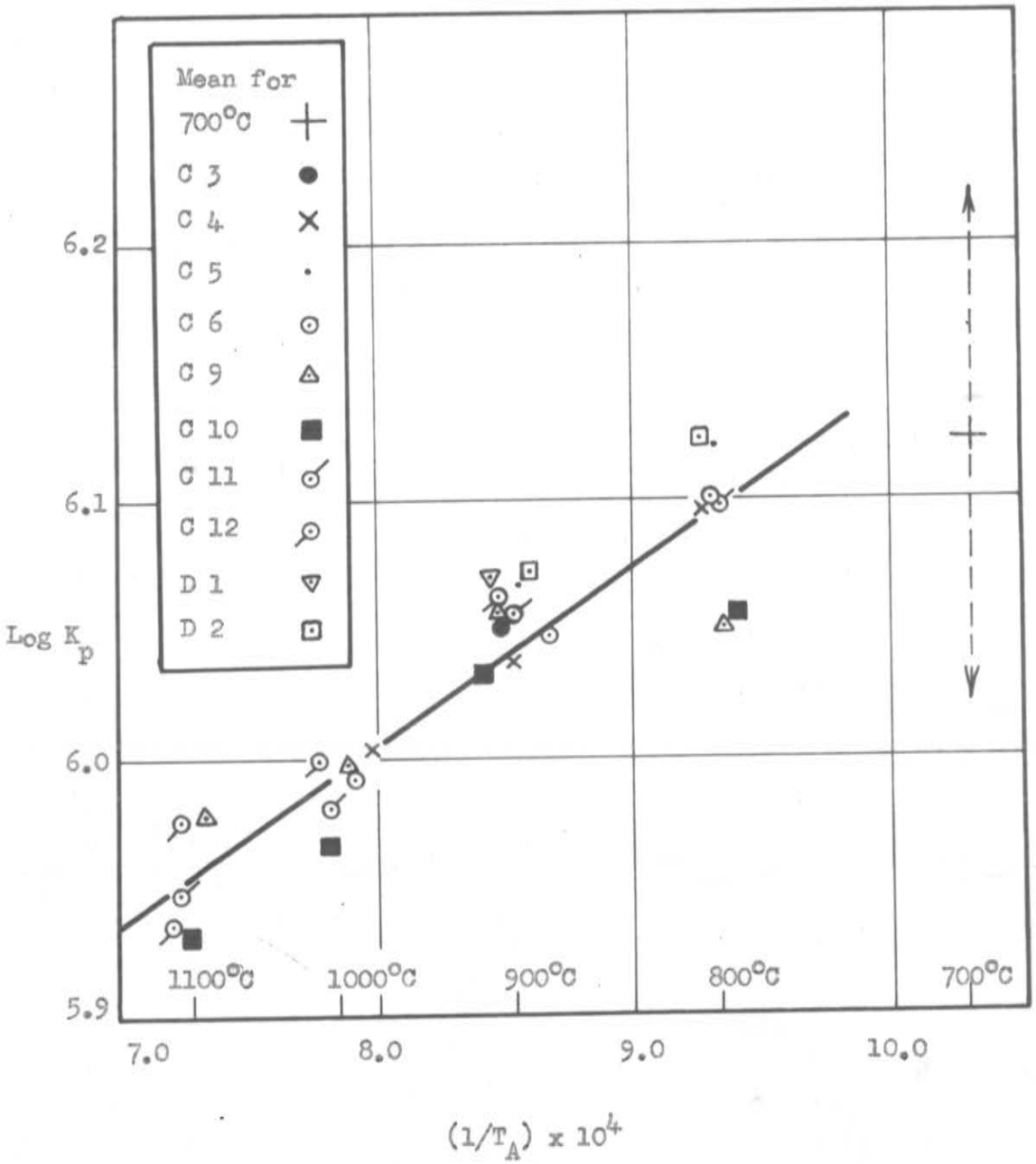

Fig. 4. Plot of experimental equilibrium data

which could be used was limited by the rate at which the barium sulphide in the reaction mass attacked the silica of the reactor bulb. Since it was felt that a reaction of this kind might possibly affect the measurements made, no data were obtained for temperatures above 1100°C.

3:3 Discussion of results

The discussion has been presented in three parts; hypotheses are developed to explain the results obtained with Series A and B samples, then the validity of the results from Series C and D samples is discussed and, finally, the experimental equilibrium constants are used to calculate the basic thermodynamic data for barium sulphide.

3:3:1 Series A and B samples

Elemental sulphur was evolved from these samples at a temperature between 800°C and 900°C and it is significant that, if a sample was brought quickly to 900°C, the rate of sulphur evolution was quite rapid for a short time and then quickly died away. This behaviour strongly suggested that some compound was decomposing and that one of the products of decomposition was sulphur vapour. Comparison of the results for these samples with the later work on iron free material (Series C and D) suggested that the evolution of sulphur and the erratic values of the equilibrium constants obtained might be due to the small quantity of iron (2%) present. Since the loss of sulphur did not produce any change in the percentage of acid soluble barium

in the reaction mass it seemed that sulphur was evolved from the barium sulphide phase and not from the barium sulphate.

There appeared to be two hypotheses which would explain the results.

(1) It seemed reasonable to assume that the interaction of barium sulphide and iron, or some iron compound, to form a barium iron complex would release sulphur which could react with the surrounding barium sulphide to produce polysulphides. Such polysulphides would affect the equilibrium measurements since it might be expected that reactions of the type,

$$BaS_3 + 2H_2 = BaS + 2H_2S \quad \text{.....(8)}$$

would readily occur and possibly lead to a high value of the ratio $(H_2O/H_2)_{equilibrium}$. Evolution of sulphur could be explained by the breakdown, between 800°C and 900°C, of the polysulphide material to give barium sulphide and elemental sulphur.

Supporting this hypothesis, it should be noted that Welles[2] reports the presence of what he assumes to be polysulphides in some products which he formed by reducing barium sulphate with hydrogen. However, Welles does not state what impurities were present in the precipitated barium sulphate which he used. Further, there was much more hydrogen sulphide present in the exit gases for Series A and B samples than for the corresponding Series C and D samples where hydrogen sulphide could be rarely detected on passing the exit gases from the reactor over a filter paper impregnated with lead acetate.

(2) It might be postulated that the high values of $(H_2O/H_2)_{equilibrium}$ obtained with Series A and B samples were due to the presence of a compound containing barium, iron, and sulphur which reacted with hydrogen to produce hydrogen sulphide; this compound losing sulphur at temperature above 850°C. This supposition is supported by the fact that the iron complex in samples reduced at 600°C was easily broken up by dilute hydrochloric acid but, after evolution of sulphur had occurred, it was necessary to digest the material with boiling acid for some time before all the iron came into solution.

Although the results obtained with Series A and B samples were inconsistent, and high, the values of $(H_2O/H_2)_{equilibrium}$ obtained were of the same order as those given by Series C and D samples and, together with the results of the Xray analyses, confirmed that, even where the barium sulphate contained small quantities of iron and silica, the reduction could be represented by equation (3). It was considered, therefore, that further investigation of the phenomenon of sulphur evolution was not justified at this stage of the investigation.

3:3:2 Series C and D samples

Inspection of Fig. 4, page 60, and Table I shows that the percentage of barium sulphide in the reaction mass had no influence on the experimental results, thus confirming the absence of solid solutions. As Welles[2] found that samples of barium sulphate which were reduced

at high temperatures lost less sulphur than those reduced at lower temperatures, Series C samples were reduced at different temperatures (see Table I) to find out if the quantity of sulphur lost from the sample through the reaction,

$$BaS + 2H_2O = Ba(OH)_2 + H_2S \quad \ldots\ldots\ldots (9)$$

had any effect on the equilibrium constant. The barium sulphide phase of Series C samples reduced at 900°C contained sulphur equivalent to 98% of the barium present while samples reduced at 1100°C only lost a quantity of sulphur corresponding to 0.5% of the stoichiometric equivalent of the barium present. Examination of Fig. 4, page 60, indicates that the sulphur loss had no effect. The results obtained

TABLE I

Temperature of reduction and composition of reaction masses

Sample	Temperature of reduction (°C)	$BaSO_4$ reduced (%)
C3	900	55
C4	900	40
C5	900	3
C6	900	65
C9	1000	30
C10	1000	5
C11	1100	15
C12	1100	21

with Series D samples, which contained considerable quantities of hydroxide material, are also consistent with the body of the work. The sulphide/hydroxide material used to make up Sample D1 contained 12% of sulphur by weight or approximately 64% of the stoichiometric equivalent of the barium present. In the case of Sample D2 the barium sulphide/hydroxide material contained a quantity of sulphur equivalent to 97% of the barium present. Hence it appears that a deficiency of sulphur in the sulphide portion of the reaction mass has little effect on the equilibrium.

It can be seen from Table II and Fig. 4, page 60, that the measurements carried out with a steam-hydrogen flow rate of 35 cm^3 per min are consistent with those carried out at 70 cm^3 per min. This, in turn, indicates that there was no appreciable loss of hydrogen from the apparatus by diffusion, since the rate of diffusion would not be affected by the flow rate.

TABLE II

Gas flow rates used in the determination of equilibrium constants

Sample number	C3	C4	C5	C6	C9	C10	C11	C12	D1	D2
Gas flow rate (cm^3/min)	35	35	35	35	70	35	35	70	35	35

The straight line correlating the experimental points in Fig. 4, page 60, was selected by the method of least squares, the points being

weighted according to the experimental error likely to be present. It was found that the mean deviation from this line, which corresponds to the equation*,

$$\log K_p = 5.447 + (697.5 \pm 52.5)/T \quad \ldots\ldots(a)$$

was approximately equal to the estimated experimental errors in the measurements; the maximum deviation at 800°C is 9% and at 1100°C is 4%; the mean deviation at 800°C is 5% and at 1100°C is 2.8%.

3:3:3 Thermodynamic calculations

Calculations of the basic thermodynamic data for barium sulphide were made to check the validity of the equilibrium constants obtained. At any given temperature $\ln K_p = \Delta S/R - \Delta H/RT$. Assuming that ΔH and ΔS remained constant over the temperature interval 1073°K to 1373°K, the terms of this equation could be identified with the corresponding terms in equation (a) to give,

$$\Delta H_{1073-1373} = 1.61 \text{ k cal/mol., and}$$

$$\Delta S_{1073-1373} = 25.1 \text{ cal/mol., } ^\circ K$$

It was further assumed that $\Delta H_{1073-1373} = \Delta H_{298}$ and $\Delta S_{1073-1373} = \Delta S_{298}$ and, combining these results with the tabulated[76)77)] thermodynamic properties of barium sulphate, hydrogen, and water, it was found that, for barium sulphide, $\Delta H_{298} = -117.4$ k cal/mol. and $S_{298} = 1.03$ cal/mol., °K. This calculated value of the heat of formation was 11% higher than the tabulated value[76)], but the value calculated for the entropy of barium sulphide was only one twentieth of the value estimated by Kireev[78)]. It appeared, therefore, that

*This statistical correlation was carried out by Dr. A.T. James of the Division of Mathematical Statistics, C.S.I.R.O.

ΔS for reaction (3) varied with temperature, although it was possible to correlate the experimental results satisfactorily by a straight line over the narrow temperature range investigated.

Published equations[79] for the variation of the specific heats of the components of reaction (3) with temperature were used to calculate $\ln K_p$ in terms of T (see Appendix A). This treatment yielded the equation,

$$R\ln K_p = -\Delta H^\circ/T - 21.00 \ln T + 5.46 \times 10^{-3} T + 4.13 \times 10^{5} T^{-2} - I \quad \ldots(b)$$

where ΔH° and I are integration constants. Equation (b) may be rewritten as,

$$\Sigma = \Delta H^\circ/T + I = -R \ln K_p - 21.00 \ln T + 5.46\times10^{-3} T + 4.13\times10^{5} T^{-2} \quad \ldots(c)$$

It follows that a plot of Σ against the reciprocal of the absolute temperature should yield a straight line. Fig. 5 shows such a plot using K_p values read from Fig. 4, page 60. The straight line correlating the plot in Fig. 5 has the equation,

$$\Sigma = 15100/T - 182.4 \quad \ldots\ldots\ldots\ldots\ldots\ldots\ldots\ldots\ldots\ldots(d)$$

and hence $\Delta H^\circ = 15100$ and $I = -182.4$. By substituting these values in equation (b) the following thermodynamic data have been calculated,

$$\Delta G_{298} = -5.48 \text{ k cal/mol.}$$

$$\Delta H_{298} = 6.55 \text{ k cal/mol.}$$

$$\Delta S_{298} = 40.4 \text{ cal/mol., } ^\circ K.$$

Using tabulated[76)77)] thermodynamic data for barium sulphate, hydrogen, and water it was calculated that, for barium sulphide

$$\Delta G_{298} = -110.4 \text{ k cal/mol.}$$

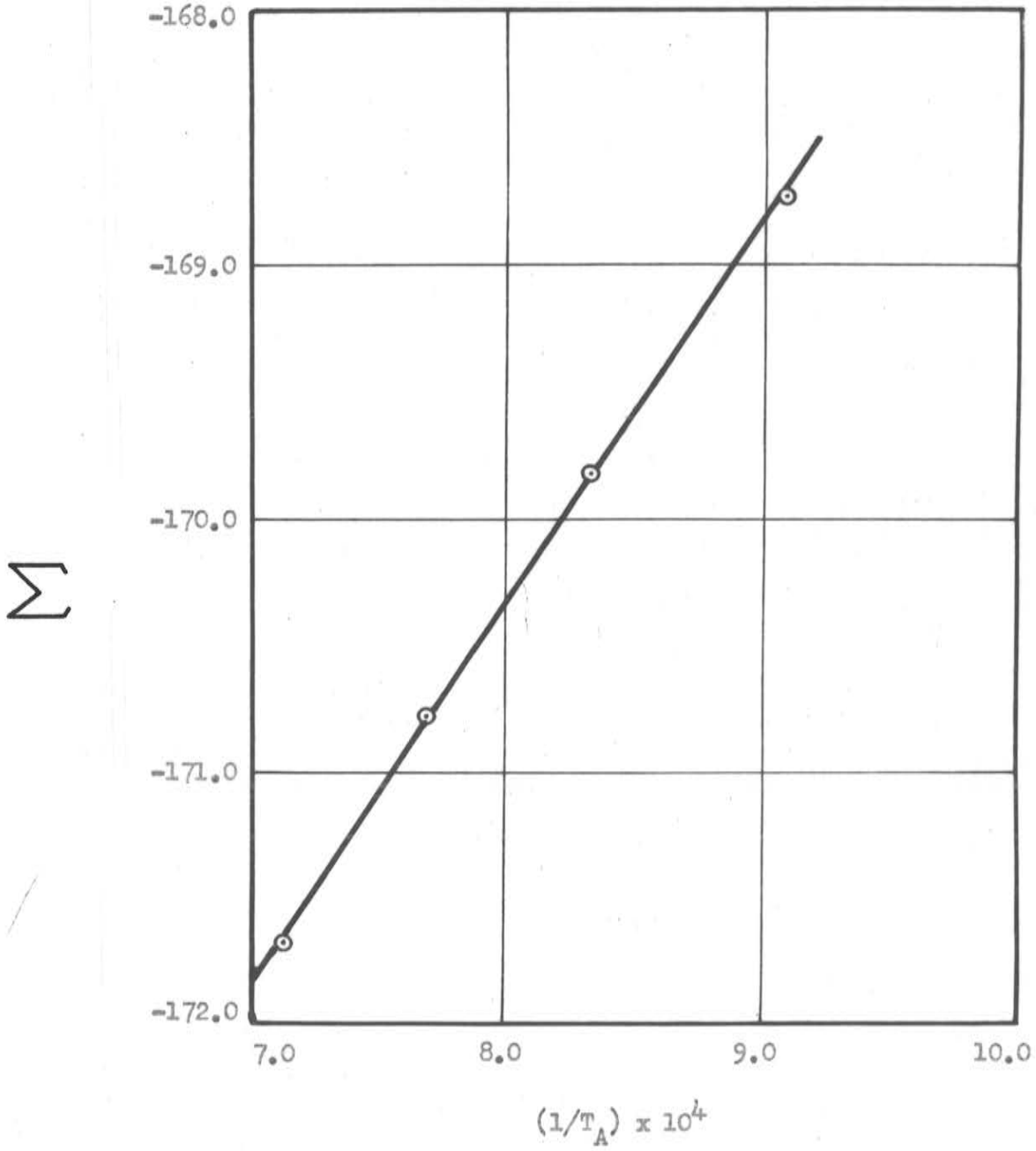

Fig. 5. Sigma plot prepared from the correlation in Fig. 4, page 60

$$\Delta H_{298} = -112.4 \text{ k cal/mol.}$$

$$S_{298} = 16.3 \text{ cal/mol., } ^{\circ}K.$$

These calculated figures compared reasonably well with the published data for barium sulphide, viz.,

$$\Delta G_{298} = -103.1 \text{ k cal/mol.}^{76)}$$

$$\Delta H_{298} = -106.0 \text{ k cal/mol.}^{76)}$$

$$S_{298} = 20.8 \pm 1.0 \text{ cal/mol., } ^{\circ}K^{78)}.$$

It is possible that an accurate expression for the variation of the specific heat of barium sulphide with temperature - assumed to be identical with that for calcium sulphide (see Appendix A) - would give even closer agreement between calculated and published values. However, the calculations did show that the experimental results were quite sound.

3:4 Conclusions

(1) The reduction process, even for impure barium sulphate, may be represented by the equation,

$$BaSO_4 + 4H_2 = BaS + 4H_2O \quad \ldots\ldots\ldots\ldots (3).$$

(2) Neither barium sulphite nor barium hydroxide are formed to any great extent.

(3) Equilibrium constants in the temperature range 800°C to 1100°C are satisfactorily correlated by the equation,

$$\log K_p = 5.447 + 697.5/T.$$

4. DETERMINATION OF REACTION RATES - FIXED BEDS

Since the aim of this project was to compare the rate at which barium sulphate is reduced by hydrogen in a fluidized bed with the rate predicted from bench scale experiments on a small fixed bed it was not intended that the kinetic investigation should be exhaustive. The objective of this part of the project was simply to gain sufficient information about the reduction process to enable a rate of reaction to be predicted for a fluidized bed.

The literature survey revealed that the only previous work on the reduction of barium sulphate by hydrogen was published by Welles[2] who obtained comparative rates for each of the alternative reducing gases, hydrogen and carbon monoxide. Welles reduced powdered material held in porcelain boats and compared the times required for complete reduction; he gave no information on the variation of the rate as the reduction proceeded and, in any case, his results applied only to the system - powdered material in a boat - which he used.

Since virtually no information on reaction rates was available it was necessary to carry out a preliminary or "sighting programme",

(1) to develop an experimental technique which would yield reproducible results,

(2) to determine the magnitude of the reaction rate and the increase in the rate as the reduction temperature was increased, and

(3) to determine the relative importance of gas diffusion, diffusion through the solid product layer, and chemical reaction rate in determining the measured rate.

This part of the work is set out in Sections 4:1 and 4:2. When this preliminary phase had been completed it was necessary to determine the relative importance of the variables (particle size, solid composition, etc.) which could affect the rate of reaction in order to provide a satisfactory basis for correlating the experimental results. This final phase of the bench scale work, together with the correlations developed, is set out in Sections 4:3 and 4:4. The conclusions are contained in Section 4:5.

4:1 Experimental procedure (Preliminary stage)

The results of the equilibrium determinations for the system $BaSO_4/BaS/H_2/H_2O$ (see Section 3:4) showed that the reduction of barium sulphate by hydrogen follows the equation,

$$BaSO_4 + 4H_2 = BaS + 4H_2O \quad \ldots\ldots\ldots(3)$$

thus the progress of the reduction could be followed, either by measuring the quantity of hydrogen consumed, or by measuring the quantities of barium sulphide and water produced.

Two types of reactors are in general use for studying reactions between gases and solids, the differential reactor and the integral reactor. In a differential reactor, where the bed is relatively thin, changes between inlet and outlet compositions are small enough

to enable the bed conditions to be taken as the arithmetic mean of inlet and outlet conditions. In an integral reactor, on the other hand, a thick bed is used, conditions vary considerably from inlet to outlet, and interpretation of the results obtained is difficult unless the mechanism of the reaction is known so that the necessary integrations may be performed. A differential type of reactor was chosen for this work since the mechanism of reaction was not known. The major disadvantage with the differential reactor is the extreme analytical precision which is required to establish a reliable rate from the small quantities of product formed. However, it is possible to make accurate determinations of small quantities of water vapour with the efficient dessicating agents available so this was not a serious drawback. A differential type of reactor was, therefore, eminently suitable for studying the rate of reduction of barytes by hydrogen.

It was also possible to follow the course of the reduction by reducing samples for varying times, stopping the reaction, and assaying to determine the quantity of barium sulphide produced. This method was very laborious since a number of samples had to be processed to obtain the same information which could be gained from a single sample by absorbing and weighing the water in the gases leaving the reactor. For this reason, the assaying method was only used in cases where it was not feasible to follow the rate of reaction by weighing the water produced.

4:1:1 Apparatus

A line diagram of the apparatus is shown in Fig. 6 and a photograph showing the general layout is presented in Fig. 7. The furnace by-pass tube shown in dashed outline in Fig. 6 was added during the later part of the investigation (see Section 4:3:1).

The reactor furnace consisted of a $1\frac{3}{4}$ inch diameter translucent silica tube wound with 18 gauge Nichrome V wire and insulated with kieselguhr. The power input to this furnace, which had a capacity of 1500 watts, was controlled by a photo-cell relay actuated by a thermocouple placed close to the wall of the furnace. The details and circuit diagram for this controller are given in Appendix H.

Before entering the reactor proper the cold hydrogen was preheated by passing through a 3 inch length of $1\frac{1}{4}$ inch diameter silica tube, packed with silica chips, which was wound on the outside with 22 gauge Nichrome V wire. The input to this winding, which had a capacity of about 500 watts, was manually controlled by a Variac autotransformer. The reactor itself consisted of a piece of translucent silica tube having an internal diameter of 1 inch into which a silica thermocouple sheath was sealed so that temperature measurements could be obtained at the centre of the barytes bed. A packing of +14-10# Mullite chips was used to hold the barytes bed in position in the reactor. The thickness of the barytes bed varied with the particle size but was generally less than two particle diameters.

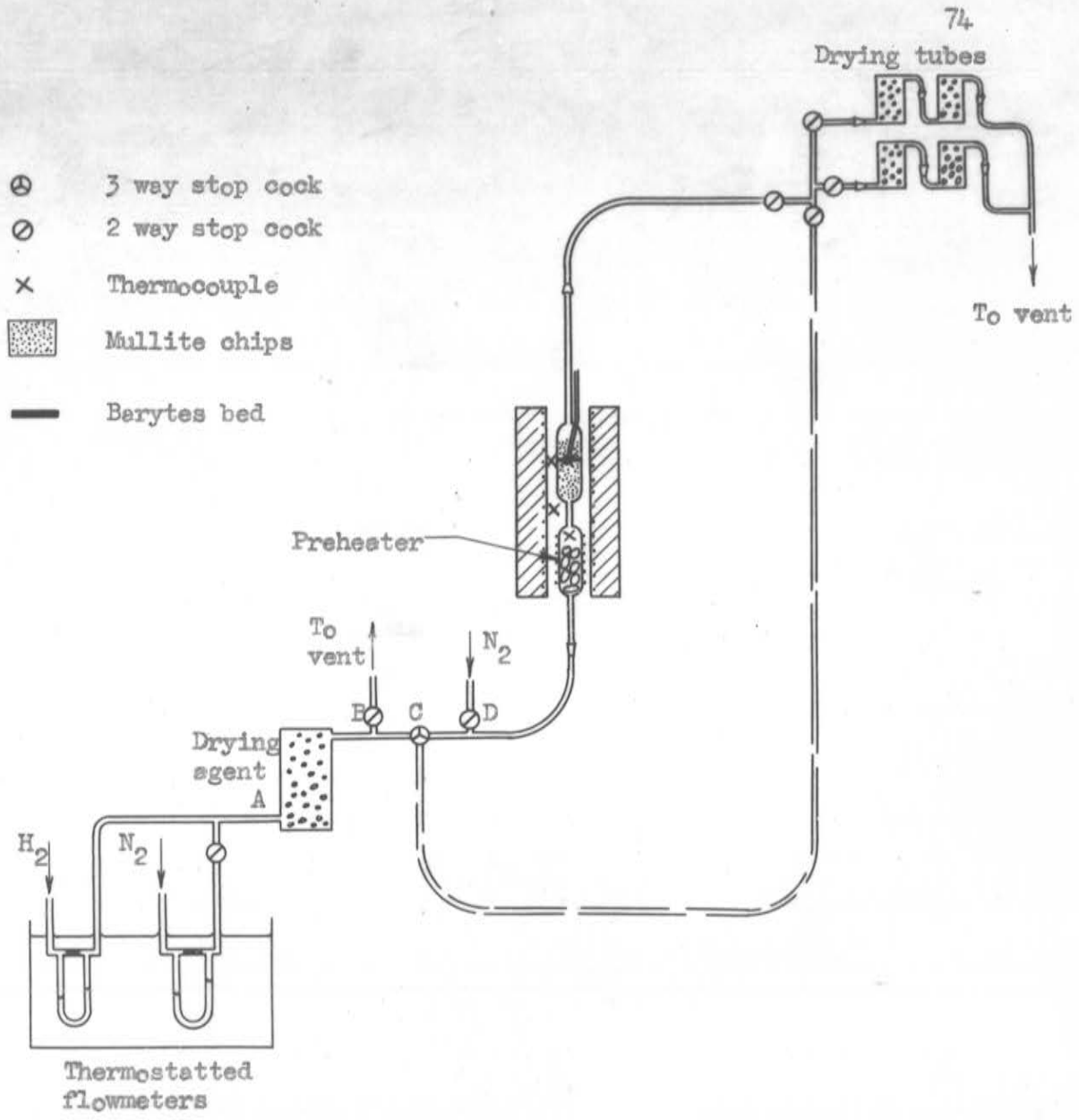

Fig. 6. Line diagram of reaction rate apparatus

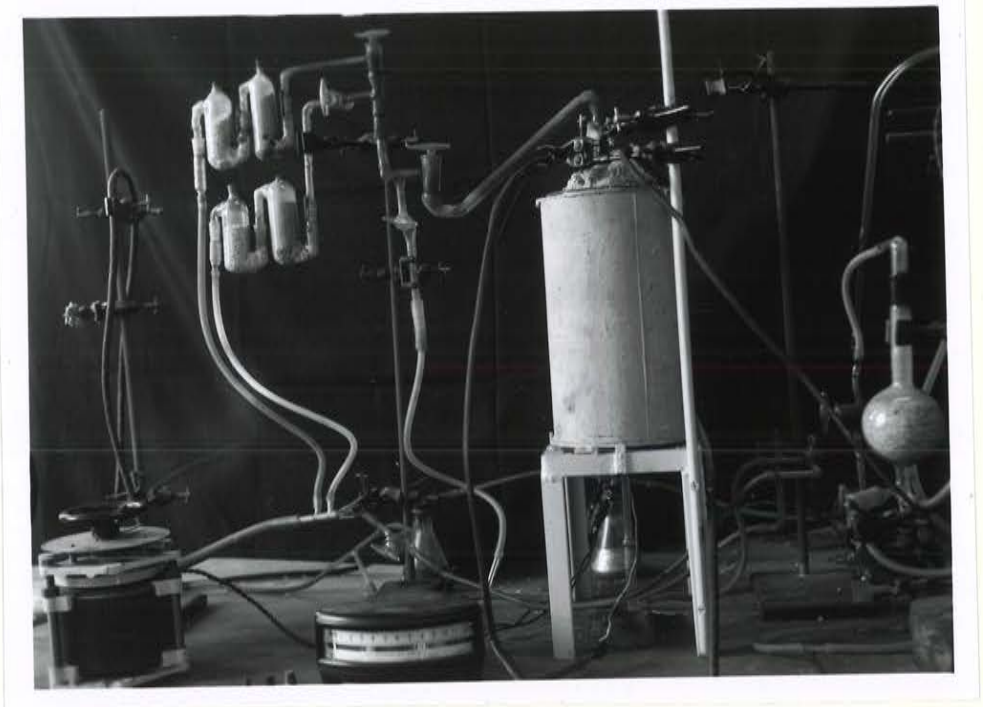

Fig. 7. Photograph of reaction rate apparatus

The temperature at the centre of the barytes bed was measured by a chromel-alumel thermocouple which had previously been standardized against a substandard Pt/Pt-Rh couple. The E.M.F. generated by the chromel-alumel couple was measured by a Cambridge Portable Potentiometer and the voltage measurements converted to temperatures by reference to the calibration curve. Since it was found that the temperature difference between the centre and outside of the bed rarely exceeded 5°C it was estimated that the maximum error encountered, at any time,

in taking the reading of the centre thermocouple as the temperature of the bed was less than $\pm 7^{\circ}C$.

The arrangement of the drying tubes may be observed in Figs. 6 and 7. Indicating Drierite (anhydrous calcium sulphate) was selected as the desiccant because it has a high efficiency and was readily available in a granular form. Calculations using the method set out in Perry[80] showed that more than 99% of the water entering a bed of Drierite 6 inches deep and 1 inch in diameter should be removed. As can be seen from Fig. 7, two beds each 3 inches deep were used in series. Tests using a third bed showed that no water escaped from the second bed so long as the indicator in that bed did not show any change from blue to pink. The drying tubes were connected to the rest of the apparatus by ground joints to facilitate removal for weighing.

Gas flow rates were measured by orifice meters of the type produced by Quickfit and Quartz Pty. Ltd.. Calibration was carried out using a wet test meter to measure the quantity of gas passed in a given time. The flowmeters were placed in a constant temperature water bath to prevent changes in calibration due to variations in ambient temperatures.

It was found that the hot gases leaving the reactor could be cooled sufficiently to be passed into the drying tubes by passage through about 18 inches of $\frac{1}{2}$ inch diameter glasstube which was left bare. The silica reactor unit was joined to the rest of the

apparatus by a combination of standard ground glass and ground silica joints. No lubricant was used on these joints but there appeared to be little or no leakage from the system at these points.

4:1:2 Experimental technique

The reactor furnace (see Fig. 7, page 74) was brought up to the control temperature with a slow stream of nitrogen passing through the reactor. The two sets of drying tubes were then weighed and attached to the apparatus and the preheating winding switched on. At this stage hydrogen was passing through stop cock B (see Fig. 6) to the vent but when the preheater temperature had reached a predetermined level the valves B and D were turned to pass the hydrogen through the reactor. A stopclock was started simultaneously and the drying tube sets were alternately removed and weighed at fixed intervals; one set being weighed while the other set was on stream. The voltage setting on the Variac transformer controlling the preheating element and the temperature level in the preheater at which hydrogen flow should be commenced were found by carrying out runs with the reactor packed only with Mullite chips.

A hydrogen flow rate of 13 litres per min N.T.P. was chosen for all of the preliminary work since this gave a value of Reynolds Number for the barytes bed of approximately 5. This was the lowest value of Reynolds Number for which accurate correlations[81] of mass transfer data were available.

4:1:3 Raw Materials

The material used for all the reaction rate work was a selected sample of mineral barytes obtained from South Australian Barytes Ltd.. This barytes had the following average analysis,

$BaSO_4$	97.5%
SiO_2	2.1%
Fe_2O_3*	1.5%
H_2O and organic matter	0.08%

The method of analysis used is set out in detail in Scott and Furman[82]. It was found that the barytes showed a marked tendency to powder and shatter when heated above about 200°C and consequently it was necessary to heat the material to approximately 600°C before crushing and screening to obtain a sample which would be quite stable to subsequent heating. The crushed material was screened to +10-8# (Tyler), giving the sample upon which rate measurements were carried out during the preliminary phase of the work.

The gases used, hydrogen and nitrogen, were of commercial quality supplied in cylinders; since hydrogen analyses gave the oxygen content as less than 0.1%, it was felt that the added refinement of purification was not justified in the exploratory stage of the investigation.

* This includes all Al_2O_3 and MnO, if any, in the sample.

4:1:4 Treatment of results

The approach adopted, viz. absorption of the water produced by the reaction, yielded a series of weight increments for known times. The results for a typical run are shown in Table III. These weights of water were successively added to give the total weight of water produced at a given time and then converted to the corresponding weight of barium sulphate reduced, in accordance with equation (3), to give the percentage reduction vs time curve.

TABLE III

Log sheet for a typical rate determination

Time (min)	Tube set	Weight (g)	Weight increment (g)	Temp. (°C)	Remarks
0	A	246.979		998	Run No. E35
	B	226.956	0.069		+8-6# crushed
1	A	247.048		997	barytes.
			0.441		
3	B	227.397		993	H_2 flow
			0.530		
5	A	247.578		995	rate of 13
			0.423		
7	B	227.820		993	litre/min
			0.343		
9	A	247.921		992	N.T.P..
			0.282		
11	B	228.102		993	
			0.308		
14	A	248.229		994	

In order to save unnecessary calculation all rates have been expressed as g of H_2O per g of barytes per minute.

4:2 Discussion of results (Preliminary stage)

The results of this part of the work (runs No. E1 to E30) are presented in Figs. 8, 9, and 10. These results were obtained at a constant mass velocity of 13 litres per min N.T.P..

It can be seen by examining Fig. 8 that the rate of reaction at 800°C is extremely slow and it seemed unlikely that any process operating on the fluidizing principle would be practicable at this temperature. Consequently, only one sample was studied at 800°C. It can also be seen from Figs. 8 and 9 that the rate vs time curves for 900°C and 1000°C rise to a maximum and then decrease as the reaction proceeds. This type of curve is typical of an auto-catalytic type of reaction where the presence of the product of the reaction materially accelerates the rate. This form of behaviour has been observed for a number of other reactions, viz. reduction of nickel oxide with hydrogen[35], reduction of copper oxide with hydrogen[83)84)], reaction between calcium and nitrogen[85], and most thermal decompositions[86)87)]. At 1100°C, however, it appears, from Fig. 10, that the maximum rate occurs at a very early stage in the reduction since the rate vs time curve appears to slope downward from the very start of the reaction.

Examination of particles incompletely reduced, and then treated with dilute hydrochloric acid to remove the barium sulphide

Fig. 8. Rate curves for 800°C and 900°C

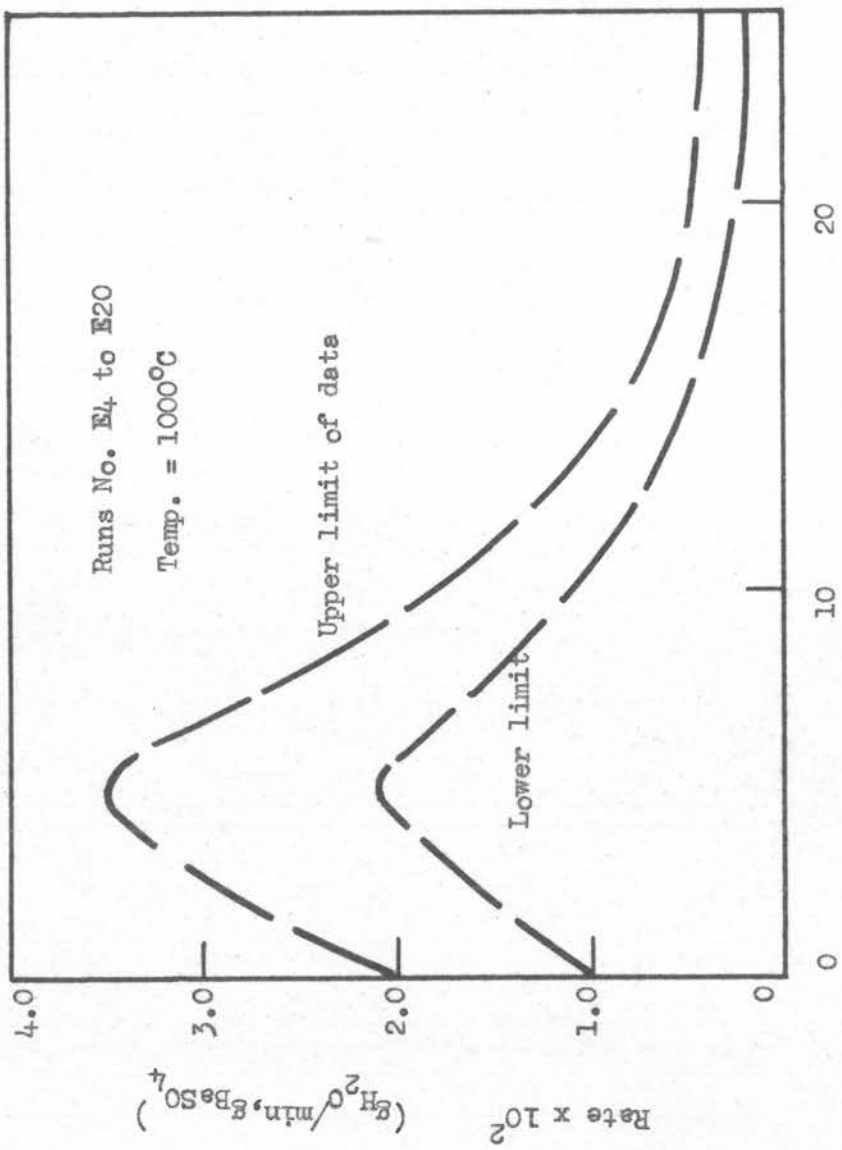

Fig. 9. Rate data for 1000°C

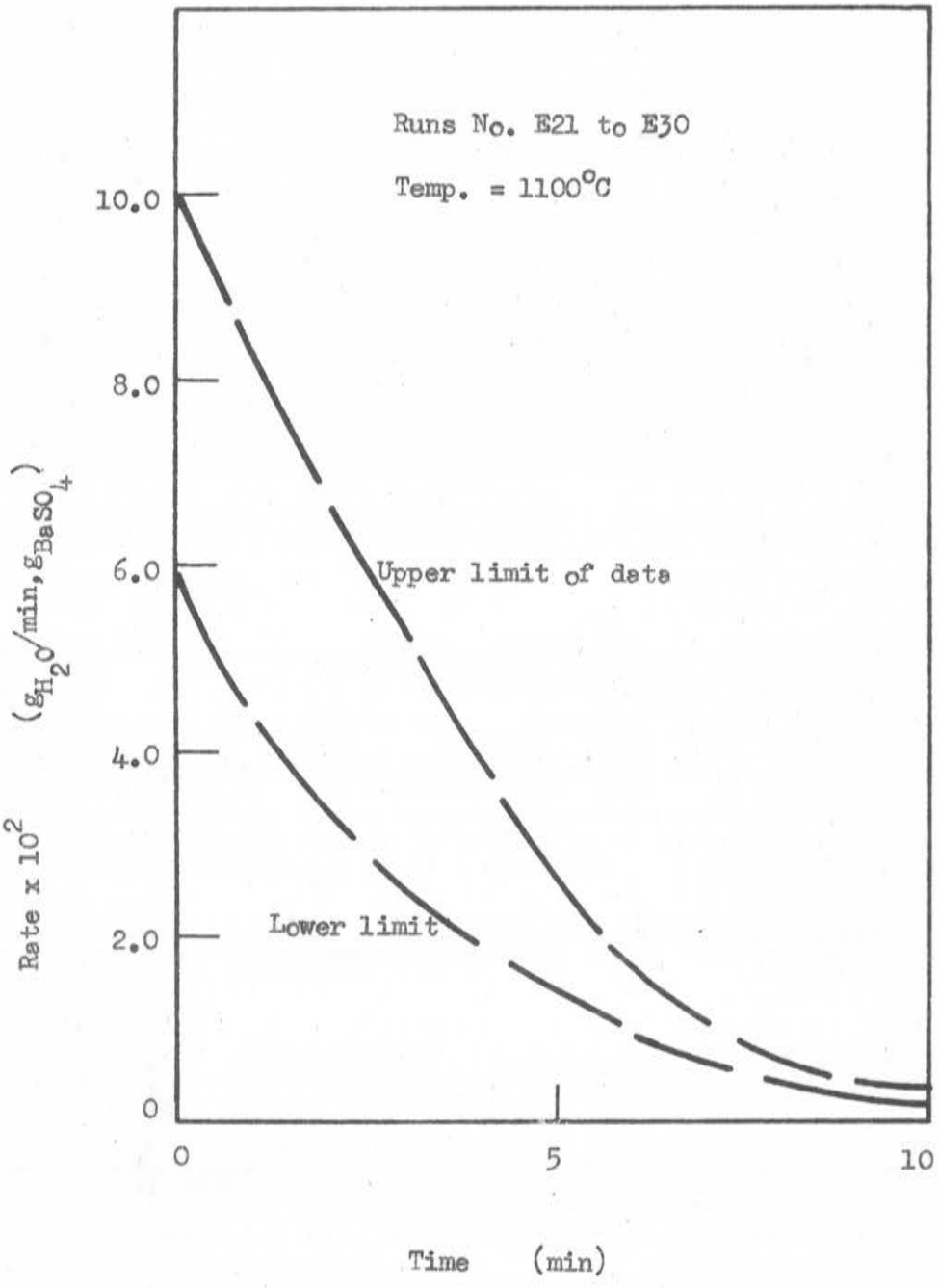

Fig. 10. Rate data at 1100°C

formed, showed that the reaction appeared to start at the surface of the barytes particle and proceeded inwards so that a barium sulphide crust was formed around the unattacked core. The reaction takes place, therefore, at the $BaSO_4$/BaS interface as shown diagrammatically in Fig. 11

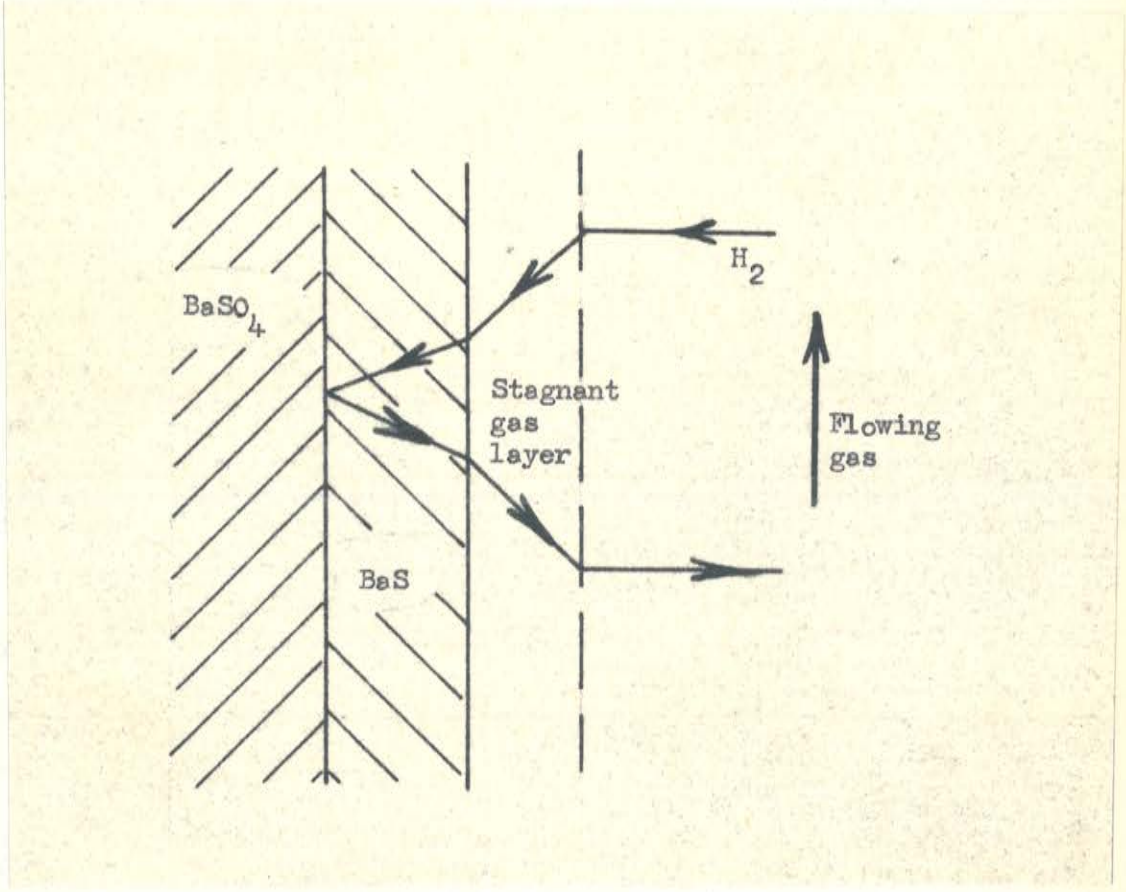

Fig. 11. Diagrammatic representation of the reduction of barytes

4:2:1 Effect of gaseous diffusion

It can be seen that, on the basis of Fig. 11, the first step in the reduction is the diffusion of hydrogen from the body of the gas, through the "stagnant" gas film surrounding the solid, to the solid surface. Since in the case of many reactions carried out at high temperatures, this rate of diffusion to the solid surface is the slowest step in the reaction, it was deemed advisable to examine the data obtained for the reduction of barytes to see if, in this case, the rate of diffusion from the body of the gas to the solid surface was a controlling factor.

Calculations, using the mass transfer data of Hobson and Thodos,[81] showed that the rate at which hydrogen could be supplied to the surface was approximately fifty times as fast as the maximum rate of reaction at 1100°C. It follows, therefore, that the rate of gaseous diffusion is not a controlling factor in the rate of reduction at temperatures up to 1100°C. This conclusion is confirmed by the plot in Fig. 12 where it is found that the maximum rate of reaction is proportional to the absolute temperature raised to the twenty second power. It is generally accepted[27] that the rate of a diffusion controlled process is proportional to the square root of the temperature.

4:2:2 Inconsistency of results

It became apparent at an early stage in the work that there was considerable, unaccountable variation in the rate curves from

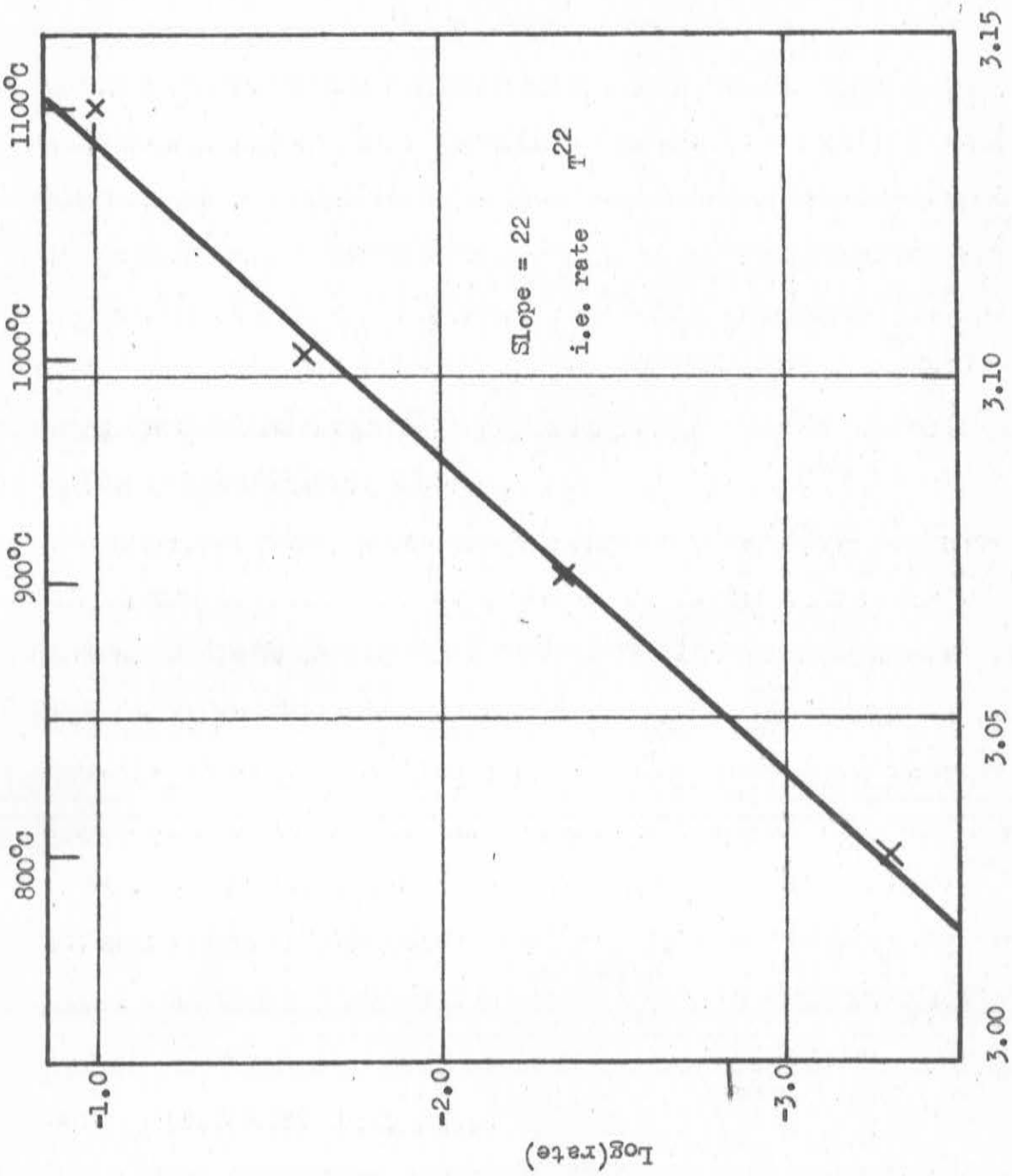

Fig. 12. Temperature dependence of the reaction rate

run to run (see spread of data in Figs. 9 and 10) and an explanation was sought for this behaviour. Three different types of packing, viz. silica, alundum, and Mullite chips, were used to find out if the barytes particles were reacting with the packing material or with the walls of the reactor, but the composition of the packing was found to have little or no effect on the rate of reaction obtained.

It was also thought possible that the temperature-time history of the sample might have some effect on the reaction rate since Benton and Emmett[35] claimed such a dependence for the nickel oxide reduction. However, samples held at 1100°C for many hours and then reduced at 1000°C did not give a rate appreciably different from those obtained with samples brought quickly to 1000°C and reduced immediately.

The possibility that the small quantity of oxygen in the commercial hydrogen (0 to 0.1%) could affect the reaction rate was also investigated, but comparisons of hydrogen analyses and reaction rates showed that there was no correlation between the two. It was found necessary, however, to deduct the quantity of water produced by the oxygen in the hydrogen from the weight of water collected in the drying tubes if errors in the later part of the percentage reduction vs time curves were to be avoided. Errors from this source never displaced the curve by more than 5%.

Finally, the belief was formed that part of the variation from run to run was caused by the wide size range of the material being used and the consequent difficulty in obtaining samples having the same surface area. The rate of gas-solid reactions depends upon the surface area of the solid (see Section 2:3:3, page 14), therefore, the rate of reaction, over the initial part of the reduction, will be sensitive to changes in the specific area of the sample. This hypothesis was confirmed by the later work with samples of known surface area (see Section 4:4:1 below).

At 1100°C it was found that the initial rates of reaction were inconsistent, even for the same run, and often appeared to be much lower than expected from the later measurements. This anomaly was finally traced to the loss of weight of the drying tubes when the air in them was replaced by hydrogen. Although the loss of weight was only of the order of 0.1g the effect on the measured rate of reaction was quite large since the weight of water collected in the first half minute was only about 0.3g. This difficulty was overcome by flushing the drying tubes with hydrogen before the initial weighing and by closing the outlets of the tubes with corks on removing from the apparatus.

4:2:3 Conclusions

The conclusions which were drawn from this exploratory phase of the investigation may be set out as follows.

(1) The reaction is auto-catalytic with a well defined maximum

occurring in the rate vs time curves obtained at temperatures of 900°C and 1000°C. At 1100°C the maximum value appears to be reached within the first half minute.

(2) The reaction takes place at the $BaSO_4$/BaS interface.

(3) Diffusion from the body of the gas phase to the solid surface does not control the rate of reduction of barytes by hydrogen at temperatures up to 1100°C.

(4) The rate of reaction is not affected by the composition of the packing material used to support the differential bed in the reactor.

(5) It is necessary to flush the drying tubes with the reducing gas and to keep the tubes tightly corked when detached from the apparatus if consistent weights are to be obtained.

(6) It appears that the specific area of the sample may have a marked effect on the rate of reaction.

4:3 Experimental procedure (Final stage)

The ultimate objective of the investigation was to obtain enough information on the reaction rate to be able to predict the rate at which barytes particles would react with a gas containing hydrogen in a fluidized system, therefore, after the preliminary stage had been completed, the next step was to obtain information on the other factors which could affect the rate of reaction, and, if possible, to identify the mechanism of the chemical reaction occurring at the $BaSO_4$/BaS interface.

The preliminary work showed that the rate of diffusion from the body of the flowing gas to the surface of the barytes particles was much faster than the rate of reaction (see Section 4:2:3). It seemed possible, however, that the rate of diffusion of water and hydrogen through the growing barium sulphide crust might be a controlling factor, especially in the later stages of the reduction when the barium sulphide layer was relatively thick. It was decided to test this possibility by diluting the reducing gas (hydrogen) first with an inert gas (nitrogen) and then with the product of reaction (water). A reduction in the partial pressure of hydrogen would produce a reduction in the diffusion rate and a consequent reduction in the rate of reaction if diffusion was a controlling factor. The dependence of the rate of reaction on variations in the partial pressures of hydrogen and water would also yield information on the reaction mechanism.

The effect of variation in the specific surface of the barytes being reduced, on the reaction rate obtained, was also investigated by preparing samples of known surface area, viz. spheres, cubes, and hemispheres, whilst samples containing varying quantities of impurities (Fe and Si) were reduced to find if the purity of the barytes had a significant effect on the reaction rate.

4:3:1 Apparatus

The apparatus used was substantially the same as that described in Section 4:1:1, page 73, the only change being the addition of

a tube by-passing the reactor furnace (see Fig. 6, page 74) so that the drying tubes could be flushed with the reducing gas before the beginning of a run.

Hydrogen-nitrogen mixtures of known composition were prepared by metering each stream through orifice meters and then mixing the gases ahead of the drying agent A (see Fig. 6). Hydrogen-water mixtures were obtained by replacing the drying agent A with a saturating tower. Distilled water was circulated, at a constant rate, over a small packed tower by a gear pump; the device was submerged in a thermostatically controlled water bath, the temperature of which was varied to give mixtures each of constant but differing water vapour contents. The humidity of the gas leaving the saturator was obtained by temperature measurements using wet and dry bulb thermometers. The equation[88] relating the humidity to the difference between wet and dry bulb temperatures for a hydrogen-water mixture shows that, for small differences, the gas may be considered as being saturated at the wet bulb temperature. This simplification was adopted in calculating the water content of all the hydrogen-water mixtures used because the difference between dry and wet bulb temperatures in no case exceeded $5^{\circ}F$. Where necessary, the tubing carrying water-hydrogen mixtures was heated to a temperature above the dew point of the mixture by playing a gas flame along it to prevent condensation.

4:3:2 Experimental technique

The method used for hydrogen and hydrogen-nitrogen mixtures was identical with that set out in Section 4:1:2, page 77, except that the drying tubes were flushed with the reducing gas before being weighed for the first time. In the case of hydrogen-water mixtures, however, it was not practicable to follow the course of the reaction by collecting and weighing the water produced. It was possible to determine the quantity of water leaving the reactor with considerable accuracy but since the rate at which water entered the reactor was proportional to the hydrogen rate which itself had a possible variation of $\pm 5\%$, the variation in the quantity of water entering the reactor was, therefore, greater than the change from inlet to outlet caused by the reaction. For this reason, it was decided to reduce similar samples of barytes for given time intervals, cool in nitrogen, and then determine the percentage reduction by assaying for acid soluble barium*.

4:3:3 Preparation of samples

Cubes of barytes were prepared by cutting up selected blocks of mineral with a diamond saw. The cubes were then heated to about 600°C in an electric muffle to eliminate any which had a tendency to decrepitate. Those remaining were used as samples for the reaction rate work. Although the barytes used for making cubes was of high purity (SiO_2 = 0.25%, Fe_2O_3 = 0.30%) and therefore relatively

* The entire sample was treated with boiling, dilute HCl to remove the barium sulphide present.

stable to heating, at least half of the cubes prepared shattered or split during the preliminary heating.

Some spheres were prepared by tumbling cubes with carborundum powder but it was later found that spheres could be produced less laboriously if rounded particles, selected from stabilized crushed material, were tumbled with carborundum. Hemispheres were made by splitting spheres with the diamond saw.

4:3:4 Treatment of results.

Rate vs time and percentage reduction vs time plots were produced from the weights of water collected in the way set out in Section 4:1:4, page 79. In the case of the runs with a reducing gas consisting of a mixture of hydrogen and water the sample assays gave the percentage reduction vs time curve directly. Where necessary this curve was differentiated graphically to give a rate vs time curve. It should be noted that, for convenience, the data for hydrogen-water mixtures of a fixed composition were included under a single run number although several samples were used to obtain the results.

4:4 Discussion of results (Final stage)

The rate vs time and percentage reduction vs time data for runs E32 to E92 are shown in Appendix C.

Refinement of the experimental method, viz., the use of closely sized samples, flushing of the drying tubes with reducing gas, and

correction of the weight of water produced to allow for the small quantity of oxygen in the hydrogen markedly improved the accuracy of the rate vs time curves obtained. Examination of the data presented in Appendix C shows that consecutive runs on the same sample under similar conditions rarely differ by more than 10% over the whole course of the reaction. This is a considerable improvement on the results obtained in the preliminary stage where the rate vs time curves show variations of the order of 50% (see Figs. 9 and 10, page 82) for consecutive runs. It can also be seen from Appendix C that the figures recorded for any one run are reasonably consistent among themselves since it was very unusual for a point to deviate by more than 10% from the curve which could be drawn through the remaining points.

4:4:1 Effect of specific surface

The preliminary work with crushed material indicated that the rate of reaction was markedly influenced by the specific area of the material being reduced. Samples consisting of sized spheres, hemispheres, and cubes were made up and the results compared to see if the effect of surface area and particle shape on the reaction rate could be put on a rational basis.

It was found that the initial rate per unit area at a given temperature was constant for samples where the composition of the barytes did not vary. This finding is illustrated by the results, shown in Table IV, for Sample F. It can also be seen that the shape

TABLE IV

Effect of specific surface and particle size on the initial rate of reaction for Sample F

Run No.	Temp. (°C)	Shape	Specific surface (cm^2/g)	Initial rate x 10^3 (g_{H_2O}/min, cm^2)
E56-57	1014	sphere	2.2	3.4
E58	1017	hemisphere	3.0	3.5
E60	1014	cube	2.7	3.5
E69	1013	sphere	3.7	3.6
E64-66	1105	sphere	2.2	18.2
E67	1105	cube	2.7	18.5
E68	1108	sphere	3.7	17.9

of the particles appeared to have no effect on the initial reaction rate.

4:4:2 Effect of changes in hydrogen partial pressure

(1) Hydrogen-nitrogen mixtures

The results of the rate work using hydrogen-nitrogen mixtures of varying composition are summarized by Figs. 13 and 14. It can be seen that, at both 1100°C and 1000°C, a change in the partial pressure of hydrogen from one atmosphere to half an atmosphere had little effect on the initial rates obtained. At 1100°C the only effect of reducing

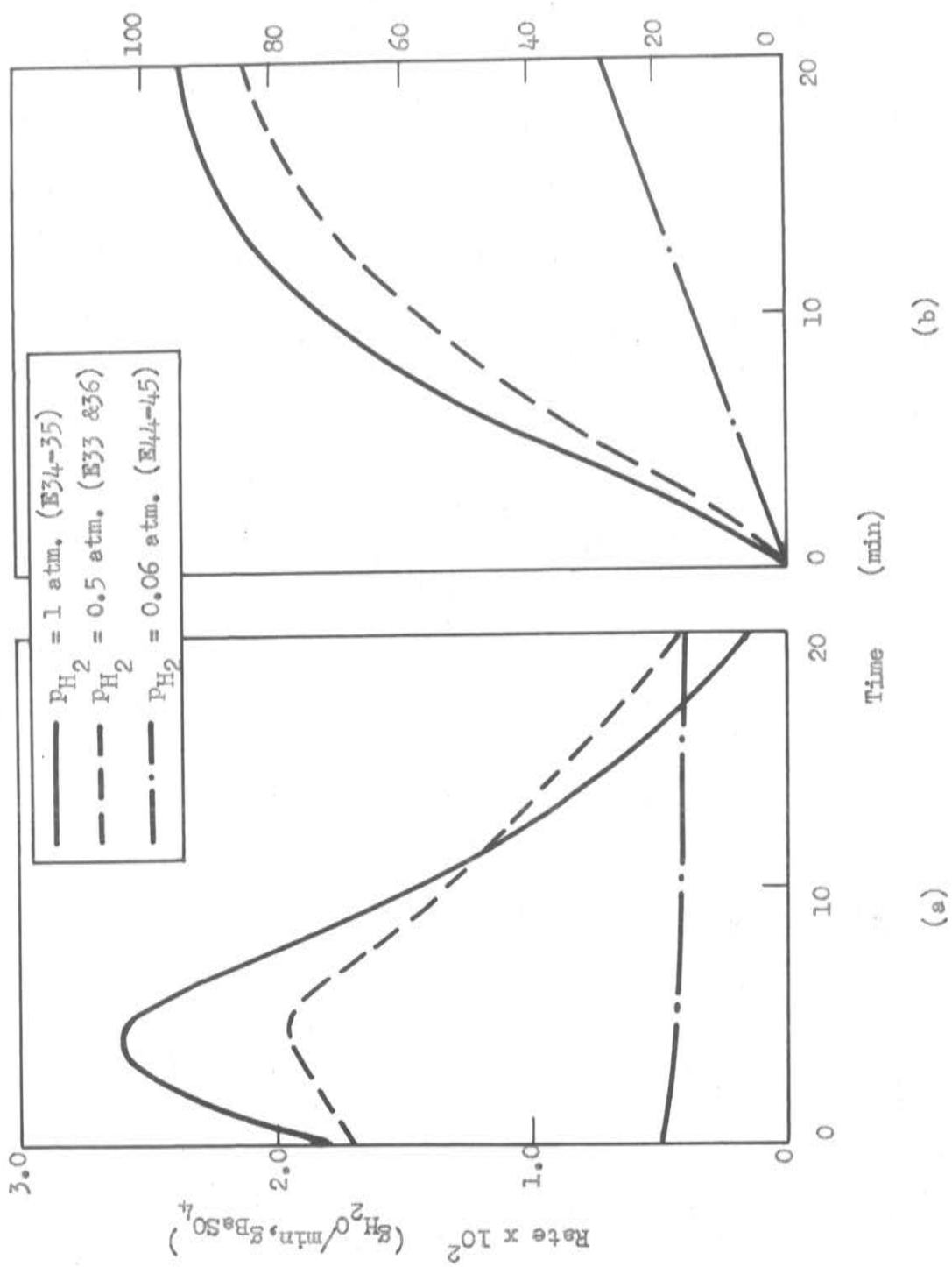

Fig. 13. Effect of variation in hydrogen partial pressure on the reaction rate at 1000°C (Nitrogen dilution)

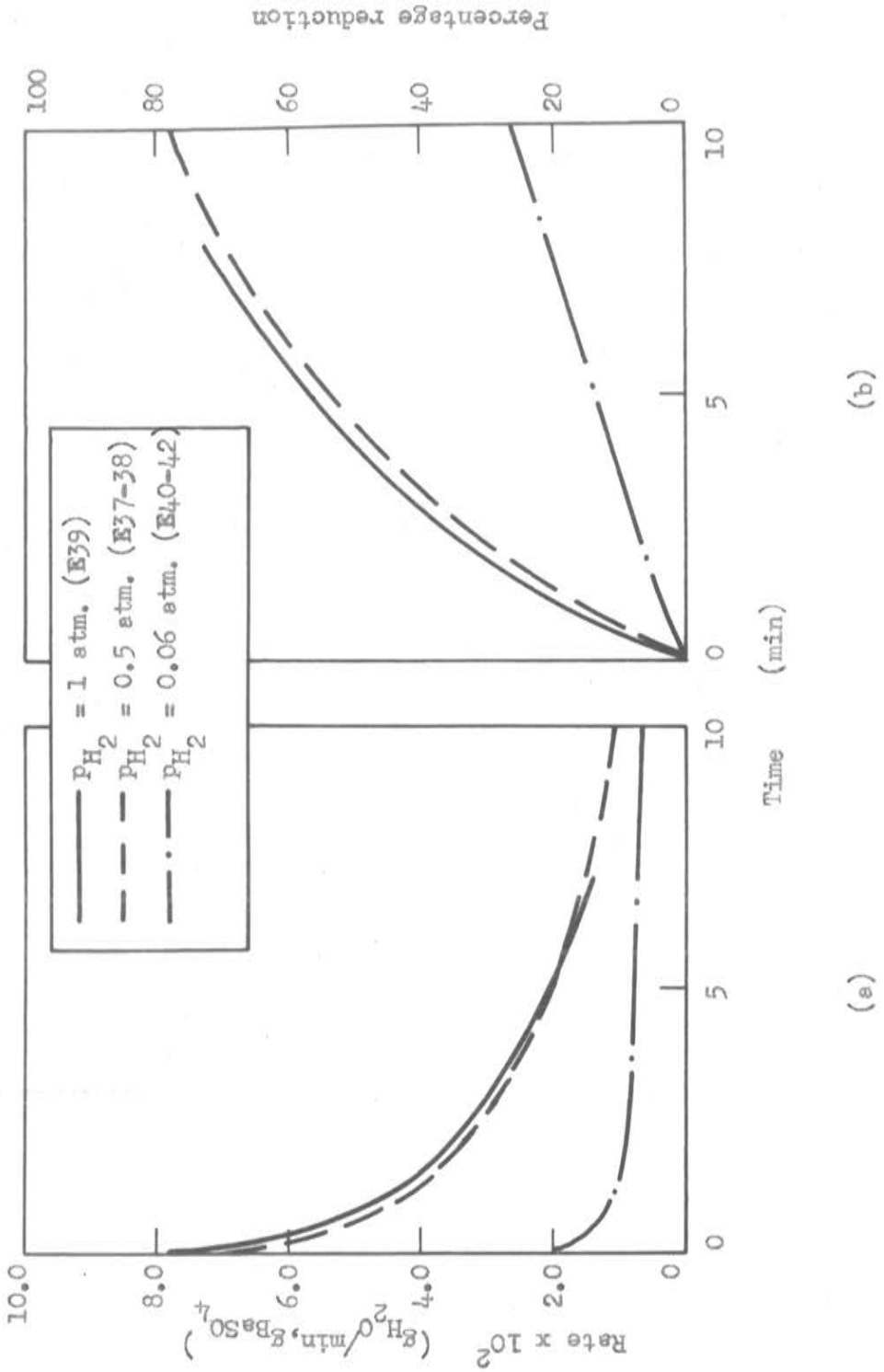

Fig. 14. Effect of variation in hydrogen partial pressure on the reaction rate at 1100°C (Nitrogen dilution)

the partial pressure of hydrogen from one to half an atmosphere was to decrease slightly the percentage reduction obtained in a given time; at 1000°C, however, this same change in hydrogen partial pressure caused a relatively large decrease in the rate of reaction once the reduction had started. It was apparent that a decrease in the partial pressure of hydrogen has a far greater retarding effect on the rate at 1000°C, where the reaction is relatively slow, than at 1100°C where the reaction is fast. This is the opposite effect to what might be expected if diffusion through the solid product layer was a controlling factor since it is generally accepted[27] that the rate of a diffusion process increases much more slowly with temperature than the rate of a chemical process. It seems unlikely, therefore, that diffusion is a controlling factor even in the last stages of the reduction.

In contrast to this behaviour, when the partial pressure of hydrogen was drastically reduced to 0.06 atmospheres, the rate of reaction obtained was almost constant (see Figs. 13a and 14a), and, since a constant rate is a characteristic of a reaction controlled by the rate of diffusion from the body of the reducing gas to the solid surface, it appears that at very low partial pressures of hydrogen the reaction becomes diffusion controlled.

(2) Hydrogen-water mixtures

It can be seen by comparing the results for hydrogen-water mixtures (Figs. 15 and 16) with the results for hydrogen-nitrogen

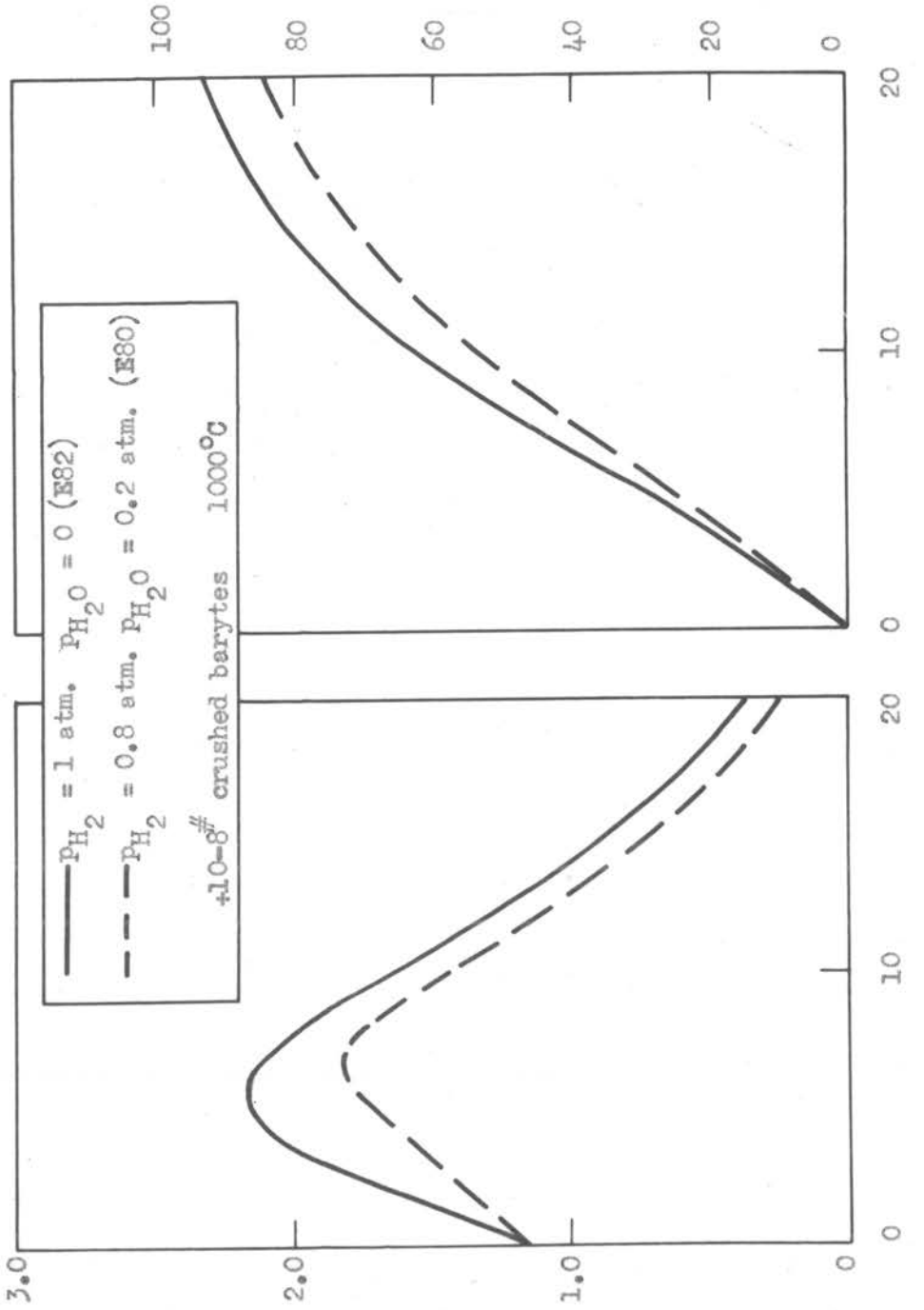

Fig. 15. Effect of variation in hydrogen partial pressure on the reaction rate at 1000°C. (Water dilution)

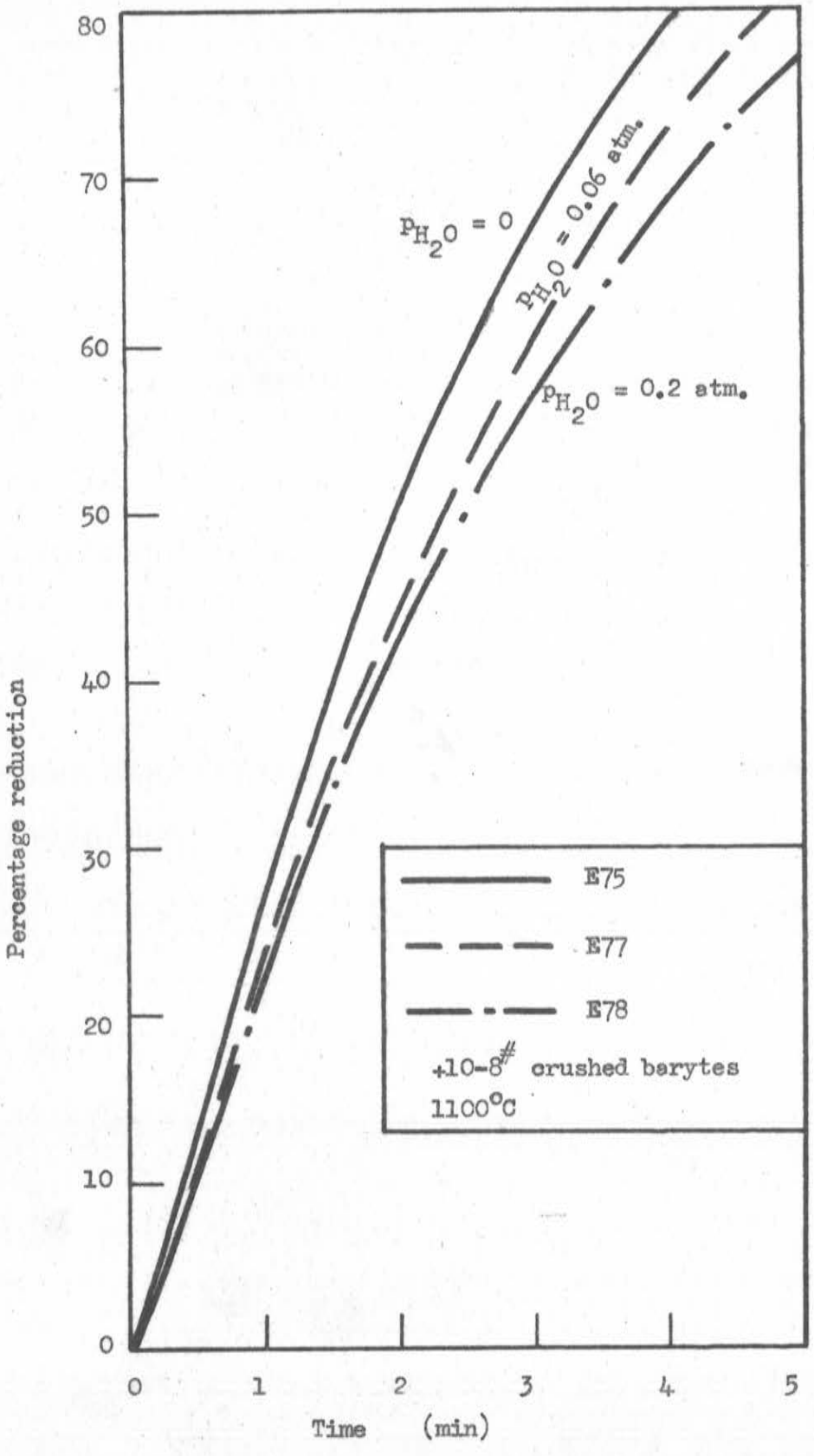

Fig. 16. Effect of variation in hydrogen partial pressure on the reaction rate at 1100°C (Water dilution)

THE UNIVERSITY OF ADELAIDE

mixtures (Figs. 13 and 14) that addition of water vapour to the reduction gas had a similar effect to the addition of nitrogen. The initial rates in each case were not reduced and the effect on the subsequent reaction rate was much greater at 1000°C than at 1100°C.

It appears that, at 1100°C, the rate of reaction is almost independent of the hydrogen partial pressure so long as that partial pressure does not fall to a very low value. At 1000°C, however, the hydrogen partial pressure has a greater effect on the rate once the reaction is under way.

4:4:3 Temperature dependence of reaction rate

Fig. 17 shows that the temperature dependence of the reaction rate did not change markedly as the reaction proceeded. Even at 80% reduction the slope of the log (rate) vs log (temperature) plot has a value of 21 which is much greater than the value of 0.5 to be expected[27] for a diffusion controlled reaction. This supports the belief that the rate is chemically controlled and is not appreciably retarded by diffusion when the partial pressure of hydrogen is high.

4:4:4 Effect of silica and iron impurities

It can be seen from Table V that the initial rate per unit area is increased by the presence of iron and silica although the limited results available do not give any information concerning the relative efficiencies of iron and silica in accelerating the initial rate.

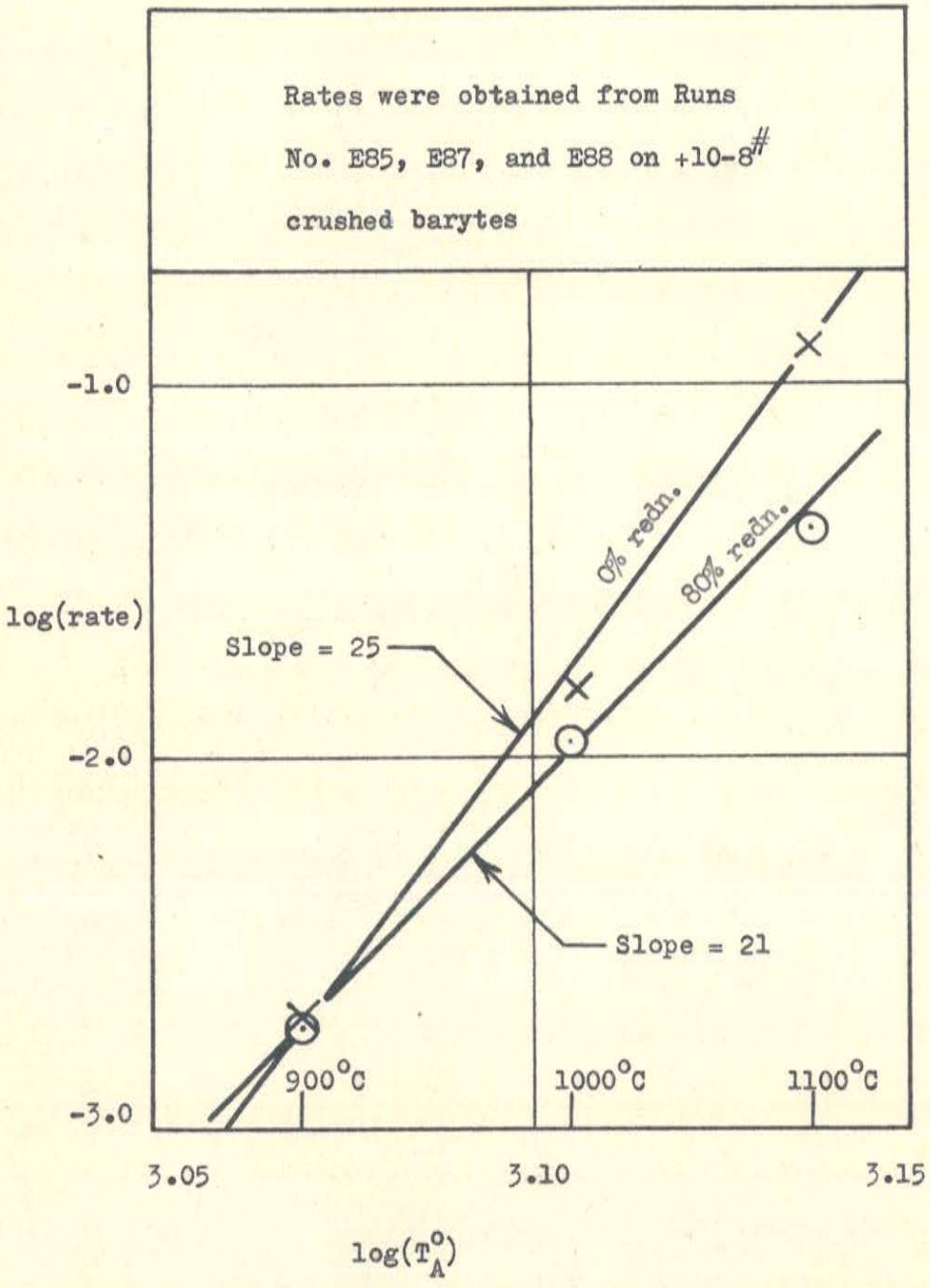

Fig. 17. Variation in temperature dependence as the reaction proceeds

TABLE V

Effect of impurities on the initial reaction rate

Sample	Assay*		Initial rate x 10^3 (g_{H_2O}/min,cm^2)	
	SiO_2	Fe_2O_3	1015°C	1105°C
E	2.0	1.3	4.0	22
F	0.25	0.30	3.5	18
H	2.5	2.0	-	27
I	1.9	1.3	-	21

A comparison of the reduction times for similar spheres of sample F and Sample H reveals that a tenfold increase in the silica and iron contents has decreased the reduction time by 25%. A 6.2 mm sphere of Sample F (E66) took twenty two minutes to reach 55% reduction at 1100°C whereas a 6.3 mm sphere of sample H (E83) required only five minutes to reach the same stage of reduction under similar conditions. These findings were partially confirmed in a communication from Dr. Rigg of Imperial Smelting Corporation Ltd., who noticed a similar effect when reducing barytes with carbon monoxide.

Examination of the rate data for Sample F at 1000°C (E56-58) reveals that the rate vs time curves show no maximum value but

* Details of the sample assays may be found in Appendix C

fall away steadily from zero time onwards. This type of curve was not obtained with any of the other samples which all contained much more silica and iron and exhibited clearly defined maxima in the rate vs time curves at 1000°C. It seems, therefore, that the presence of impurities in the barytes may well be responsible for the maximum in the rate vs time curve.

4:4:5 Effect of heating barytes above the transformation temperature

It had been noticed that, when samples were accidentally heated to above 1150°C before being reduced, the rate of reaction was greatly accelerated. Since barium sulphate undergoes a transformation from rhombic to monoclinic crystal structure at 1149°C[89] it seemed likely that these phenomena were inter-related. Accordingly Run No. E87 was carried out on a sample which had been heated to 1130°C before being reduced at 1100°C, while a sample which had been heated to 1160°C was used in Run No. 86. The rates obtained for these two samples are compared in Table VI with the rate obtained from a sample (E92) which was heated to 1100°C and immediately reduced. It can be seen that the critical temperature, as far as acceleration of the reaction rate is concerned, lies between 1130°C and 1160°C, and it is reasonable to assume that this critical temperature is in fact the temperature at which rhombic barium sulphate transforms to monoclinic barium sulphate. This behaviour will be considered further in the discussion on reaction mechanism (see Section 4:4:7).

TABLE VI

Effect on the reaction rate at 1100°C of heating samples above 1150°C

Time (min)	Rate x 10^2 (g_{H_2O}/min, g_{BaSO_4})*		
	Run No. E86** (Heated to 1160°C before reduction)	Run No. E87** (Heated to 1130°C before reduction)	Run No. E92** (Heated to 1100°C and reduced)
0	25.0	12.3	12.0
0.5	21.0	11.0	11.0
1.0	5.9	8.9	8.5
2.0	0.9	3.9	3.5
4.0	0.05	0.8	0.7
6.0	-	0.05	-
8.0			

* All samples were reduced with hydrogen at 1100°C

** These rate data have been extracted from Appendix C.

4:4:6 Correlation of results.

It was found that, once the point of maximum rate had been passed, the reaction obeyed a first order law, i.e.,

$$\log(1 - f) = kt \quad \ldots\ldots\ldots\ldots\ldots\ldots\ldots\ldots (a)$$

Where f = the fraction of barium sulphate reduced at time t

t = time

k = a constant.

Plots of $\log(1 - f)$ vs t for typical samples reduced at 1000°C and 1100°C can be seen in Figs. 18 and 19 respectively. The first order law holds quite well for the later stages of the reduction at 1000°C and for the whole reduction period at 1100°C; however, it can be seen that the slope of the lines, and consequently the value of the rate constant, varies with the particle size, partial pressure of hydrogen, and solid composition. Thus it was necessary to eliminate the effect of some of these variables if a useful correlation was to be developed.

It had been found (Section 4:4:1) that the initial rate per unit area was a constant for a given temperature and this suggested a convenient method of eliminating the effect of particle size variation from the correlation, viz. to divide the rate of reaction by the specific surface of the sample. A plot of (R/s) vs $(1 - f)$ for three different samples at 1100°C is shown in Fig. 20 and it can be seen that the results correlate reasonably well on a straight

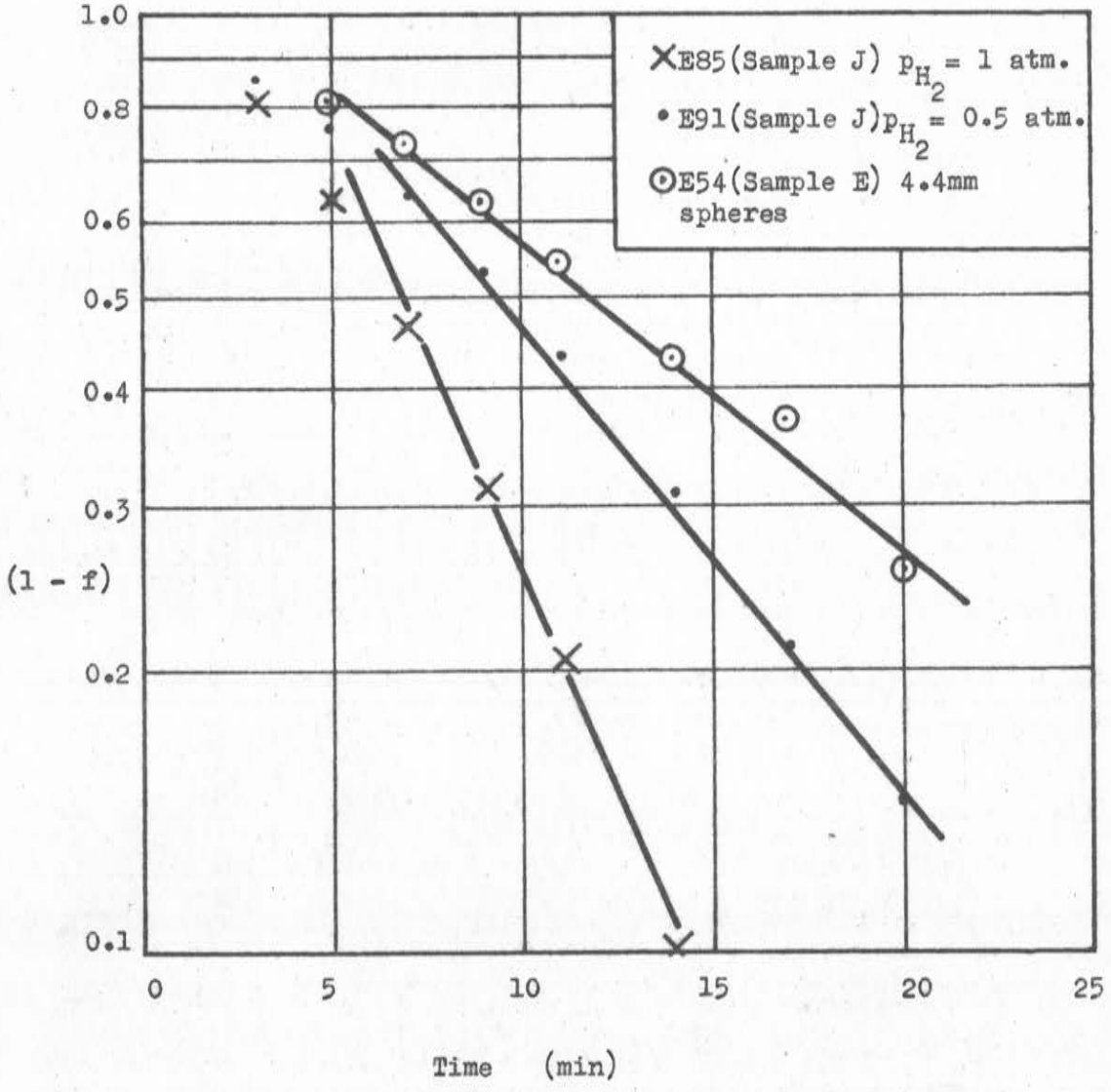

Fig. 18. First order plot for data at 1000°C

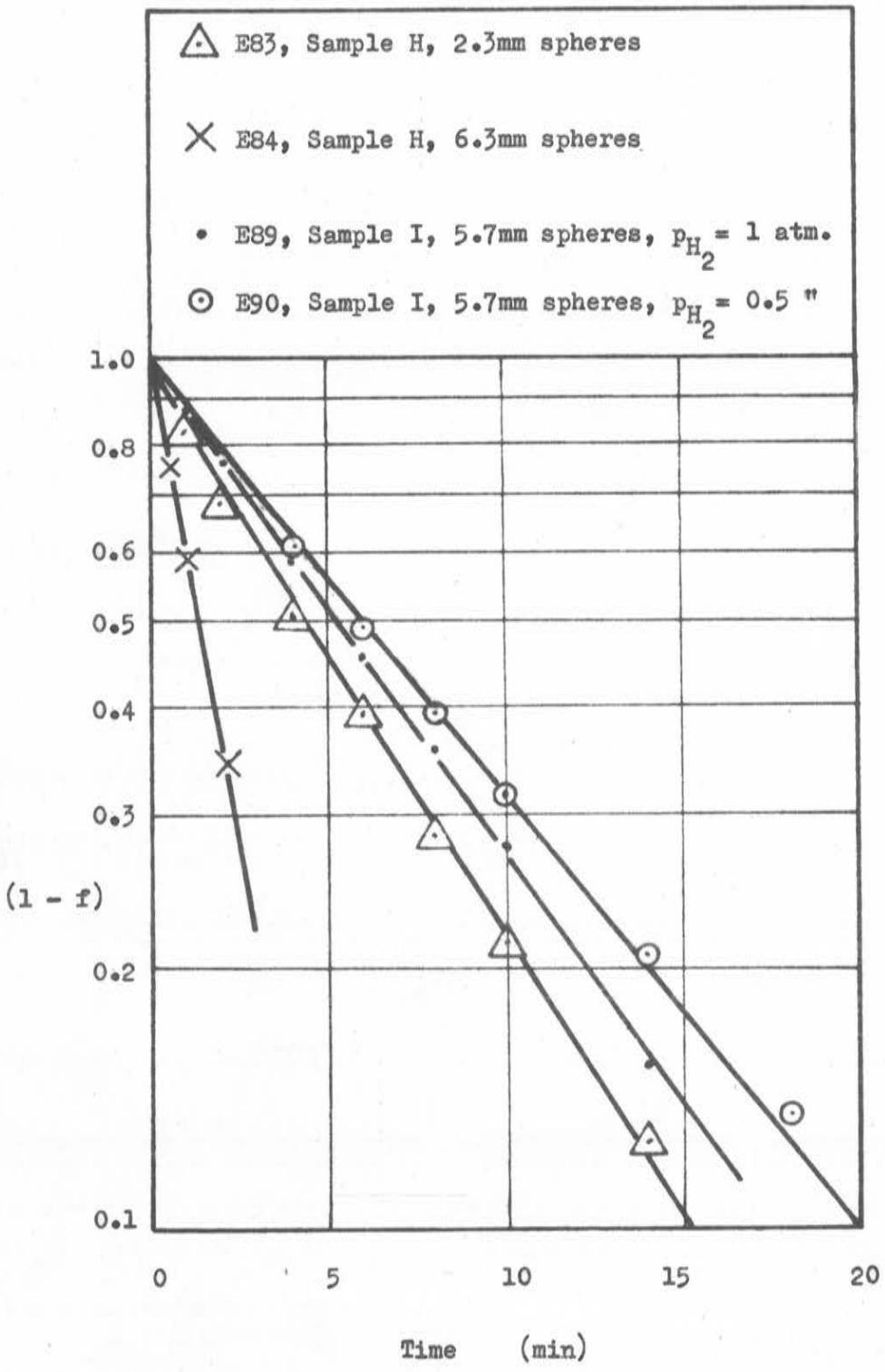

Fig. 19. First order plot for data at 1100°C

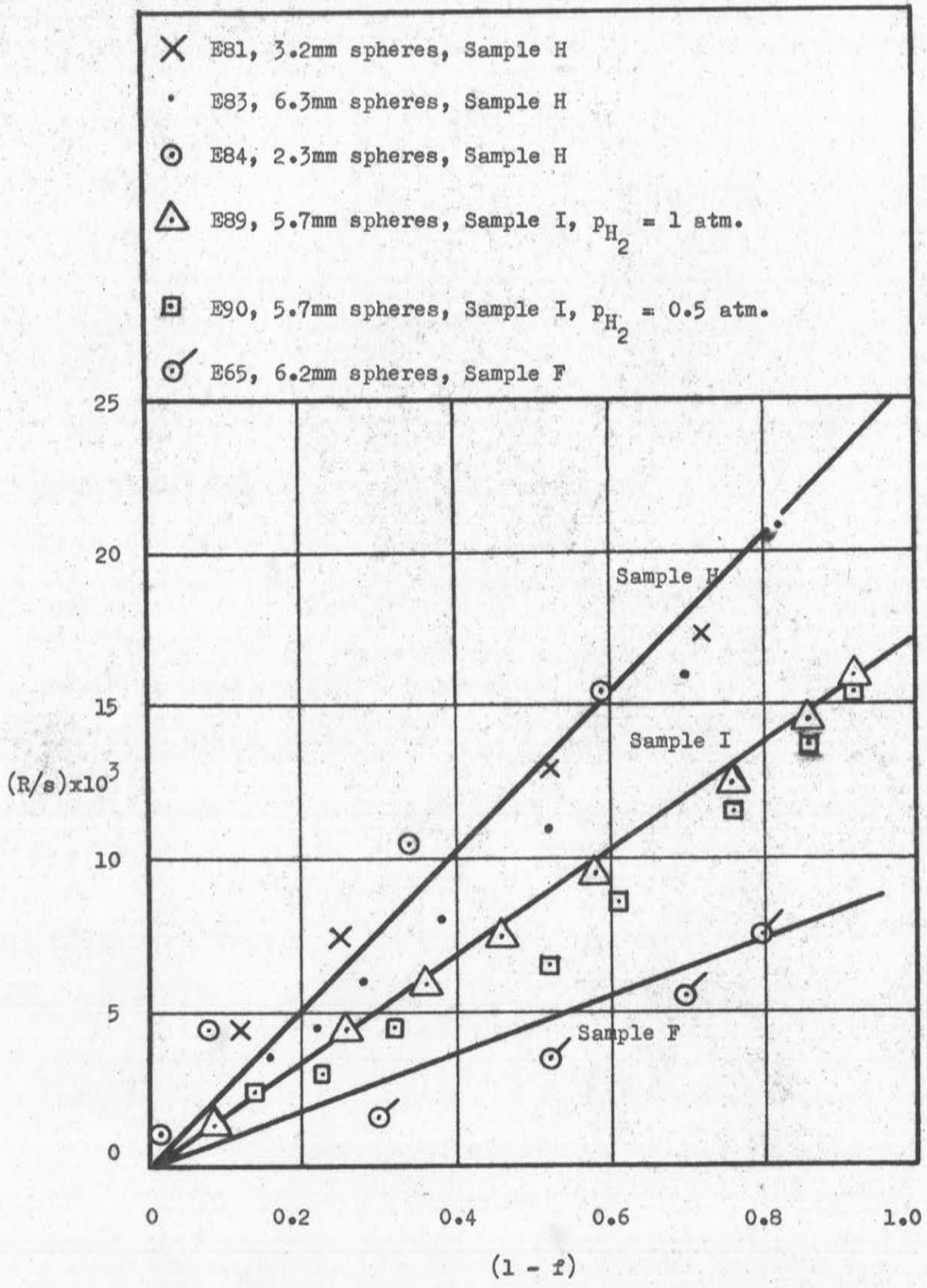

Fig. 20. Correlation of results for Sample F, H, and I at 1100°C

line, the slope of which depends upon the composition of the sample. Fig. 21 gives values of the slope (K), read from Fig. 20 for different percentages of impurity. This correlation takes no account of the slight variations in the rate of reaction caused by variations in the partial pressure of hydrogen. However, for most purposes, the rate of reaction at 1100°C can be satisfactorily represented by the equation,

$$R/s = K(1 - f)/100 \quad \text{.....(b)}$$

Where R = the rate of reaction

$(g_{H_2O}/\text{min}, g_{BaSO_4})$

s = the specific area of the barytes sample (cm^2/g)

f = the fraction reduced

K = the rate constant (obtained from Fig. 21)

The time at any point on the (R/s) vs (1 - f) curve may be found by dividing increments of f by the average rate for that increment and summing the times obtained. Consequently rate vs time and percentage reduction vs time curves may be easily constructed.

It was also discovered that the results for spheres at 1100°C could be correlated very satisfactorily by an equation of the form,

$$s/R = A_c/K_1A_i + SA_c/K_2A_m \quad \text{.....(c)}$$

Where R = the rate of reaction

$(g_{H_2O}/\text{min}, g_{BaSO_4})$

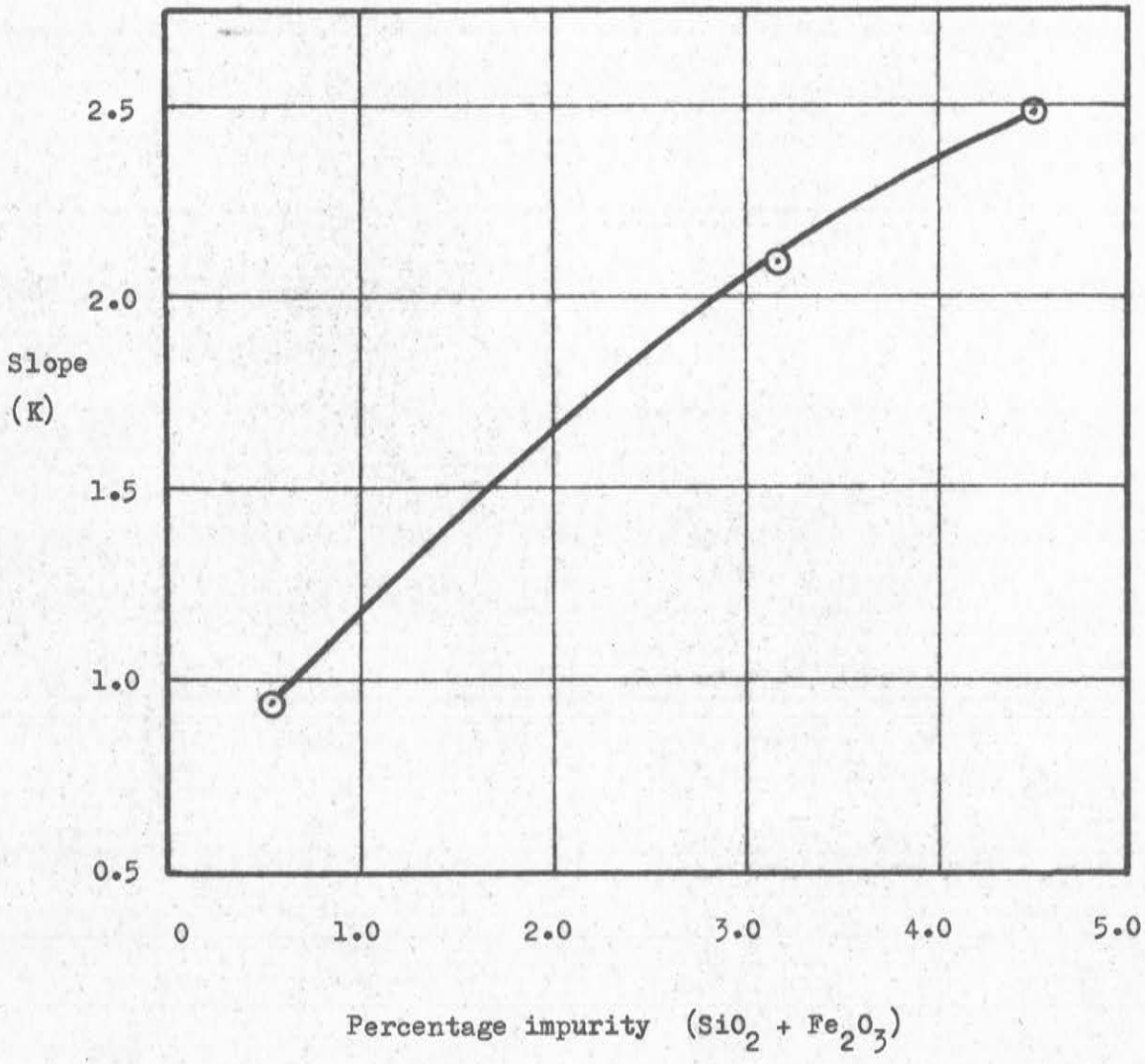

Fig. 21. Variation of K with the percentage impurity in the barytes

s = the specific surface (cm^2/g)

A_o = the outside area of the sphere (cm^2)

A_i = the area of the $BaSO_4/BaS$ interface (cm^2)

S = the thickness of the BaS layer (cm)

$A_m = (A_o A_i)^{0.5}$

K_1 and K_2 are constants.

This equation was developed by extending the method used by Wilhelm[27] for combining chemical and diffusion rates in catalytic reactions to cover the case of a chemical reaction, taking place at a product/reactant interface, which is progressively retarded by diffusion of the gaseous reactants through the solid product layer. Although the experimental data for spheres fit this equation very well it should be noted that such retardation of the rate of reaction is unlikely; the close fit is probably due to the use of two constants in equation (c) as compared with equation (b) where there is only one constant.

It was found that K_1, which could easily be found from the experimental rate vs time curve by substituting the value of the rate at zero time in equation (c), was independent of the particle size and showed the same dependence on the solid composition as the initial rate. Constant K_2, on the other hand, was very sensitive to changes in barytes composition and varied only slightly with particle size. Some typical values of K_1 and K_2 are shown in Table VII.

TABLE VII

Values of K_1 and K_2 for various spherical samples

Run No.	Sample	Dia. (mm)	K_1	K_2
E63	E	4.4	22×10^{-3}	5×10^{-3}
E68	F	3.7	18×10^{-3}	5×10^{-4}
E65	F	6.2	18×10^{-3}	3×10^{-4}
E84	H	2.3	28×10^{-3}	2×10^{-3}
E81	H	3.2	25×10^{-3}	3×10^{-3}
E83	H	6.3	30×10^{-3}	2×10^{-3}
E89	I	5.7	21×10^{-3}	1×10^{-3}
E90*	I	5.7	21×10^{-3}	8×10^{-4}

*Run E90 was carried out using an equimolar mixture of nitrogen and hydrogen as reducing gas. Pure hydrogen was used for the other runs.

This correlation is not as useful as the previous one (b), although it fits the experimental results more precisely, because it requires accurate knowledge of the ratio between the surface area and the area of the interface at which the reaction is taking place and this, in turn, depends upon the shape of the particle being reduced. The ratio can only be determined accurately for spheres and consequently this correlation is limited in application to spherical or near spherical particles.

Similar correlations were attempted at 1000°C but the results obtained were unsatisfactory due to difficulty in predicting the maximum rate to be obtained. Unlike the initial rate per unit area, which is independent of particle size and shape (see Section 4:4:1, page 94), the maximum rate divided by the specific area still depends upon the particle size. The effect of variation in hydrogen partial pressure is also much greater at 1000°C than at 1100°C where it was possible to neglect this factor. No satisfactory basis could be found for correlating the data at 1000°C.

4:4:7 Reaction mechanism

Although the experimental programme was developed to meet the needs of the investigation for rate data which could be used to predict rates of reaction in a fluidized reactor it was also possible, using the information obtained, to set up some hypotheses regarding the mechanism of the reaction.

It was pointed out in Section 4:4:3, page 103, that the rate of reaction, at partial pressures of hydrogen of the order of a half to one atmosphere, depends upon the rate of the process occurring at the $BaSO_4$/BaS interface since diffusion through the gas phase and diffusion through the product layer do not seem to be important. The salient features of this process are,

(1) the initial rate is not affected by variations in the partial pressures of hydrogen and water so long as the partial pressure of hydrogen does not fall to a very low value,

(2) the reaction is autocatalytic,

(3) the rate of reaction appears to be accelerated by the presence of iron and silica, and

(4) the rate of reaction is accelerated by changes in the crystal structure of the barytes.

Initially, the barium sulphate reduction is equivalent to a catalytic reaction which may be represented by,

$$H_{2(g)} \rightleftharpoons H_2{}^{0}{}_{(g)} \quad \ldots\ldots\ldots\ldots\ldots\ldots (10)$$

It should be possible, therefore, to interpret the initial rate data by a technique similar to that used for interpreting kinetic data for catalytic reactions of the type,

$$A_{(g)} \rightleftharpoons B_{(g)} \quad \ldots\ldots\ldots\ldots\ldots\ldots (11)$$

Corrigan[23] postulates that the mechanism of this type of reaction involves three steps,

$A_{(g)} + c \rightleftharpoons Ac$ (chemisorption)

$Ac \rightleftharpoons Bc$ (single site surface reaction)

$Bc \rightleftharpoons B_{(g)} + c$ (desorption)

where c indicates an active centre or high energy site on the solid surface. The form of the rate equation depends upon which step, viz. chemisorption, reaction, or desorption, is slowest, i.e. controls the rate. The rate equations which Corrigan[23] derives for each case are,

$$r = k(p_A - p_A^*)/(1 + K_B p_B + K_i p_i) \ldots\ldots\ldots (d)$$

(rate of chemisorption of A controlling)

$$r = k(p_A - p_A^*)/(1 + K_B p_B + K_A p_A + K_i p_i) \ldots (e)$$

(rate of surface reaction controlling)

$$r = k(p_A - p_A^*)/(1 + K_A p_A + K_i p_i) \text{.....(f)}$$

(rate of desorption of B controlling)

Where K = the equilibrium chemisorption constant

k = the rate constant

p = partial pressure

$p_A^* = p_B/K_e$

K_e = the equilibrium constant for reaction (11)

r = the reaction rate

and the subscript i refers to an inert gas

The application of these equations to the barytes reduction may now be examined where, (1) hydrogen-nitrogen mixtures and, (2) hydrogen-water mixtures were used as reducing agents.

(1) Hydrogen-nitrogen mixtures

In this case the partial pressure of water is small and may be neglected without serious error so that the initial rates are given by the equations,

$$r_o = kp_{H_2}/(1 + K_{N_2} p_{N_2}) \text{ .....(g)}$$

(chemisorption of hydrogen controlling)

$$r_o = kp_{H_2}/(1 + K_{H_2} p_{H_2} + K_{N_2} p_{N_2}) \text{ .....(h)}$$

(surface reaction controlling)

$$r_o = kp_{H_2}/(1 + K_{H_2} p_{H_2} + K_{N_2} p_{N_2}) \text{ .....(i)}$$

(desorption of water controlling)

If it is assumed that K_{N_2} is small enough to be neglected which seems probable since nitrogen does not react with barium sulphate and is, therefore, unlikely to be chemisorbed at the barium sulphate surface, then the equations become,

$$r_o = kp_{H_2} \quad \text{.....(j)}$$

(rate of chemisorption of hydrogen controlling)

$$r_o = kp_{H_2}/(1 + K_{H_2} p_{H_2}) \quad \text{.....(k)}$$

(rate of surface reaction controlling)

$$r_o = kp_{H_2}/(1 + K_{H_2} p_{H_2}) \quad \text{.....(l)}$$

(rate of desorption of water controlling)

Now it was found that the initial rate of reaction is not sensitive to variations in hydrogen partial pressure, hence the rate of chemisorption of hydrogen can be eliminated as a controlling factor by inspection of equations (j), (k), and (l).

(2) Water-hydrogen mixtures

In the case where water-hydrogen mixtures were used as the reducing gas, $p^*_{H_2}$ is small because of the large value of the equilibrium constant ($K_e \doteq 10^6$) for the reduction of barium sulphate by hydrogen. There is no inert gas present so p_i is zero and equations (e) and (f) become,

$$r_o = kp_{H_2}/(1 + K_{H_2O} + p_{H_2}(K_{H_2} - K_{H_2O})) \quad \text{.....(m)}$$

(rate of surface reaction controlling)

$$r_o = kp_{H_2}/(1 + K_{H_2} p_{H_2}) \quad \text{.....(n)}$$

(rate of desorption of water controlling)

As information is not available regarding the relative magnitudes of the chemisorption equilibrium constants K_{H_2} and K_{H_2O} it is not possible to eliminate either of these alternative controlling factors (surface reaction rate and desorption rate) by inspection of equations (m) and (n) since either equation could satisfy the condition that the initial rate be insensitive to variation of the partial pressure of water (and hence hydrogen) in the reducing gas. Insufficient experimental data are available to attempt the evaluation of any of the constants in equations (k), (l), (m), and (n).

It may be concluded from the analysis under (1) and (2) that if hydrogen is strongly chemisorbed on the surface of the barytes then the rate of reaction is determined either by the number of hydrogen atoms, or molecules, combining with an adjacent oxygen atom in the underlying barium sulphate lattice or by the rate of desorption of the water molecules so formed.

It is difficult to explain the variation in the rate per unit area of interface as the reaction proceeds (see Fig. 22) in terms of desorption control since it might be expected[90], that under such circumstances, the rate of reaction per unit area of interface would be constant for the whole course of the reaction. Fig. 22 shows that the rate per unit area at 1000°C varies by as much as 50% during the course of the reaction. Control of the rate of reaction by the surface reaction does, therefore, seem to offer a more satisfactory

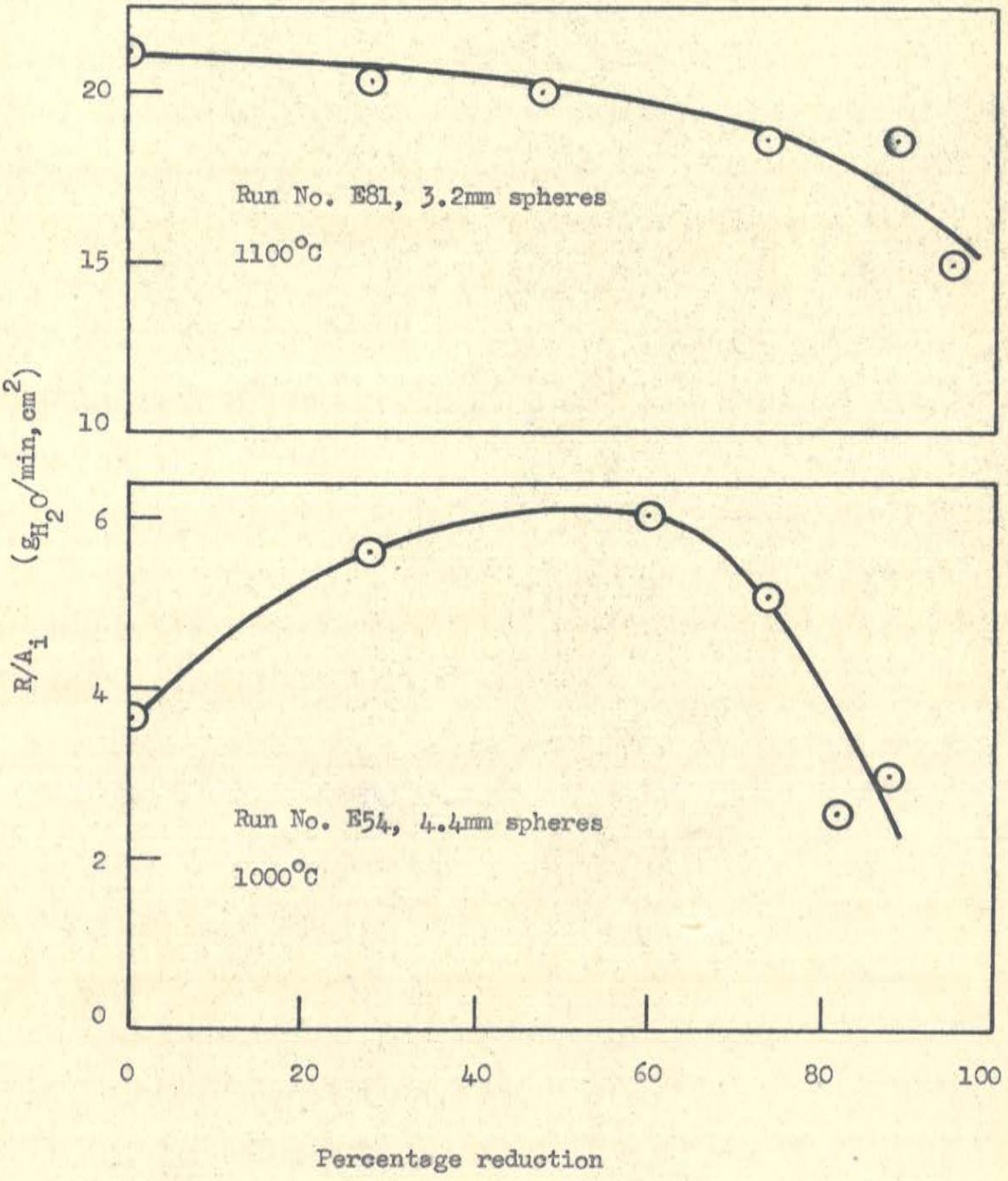

Fig. 22. Variation of the rate per unit area of interface as the reaction proceeds

explanation for the reaction mechanism.

It might be considered that the rate determining factor was the rate at which hydrogen atoms in the chemisorbed hydrogen layer were raised to a sufficiently high energy level to react with the underlying barium sulphate lattice or, alternatively, that the controlling step was the creation, at the solid surface, of a site having sufficient energy to react with a chemisorbed hydrogen atom. This last explanation is quite attractive in the present case since it was found that variations in the solid properties, viz. percentage of impurities and crystal structure, cause variations in the initial and subsequent reaction rates. This type of mechanism has been put forward by Roberts and Anderson[91] to explain the reduction of zinc oxide by hydrogen although Roberts and Anderson doubt the existence of a chemisorbed hydrogen layer at the surface of the zinc oxide. They point out that there is some evidence to suggest that reaction takes place directly a hydrogen molecule bombarding the surface strikes a suitable high energy site. However, the presence or absence of a chemisorbed hydrogen layer does not affect the argument if the rate of formation of high energy sites or lattice defects is the rate controlling factor since, in either case, the reaction rate will be insensitive to changes in hydrogen and water vapour partial pressures.

Roberts and Anderson[91] enumerate two classes of lattice defects which provide suitable sites for reaction. They are (a) thermal

defects caused by the migration of an atom in the crystal lattice from its normal position to an interstitial position, and (b) "biographical" defects caused by foreign atoms or ions in normal crystal lattice positions or by ions of abnormal valency in normal lattice positions. This provides a ready explanation for the acceleration of the reaction rate by silica and iron impurities. Compounds such as iron, which readily gain or loose electrons, are capable of forming both types of "biographical" crystal defects and hence are efficient in accelerating reactions which depend on the rate of formation of lattice defects.

Prout and Tompkins[87] have suggested that the lattice defect theory provides a satisfactory basis for explaining the autocatalytic type of rate curves obtained during the thermal decomposition of potassium permanganate. They point out that the product layer will, in general, have a crystal structure differing in geometric form and dimensions from the underlying solid reactant. Consequently there will be a zone between the two solid phases, possibly a small multiple of the unit crystal cell length in thickness, where collapse of the original crystal structure and formation of the product structure will be taking place. The result is that the interfacial region will be one of high energy or will contain a high concentration of lattice defects. If it is assumed that the reaction is initiated at a few high energy points on the surface of the solid and that the reaction zones then spread over the surface as well as moving inwards, it can be seen that the interfacial area during the initial stages of the reaction will

increase and this, in turn, means that the number of high energy sites available for reaction will also increase rapidly and consequently the reaction will be autocatalytic. The maximum rate will occur when the reaction zone covers the surface of the particle. The reduction of barium sulphate appears to conform to the requirements of this theory since the crystal structure of the barium sulphide (cubic) is different to the structure of the barium sulphate (rhombic). Also, heating barytes for a short time to above the temperature at which transformation to a monoclinic structure takes place and then reducing at a lower temperature accelerates the rate of reaction. This appears to confirm the theory of Prout and Tompkins[87] that decay of one type of crystal structure and growth of another type leads to formation of high energy sites suitable for reaction with the gas phase.

It follows from the theory of lattice defects presented by Roberts and Anderson[91] that the number of thermally produced defects will increase with rising temperature while the number of "biographical" defects will remain constant. It seems reasonable to suppose, therefore, that there will be more lattice defects initially present on the surface of a barytes particle at 1100°C than at 1000°C. This means that the reaction will be initiated at a much larger number of points on the surface at the higher temperature and consequently the individual reaction zones will cover the surface at a much earlier

stage in the reaction. This may possibly explain why the rate vs time curves at 1100°C show no maximum value in contrast to those at 1000°C and 1050°C (E72) which show a well defined maximum.

This hypothesis is, however, unable to explain why Sample F, which was low in silica and iron, gave rate vs time curves which showed no maximum value. These results, although scanty, do appear to indicate that the autocatalytic nature of the reaction may in part, at least, be due to the presence of impurities.

4:5 Conclusions

The immediate requirements of the investigation were satisfied by the information summarised below.

(1) The rate of reduction of barytes by hydrogen is not controlled by diffusion at temperatures up to 1100°C.

(2) At 1100°C the rate is of the first order with respect to the barium sulphate phase and of zero order with respect to the gas phase so long as the hydrogen partial pressure does not fall to a very low value.

(3) The rate of reaction at 1100°C is satisfactorily correlated by the empirical equation,

$$R/s = K(1 - f)/100$$

for which values of K, depending on the solid composition, may be obtained from Fig. 21, page 113. This equation should provide a

sound basis for predicting the rate of reduction to be expected in a fluidized reactor at 1100°C.

5. PREDICTION OF RATES FOR FLUIDIZED BEDS

The aim of this project was to elucidate the problems associated with the prediction of rates of reaction in dynamic (fluidized) systems using the results of bench scale tests on small fixed beds. A comparison was to be made of the rate at which barytes was reduced by hydrogen in a fluidized bed with the corresponding rate predicted from the results of bench scale experiments on a fixed differential bed. This Section deals with the prediction of rates using the rate data previously obtained (see Section 4) using a differential bed reactor. Although these calculations were necessarily carried out concurrently with the experimental determination of rates in the fluidized reactor it is convenient to discuss the problem under a single heading. Further, since this Section anticipates some of the information contained in Section 6, it enables the reader to make a smooth transition from rate work in fixed differential beds to rate work in fluidized beds.

It will be recalled that, only at 1100°C, could the rate data obtained from fixed differential beds be satisfactorily correlated and, consequently, attention was focussed on this temperature when working with fluidized beds. However, in developing an operating technique with the fluidized reactor it was necessary to carry out a number of tests at 1000°C before proceeding to the higher temperature, and, therefore, an attempt was made to predict rates

for this temperature using the rate vs time curves obtained from differential bed experiments with material similar to that used for fluidizing. These predictions were not as precise as those made for 1100°C but, never-the-less, they did provide a basis for some useful comparisons between predicted and experimental rates at the lower temperature.

The experimental programme at 1100°C included the following tests.

(1) Reduction by hydrogen, of a fixed bed containing 1500g of +14-10# barytes to test the validity of the work on differential beds.

(2) Reduction, by hydrogen, and by nitrogen-hydrogen mixtures, of fluidized beds containing 1500g of +14-10# barytes to check the method used for predicting rates in fluidized beds.

(3) Reduction, by hydrogen, of fluidized beds containing 750g of +14-10# barytes to check the effect of variation in bed depth on the method of rate prediction.

During the preliminary stage of the experimental work on the fluidizer, fixed and fluidized beds were reduced by hydrogen at 1000°C, and later, fluidized beds were also reduced at 900°C to obtain information on some points arising out of this preliminary work.

The prediction of rates for each of these cases will be considered in turn.

5:1 Prediction of rates at 1100°C

Although it was not possible to obtain rate data in a differential bed for +14-10# barytes because of the short time interval required for complete reduction, the correlation developed (see Section 4:4:6, page 110) permitted a rate vs time curve for this material to be deduced (see Appendix G). The results of these calculations are summarised in Table VIII.

TABLE VIII

Rate data for a +14-10# sample of barytes reduced in a differential bed at 1100°C

% Redn.	Rate x 10^2 (g_{BaSO_4}/min, g_{sample})	Time (min)
0	70	0
20	56	0.3
40	42	0.7
60	28	1.3
80	14	2.3
100	0	9

5:1:1 Initial bed weight of 1500g

It is logical to consider the prediction of a rate of reaction for a fixed bed before proceeding to the more complex case of a fluidized bed.

(1) Fixed bed using hydrogen as reducing gas

A fixed bed containing 1500g of +14-10# barytes is to be reduced at 1100°C using a hydrogen flow rate of 60 litre/min N.T.P.. It was found when working with differential beds (see Section 4:4:2, page 95) that the initial rate of reaction at 1100°C was not sensitive to variations in the water vapour content of the reducing gas so the initial rate of reaction for a 1500g bed would be 1050g_{BaSO_4}/min, g_{sample} if sufficient hydrogen was available. However this rate of reaction is equivalent to a hydrogen consumption rate of 400 litre/min N.T.P. which is much greater than the rate of 60 litre/min at which hydrogen is being pumped into the bed. Consequently, the initial rate of reaction will be limited by the availability of hydrogen and the gas leaving the bed will, initially, have a water vapour content close to the equilibrium concentration of 97% by volume. In this case the composition of the gas leaving the bed will be taken as 95% by volume of water vapour. The initial rate of reaction for a 1500g bed will, therefore, be 10×10^{-2} g_{BaSO_4}/min, g_{sample}.

The work on differential beds also indicated that, not only was the initial rate independent of the water vapour concentration, but the subsequent rate of reaction was also virtually unaffected, therefore, the measured rate of reaction will remain constant until the barytes is reduced to such an extent that the measured rate of reaction, determined by the rate at which hydrogen is supplied, is equal to the rate which would be obtained in a differential bed. Plotting the data in Table VIII reveals that a sample of +14-10# barytes would give a

rate of reaction of 10×10^{-2} $g_{BaSO_4}/min, g_{sample}$ at 86% reduction. At a constant rate of 10×10^{-2} $g_{BaSO_4}/min, g_{sample}$ it will take 8.6 minutes to reach this degree of reduction in the 1500g bed. After 8.6 minutes the rate vs time curve will fall away along a curve similar to the one for a differential bed. Thus curve (1) in Fig. 23a may be obtained.

(2) Fluidized bed using hydrogen as reducing gas

In predicting the rate of reaction for a fluidized bed it must be realised that part of the gas will pass up through the bed as bubbles and have little contact with the solid particles. Toomey and Johnstone[33] suggest that all gas in excess of that required to produce incipient fluidization will pass up through a bed of coarse material as bubbles. They picture the fluidized bed as consisting of two phases, a continuous phase having a porosity equal to the porosity which the bed had at the point of incipient fluidization, wherein the gas is in intimate contact with the solid, and a discontinuous phase, comprising the bubbles of gas passing up through the bed. It is generally agreed [45)55)70)] that this by-passed gas will pass through a shallow bed relatively unaffected by any reaction taking place in the bed, however, the only experimental data available on the rate of mass transfer between continuous and discontinuous phases is that due to Shen and Johnstone[32] who studied the rate of decomposition of nitrous oxide in a fluidized catalyst bed. They carried out their work on 100# material (particle density = 2 g/cm^3) in beds having L/D ratios of between 20 and 50. In the

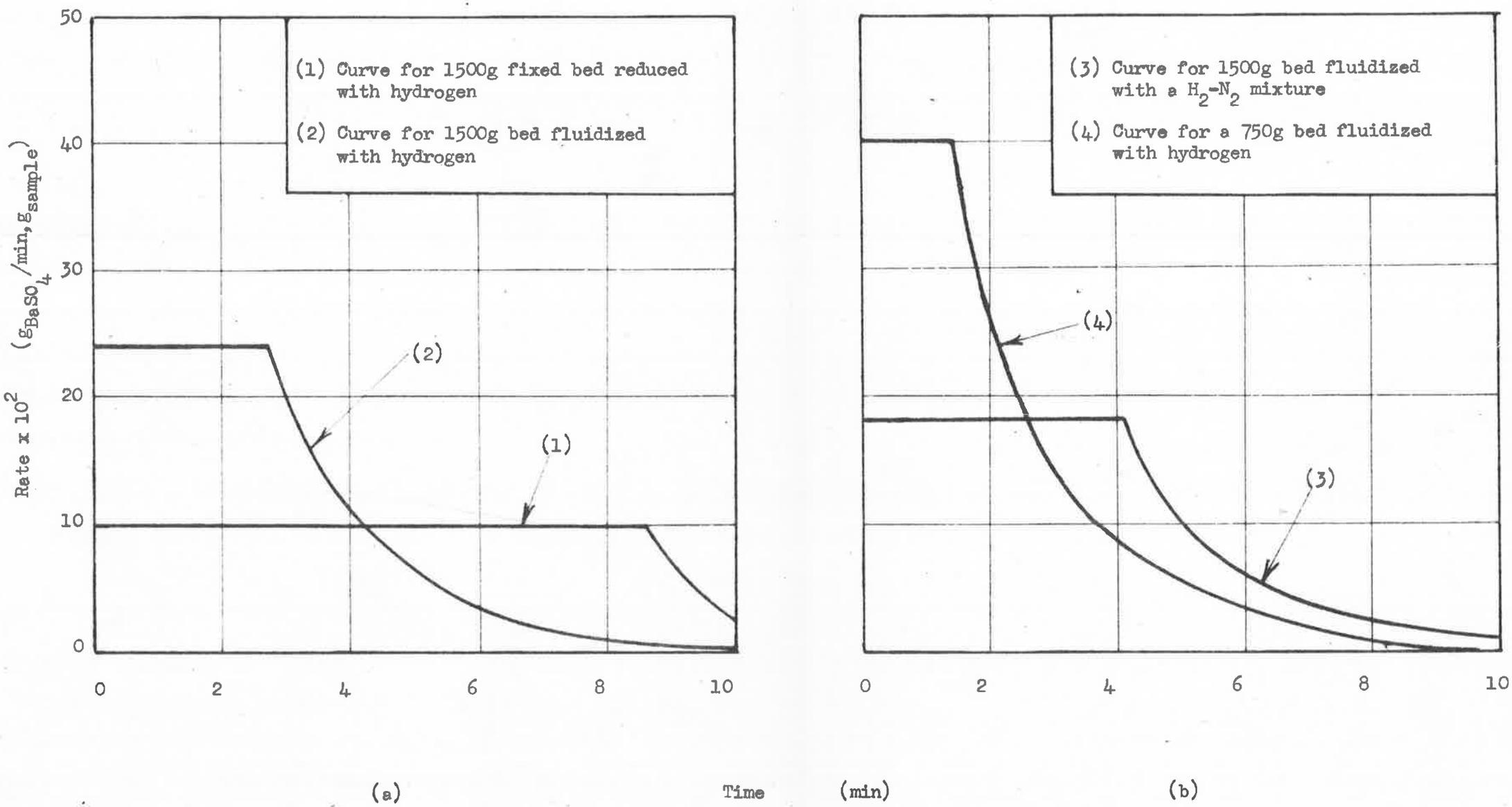
(1) Curve for 1500g fixed bed reduced with hydrogen
(2) Curve for 1500g bed fluidized with hydrogen
(3) Curve for 1500g bed fluidized with a H_2-N_2 mixture
(4) Curve for a 750g bed fluidized with hydrogen
Rate x 10^2 (g_{BaSO_4}/min, g_{sample})
Time (min)
0
10
20
30
40
50
0
2
4
6
8
10
(a)
(b)

Fig. 23. Predicted rate vs time curves for fluidized and fixed beds of +14-10# barytes reduced at 1100°C

present case it was necessary (see Appendix E, page 243) to work with +14-10# barytes (particle density = 4.3 g/cm^3) in beds having L/D ratios of between 1 and 3. Since particle size and density, together with the L/D ratio, have a very marked effect on the properties of a fluidized bed it was felt that such serious errors would be involved in extrapolating the results of Shen and Johnstone[32] for the system N_2O-N_2-O_2 to the present case of the system H_2-H_2O that the complication of such an extrapolation was not justified. It was decided, therefore, simply to estimate the percentage of water vapour in the by-passed gas leaving the bed, using the results obtained by Shen and Johnstone as a qualitative guide.

Consideration of the data in Table VIII shows that initial rate of reaction for a 1500g bed of +14-10# barytes would be 1050g$_{BaSO_4}$/min, if sufficient hydrogen was available. However, this rate of reaction is equivalent to a hydrogen consumption rate of 400 litre/min N.T.P. which is greater than the rate of 185 litre/min N.T.P. at which hydrogen is being pumped into the bed and, consequently, the initial rate of reaction will be limited by the availability of hydrogen. Since the initial rate of reaction at 1100°C is not sensitive to the presence of water vapour it is probable that the gas leaving the continuous phase of the bed where gas and solid are in intimate contact will, initially, have a water vapour content close to the equilibrium concentration of 97% by volume. The water vapour content of this gas will, therefore, be taken as 95% by volume.

At 1100°C, the minimum flow rate of hydrogen needed to produce fluidization is 110 litre/min N.T.P. (see Appendix F, page 297) so that, adopting the practice of Shen and Johnstone[32], it may be considered that 110 litre/min N.T.P. of hydrogen is passing up through the continuous phase of the bed while the balance of the hydrogen supplied, 75 litre/min N.T.P., passes up through the bed as bubbles. Although the hydrogen passing through the bed as bubbles is not in intimate contact with the barytes particles there will be a considerable transfer of water vapour between continuous and discontinuous phases since the bed is nine inches deep and the gas composition in the upper part of the continuous phase is near 100% water vapour. It will be assumed that the gas leaving the discontinuous phase of the bed initially contains 50% by volume of water yielding an initial rate of reaction for a 1500g bed of 24×10^{-2} $g_{BaSO_4}/min, g_{sample}$.

This initial rate may be combined with the rate data in Table VIII, page 127, to give the rate vs time curve for a 1500g bed of barytes, reduced with hydrogen at 1100°C. This is curve (2) in Fig. 23a, page 130.

(3) Fluidized bed using hydrogen-nitrogen mixture as reducing gas

In this case a bed of +14-10# barytes having an initial weight of 1500g is to be fluidized, at 1100°C, with 150 litre/min N.T.P. of a hydrogen-nitrogen mixture containing 10% by volume of nitrogen.

Under these conditions the minimum flow rate needed to produce fluidization is 90 litre/min N.T.P.. This means that 60 litre/min

N.T.P. of the gas will be by-passed through the bed in bubbles. Since the gas mixture contains 10% of nitrogen the gas leaving the continuous phase of the bed will initially contain 85% by volume of water vapour. Reynolds Number for the bed is the same in this case as it was for fluidization with hydrogen so the gas leaving the discontinuous phase will be assumed to contain the same percentage of water vapour as previously, viz. 50% by volume, since Shen and Johnstone[32] found that the transfer coefficient between continuous and discontinuous phases depended upon the value of Reynolds Number for the bed. Consequently, the maximum rate of reaction possible for a 1500g bed is $18 \times 10^{-2} g_{BaSO_4}$/min, g_{sample}.

Combination of this maximum rate with the rate vs composition and rate vs time data in Table VIII, page 127, leads to the rate vs time curve (3) shown in Fig. 23b, page 130.

5:1:2 Initial bed weight of 750g

The only case to be considered is for a 750g bed of +14-10# barytes fluidized with hydrogen at a flow rate of 185 litre/min, measured at N.T.P..

The data in Table VIII, page 127, shows that the initial rate of reaction for a 750g bedof +14-10# barytes would be equivalent to a hydrogen consumption of 200 litre/min N.T.P.. This rate of consumption is greater than the rate of 185 litre/min N.T.P. at which hydrogen is being pumped into the bed, therefore, it appears likely that the gas initially leaving the continuous phase of the bed will

contain 95% by volume of water vapour.

Since the hydrogen flow rate needed to produce incipient fluidization is 110 litre/min N.T.P. it follows that 75 litre/min N.T.P. of hydrogen will be by-passed through the bed in bubbles. However, in this case, the bed depth is only four inches so there will be less transfer of water vapour from the continuous to the discontinuous phase than was the case for a 1500g bed (see above); there is less bed agitation and a smaller contact time. Therefore, it will be assumed that the by-passed gas leaving the bed at the beginning of the reaction contains 10% by volume of water vapour.

These figures for the water vapour contents of the exit gases give a maximum rate of reaction, for a 750g bed of +14-10# barytes at 1100°C, equal to 40×10^{-2} $g_{BaSO_4}/min, g_{sample}$ and yield the rate vs time curve (4) in Fig. 23b, page 132.

5:2 Prediction of rates at 1000°C

The rate vs time data for a typical +14-10# sample of barytes, reduced in a differential bed at 1000°C, are contained in Table IX.

5:2:1 Initial bed weight of 1500g

Here again the case for a fixed bed will be considered before proceeding to fluidized beds

(1) Fixed bed using hydrogen as reducing gas

A fixed bed containing 1500g of +14-10# barytes is to be reduced with hydrogen at a flow rate of 120 litre/min N.T.P..

TABLE IX

Rate data for Run No. E52* (+14-10#) obtained at 1000°C in a differential bed

Time (min)	Rate x 10^2 (g_{BaSO_4}/min, g_{sample})
0	8.8
1	10.4
3	11.4
5	9.1
7	6.5
9	3.9
11	1.6
14	0.3
17	

* Taken from Appendix C, page 204

It was found (see Section 4:4:2, page 101) that the presence of water vapour had little effect on the initial rate of reaction and consequently the initial rate for this case should be the same as the initial rate of 8.7×10^{-2} g_{BaSO_4}/min, g_{sample} (see Table IX) obtained in a differential bed. This means that the gas leaving the 1500g bed at the beginning of reduction will contain 50% by volume of water vapour. It will be assumedthat the mean water vapour content of the gas in the bed may be taken as the arithmetic mean of inlet and outlet concentrations,

i.e. 25% by volume. Examination of Fig. 15, page 49, shows that the presence of 20% of water vapour in the reducing gas retards the maximum rate by about 20%. Reconciling this information with the data in Table IX gives a maximum rate of reaction for a 1500g bed equal to 9×10^{-2} $g_{BaSO_4}/min, g_{sample}$ occurring about 5.5 minutes after the start of reduction.

The mean water vapour content of the gases in the bed will decrease as the reaction progresses and, since detailed information on the retarding effect of water vapour is not available, the rate vs time curve will, for simplicity, be represented by two straight lines intersecting at the point of maximum rate. The area under a rate vs time curve is equal to the fraction of the sample reduced so the curve for a 1500g bed of +14-10# barytes can be simply constructed; the initial and maximum rates are known together with the time at which the maximum rate occurs. This curve is labelled (1) in Fig. 24.

(2) Fluidized bed using hydrogen as the reducing gas

In this case a fluidized bed containing 1500g of +14-10# barytes is to be reduced with hydrogen at a flow rate of 185 litre/min N.T.P.

A hydrogen flow rate of 130 litre/min N.T.P. is needed to produce incipient fluidization (see Appendix F, page 296) so that 55 litre/min N.T.P. may be considered to pass up through the bed in bubbles. The water vapour content of this by-passed gas leaving the discontinuous phase of the bed will be lower than that of the

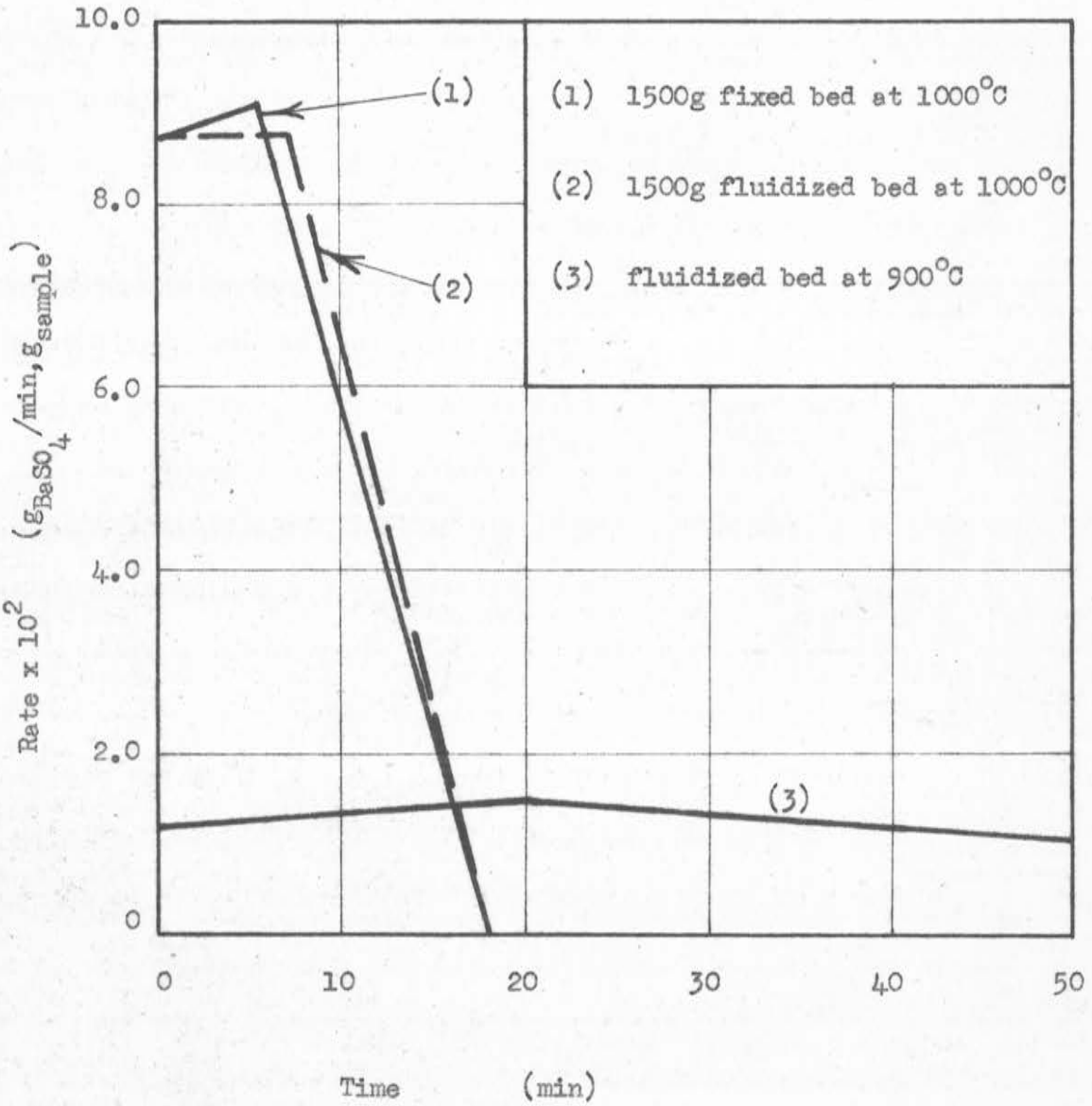

Fig. 24. Predicted rate vs time curves for +14-10# barytes reduced in fixed and fluidized beds at 1000°C and 900°C

gas leaving the continuous phase, where gas and solid are in intimate contact.

The initial rate of reaction should be the same for the fluidized bed as for the fixed bed, viz. 8.7×10^{-2} $g_{BaSO_4}/min, g_{sample}$, since the initial rate is not sensitive to changes in the water vapour partial pressure. This means that the average water vapour content of the gas leaving the bed during the initial phase of the reaction will be 35% by volume. If the water vapour content of the gas leaving the discontinuous phase of the bed, during this initial period, is taken as 10% then the concentration of water vapour in the gas leaving the dense phase must be 45%.

In order to estimate the mean value of the water vapour concentration in the continuous phase of the bed it is necessary to have some idea of the degree of back mixing occurring in the gas. Gilliland and Mason[55], using tracer gases, found that there was little or no back mixing in the gas phase of fluidized beds of this diameter, however, in this case, where a gas-solid reaction is taking place and vigorous mixing of the solids is occurring, it seems probable that some of the gas will be carried round the bed by the reacting solid. Consequently there will be some back mixing of water vapour in the gas phase of the bed. This will lead to a higher mean partial pressure of water vapour in the continuous phase of the bed than would have been the case if there was no back mixing. Therefore, the maximum mean water vapour concentration for the continuous phase of the bed will be taken as 30% by volume.

No data are available for reaction rates at water vapour concentrations greater than 20%. However, it seems reasonable to assume that the maximum rate of reaction at a water vapour concentration of 30% will be lower than the corresponding case for 20% so the maximum rate of reaction for the fluidized bed will be taken as equal to the initial rate of 8.7×10^{-2} $g_{BaSO_4}/min, g_{sample}$. The rate, vs time curve for a fluidized bed containing 1500g of +14-10# barytes will, therefore, take the shape of curve (2) in Fig. 24.

5:2:2 Initial bed weight of 750g

Here again the initial rate of reaction for a bed of +14-10# barytes fluidized with 185 litre/min N.T.P. of hydrogen will be 8.7×10^{-2} $g_{BaSO_4}/min, g_{sample}$. Therefore, if it is assumed that there is no water vapour in the by-passed gas leaving the bed, then the gas leaving the continuous phase will have a water vapour content of 30% by volume during the initial stages of the reaction. If it is further assumed that the mean water vapour content of the gas in the continuous phase, during this period, is 20% then the rate vs time curve for a 750g fluidized bed will be identical with the curve for a 1500g fixed bed, i.e. curve (1) in Fig. 24, page 137.

5:3 Prediction of rates at 900°C

No samples of +14-10# barytes were reduced in a differential bed at 900°C. However, data were obtained for +10-8# material at both 900°C and 1000°C. Assuming that the initial rate of reaction at 900°C is proportional to the surface area of the solid, as was

the case at 1000°C and 1100°C, then it can be calculated (see Appendix G) that the initial rate of reaction for +14-10# material at 900°C is 1.2×10^{-2} $g_{BaSO_4}/min, g_{sample}$.

A rate vs time curve is to be predicted for only one case, a 1500g bed of +14-10# barytes fluidized with hydrogen at a flow rate of 185 litre/min N.T.P..

The results of the work on differential beds at 1000°C (see Section 4:4:2, page 101) suggest that the initial rate of reaction at 900°C will not be sensitive to variations in water vapour concentration. Accordingly, the average percentage of water in the gas leaving the 1500g bed at the beginning of the reaction may be taken as 3% by volume. In the absence of experimental data regarding the retardation of the rate of reaction at 900°C by water vapour it will be assumed that a concentration of 3% would not seriously retard the maximum rate of reaction. Therefore, the maximum rate for +14-10# material will be taken as 130% of the initial rate, as was the case for Run No. E88 (See Appendix C, page 220), occurring twenty minutes after the beginning of reduction.

Curve (3) in Fig. 24, page 137, is obtained by assuming that the rate vs time curve for +14-10# barytes reduced at 900°C may be satisfactorily represented by two straight lines intersecting at the point of maximum rate.

6. DETERMINATION OF REACTION RATES - FLUIDIZED BEDS

In Section 5 the rate data, obtained by reducing barytes with hydrogen in a small differential bed, were used to predict the rate at which barytes would be reduced in a fluidized bed. The objective being to compare these predicted rates with the rates obtained by experiment on a fluidized reactor so that the problems associated with such predictions might be elucidated. This Section sets out the results of the work on the fluidized reactor, including a comparison of measured and predicted rates.

It was necessary to carry out a series of preliminary experiments on the fluidizer to develop an experimental technique which would yield reproducible results; the data so obtained, although not highly accurate, also served as a basis for planning the following tests. The results of this preliminary phase of the work are presented in Sections 6:1 and 6:2. Throughout the discussion the actual rates obtained are compared with the predicted rates calculated in Section 5.

The results of the preliminary experiments showed that, at 1000°C, the measured rate of reaction was much slower than the predicted rate so the final series of tests were designed,

(1) to obtain rate data at 1100°C,

(2) to find out if there was any better agreement between measured and predicted rates at 900°C than was the case at 1000°C.

(3) to see if the presence of water vapour in the gas phase of the fluidized beds had a greater retarding effect on the rate of

reaction than the tests on differential beds had indicated, and

(4) to find out if the presence of hydrogen sulphide seriously retarded the rate of reaction.

Descriptions of these experiments and the results obtained are set out in Sections 6:3 and 6:4. The conclusions drawn from this part of the work are contained in Section 6:5.

6:1 Experimental procedure (Preliminary stage)

The fluidized reactor was operated on a batch system since it was necessary that the dispersed solids in the bed should be held in contact with the reducing gas for a determinable period of time. Thus the progress of reduction could have been followed by metering the quantities of any of the reactants or products participating in the reaction

$$BaSO_4 + 4H_2 = BaS + 4H_2O \quad \ldots\ldots\ldots\ldots\ldots\ldots (3)$$

In this case the simplest approach, experimentally, was to measure the rate at which hydrogen was consumed.

6:1:1 Apparatus

The design of the fluidizing apparatus is covered in detail in Appendix E. The flowsheet which was evolved is shown in Fig. 25 and an arrangement drawing showing the various components is given

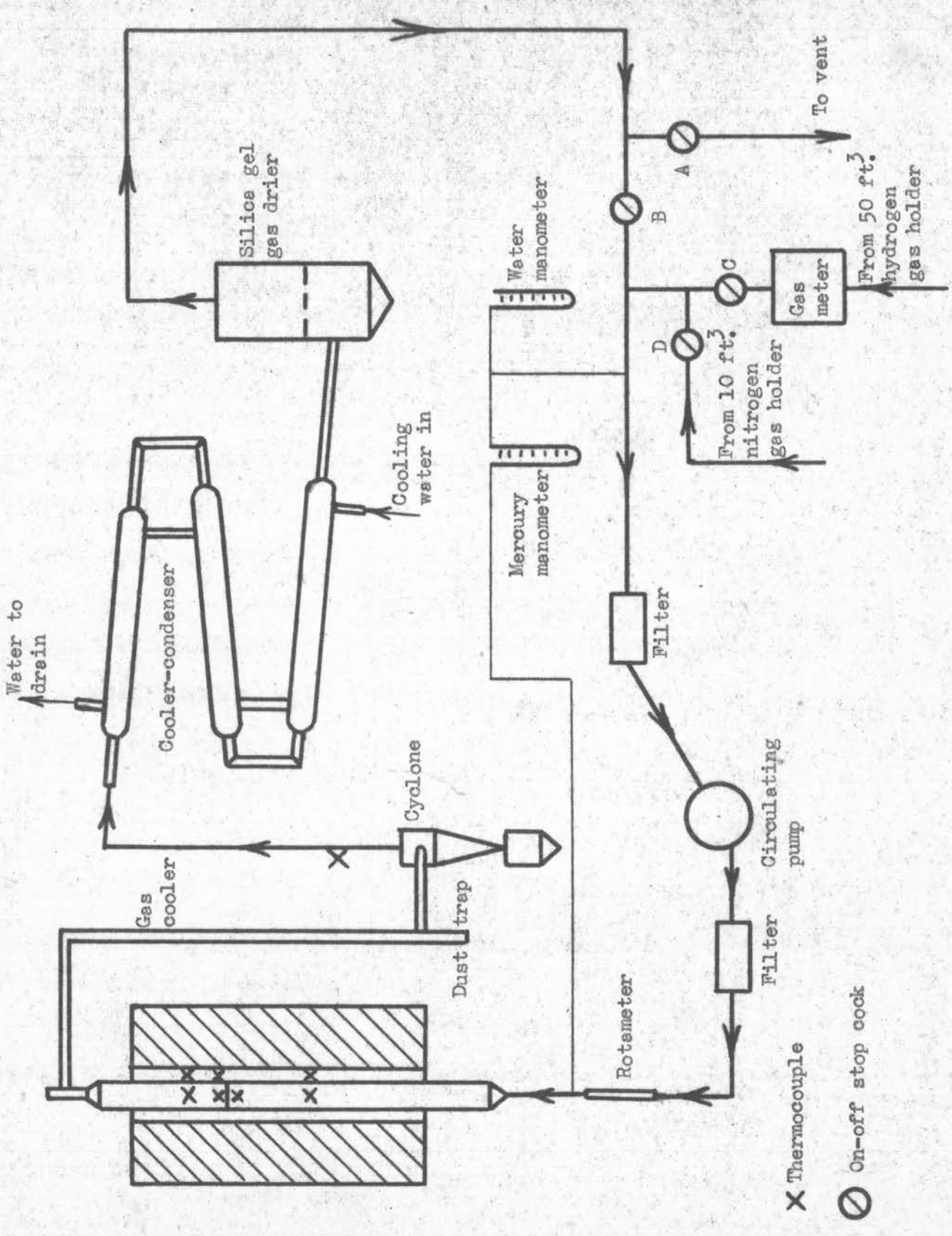

Fig. 25. Schematic flowsheet for fluidizing apparatus

in Fig. 26. Fig. 27 is a photograph showing the general layout of the plant. In Appendix F the performance of the fluidizing apparatus is compared with the performance predicted from the design calculations.

The temperature of the fluidized bed was measured by two centrally placed chromel-alumel thermocouples which had previously been standardized against a substandard Pt/Pt-Rh couple. These thermocouples were protected by a silica sheath. The measuring element was a Cambridge wall-pattern temperature indicator to which the thermocouples were connected through a multi-position switch. The temperature indicator had been standardized using a Cambridge portable potentiometer and it was estimated that the set up would permit measurement of the temperatures at the thermocouple junction to an accuracy exceeding $\pm 5^{\circ}C$ at $1000^{\circ}C$. The silica thermocouple sheath was rammed into the stainless steel pipe at the top of the reactor with asbestos paper, which had previously been soaked in a suspension of magnesium hydroxide, to provide a gas tight joint. Details of this joint and of the joint supporting the silica thermocouple sheath in the preheater tube are shown in Fig. 28.

Caustic soda pellets were placed in the bottom of the silica gel gas drier (see Figs. 25 and 26) to absorb any hydrogen sulphide which might be present in the gases leaving the cooler-condenser.

The volume of make-up hydrogen entering the circulating system, and hence the rate of reaction, was measured by a bellows type meter

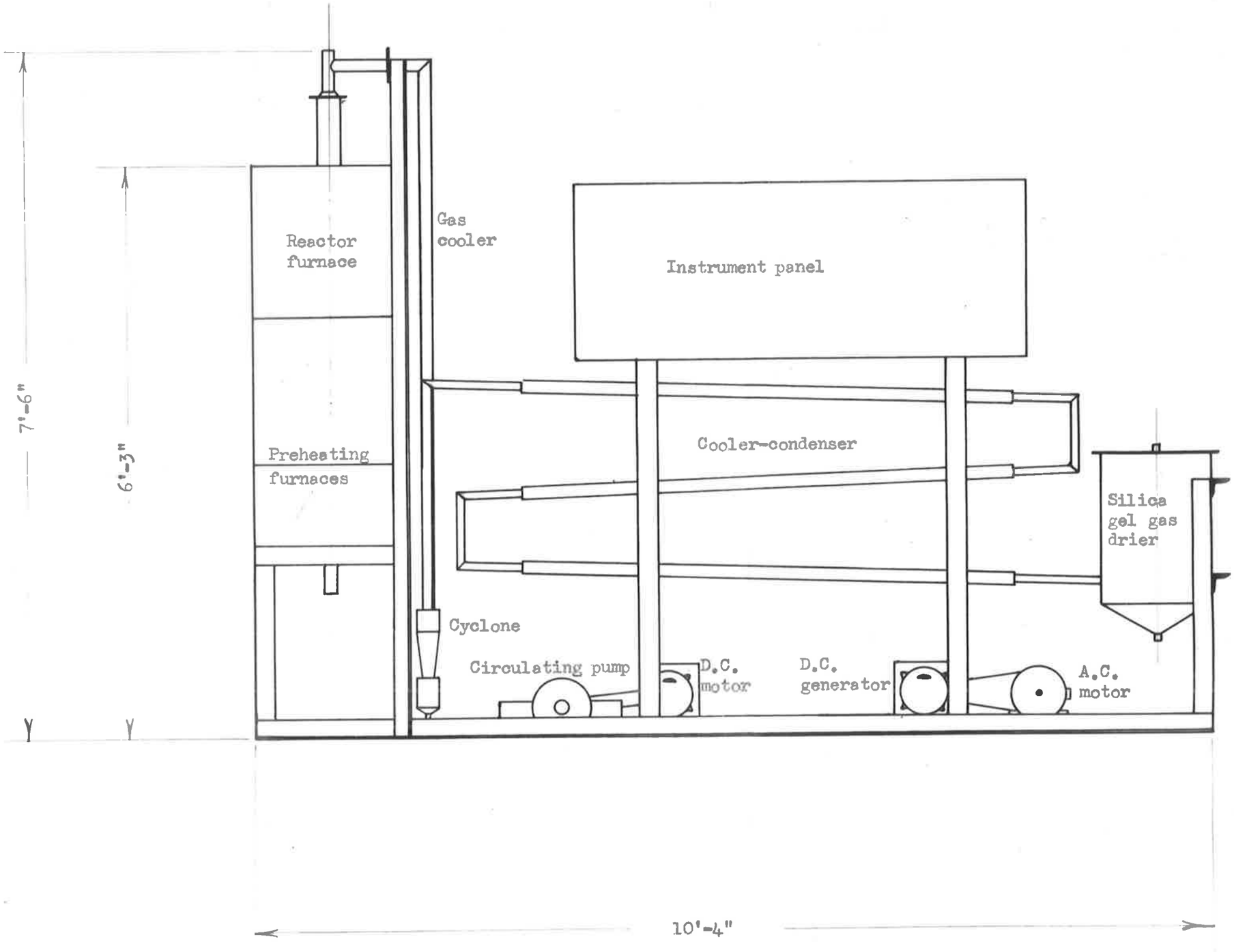

Fig. 26. Arrangement drawing of fluidizer

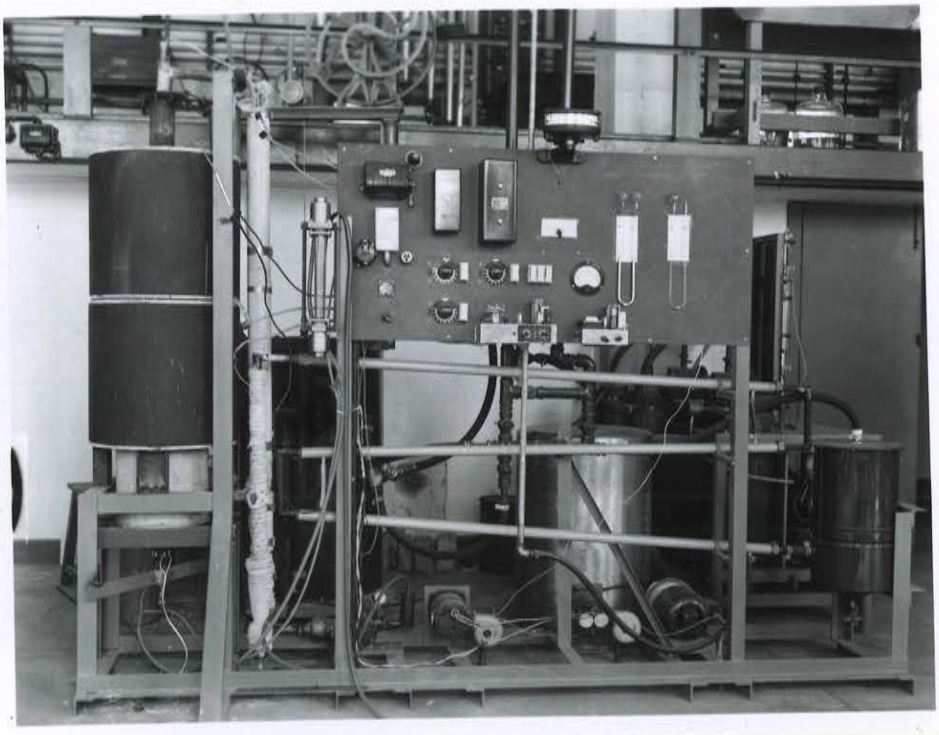

Fig. 27. Photograph of the fluidizer

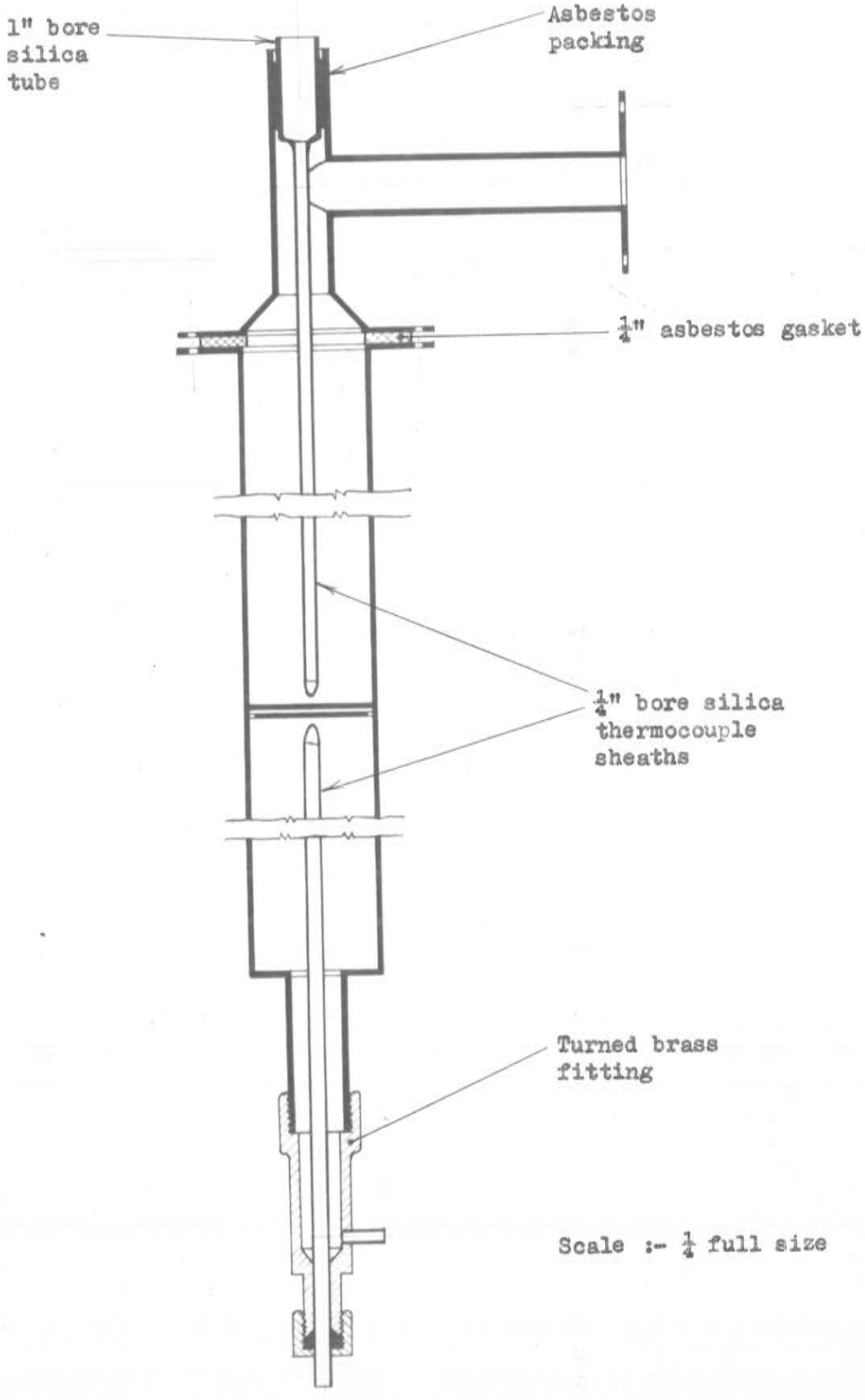

Fig. 28. Detail of the fluidizing reactor showing thermocouple sheaths

obtained from the South Australian Gas Co.. This meter had been specially calibrated and was guaranteed to be accurate to ±2%. The scale was divided into quarter cubic foot intervals.

A perspex replica of the stainless steel reactor was also made up and barytes beds were fluidized in this to permit visual observation of the type of fluidization likely to be obtained in the reactor.

6:1:2 Experimental technique

After a bed of crushed barytes had been loaded into the reactor and subsequent assembly of the unit had been completed, valves A and D (see Fig. 25, page 143) were opened and all the air in the apparatus was purged through the vent by pumping nitrogen from the ten cubic foot gas holder. Valve A was then closed and valve B opened so that nitrogen could be circulated around the apparatus. The furnaces were then switched on and the bed and preheater were brought up to temperature while the nitrogen flow rate was adjusted to keep the bed fluidized. When the bed temperature had stabilized at the set value required for a run, the preheater temperatures were lowered to levels which had previously been ascertained by trial and error. At this point hydrogen was admitted to the apparatus by opening valve C and closing D; the stop clock was started simultaneously with the opening of C. Venting to atmosphere of the gas leaving the drier was continued until all the nitrogen in the apparatus had been replaced by hydrogen (usually required the passage of about 5 cubic feet of hydrogen) and then valves A and B were turned so that the gas leaving

the drier again passed to the inlet of the circulating pump. Timing of the volumes measured by the gas meter was then commenced and these observations were continued until no more hydrogen was consumed or until the rate of consumption decreased to a constant value equal to the rate at which hydrogen was leaking from the apparatus.

Great care was taken to ensure that the pressure at the inlet to the circulating pump, which was the point of lowest pressure, was always one or two inches of water above atmospheric. Both hydrogen and nitrogen gas holders were counterbalanced so that a positive pressure was maintained at this point under all conditions. This ensured that no air could leak into the apparatus and so eliminated the danger of confined explosions.

6:1:3 Raw materials

The barytes used for fluidizing was the same as that used in the work on fixed beds, viz. a mineral having the average composition shown.

$BaSO_4$	97.5%
SiO_2	2.1%
Fe_2O_3	1.5%

Before crushing and screening the lumps of mineral were heated to about 800°C in a muffle furnace to give material which would not decrepitate on subsequent heating. Most of the tests were carried out on a +14-10# (Tyler) crushed, screened, and washed sample.

Hydrogen was generated from caustic soda solution in a Knowles "double depth" electrolytic cell and then stored in a fifty cubic foot gas holder until required. The purity of the hydrogen produced and stored in this way was found to be about 99.9%.

Nitrogen was purchased in cylinders and fed into the ten cubic foot gas holder through a reducing valve.

6:1:4 Treatment of results

The approach adopted, viz. measuring the time for a known volume of hydrogen to be consumed, yielded a series of times for constant increments of volume. These volumes (usually one cubic foot) were converted to the equivalent weight of barium sulphate and divided by the time of consumption and bed weight to give the average rate of reaction, in grammes of barium sulphate per minute per gramme of sample, for that time interval. This average rate of reaction was then plotted at the time in the middle of the time interval to yield a rate vs time curve.

6:2 Discussion of results (Preliminary stage)

Before work was commenced on the fluidizer a number of samples of close sized barytes was fluidized with air and with hydrogen in a perspex replica of the stainless steel reactor so that visual observations could be made of the fluidization patterns obtained. These tests also gave a check on the design calculations contained in Appendix E where the minimum fluidizing velocity for a +14-10# sample of barytes was estimated.

A number of barytes beds was then reduced in the fluidizing apparatus at 1000°C using relatively low hydrogen velocities, i.e. fixed beds, in order to acquire the operating technique which would enable the bed temperature to be controlled accurately. Work was commenced with low hydrogen velocities since it was found that temperature control became more difficult at high flow rates. When the operating technique had been mastered using fixed beds a number of fluidized beds were reduced at 1000°C until all the remaining difficulties in the operation of the fluidizing unit had been overcome. The results of the runs on fixed beds are presented in Fig. 29 while Fig. 30 summarises the data obtained using fluidized beds.

6:2:1 Fluidization in perspex model

Most of the data obtained using the three inch diameter perspex replica of the stainless steel fluidizer can be found in Appendix F where the fluidizer performance predicted from design calculations is compared with the actual performance of the unit which was built.

It was found that close sized samples of barytes tended to slug violently at flow rates in excess of about 200% V_{mf}. This behaviour was aggravated by increase in bed depth and it was found that a bed having an unfluidized depth of six inches was about the deepest which could be handled satisfactorily if excessive ejection of the bed material into the free-board above the bed was to be avoided. It was also noticed that, at all gas velocities exceeding the minimum required for fluidization (V_{mf}), there were bubbles of gas passing

up through the bed. This behaviour appears to be in agreement with the theory of Toomey and Johnstone[33], viz. that all gas in excess of that required for incipient fluidization passes up through the bed as bubbles. The small bubbles present in the bed just above the constriction plate rapidly coalesced until, at a height of about four inches above the bottom of the bed, they formed large bubbles which occupied the entire cross section of the bed. This behaviour led to slugging in beds which were deeper than about four inches.

6:2:2 Comparison of measured and predicted rates of reaction

Figs. 29 and 30 summarise the data obtained with fixed and fluidized beds respectively. The spread of data is indicated by the dotted lines, and the predicted rate vs time curves are also shown so that a ready comparison can be made between measured and predicted data.

(1) Fixed beds

It can be seen from Fig. 29 that the actual rate of reaction obtained for a bed containing 1500g of +14-10# barytes was substantially slower than the rate predicted from the results of tests on small differential beds. Examination of Fig. 29 also shows that the measured rate vs time curve does not rise to a maximum value as does the predicted curve, but falls away steadily from the start of reduction. This may have been caused by a few of the barytes particles which appeared to break down on heating and consequently made it impossible to obtain a bed which did not contain a small

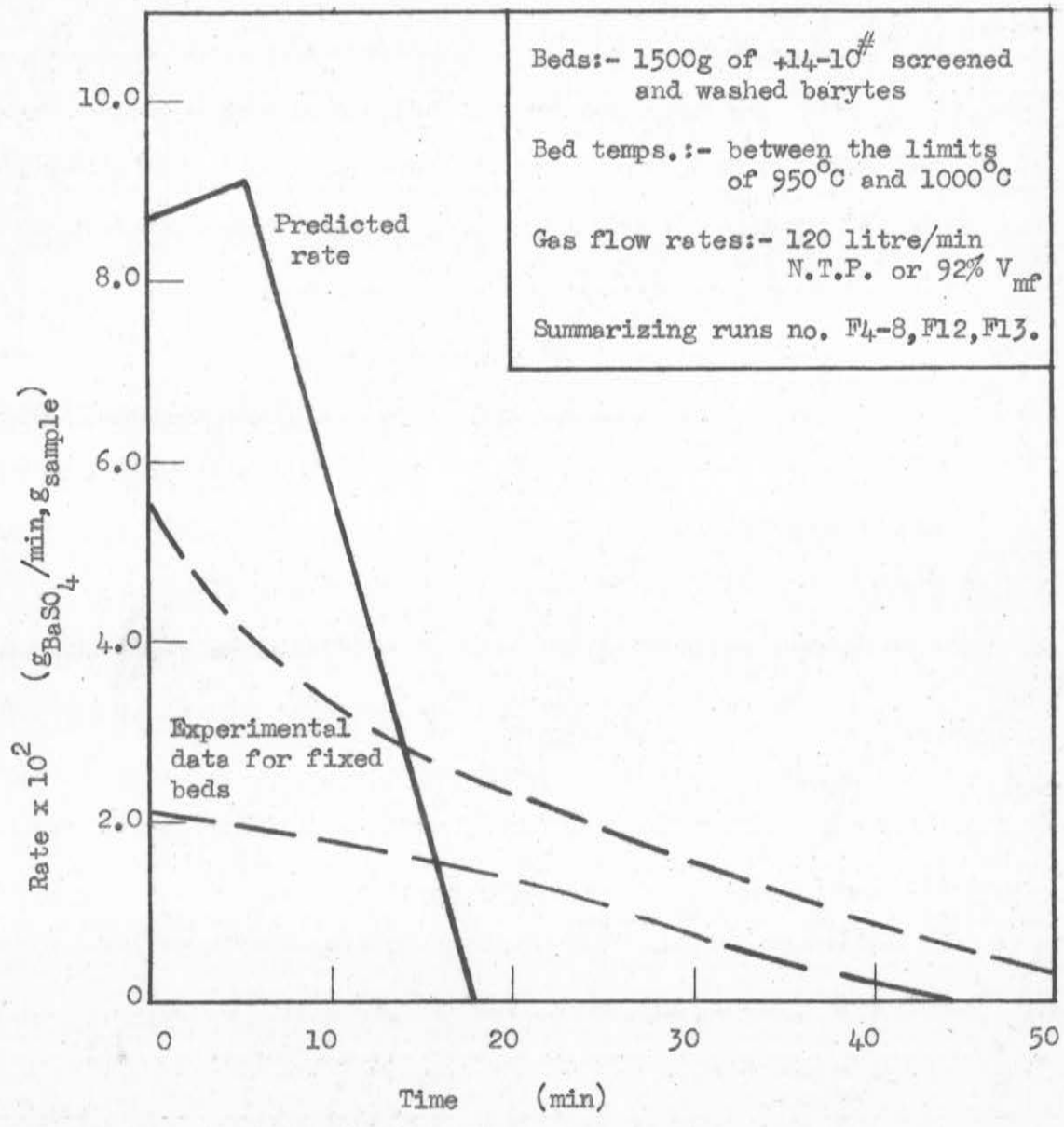

Fig. 29. Rate data for fixed beds at 1000°C

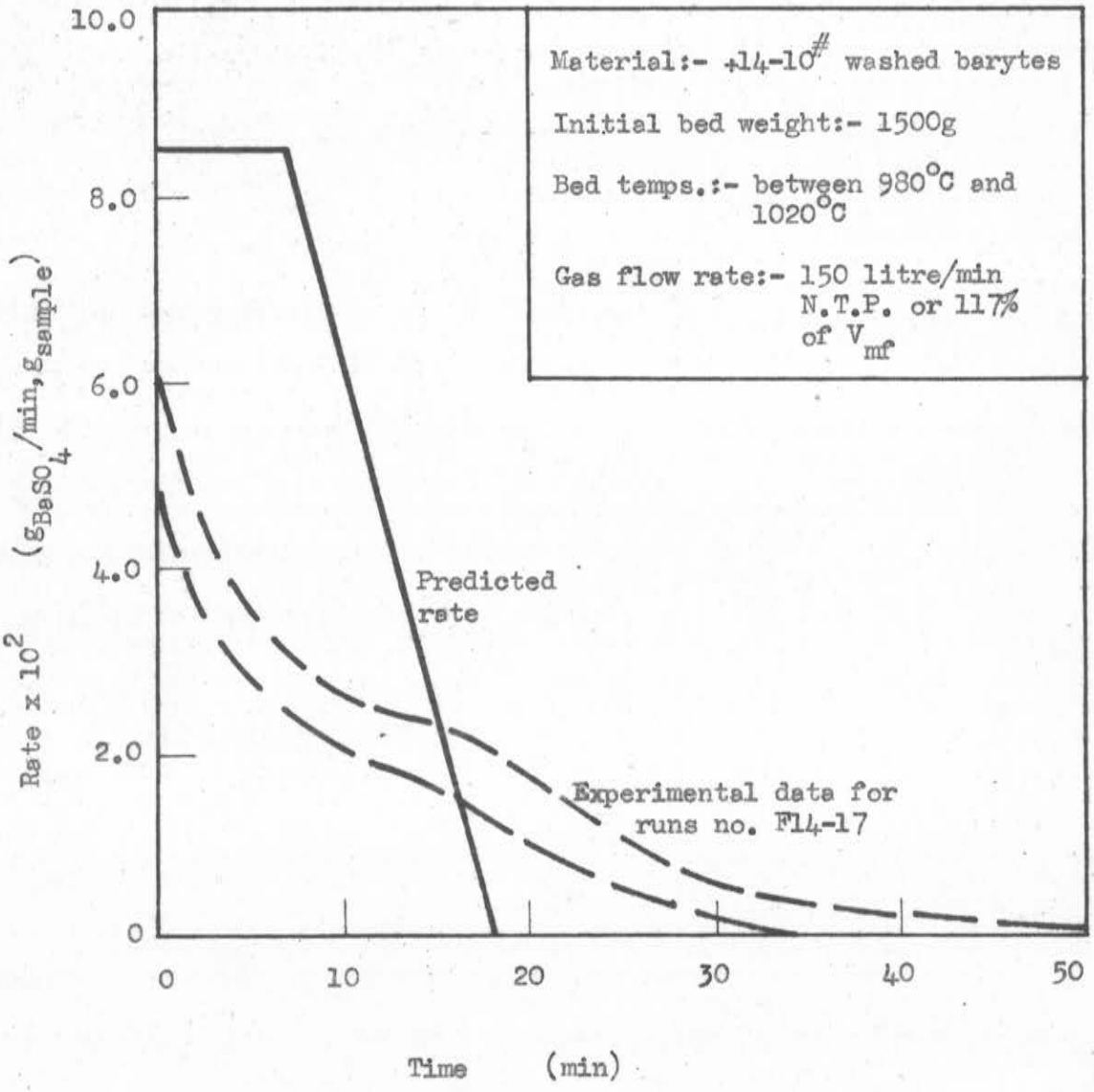

Fig. 30. Rate data for fluidized beds at 1000°C

quantity of about 100# material. It seems certain that when hydrogen was admitted to the bed this fine material, having a large specific surface area, would react very rapidly giving an abnormally large rate of reaction which would fall away to the true value for +14-10# material. This effect may have masked the auto-catalytic nature of the reaction.

(2) Fluidized beds

Examination of Fig. 30, page 154, shows that, in this case also, the rate of reaction obtained in practice was much slower than the predicted rate. It was thought that there were two possible reasons for the discrepancy between measured and predicted rates. These were, (1) that the retardation of the reaction rate caused by the presence of water vapour was much more severe than the data obtained (see Section 4:4:2), page 95) from the tests on differential beds indicated, or (2) that the rate may have been retarded by the presence of hydrogen sulphide formed by the secondary reaction,

$$BaS + 2H_2O = Ba(OH)_2 + H_2S \quad .....(9)$$

which proceeds to a limited extent.

It was decided that more information about the influence of water vapour concentration on the reaction rate could be obtained by varying the bed depth and hydrogen flow rate while the effect of hydrogen sulphide could be studied by reducing a bed of barytes with a mixture of hydrogen and hydrogen sulphide.

6:2:3 Factors producing inconsistency in experimental results

It can be seen from Figs. 29 and 30, pages 153 and 154, that the rates obtained from successive runs differed by as much as 50%. This was due primarily to the difficulty experienced in keeping the bed temperature at a constant set value during the early part of a run. It was found that, for a given heat flux, the wall temperature of the preheater tube was much lower when hydrogen was passing through the tube than when nitrogen was being used, due probably, to the high conductivity of hydrogen compared with nitrogen. It was, therefore, necessary to adjust the input to the preheating furnaces during the few minutes before hydrogen was switched on so that the temperature of the preheater walls decreased to a value which experience showed to be correct for the hydrogen flow rate being used. The preheater furnace controls were then advanced again to the set points when hydrogen was admitted to the apparatus. Failure to observe this procedure caused a sudden rise of up to 50°C in the bed temperature during the first two or three minutes of a run. The preliminary tests provided valuable operating experience so that, by the time Run No. F17 had been reached, the temperature of the bed throughout a run could be held within $\pm 10^{\circ}$C of the average for the run and the average could be held within 10°C of the predetermined temperature.

Some difficulty was also encountered through hydrogen leaking out of the apparatus. Such leaks were very serious since, as pointed

out in Section 6:1:4, page 150, the rate of reaction was measured by timing the volume of make-up hydrogen entering the apparatus. Some allowance for leakage could be made by measuring the rate of hydrogen consumption at the end of a run, when all the barytes had been reduced, and then subtracting this rate from the previous measurements; it was necessary to assume that the rate of leakage was constant over the whole period for a test if this correction was to be valid. The most serious leak was found to occur at the flange on top of the preheater-reactor tube (see Fig. 28, page 147) where the asbestos gasket began to break down when the metal temperature exceeded about 600°C. The leak rate at this point usually increased steadily during a run and it was found necessary to cool the outside of the flange with a water spray in order to maintain a gas tight seal; care was also needed during assembly of the apparatus after loading to ensure that all other joints were leak proof. After this modification had been made it was generally possible to limit the leak rate to about one cubic foot of hydrogen per hour. This was equivalent to a reaction rate of 1×10^{-3} $g_{BaSO_4}/min, g_{sample}$ for a 1500g bed, i.e. about 5% of the maximum rate measured at 1000°C. Most of this leakage occurred from the gland of the circulating pump and it was found that the rate of hydrogen loss from this point was substantially constant so that the measured rate of reaction could be corrected by subtracting the leakage rate obtained at the end of a run.

6:2:4 Conclusions

The conclusions which were drawn from the preliminary experiments may be set out as follows.

(1) The rate of reaction obtained for both fixed and fluidized beds of +14-10# barytes at 1000°C is only about half the rate predicted from the work on differential beds.

(2) It is possible that this retardation of the rates of reaction may be caused by water vapour having an unexpectedly large effect on the rate of reaction or by the presence of hydrogen sulphide in the gas phase of the beds.

6:3 Experimental procedure (Final stage)

The primary objective of the preliminary work was to provide operating experience so that accurate rate data could be obtained from the fluidizer at 1100°C. Attention was focussed upon this temperature because, only at 1100°C, could the data obtained from differential beds be satisfactorily correlated in a form suitable for rate prediction. Consequently, the most precise rate predictions made (see Section 5) were for fixed and fluidized beds at 1100°C.

The tests planned for 1100°C may be set out as follows.

(1) Reduction, by hydrogen, of a fixed bed containing 1500g of +14-10# barytes to test the validity of the work on differential beds.

(2) Reduction, by hydrogen and a hydrogen-nitrogen mixture, of

fluidized beds containing 1500g of +14-10# barytes to check the method used for predicting rates in fluidized beds.

(3) Reduction, by hydrogen, of fluidized beds containing 1500g of +14-10# barytes to check the effect of variation in bed depth on the method of rate prediction.

The preliminary work also showed that the rate of reaction obtained at 1000°C, in both fixed and fluidized beds, was lower than the rate predicted from the previous work on differential beds so it was decided to reduce samples of +14-10# barytes in fluidized beds at 1000°C, varying both the initial bed weight and the gas velocity, to try to find the cause of this discrepancy. This would have the effect of varying the mean water vapour partial pressure in the beds and give some check on the work done on differential beds with water-hydrogen mixtures. It was also decided to reduce a sample at 1000°C with a mixture of hydrogen and hydrogen sulphide to see if the hydrogen sulphide retarded the rate of reaction.

Rates of reaction were to be obtained for fluidized beds of +14-10# barytes at 900°C to see if there was any better agreement between predicted and measured rates at this temperature than was the case at 1000°C.

A sample of +65-48# barytes was also to be reduced to give some idea of the rate of reaction likely to be obtained with material in this size range.

6:3:1 Apparatus

The only modifications to the unit as described in Section 6:1:1, page 142, were the addition of a water spray to cool the outside of the flange at the top of the preheater-reactor tube (see Fig. 31) and the insertion of three Birco Inconel rod heating elements in the preheating tube. The three 2500 watt elements were connected in series and the voltage across them controlled by a Variac auto-transformer. These elements increased the maximum energy input to the preheating section by approximately one kilowatt. It was found that this extra preheating capacity was required when the hydrogen flow rate exceeded about 190 litre/min N.T.P.

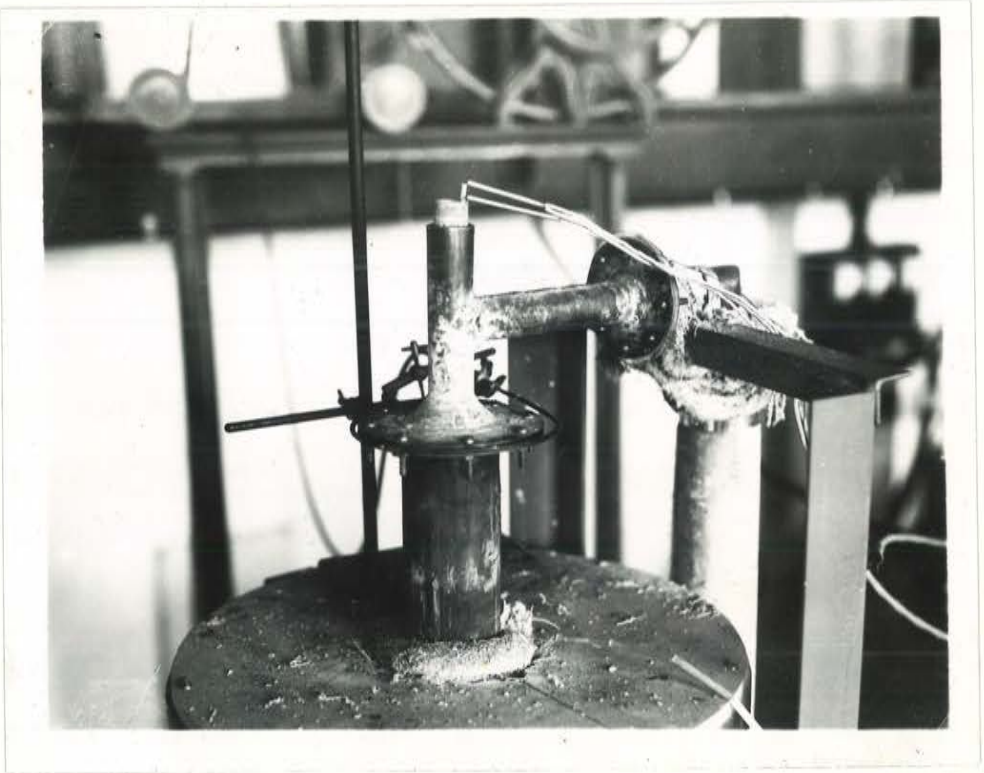

Fig. 31. Photograph of the top of the reactor tube showing the cooling spray in position

6:3:2 Experimental technique

The procedure adopted was identical with that set out in Section 6:1:2, page 148.

6:3:3 Treatment of results

Rate vs time curves were produced from the volume vs time observations in the way set out in Section 6:1:4, page 148.

6:4 Discussion of results (Final stage)

The volume vs time records and the derived rates of reaction for runs number F18 to F32 inclusive are presented in tabular form in Appendix D.

A comparison of runs on similar samples, carried out under the same conditions, e.g. F19 and F20 or F22 and F25, shows that the rates obtained rarely differed by more than 10% over the course of the reaction. This improvement on the accuracy of the data presented in Fig. 29, page 155, may be attributed to the elimination of hydrogen leaks and to the more accurate control of the bed temperature due to improved operating technique.

Fixed and fluidized beds of +14-10# barytes were reduced at 1100°C and fluidized beds of varying weights were reduced at 1000°C and 900°C. The rate vs time curves obtained at 1100°C are presented in Figs. 32, 33, 34, and 35, while the results of the tests at 1000°C and 900°C are set out in Figs. 36 and 37, respectively. The appropriate predicted rate vs time curves, taken from Section 5, are also

provided in each case to facilitate the comparison of measured and predicted rates.

Because of its importance, the work at 1100°C will be discussed before proceeding to consider the effects of bed depth and flow rate on the reaction rates at 1000°C and 900°C. Finally the results of the test on +65-48# material will be dealt with.

6:4:1 Comparison of measured and predicted rates at 1100°C

Examination of Fig. 32, which compares the predicted and actual curves for a fixed bed containing 1500g of +14-10# barytes, shows that the measured rate was only 10% less than the predicted rate over the constant rate period. It should be noted, however, that a hydrogen flow rate of 130 litre/min N.T.P. was used during the first two minutes of the test (see Appendix D, page 241) to purge all nitrogen from the system and this had the effect of shifting the measured curve to the left along the time axis. Rate measurements were impossible during this period but the probable shape of the curve which would be obtained at a flow rate of 130 litre/min N.T.P. has been indicated on Fig. 32 by a dashed line.

The excellent agreement between measured and predicted rates shows that the work carried out on differential beds was quite sound and confirms that, for most practical purposes, the reaction between hydrogen and barium sulphate at 1100°C may be taken as being of zero order with respect to hydrogen and of the first order with respect to barium sulphate. The fact that the measured rate is 10% lower than

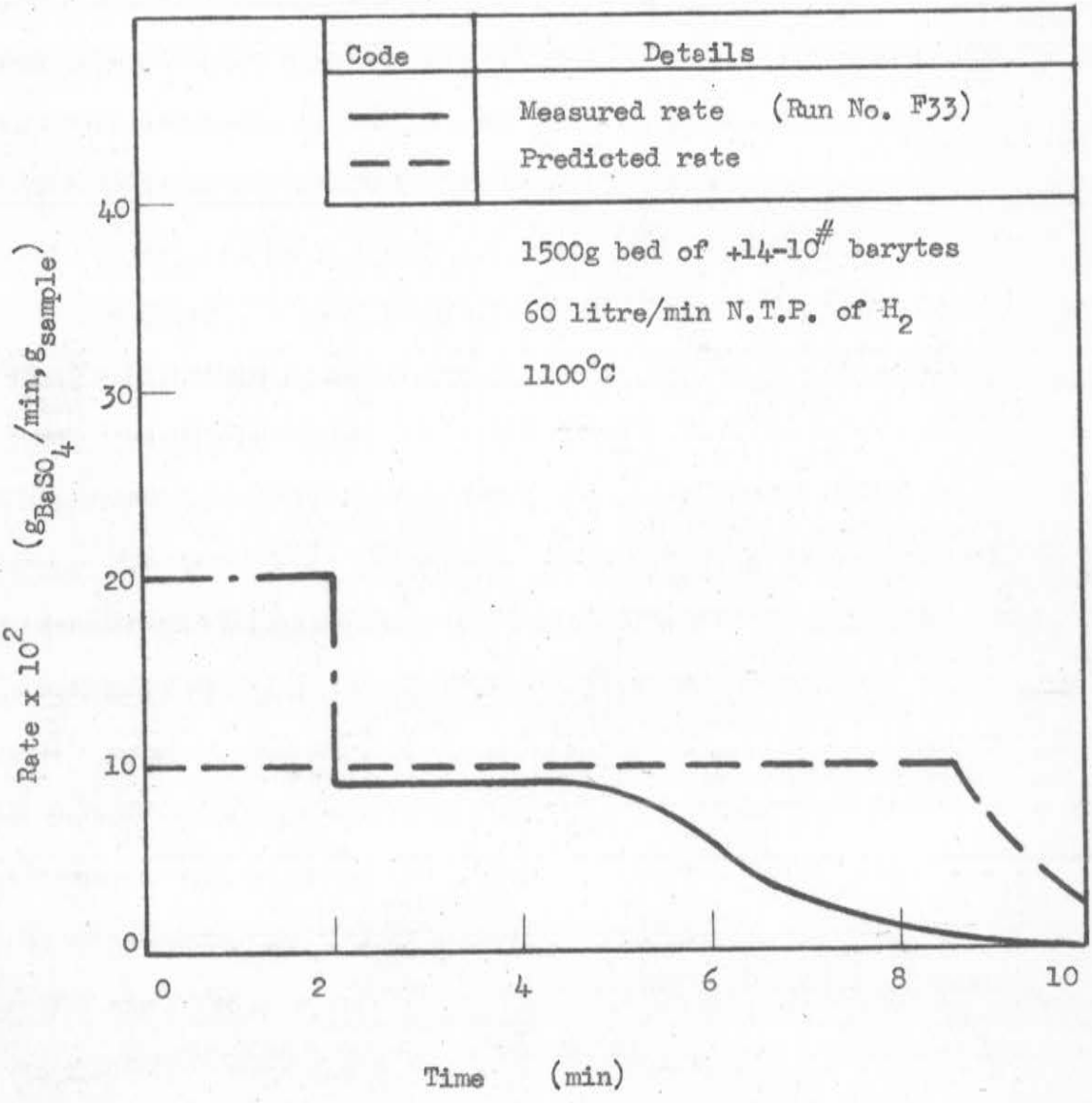

Fig. 32. Comparison of measured and predicted rates of reaction for a 1500g fixed bed at 1100°C

the predicted rate also confirms the finding of the previous work (see Section 4:4:2, page 103) that the reaction is slightly retarded by the presence of water vapour. Additional information about the effect of water vapour on the reaction rate would probably have led to an even more precise rate prediction.

Figs. 33 and 34 show that the measured and predicted rate vs time curves for 1500g fluidized beds were almost identical. In the case of the 750g fluidized bed (Fig. 35) the initial measured rate is 25% lower than the predicted rate but agreement between measured and predicted curves is still quite good.

The success of these predictions for fluidized beds shows that the two phase theory of fluidization, developed by Johnstone and his co-workers[31)32)33)], which was utilized in the calculations pertaining to the prediction of rates (see Section 5) is correct. It will be recalled, however, that during these calculations, assumptions had to be made regarding the rate of mass transfer between the continuous and discontinuous phases of the fluidized beds; lack of experimental values of the coefficient for this transfer process provides the major difficulty in applying the two phase theory to practical problems.

It was considered that the experimental data might be used to calculate values of the transfer coefficient between continuous and discontinuous phases as Shen and Johnstone[32)] did but close examination showed that more detailed information on the effect of water vapour

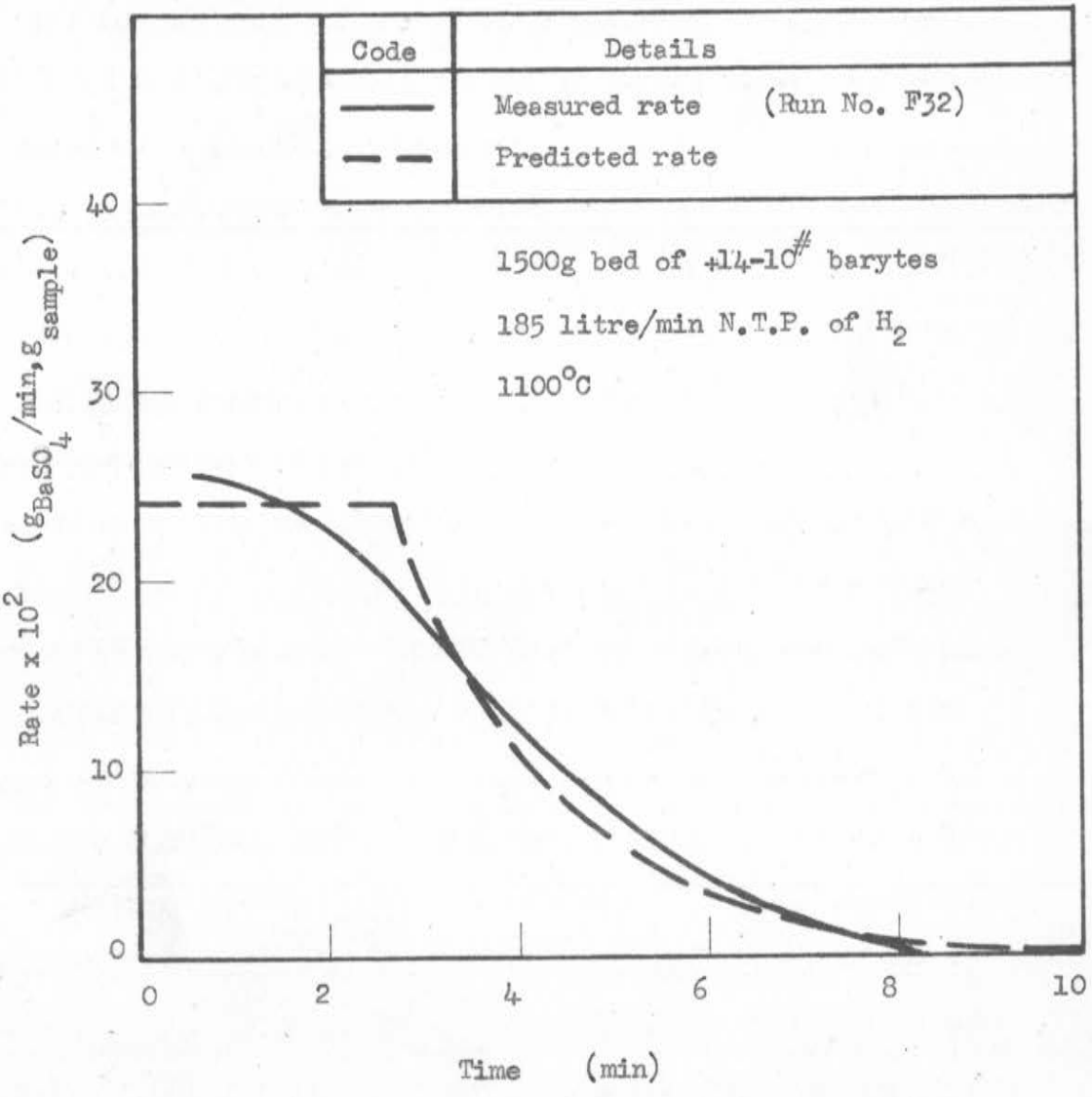

Fig. 33. Comparison of measured and predicted rates of reaction for a 1500g bed fluidized with hydrogen at 1100°C

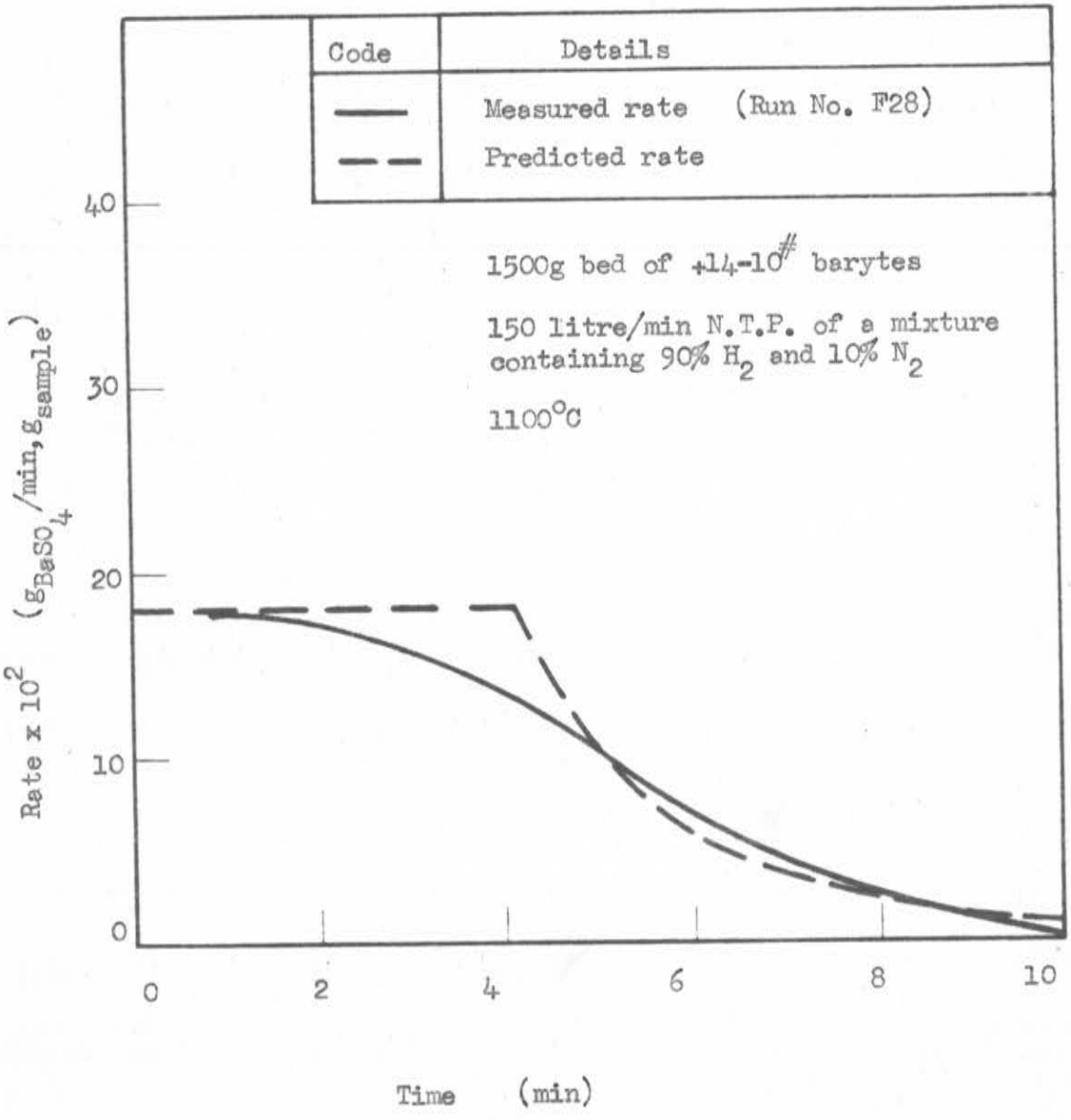

Fig. 34. Comparison of measured and predicted rates of reaction for a 1500g bed fluidized with a H_2-N_2 mixture at 1100°C

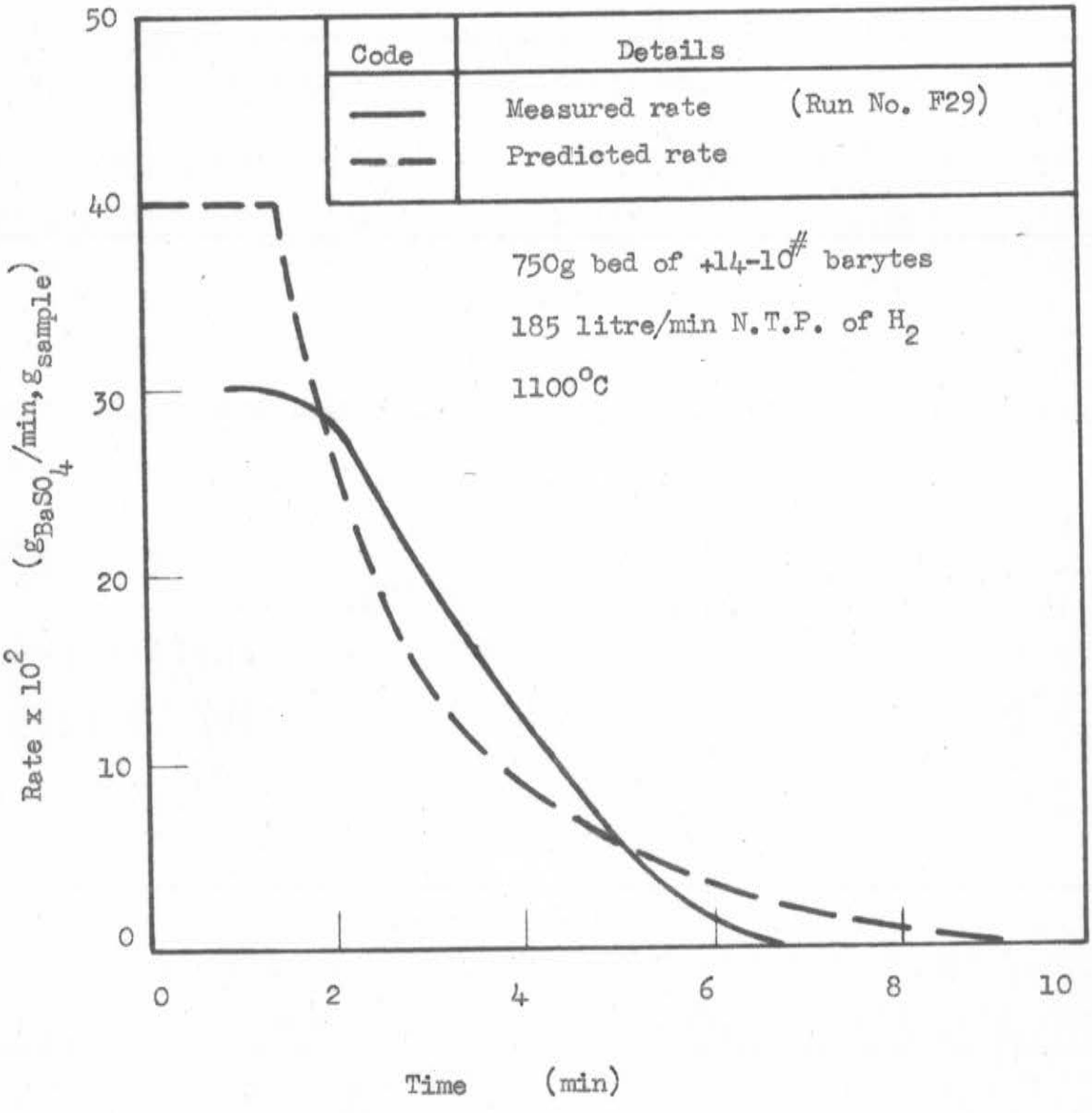

Fig. 35. Comparison of measured and predicted rates of reaction for a 750g bed fluidized with hydrogen at 1100°C

partial pressure on the reaction rate and on the gas flow pattern in the bed* would be required if these coefficients were to be more than a verification of the two phase theory of fluidization. Since the comparison of actual and predicted rates provided a graphic confirmation of this theory transfer coefficients were not calculated.

6:4:2 Effect of variation in bed depth and gas flow rate on the rate of reaction obtained in fluidized beds at 1000°C and 900°C

Examination of Figs. 36 and 37 shows that, at both 1000°C and 900°C, the rate of reaction per unit mass was greater for a 750g bed than for the corresponding 1500g bed, although still less than the predicted rate. Also, in both cases, the maximum in the rate vs time curve was more prominent for the shallow bed than for the deep bed. The maximum in curve (3) of Fig. 36 may have been slightly accentuated by temperature variations since the highest bed temperatures for these runs - 15°C above the maximum - occurred close to the point of maximum rate, however, consideration of the temperature records for these runs, suggested that the sharp maximum in the curves was not entirely caused by the high temperature during the initial phase of the reaction.

If the discrepancy between predicted and measured rates is disregarded the experimental data obtained by varying bed depths and gas flow rates can be explained in terms of retardation of the rate of reaction by water vapour; the water vapour content of the gas in the

* It seems probable (see Appendix F, page 296) that the volume of gas by-passed through a bed depends partly on the rate of reaction.

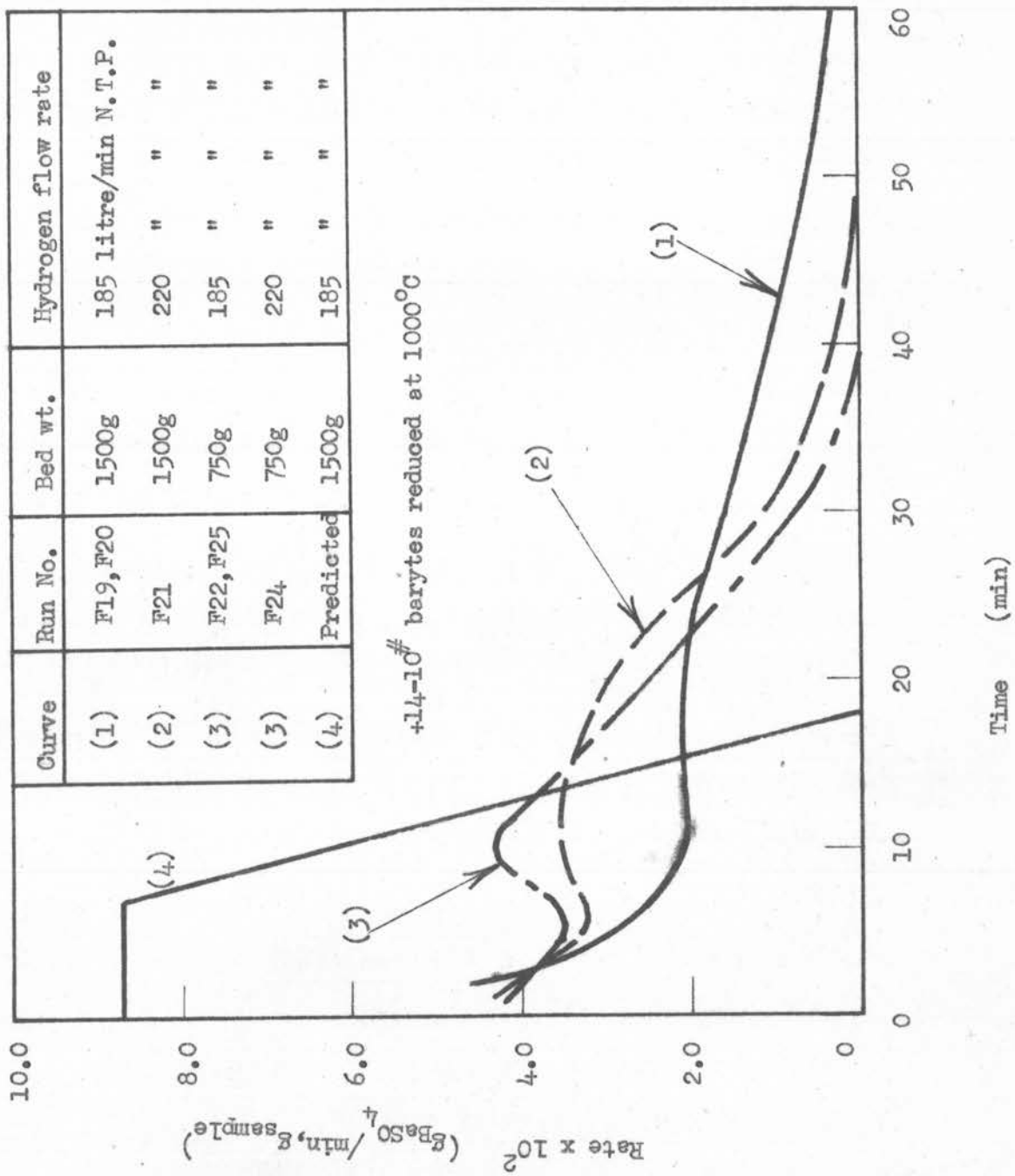

Fig. 36. Effects of variations in the initial bed weights and hydrogen flow rate on the rate of reaction at 1000°C

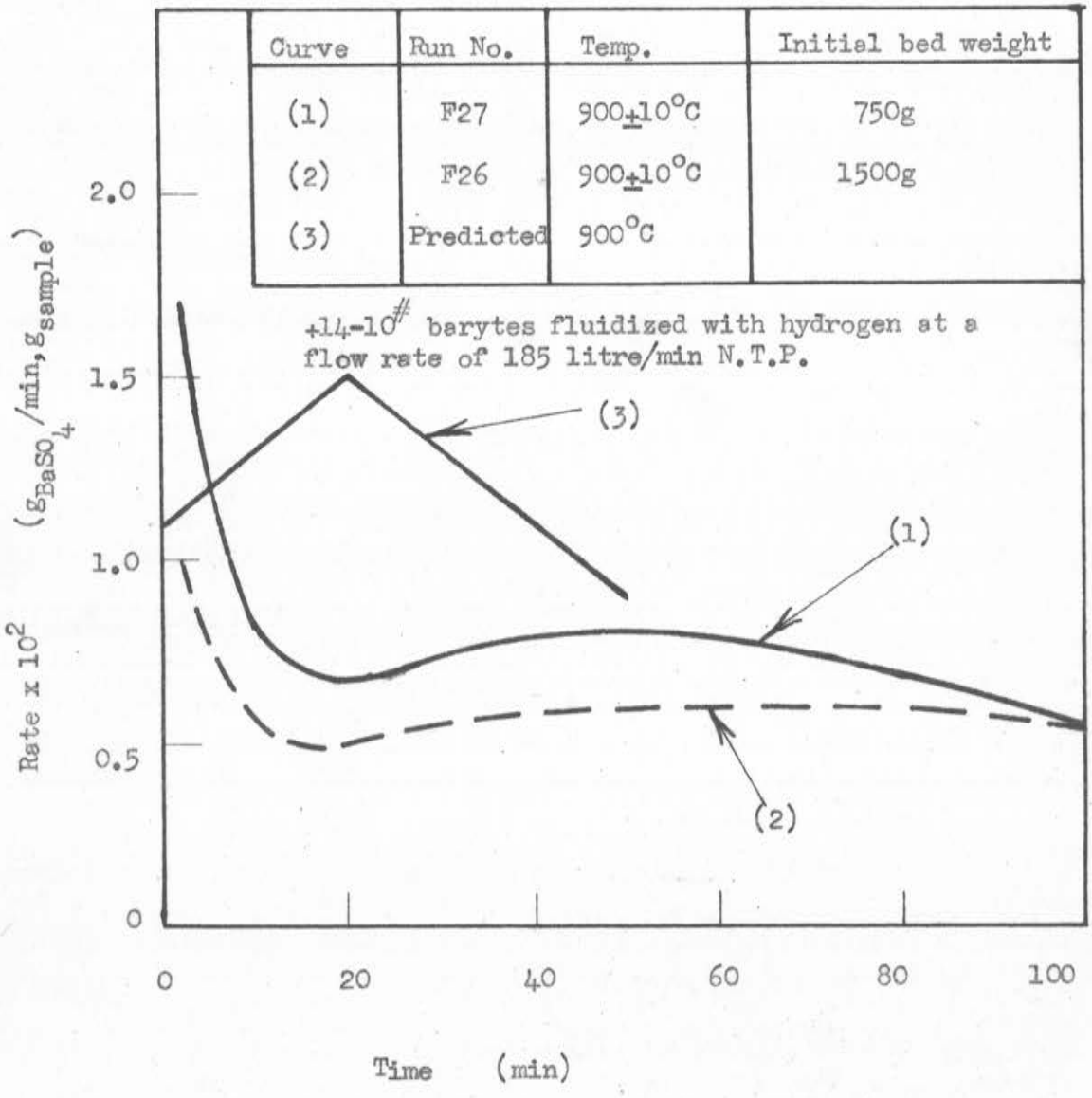

Fig. 37. Effect of variation in the initial bed weight on the rate of reaction at 900°C

continuous phase of the bed will depend upon the amount of gas being by-passed through the bed as bubbles.

Shen and Johnstone[32] found that the rate of mass transfer per unit volume of bed, between continuous and discontinuous phases, increased with gas velocity and with bed depth. This is quite logical since, if the volume of by-passed gas is increased, the area available for mass transfer between continuous and discontinuous phases will also increase and, consequently, the rate of mass transfer between the phases will become larger. This rate of mass transfer will also be increased by increased turbulence in the bed and, therefore, the rate of mass transfer will be greater for a deep bed, where there is considerable agitation due to slugging, than for the corresponding shallow bed. The partial pressure of water vapour in the gas of the continuous phase of the fluidized bed will increase from inlet to outlet due to the reaction taking place but this rate of increase will be modified by the rate of mass transfer between the continuous and discontinuous phases. Fig. 38 shows the probable mode of variation of the water vapour concentration in the gas flowing through the continuous phase of the bed, as the distance from the inlet increases, for the two gas flow rates used. The water vapour concentration at the inlet has not been assumed to be zero; there will probably be some back mixing in the gas phase of the bed (see Section 5:2:1, page 138).

It is assumed that the reaction rate is retarded by the presence of water vapour then, it can be seen from Fig. 38 that, at both flow rates, the rate of reaction per unit mass will be higher for a

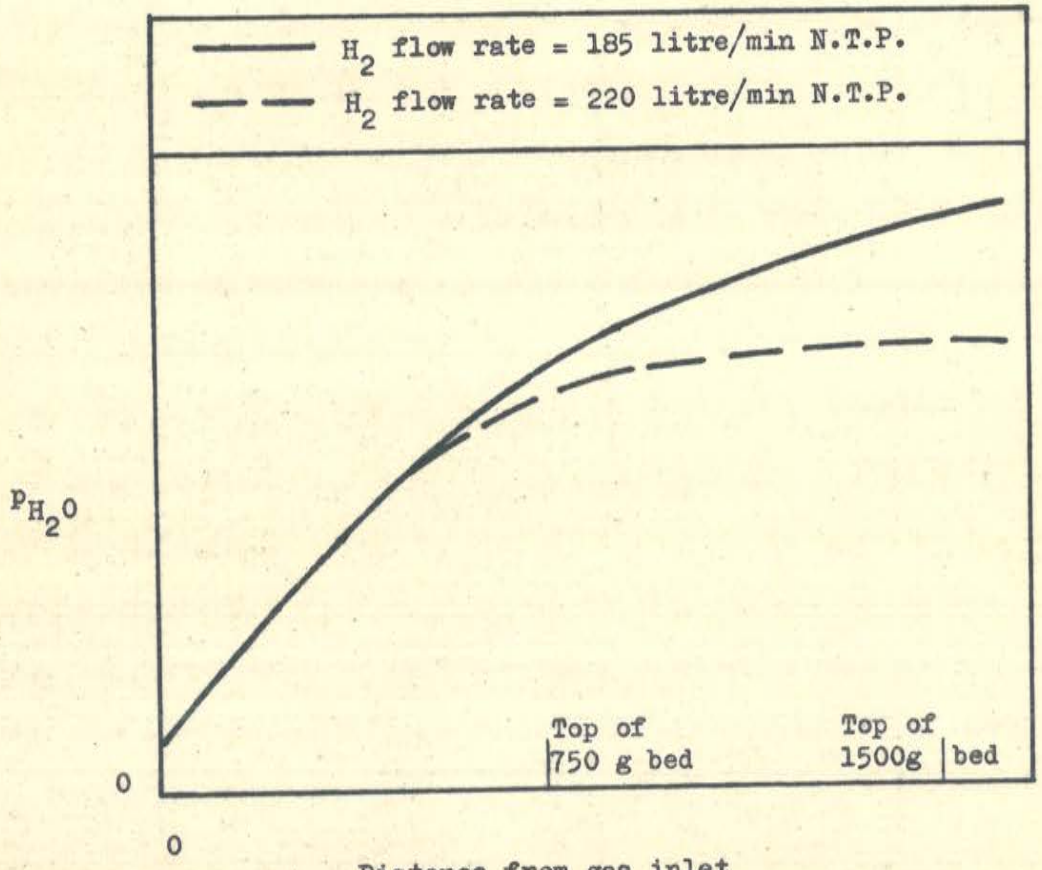

Fig. 38. Variation of water vapour partial pressure in the continuous phase of a fluidized bed with distance from the gas inlet

750g bed than for the corresponding 1500g bed because the mean value of the water vapour partial pressure will be highest, in each case, for a deep bed. It can also be seen that the increase in rate due to halving the bed depth will be more pronounced at a low hydrogen flow rate than at a high flow rate. The lower mean partial pressure of water vapour in the 750g bed also suggests that the maximum in the rate vs time curve would be more prominent in this case than for the corresponding 1500g bed since it was found (see Fig. 15, page 99) that the presence of water vapour appeared to retard the maximum rate of reaction preferentially.

Examination of Fig. 36, page 169, shows that the behaviour observed in practice was the same as that predicted on the basis of Fig. 38, however, the fact remains that the rate vs time curves predicted, using the limited data obtained previously about the retarding effect of water vapour, differs considerably from the measured curves. The only likely explanations for this discrepancy appear to be,

(1) that the retardation of the rate of reaction by water vapour is much greater than indicated by the work on differential beds, or

(2) that the rate of reduction is retarded by the presence of hydrogen sulphide formed by the reaction,

$$BaS + 2H_2O = Ba(OH)_2 + H_2S \quad \ldots\ldots\ldots\ldots\ldots\ldots (9)$$

6:4:3 Effect of hydrogen sulphide on the reaction rate at 1000°C

A 750g bed of +14-10# barytes was reduced with a hydrogen-hydrogen sulphide mixture to determine whether the rate of reaction

was retarded by the presence of hydrogen sulphide. In Fig. 39 the rate vs time curve for the barytes sample reduced with a mixture of hydrogen and hydrogen sulphide containing 2% by volume of hydrogen sulphide is compared with the corresponding curve using pure hydrogen. It can be seen that the presence of the hydrogen sulphide has markedly reduced the rate of reaction.

The percentage of hydrogen sulphide present in this case is considerably larger than the amount likely to be produced from the interaction of barium sulphide and water according to reaction (9) since the thermodynamic investigation of reaction (9) (see Appendix A, page 188) showed that, at equilibrium, the hydrogen sulphide produced is only 0.01% by volume of the water present. Never-the-less the results of this test do indicate that hydrogen sulphide retards the reduction of barytes by hydrogen at 1000°C and it seems possible that the discrepancy between measured and predicted rates of reaction at 1000°C and 900°C is due to this effect. The concentration of hydrogen sulphide in the gas phase of the beds will be a function of the water vapour concentration and hence the hypothesis set out in Section 6:4:2 to explain the variation of reaction rate with bed depth should still be applicable.

6:4:4 Reduction of +65-48# barytes

Most commercial processes using fluidization techniques utilize beds of about 100# material with gas velocities two to three times that (V_{mf}) needed to produce incipient fluidization in order to get

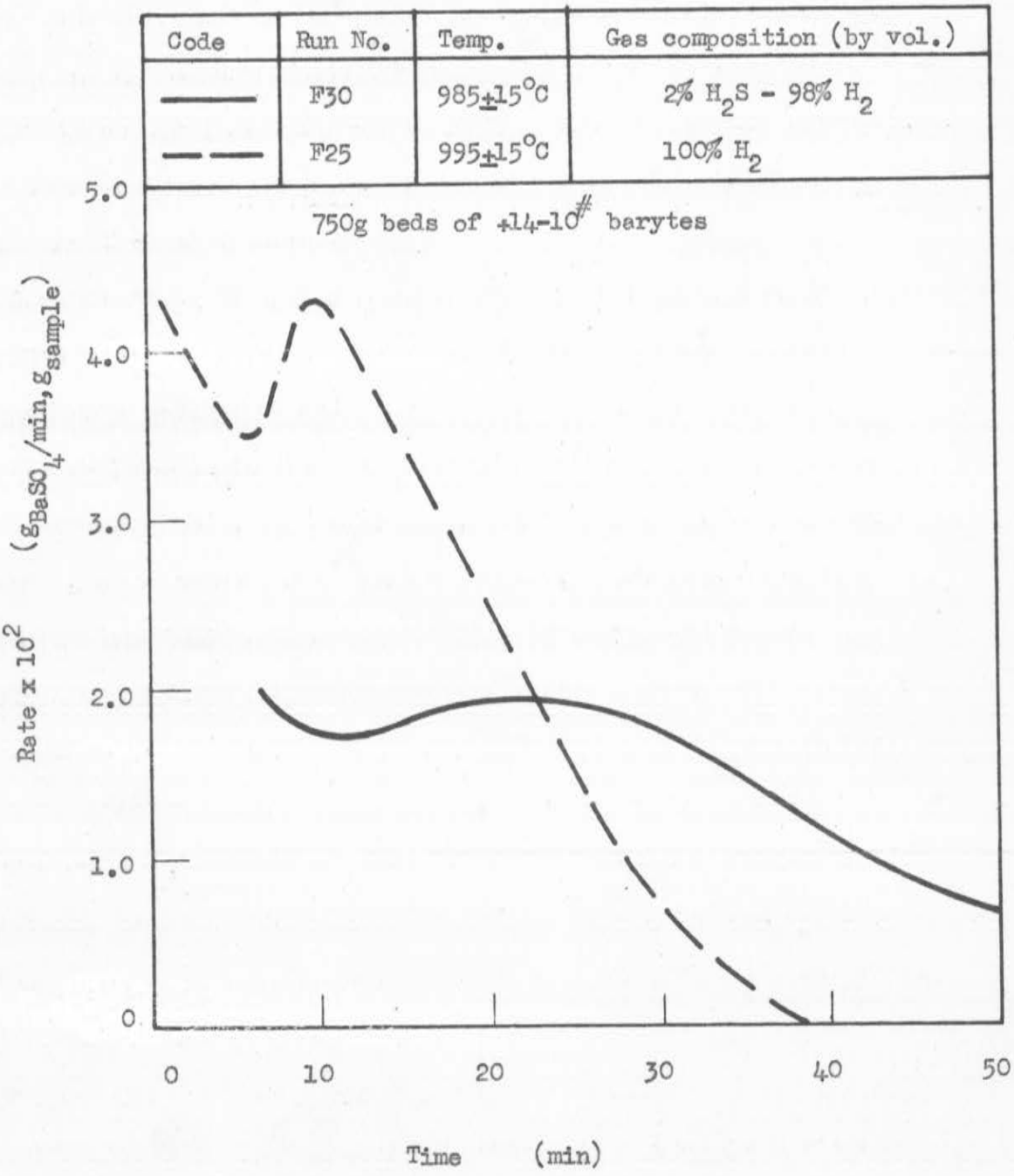

Fig. 39. Effect of hydrogen sulphide on the rate of reaction at 1000°C

rapid reaction rates. It was decided, therefore, to reduce a +65-48# (Tyler) sample of barytes at a hydrogen velocity of about 300% V_{mf} to find out what rate of reaction could be obtained under these conditions. Data were first obtained at 900°C and then the temperature was rapidly increased to 1000°C and stabilized at this value while further rate measurements were made. In this way rate data were obtained for two different temperatures using only one sample. The results of this test are shown in Fig. 40.

Assuming, for simplicity, that the gas leaving the dense phase of the bed is 100% water vapour and the by-passed gas is 100% hydrogen, the maximum rate of reaction possible at 900°C, with a hydrogen flow rate of 26 litre/min N.T.P. (325% V_{mf}), is $2.7 \times 10^{-2} g_{BaSO_4}/min, g_{sample}$. However, it can be seen from Fig. 40 that the measured rate of reaction at 900°C was only $0.6 \times 10^{-2} g_{BaSO_4}/min, g_{sample}$ or 20% of the predicted rate.

Making the same assumptions at 1000°C it is found that the maximum rate of reaction would be $2.3 \times 10^{-2} g_{BaSO_4}/min, g_{sample}$. Examination of Fig. 40 shows that the actual rate of reaction at 1000°C considerably exceeds the predicted rate. This means that there is some water vapour in the gas leaving the discontinuous phase of the bed, as might be expected, since the gas in the top of the continuous phase probably contains near 100% of water vapour. The measured rate corresponds to a water vapour concentration of 10% in the gas leaving the discontinuous phase of the bed.

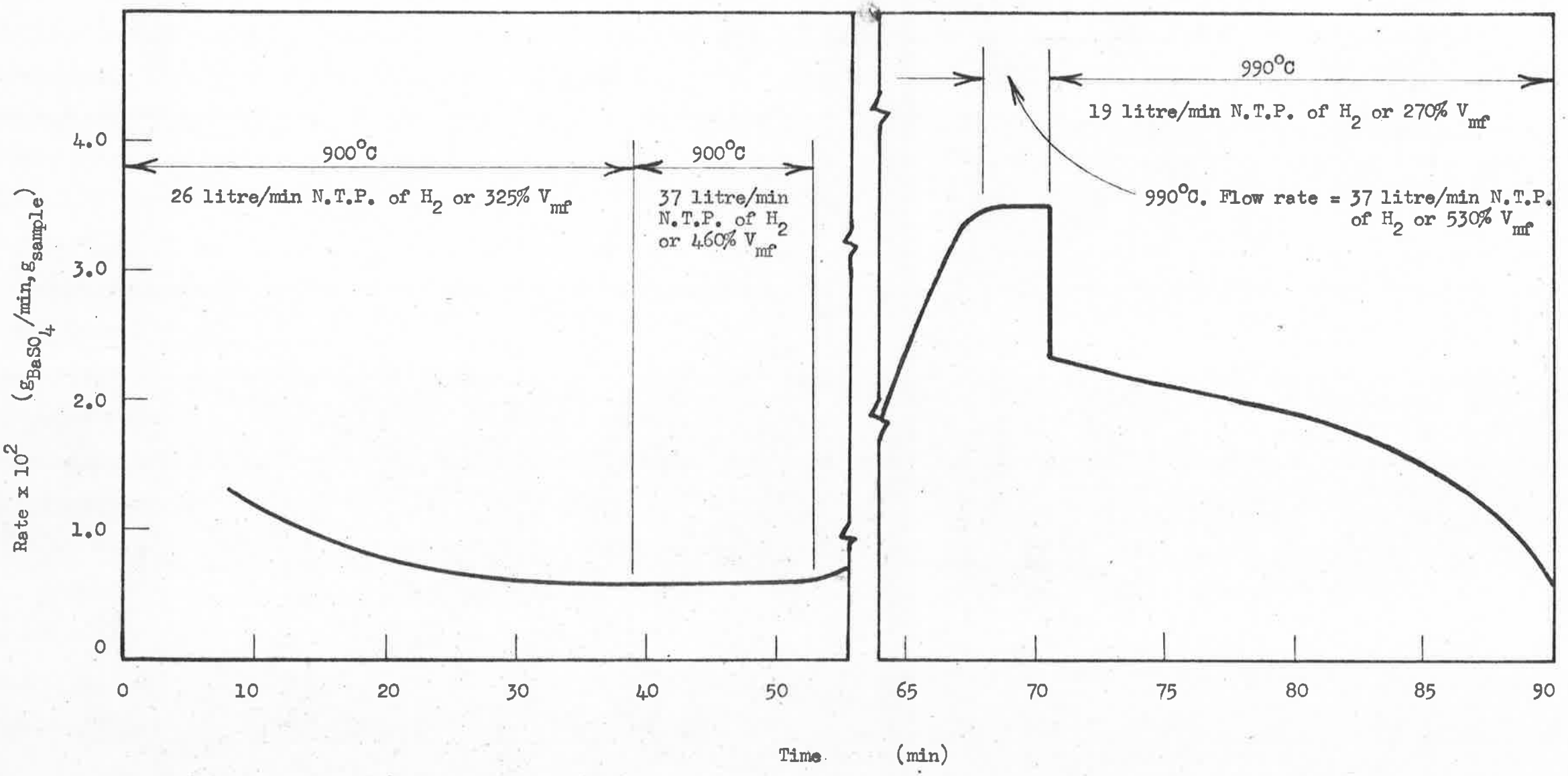

Fig. 40. Rate data for a fluidized bed of +65-48# barytes

This test shows that, even with material as fine as +65-48#, it is still necessary to operate at a temperature of about 1000°C if the efficient gas-solid contacting made possible by the fluidization technique is to be fully utilized to give a high conversion of the reducing gas, i.e. to minimized pumping requirements and give the highest possible rate of reaction.

6:5 Conclusions

The conclusions drawn from this final phase of the project may be set out as follows.

(1) The work on fixed, differential beds and the correlation developed to describe the data obtained at 1100°C appear to be quite sound since accurate rate predictions could be made for a thick bed of +14-10# barytes at 1100°C.

(2) The rate of reduction of +14-10# (Tyler) barytes in beds fluidized with hydrogen at 1100°C may be predicted from the results of tests on differential beds if the "two phase" theory of fluidization is accepted. Lack of experimental values of the coefficient for mass transfer between the two phases - continuous and discontinuous - in a fluidized bed is the major obstacle encountered in making such rate predictions.

(3) At 900°C and 1000°C the rates of reaction obtained by reducing +14-10# barytes in fluidized beds are only half the rates predicted from the work on differential beds. There is some evidence to suggest

that this discrepancy may be due to the retarding effect of hydrogen sulphide on the rate of reaction.

(4) Even when samples as fine as +65-48# (Tyler) are reduced, a bed temperature of about 1000°C is required to utilize the rapid rates of reaction made possible by the efficient gas-solid contacting obtained in a fluidized bed. However, if the bed temperature is increased to 1100°C, material in the size range +14-10# (Tyler) can be handled efficiently.

(5) There appear to be no technical difficulties connected with the reduction of barytes in a fluidized bed to produce barium sulphide, although, it must be realised, that the process has only been operated on a batch basis.

7. SUMMARY AND CONCLUSIONS

The reduction of barytes by hydrogen has been used as a medium to investigate the problems associated with the prediction of reaction rates for a fluidized system from the results of tests on a small fixed bed.

A literature survey revealed that, although no work of a quantitative nature had been published on the reduction of barium sulphate by hydrogen, it appeared to be a simple, uncomplicated reaction which would form a suitable basis for the project. However, it was necessary to carry out equilibrium determinations for the system $BaSO_4/BaS/H_2O/H_2$ to verify this point; the following information was obtained.

(1) The reduction process, even for impure barium sulphate, may be represented by the equation,

$$BaSO_4 + 4H_2 = BaS + 4H_2O$$

(2) Neither barium sulphite nor barium hydroxide are formed to any great extent when barium sulphate is reduced by hydrogen, showing that there are no extensive side reactions taking place.

(3) Equilibrium constants in the temperature range 800°C to 1100°C are satisfactorily represented by the equation,

$$\log K_p = 5.447 + 697.5/T$$

with a maximum uncertainty of $\pm 5\%$ in K_p at 800°C

The equilibrium determinations confirmed that the reduction of barytes by hydrogen fulfilled the requirements of the project for a process uncomplicated by extensive side reactions so samples of mineral barytes were then reduced in a fixed differential bed to obtain rate data which could be used to predict the rate of reaction for a fluidized bed. The information gained from this phase of the project may be summarised as follows.

(1) The rate of reduction of barytes, by hydrogen, is not controlled by diffusion at temperatures up to 1100°C so long as the hydrogen concentration does not fall to a very low value.

(2) For most practical purposes, the reaction rate at 1100°C may be taken as being of the first order with respect to barium sulphate and of zero order with respect to hydrogen. Water vapour has a slight retarding effect on the reaction but this can be neglected in most cases. The experimental data at 1100°C were satisfactorily correlated by the empirical equation,

$$R/s = K(1 - f)/100$$

Where R = the rate of reaction

s = the specific surface of the barytes sample

K = a constant depending upon the barytes composition

f = the fraction of the barytes reduced.

(3) At 1000°C and 900°C the rate vs time curves obtained exhibited a maximum value and it was not possible to derive an expression which would correlate the experimental data. There was some evidence to suggest that the maximum in the rate vs time curves may have been due to the presence of impurities in the mineral barytes used. Water vapour also appeared to have a greater retarding effect on the rate of reaction than was the case at 1100°C.

In the final stage of the project the method of rate prediction adopted was tested by comparing the predicted rates of reduction with the rates obtained by experiment on a fluidized reactor. The conclusions drawn from these comparisons are enumerated below.

(1) The work on fixed differential beds and the correlation developed to describe the experimental data at 1100°C are quite sound.

(2) If the "two phase" theory of fluidization is accepted the rate of reduction of barytes, in beds fluidized with hydrogen at 1100°C, may be predicted satisfactorily from the results of tests on differential beds. The only obstacle to making rate predictions is the lack of experimental coefficients for mass transfer between the two phases - continuous and discontinuous - in a fluidized bed. However, even where these rates of mass transfer must be estimated, as they were in this work, rate predictions may be made with fair

accuracy for a gas-solid reaction, such as the reduction of barytes at 1100°C, where the reaction is virtually unaffected by variation in gas concentrations.

(3) At 900°C and 1000°C the rates of reaction obtained by reducing +14-10# barytes in fluidized beds are only half the rates predicted from the work on differential beds. There is some evidence to suggest that this discrepancy may be due to the retarding effect of hydrogen sulphide on the rate of reaction.

It was realised that the reduction of barytes in a fluidized bed might have practical application in the small scale production of barium sulphide, and, in this connection, the following conclusions were reached.

(1) There appear to be no technical difficulties connected with the reduction of barytes in a fluidized bed to produce barium sulphide, although, it must be realised, that the process has only been operated on a batch basis.

(2) Even when samples as fine as +65-48# (Tyler) are reduced, a bed temperature of about 1000°C is required to utilize the rapid rates of reaction made possible by the efficient gas-solid contacting obtained in a fluidized bed. However, if the bed temperature is increased to 1100°C, material in the size range +14-10# (Tyler) can be handled efficiently.

8. RECOMMENDATIONS FOR FUTURE WORK

Since the objective of this project was to elucidate the problems associated with rate prediction in a fluidized bed, it is natural that a topic was encountered about which further information is desirable if accurate predictions are to be made.

(1) Data are required which will permit calculation of the rate of mass transfer between the continuous and discontinuous phases of a fluidized bed.

(2) The reduction of barytes by hydrogen appears to be a suitable medium for obtaining such mass transfer data since it is uncomplicated by extensive side reactions. However, in order to determine accurate mass transfer data it would be necessary to have complete knowledge of the retarding effect of water vapour on the rate of reaction. Although this effect is slight, it is significant where high conversions are obtained in the gas phase of a fluidized bed. An exhaustive study of the effect of water vapour on the rate of reaction should, therefore, be undertaken.

(3) The mechanism by which barium sulphate is reduced by hydrogen should also be determined. Such a study could be made by reducing samples of pure barium sulphate with hydrogen, hydrogen-nitrogen, and hydrogen-water mixtures. Conventional rate equations could then be fitted to the curves obtained and the unsatisfactory mechanisms eliminated. It appears that a satisfactory diagnosis of reaction mechanism cannot be made while working with mineral barytes since

small quantities of impurity appear to have a marked effect on the rate vs time curves obtained. Although the work on reaction mechanism is of a fundamental nature such information is necessary to give a sound basis for correlating the rate data obtained above.

APPENDIX A

Thermodynamic investigation of the reduction of barium sulphide by hydrogen

Appendix A **Thermodynamic investigation**

It was necessary to determine what reactions are likely to occur in the system $BaSO_4$-H_2. The method of attack used is that advocated by Hougen and Watson[92], viz., the derivation of the free energy change as a function of temperature for each reaction being investigated. The data required for the derivation of these functions were, (1) the heat of formation of each component at a known temperature, (2) the specific heat equation for each component, and (3) either the free energies of formation of each component at a known temperature, or the molal entropy for each component at a known temperature.

All the possible reactions were subjected to a preliminary investigation by means of the equation,

$$\Delta F^{\circ}_{T} = \Delta H^{\circ}_{298} - T \Delta S_{298} \qquad \text{.....(a)}$$

If these results were at all promising, i.e. ΔF°_{T} was less than 10 k cal per g mol. at any temperature within the range 400°C to 1100°C, then, where specific heat equations were available, the reaction was examined more thoroughly in the way described by Hougen and Watson[92]. The results of the investigation are summarised below.

(1) $$BaSO_4 + 4H_2 = BaS + 4H_2O$$

$$\Delta F^{\circ}_{T} = 21550 + 21.00T \ln T - 5.46\times10^{-3}T^{2} - 4.13\times10^{5}T^{-1} - 187T \qquad \text{.....(b)}$$

$$\Delta F^{\circ}_{673} = -15.3 \text{ k cal}$$

$$\Delta F^{\circ}_{1373} = -37.1 \text{ k cal}$$

Appendix A

(2) $BaSO_4 + H_2 = BaSO_3 + H_2O$

$\Delta F^\circ_T = 9800 - 11.3T$ .....(c)

$\Delta F^\circ_{673} = 2.2$ k cal

$\Delta F^\circ_{1373} = -5.7$ k cal

(3) $BaSO_3 + 3H_2 = BaS + 3H_2O$

$\Delta F^\circ_T = 3200 - 33.5T$ .....(d)

$\Delta F^\circ_{673} = -19.30$ k cal

$\Delta F^\circ_{1373} = -42.8$ k cal

(4) $BaS + H_2O = BaO + H_2S$

$\Delta F^\circ_T = 26030 + 0.56T \ln T - 1.26\times10^{-3}T^2 + 0.04\times10^{5}T^{-1} - 3.0T$.(e)

$\Delta F^\circ_{673} = 25.9$ k cal

$\Delta F^\circ_{1373} = 25.1$ k cal

(5) $BaS + 3BaSO_4 = 4BaO + 4SO_2$

$\Delta F^\circ_T = 345700 + 30.9T \ln T - 26.2\times10^{-3}T^2 + 2.84\times10^{5}T^{-1} - 377T$.(f)

$\Delta F^\circ_{673} = 216.2$ k cal

$\Delta F^\circ_{1373} = 86.9$ k cal

It can be seen that the only reactions which appear likely to proceed at temperatures below 1100°C are (1), (2), and (3) above. This means that the reduction of barium sulphate by hydrogen may proceed by way of two alternative paths, direct formation of barium sulphide, or formation of barium sulphite followed by further reduction to yield the sulphide.

The thermodynamic data used in the derivation of equations (b), (c), (d), (e), and (f) are presented in Tables X and XI.

Appendix A

Table X

Specific heats as functions of temperature

Substance	Heat capacity[79]	(cal/mol., °C)
BaS	$10.2 + 3.8\times10^{-3}T$	(same as for CaS)[98]
BaO	$9.97 + 5.21\times10^{-3}T$	
$BaSO_4$	$33.80 - 8.43\times10^{5}T^{-2}$	
$H_2(g)$	$6.52 + 0.78\times10^{-3}T + 0.12\times10^{5}T^{-2}$	
$H_2O(g)$	$7.17 + 2.56\times10^{-3}T + 0.08\times10^{5}T^{-2}$	
$SO_2(g)$	$10.38 + 2.54\times10^{-3}T - 1.42\times10^{5}T^{-2}$	
$H_2S(g)$	$7.02 + 3.68\times10^{-3}T$	

Table XI

Standard heats of formation and molal entropies

Substance	$(\Delta H_f)_{298}$ (k cal/g mol.)[76]	S_{298} (E.U.)[77]
BaS	-106.0	20.8 ± 1.0[78]
BaO	-133.0	16.8 ± 0.3
$BaSO_3$	-282.6	29.0 ± 1.0*
$BaSO_4$	-350.2	31.6 ± 0.2
$H_2(g)$		31.22 ± 0.01
$H_2O(g)$	-57.8	45.13 ± 0.03
$SO_2(g)$	-70.96	59.24 ± 0.1
$H_2S(g)$	-4.81	49.10 ± 0.1

*Calculated in the way indicated for BaS[78]

APPENDIX B

Data from the equilibrium determinations

Appendix B

TABLE XII

Values of the ratio $(H_2O/H_2)_{equilibrium}$ for Series C and D samples

Sample	Temp.(°C)	$(H_2O/H_2)_{equilibrium}$	Remarks
C3	905	32.6±0.5	55% of the $BaSO_4$ was reduced at 900°C. H_2O-H_2 flow rate = 35 cm^3/min N.T.P.
C4	805	33.5±1.0	40% of the $BaSO_4$ was reduced at 900°C. H_2O-H_2 flow rate = 35 cm^3/min N.T.P.
	900	32.3±1.0	
	982	31.7±1.0	
C5	705	36.0±2.0	3% of the $BaSO_4$ was reduced at 900°C. H_2O-H_2 flow rate = 35 cm^3/min N.T.P.
	800	34.0±1.0	
	895	32.9±1.0	
C6	805	34.5±2.0	65% of the $BaSO_4$ was reduced at 900°C. H_2O-H_2 flow rate = 35 cm^3/min N.T.P.
	880	32.5±0.5	
	990	31.5±0.5	
C9	690	34.0±2.0	30% of the $BaSO_4$ was reduced at 1000°C. H_2O-H_2 flow rate = 70 cm^3/min N.T.P.
	797	32.6±1.0	
	905	32.7±1.0	
	993	31.5±0.5	
	1090	31.2±0.5	

Appendix B

Table XII (cont.)

Sample	Temp.(°C)	$(H_2O/H_2)_{equilibrium}$	Remarks
C10	710	34.5±1.0	5% of the $BaSO_4$ was
	793	32.7±1.0	reduced at 1000°C.
	917	32.2±0.5	H_2O-H_2 flow rate =
	1007	31.0±0.5	35 cm^3/min N.T.P.
	1104	30.4±0.3	
C11	710	34.0±2.0	15% of the $BaSO_4$ was
	800	33.5±1.0	reduced at 1100°C.
	903	32.7±0.5	H_2O-H_2 flow rate =
	1005	31.3±0.5	35 cm^3/min N.T.P.
	1106	30.7±0.3	
	1106	30.7±0.3	
C12	907	32.8±1.0	21% of the $BaSO_4$ was
	1010	31.6±0.5	reduced at 1100°C.
	1106	31.2±0.5	H_2O-H_2 flow rate =
	1111	30.4±0.3	70 cm^3/min N.T.P.
D1	910	33.0±1.0	50% $BaSO_4$, 50% BaS-$Ba(OH)_2$
			BaS-$Ba(OH)_2$ material
			contained S equivalent to
			64% of the Ba present.

Appendix B

Table XII (cont.)

Sample	Temp.(°C)	$(H_2O/H_2)_{equilibrium}$	Remarks
D2	800	34.0±1.0	50% $BaSO_4$, 50% $BaS-Ba(OH)_2$
	890	33.0±1.0	$BaS-Ba(OH)_2$ material contained S equivalent to 97% of the Ba present. H_2O-H_2 flow rate = 35 cm^3/min N.T.P.

APPENDIX C

Rate data obtained from fixed beds

Appendix C

TABLE XIII

Rate data - fixed beds

It should be noted that all rates are expressed as grammes of water per minute per gramme of barytes.
All runs were carried out at a gas flow rate of 13 litre/min N.T.P. unless otherwise specified.
The uncertainty given in the temperature measurements represents the maximum variation in the measured temperature during a run.
All runs were carried out with hydrogen as the reducing gas unless otherwise stated.
Sample assays are given in Table XIV, page 223.

Run No.	Time (min)	%Redn.	Rate	Remarks
E32	0	0		Sample B
			1.7×10^{-2}	
	1	5.5		+8-6# crushed barytes
			1.75	
	3	16.9		Temp. = 992±5°C
			1.8	
	5	28.6		Inlet conditions
			1.8	
	7	40.3		p_{H_2} = 0.52 atm.
			1.65	
	9	51.0		p_{N_2} = 0.48 atm.
			1.4	
	12	64.6		
			1.1	
	15	75.4		
			0.75	
	18	82.5		
			0.5	
	21	87.4		
E33	0	0		Sample B
			1.7×10^{-2}	
	1	5.5		Temp. = 995±2°C
			1.8	
	3	17.2		Inlet conditions
			2.0	
	5	30.4		p_{H_2} = 0.52 atm.
			1.7	
	7	41.3		p_{N_2} = 0.48 atm.
			1.5	

Appendix C

Table XIII (Cont.)

Run No.	Time (min)	% Redn.	Rate	Remarks
E33 (cont.)	9	51.2	1.3×10^{-2}	
	11	59.6	1.0	
	14	69.4	0.75	
	17	76.2	0.5	
	20	81.3		
E34	0	0	1.8×10^{-2}	Sample B
	1	5.9	2.5	Temp. = 994±2°C
	3	22.0	2.8	
	5	40.4	2.3	
	7	55.0	1.9	
	9	67.5	1.35	
	11	76.2	0.9	
	14	88.1		
E35	0	0	1.9×10^{-2}	Sample B
	1	6.2	2.25	Temp. = 993±2°C
	3	20.7	2.65	
	5	38.0	2.1	
	7	51.5	1.7	
	9	62.8	1.4	

Appendix C

Table XIII (cont.)

Run No.	Time (min)	% Redn.	Rate	Remarks
E35 (cont.)	11	71.8	1.0×10^{-2}	
	14	81.6	0.6	
	17	87.5	0.3	
	20	93.5		
E36	0	0	1.6×10^{-2}	Sample B
	1	5.1	1.8	Temp. = 990±2°C
	3	16.8	1.9	Inlet conditions
	5	29.3	1.7	p_{H_2} = 0.52 atm.
	7	40.2	1.6	p_{N_2} = 0.48 atm.
	9	50.6	1.35	
	11	59.4	1.1	
	14	70.2	0.8	
	17	77.8	0.5	
	20	82.6		
E37	0	0	6.0×10^{-2}	Sample B
	0.5	10.0	4.5	Temp. = 1094±5°C
	1	16.8	4.1	Inlet conditions
	2	30.2	2.9	p_{H_2} = 0.52 atm.
	4	49.0	2.2	p_{N_2} = 0.48 atm.
	6	63.1	1.5	

Appendix C

Table XIII (cont.)

Run No.	Time (min)	% Redn.	Rate	Remarks
E37 (cont.)	8	73.0	0.8×10^{-2}	
	11	80.8	0.3	
	14	83.5		
E E38	0	0	6.2×10^{-2}	Sample B
	0.5	9.9	5.0	Temp. = $1099 \pm 2^{\circ}C$
	1	16.3	4.0	Inlet conditions
	2	31.1	3.4	p_{H_2} = 0.52 atm.
	4	53.5	2.5	p_{N_2} = 0.48 atm.
	6	69.5	1.5	
	8	79.5	0.8	
	11	86.8	0.3	
	14	90.0		
E39	0	0	6.9×10^{-2}	Sample B
	0.5	11.0	5.2	Temp. = $1109 \pm 5^{\circ}C$
	1	19.3	4.2	
	2	33.0	3.0	
	4	52.4	2.3	
	6	67.5	1.4	
	8	76.6		

Appendix C Table XIII (cont.)

Run No.	Time (min)	% Redn.	Rate	Remarks
E40	0	0		Sample B
			1.8×10^{-2}	
	0.5	3.0		Temp. = 1088±5°C
			1.2	
	1	4.8		Inlet conditions
			0.9	
	2	7.9		p_{H_2} = 0.06 atm.
			0.8	
	4	13.0		p_{N_2} = 0.94 atm.
			0.8	
	6	18.3		
			0.8	
	8	24.5		
			0.7	
	10	28.0		
E41	0	0		Sample B
			1.6×10^{-2}	
	1	5.2		Temp. = 1095±5°
			1.4	
	2	9.6		Inlet conditions
			1.0	
	4	16.3		p_{H_2} = 0.06 atm.
			0.9	
	6	22.1		p_{N_2} = 0.94 atm.
			0.8	
	9	27.1		
			0.7	
	12	31.2		
E42	0	0		Sample B
			1.6×10^{-2}	
	1	5.1		Temp. = 1095±2°C
			1.1	
	2	8.9		Inlet conditions
			0.9	
	4	14.5		p_{H_2} = 0.06 atm.
			0.8	
	6	20.0		p_{N_2} = 0.94 atm.
			0.8	

Appendix C Table XIII (cont.)

Run No.	Time (min)	% Redn.	Rate	Remarks
E42 (cont.)	8	25.0		
			0.7	
	9	29.4		
			0.7	
	12	36.2		
			0.6	
	15	42.2		
			0.5	
	19	48.7		
			0.4	
	23	54.0		
E43	0	0		Sample B
			1.3×10^{-2}	
	1	4.1		Temp. = $1099 \pm 2^{\circ}C$
			1.2	
	2	8.1		Flow rate = 0.86 litre/
			3.0	
	4	28.7		min N.T.P. of pure H_2
			2.9	
	7	55.7		
			1.7	
	10	72.5		
E44	0	0		Sample B
			0.5×10^{-2}	
	1	1.7		Temp. = $1016 \pm 5^{\circ}C$
			0.4	
	2	3.0		Inlet conditions
			0.4	
	4	5.5		p_{H_2} = 0.06 atm.
			0.4	
	7	8.2		p_{N_2} = 0.94 atm.
			0.4	
	10	12.0		
			0.4	
	13	15.8		
			0.4	
	17	19.8		
			0.35	
	21	22.8		

Appendix C Table XIII (cont.)

Run No.	Time (min)	% Redn.	Rate	Remarks
E45	0	0		Sample B
			0.5×10^{-2}	
	2	3.4		Temp. = 1015±2°C
			0.6	
	4	7.2		Inlet conditions
			0.6	
	7	13.1		p_{H_2} = 0.06 atm.
			0.6	
	10	18.8		P_{N_2} = 0.94 atm.
			0.6	
	15	28.5		
			0.5	
	20	36.6		
			0.5	
	25	44.7		
			0.4	
	30	51.2		
E46	0	0		Sample B
			0.8×10^{-2}	
	1	2.5		Temp. = 1019±2°C
			0.7	
	4	9.5		Flow rate = 0.86 litre/
			1.4	
	8	27.5		min N.T.P. of pure H_2
			1.4	
	12	45.5		
			1.3	
	16	62.5		
			1.0	
	20	75.5		
E47	0	0		Sample B
			0.4×10^{-2}	
	2	2.7		Temp. = 1016±2°C
			0.5	
	5	7.6		Inlet conditions
			0.4	
	8	11.3		p_{H_2} = 0.06 atm.
			0.4	
	11	15.2		p_N = 0.94 atm.
			0.4	

Appendix C Table XIII (cont.)

Run No.	Time (min)	% Redn.	Rate	Remarks
E47 (cont.)	15	20.5	0.4	
	19	25.6		
E48	0	0	0.6×10^{-2}	Sample B
	2	3.9	0.8	Temp. = $1016 \pm 2^{\circ}C$
	4	9.0	1.1	Flow rate = 0.86 litre/
	7	20.0	1.0	min N.T.P. of pure H_2
	10	29.5	1.4	
	14	43.0	1.2	
	18	58.7	0.8	
	23	71.8		
E49	0	0	0.5×10^{-2}	Sample B
	2	3.2	0.7	Temp. = $980 \pm 5^{\circ}C$
	4	7.7	1.2	Flow rate = 0.86 litre/
	8	24.6	1.0	min N.T.P. of pure H_2
	12	37.5	1.0	
	16	50.6	0.9	
	20	62.5		

Appendix C Table XIII (cont.)

Run No.	Time (min)	% Redn.	Rate	Remarks
E50	0	0		Sample C
			1.6×10^{-2}	
	1	5.2		+6-4# crushed barytes
			2.1	
	3	18.6		Temp. = 996±2°C
			2.2	
	5	33.2		
			1.9	
	7	45.4		
			1.7	
	9	56.5		
			1.5	
	11	71.0		
			1.2	
	14	82.7		
			0.8	
	17	90.5		
			0.4	
	20	94.4		
			0.2	
	25	97.5		
E51	0	0		Sample C
			1.7×10^{-2}	
	1	5.6		Temp. = 996±2°C
			2.0	
	3	18.6		
			2.0	
	5	31.4		
			1.8	
	7	43.2		
			1.7	
	9	54.3		
			1.3	
	11	62.6		
			1.1	
	14	73.5		
			0.8	
	17	81.1		
			0.6	
	20	87.0		

Appendix C Table XIII (cont.)

Run No.	Time (min)	% Redn.	Rate	Remarks
E52	0	0		Sample D
			2.7×10^{-2}	
	1	8.7		+14-10# crushed
			3.2	
	3	29.6		barytes of the same
			3.5	
	5	52.2		composition as Sample
			2.8	
	7	70.4		C.
			2.0	
	9	83.5		Temp. = 996±2°C
			1.2	
	11	91.1		
			0.5	
	14	96.1		
			0.1	
	17	97.0		
E53	0	0		Sample D
			2.1×10^{-2}	
	1	6.9		Temp. = 1006±2°C
			3.1	
	3	27.0		
			3.5	
	5	49.7		
			2.7	
	7	67.2		
			2.2	
	9	81.5		
			1.3	
	11	89.8		
			0.6	
	15	97.5		
			0.1	
	19	99.0		

Appendix C Table XIII (cont.)

Run No.	Time (min)	% Redn.	Rate	Remarks
E54	0	0		Sample E
			1.0×10^{-2}	
	1	3.2		4.4 mm spheres
			1.1	
	3	10.4		Specific area =
			1.3	
	5	18.8		3.2 cm^2/g
			1.4	
	7	27.9		Temp. = 100±5°C
			1.4	
	9	37.0		
			1.3	
	11	45.5		
			1.2	
	14	57.0		
			1.0	
	17	67.0		
			0.8	
	20	74.5		
			0.5	
	25	82.8		
			0.3	
	30	87.6		
			0.2	
	35	91.0		
			0.1	
	40	92.5		
E55	0	0		Sample E
			1.6×10^{-2}	
	1	5.2		4.4 mm spheres
			1.3	
	3	13.7		Temp. = 100±5°C
			1.4	
	5	22.8		
			1.3	
	7	31.2		
			1.2	
	9	39.0		
			1.2	

Appendix C Table XIII (cont.)

Run No.	Time (min)	% Redn.	Rate	Remarks
E55 (cont.)	11	46.7		
			1.1	
	14	57.5		
			1.0	
	17	67.3		
			0.8	
	20	75.0		
			0.7	
	25	86.5		
E56	0	0		Sample F
			0.8×10^{-2}	
	1	2.6		6.2 mm spheres
			0.6	
	3	6.5		Specific surface =
			0.6	
	5	10.5		2.2 cm^2/g
			0.6	
	7	14.4		Temp. = 1014±5°C
			0.5	
	9	17.5		
			0.5	
	11	21.0		
			0.5	
	14	26.0		
			0.5	
	17	30.0		
			0.5	
	20	35.4		
			0.4	
	30	48.0		
			0.3	
	40	58.0		
E57	0	0		Sample F
			0.7×10^{-2}	
	1	2.4		6.2 mm spheres
			0.5	
	3	5.6		Temp. = 1007±5°C
			0.5	

Appendix C Table XIII (cont.)

Run No.	Time (min)	% Redn.	Rate	Remarks
E57 (cont.)	5	8.8		
			0.4	
	7	11.4		
			0.4	
	10	15.4		
			0.4	
	13	19.2		
			0.35	
	17	23.7		
			0.35	
	20	27.0		
			0.3	
	30	36.8		
			0.3	
	40	46.2		
E58	0	0		Sample F
			1.0×10^{-2}	
	1	3.2		6.8 mm hemispheres
			0.9	
	3	9.1		Specific surface =
			0.8	
	5	14.4		3.0 cm^2/g
			0.8	
	7	19.5		Temp. = $1017 \pm 2^{\circ}C$
			0.7	
	10	26.3		
			0.6	
	13	32.1		
			0.6	
	17	39.8		
			0.5	
	21	46.5		
			0.5	
	25	53.0		
			0.4	
	30	59.5		

Appendix C Table XIII (cont.)

Run No.	Time (min)	% Redn.	Rate	Remarks
E59	0	0		Sample E
			1.4×10^{-2}	
	1	4.6		4.4 mm spheres
			1.5	
	3	14.3		Specific surface =
			1.4	
	5	23.5		3.2 cm^2/g
			1.4	
	7	32.6		Temp. = 1011±3°C
			1.2	
	10	44.3		
			1.1	
	13	54.7		
			0.9	
	17	66.5		
			0.6	
	21	74.4		
			0.5	
	25	80.9		
E60	0	0		Sample F
			0.9×10^{-2}	
	1	2.9		5 mm cubes
			0.7	
	3	7.4		Specific surface =
			0.7	
	5	12.2		2.7 cm^2/g
			0.6	
	7	15.9		Temp. = 1014±2°C
			0.6	
	10	21.8		
			0.6	
	13	27.7		
			0.55	
	17	35.0		
			0.5	
	21	41.3		
			0.5	
	25	47.6		
			0.45	
	30	54.6		
			0.4	
	35	61.5		

Appendix C Table XIII (cont.)

Run No.	Time (min)	% Redn.	Rate	Remarks
E61	0	0		Sample D
			2.7×10^{-2}	
	1	8.8		+14-10# crushed barytes
			3.6	
	3	32.0		Temp. = 1013±5°C
			3.7	
	5	56.1		
			3.0	
	7	75.5		
			2.0	
	9	88.5		
			1.0	
	11	95.0		
			0.3	
	15	99.0		
			0.1	
	20	100.0		
E62	0	0		Sample E
			6.6×10^{-2}	
	0.5	10.7		4.4 mm spheres
			6.0	
	1	20.5		Specific surface =
			5.4	
	2	38.0		3.2 cm^2/g
			3.9	
	4	63.3		Temp. = 1103±2°C
			2.3	
	6	78.1		
			1.6	
	8	88.6		
			1.0	
	10	95.1		
			0.4	
	14	100.0		
			0.2	
	18	102		

Appendix C Table XIII (cont.)

Run No.	Time (min)	% Redn.	Rate	Remarks
E63	0	0		Sample E
			6.6×10^{-2}	
	0.5	10.3		4.4 mm spheres
			5.7	
	1	19.9		Temp. = 1101±2°C
			5.1	
	2	36.6		
			3.6	
	4	60.0		
			2.4	
	6	75.6		
			1.7	
	8	87.4		
			1.2	
	10	94.8		
E64	0	0		Sample F
			4.0×10^{-2}	
	0.5	6.5		6.2 mm spheres
			2.7	
	1	11.1		Specific surface =
			2.0	
	2	17.6		2.2 cm^2/g
			1.7	
	4	28.6		Temp. = 1103±5°C
			1.4	
	6	37.7		
			1.0	
	8	44.2		
			0.9	
	10	50.0		
			0.8	
	14	60.5		
			0.6	
	18	68.1		

Appendix C Table XIII (cont.)

Run No.	Time (min)	% Redn.	Rate	Remarks
E65	0	0		Sample F
			3.4×10^{-2}	
	0.5	5.5		6.2 mm spheres
			2.4	
	1	9.4		Temp. = $1105 \pm 5^{\circ}C$
			2.0	
	2	15.9		
			1.6	
	4	26.0		
			1.2	
	6	33.8		
			0.9	
	8	39.6		
			0.8	
	10	44.6		
			0.6	
	14	53.0		
			0.5	
	18	60.0		
			0.4	
	22	65.6		
			0.3	
	26	70.4		
E66	0	0		Sample F
			3.2×10^{-2}	
	0.5	5.2		6.2 mm spheres
			2.3	
	1	8.8		Temp. = $1108 \pm 2^{\circ}C$
			1.9	
	2	15.1		
			1.4	
	4	24.0		
			1.0	
	6	30.6		
			0.8	
	8	35.9		
			0.6	
	10	39.7		
			0.5	
	14	46.2		

Appendix C Table XIII (cont.)

Run No.	Time (min)	% Redn.	Rate	Remarks
E67	0	0		Sample F
			4.7×10^{-2}	
	0.5	7.8		5 mm cubes
			3.9	
	1	14.4		Specific surface =
			2.8	
	2	23.7		2.7 cm^2/g
			2.1	
	4	37.4		Temp. = $1106 \pm 2^{\circ}C$
			1.6	
	6	47.0		
			1.3	
	8	56.0		
			1.1	
	10	62.1		
			0.9	
	14	75.6		
			0.7	
	18	84.0		
E68	0	0		Sample F
			6.0×10^{-2}	
	0.5	9.8		3.75 mm spheres
			5.0	
	1	17.8		Specific area =
			3.8	
	2	30.1		3.7 cm^2/g
			2.6	
	4	47.3		Temp. = $1108 \pm 2^{\circ}C$
			2.0	
	6	60.0		
			1.4	
	8	69.0		
			1.1	
	10	76.0		
			0.7	
	14	86.0		
			0.5	
	18	92.6		

Appendix C Table XIII (cont.)

Run No.	Time (min)	% Redn.	Rate	Remarks
E69	0	0		Sample F
			1.3×10^{-2}	
	1	4.3		3.75 mm spheres
			1.2	
	3	12.0		Temp. = $1013 \pm 2^{\circ}C$
			1.0	
	5	18.3		
			0.8	
	7	24.1		
			0.7	
	9	28.2		
			0.6	
	11	32.5		
			0.6	
	14	38.0		
			0.5	
	17	43.1		
			0.4	
	20	48.6		
			0.4	
	25	56.2		
			0.4	
	30	65.1		
E70	0	0		Sample G
			9.5×10^{-2}	
	0.5	15.4		+10-8# crushed barytes
			8.9	
	1	29.8		Temp. = $1097 \pm 5^{\circ}C$
			6.9	
	2	52.5		
			4.3	
	4	79.1		
			1.9	
	6	92.2		
			0.7	
	8	96.6		
			0.3	
	10	98.6		

Appendix C Table XIII (cont.)

Run No.	Time (min)	% Redn.	Rate	Remarks
E71	0	0		Sample G
			8.6×10^{-2}	
	0.5	14.0		Temp. = 1095±5°C
			8.4	
	1	28.0		
			7.2	
	2	51.2		
			4.6	
	4	79.8		
			2.0	
	6	93.8		
			0.7	
	8	98.4		
			0.2	
	10	100.0		
E72	0	0		Sample G
			3.6×10^{-2}	
	0.5	5.7		Temp. = 1061±3°C
			4.0	
	1	12.4		
			4.3	
	2	26.9		
			4.0	
	4	52.1		
			2.9	
	6	71.5		
			1.7	
	8	82.4		
			1.1	
	10	91.0		
			0.5	
	14	95.7		
E73	0	0		Sample H
			6.1×10^{-2}	
	0.5	9.9		3.06 mm spheres
			6.5	
	1	20.4		
			5.7	

Appendix C Table XIII (cont.)

Run No.	Time (min)	% Redn.	Rate	Remarks
E73 (cont.)	2.5	48.3		Specific surface =
			4.2	
	4	68.6		4.4 cm^2/g
			2.6	
	6	85.4		Temp. = 1099±2°C
			1.3	
	8	93.8		N.B. Initial rate is
			0.5	
	10	97.0		probably low
			0.2	
	14	99.5		
E74	0	0		Sample H
			9.0×10^{-2}	
	0.5	14.6		2.3 mm spheres
			8.3	
	1	28.0		Specific surface =
			7.2	
	2	51.4		5.8 cm^2/g
			4.5	
	4	80.6		Temp. = 1103±3°C
			2.0	
	6	93.5		N.B. Initial rate is
			0.6	
	8	97.5		probably low.
			0.3	
	10	99.5		
E75	0	0		Sample G
			8.4×10^{-2}	
	0.5	13.6		+10-8# crushed barytes
			7.6	
	1	26.0		Temp. = 1109±5°C
			7.4	
	2	50.0		
			4.7	
	4	80.5		
			2.0	

Appendix C Table XIII (cont.)

Run No.	Time (min)	% Redn.	Rate	Remarks
E75 (cont.)	6	93.5	0.6	
	8	97.5	0.1	
	12	99.0		
E76	0	0		Sample G
	1	22.3		Temp. = 1100±10°C
	2	43.7		Inlet conditions
	4	75.8		p_{H_2O} = 0.03 atm.
				p_{H_2} = 0.97 atm.
E77	0	0		Sample G
	0.5	13.0		Temp. = 1100±10°C
	1	25.7		Inlet conditions
	2	34.5		p_{H_2O} = 0.06 atm.
	4	69.5		p_{H_2} = 0.94 atm.
	5	82.7		
E78	0	0		Sample G
	0.5	13.7		Temp. = 1100±10°C
	1	24.3		Inlet conditions
	2	44.8		p_{H_2O} = 0.2 atm.
	4	68.3		p_{H_2} = 0.8 atm.

Appendix C Table XIII (cont.)

Run No.	Time (min)	% Redn.	Rate	Remarks
E79	0	0		Sample G
	0.5	13.8		Temp. = 1100±10°C
	1	25.2		
	1.5	37.6		
	4	79.6		
E80	0	0		Sample G
	1	4.0	1.2×10^{-2}	Temp. = 1000±10°C
	3	16.2	1.9	Inlet conditions
	5	25.8	1.5	p_{H_2O} = 0.2 atm.
	7	37.0	1.7	p_{H_2} = 0.8 atm.
	10	54.2	1.8	
	20	84.4	1.2	
E81	0	0		Sample H
	0.5	15.4	9.5×10^{-2}	3.25 mm spheres
	1	27.9	7.7	Specific surface =
	2	48.0	6.2	4.15 cm^2/g
	4	74.5	4.1	Temp. = 1102±5°C
	6	89.0	2.2	
	8	95.6	1.0	
	10	98.5	0.4	
	14	99.0	0.02	

Appendix C Table XIII (cont.)

Run No.	Time (min)	% Redn.	Rate	Remarks
E82	0	0		Sample G
			1.3×10^{-2}	
	1	4.5		+10-8# crushed barytes
			1.7	
	3	15.7		Temp. = 995±10°C
			2.1	
	5	29.7		
			2.2	
	7	44.0		
			2.0	
	9	57.4		
			1.6	
	11	68.2		
			1.2	
	14	80.6		
			0.8	
	17	88.6		
			0.5	
	20	93.5		
			0.2	
	25	97.4		
E83	0	0		Sample H
			6.1×10^{-2}	
	0.5	9.9		6.3 mm spheres
			4.7	
	1	17.5		Specific surface =
			3.9	
	2	30.3		2.1 cm^2/g
			2.9	
	4	48.8		Temp. = 1107±5°C
			2.0	
	6	61.7		
			1.5	
	8	71.2		
			1.1	
	10	78.3		
			0.7	
	14	87.4		
			0.5	
	18	93.2		
			0.2	

Appendix C Table XIII (cont.)

Run No.	Time (min)	% Redn.	Rate	Remarks
E83 (cont.)	22	96.8	0.1×10^{-2}	
	26	97.0		
E84	0	0	15.1×10^{-2}	Sample H
	0.5	24.5	10.2	2.3 mm spheres
	1	41.1	7.6	Specific surface =
	2	65.9	3.9	5.8 cm^2/g
	4	91.3	0.9	Temp. = 1103±5°C
	7	100.0		
E85	0	0	1.6×10^{-2}	Sample J
	1	5.5	2.1	+10-8 # crushed barytes
	3	19.8	2.5	Temp. = 1004±5°C
	5	36.8	2.5	
	7	53.5	2.2	
	9	68.1	1.7	
	11	79.5	1.1	
	14	90.1	0.6	
	17	95.6	0.2	
	20	98.0	0.1	
	25	98.5		

Appendix C Table XIII (cont.)

Run No.	Time (min)	% Redn.	Rate	Remarks
E86	0	0		Sample J
			25.0×10^{-2}	
	0.5	40.5		Heated to 1160°C
			21.0	
	1	75.0		before being reduced.
			5.9	
	2	94.0		Temp. = 1105±3°C
			0.9	
	4	99.5		
			0.05	
	6	100.0		
E87	0	0		Sample J
			12.3×10^{-2}	
	0.5	20.0		Heated to 1130°C
			11.0	
	1	37.8		before being reduced.
			8.9	
	2	66.6		Temp. = 1100±3°C
			3.9	
	4	92.0		
			0.8	
	6	97.1		
			0.05	
	8	97.6		
E88	0	0		Sample J
			2.1×10^{-3}	
	10	6.8		Temp. = 899±2°C
			2.4	
	20	14.7		
			2.7	
	30	23.7		
			3.0	
	40	33.4		
			2.9	
	50	43.1		
			2.7	
	60	52.4		
			2.6	

Appendix C Table XIII (cont.)

Run No.	Time (min)	% Redn.	Rate	Remarks
E88 (cont.)	70	60.5	2.4×10^{-3}	
	80	68.2	2.2	
	90	74.9		
E89	0	0	4.7×10^{-2}	Sample I
	0.5	7.6	3.5	5.7 mm spheres
	1	13.3	3.2	Specific surface =
	2	23.7	2.7	2.4 cm^2/g
	4	41.2	2.1	Temp. = 1102±2°C
	6	54.4	1.6	
	8	64.5	1.3	
	10	72.8	0.9	
	14	84.5	0.5	
	18	91.8	0.3	
	22	95.5		
E90	0	0	4.8×10^{-2}	Sample I
	0.5	7.8	3.5	5.7 mm spheres
	1	13.5	3.0	Temp. = 1102±5°C
	2	23.4	2.4	Inlet conditions
	4	39.3	1.8	p_{H_2} = 0.52 atm.
	6	50.8	1.4	p_{N_2} = 0.48 atm.

Appendix C Table XIII (cont.)

Run No.	Time (min)	% Redn.	Rate	Remarks
E90 (cont.)	8	60.4	1.2×10^{-2}	
	10	68.2	0.8	
	14	79.2	0.5	
	18	86.4	0.3	
	22	90.3	0.1	
	26	92.1	0.05	
	30	93.6		
E91	0	0	1.4×10^{-2}	Sample J
	1	4.7	1.5	+10-8# crushed barytes
	3	14.4	1.6	Temp. = 1000±5°C
	5	25.1	1.7	Inlet conditions
	7	35.9	1.6	p_{H_2} = 0.52 atm.
	9	46.5	1.5	p_{N_2} = 0.48 atm.
	11	56.6	1.3	
	14	69.6	1.0	
	17	78.8	0.6	
	20	85.4	0.3	
	25	89.8	0.1	
	30	91.6		
E92	0	0	12.0×10^{-2}	Sample J
	0.5	19.5	11.1	Temp. = 1100±2°C

Appendix C Table XIII (cont.)

Run No.	Time (min)	% Redn.	Rate	Remarks
E92 (cont.)	1	37.8		
			8.5	
	2	65.0		
			3.5	
	4	88.9		
			0.7	
	6	92.6		

TABLE XIV.

Sample Assays

Sample	Assay	
	SiO_2 (%)	Fe_2O_3 (%)
B, C, and D	not assayed	not assayed
E	2.0	1.3
F	0.25	0.30
G	2.0	1.2
H	2.5	2.0
I	1.9	1.3
J	2.1	3.0

APPENDIX D

Rate data obtained from fluidized beds

Appendix D

TABLE XV

Rate data - fluidized beds

It should be noted that all rates are expressed as grammes of barium sulphate per minute per gramme of barytes sample.
The uncertainty given for the temperature measurement represents the maximum variation of the measured temperature during a run.
All runs were carried out with hydrogen as the reducing gas unless otherwise stated.
All beds were of +14-10# barytes unless otherwise stated.

Run No.	H_2 Volume ($ft.^3$)	Time (min)	Rate x 10^2	Remarks
F18	0	0		1500g bed
	6	0.97	9.2	Temp. = 1080±20°C
	7	1.43	8.6	Gas flow rate
	8	1.92	8.5	= 185 litre/min
	9	2.42	8.5	N.T.P.
	10	2.92	8.0	Amb. temp. = 25°C
	11	2.45	8.0	
	12	2.98	7.7	
	13	3.53	7.2	
	14	5.12	7.3	
	15	5.70	6.8	
	16	6.32	6.5	
	17	6.97	5.7	
	18	7.70	4.8	
	19	8.57	4.1	
	20	9.57	3.2	

Appendix D

Table XV (cont.)

Run No.	H_2 Volume ($ft.^3$)	Time (min)	Rate x 10^2	Remarks
F18 (cont.)	21	10.83		
			2.9	
	22	12.23		
			2.3	
	23	14.00		
			1.7	
	24	16.23		
			1.2	
	25	19.33		
			0.7	
	26	23.92		
			0.1	
	27	36.92		
			0	
	28	58.92		
F19	0	0		1500g bed
	6	0.97		Temp.= 1005±10°C
			4.9	
	7	1.80		Gas flow rate
			4.1	
	8	2.78		= 185 litre/min
			3.1	
	9	4.03		N.T.P.
			2.6	
	10	5.53		Amb. temp. = 26°C
			2.3	
	11	7.17		
			2.3	
	12	8.82		
			2.1	
	13	10.60		
			2.1	
	14	12.37		
			2.2	
	15	14.10		
			2.2	
	16	15.83		
			1.7	

Appendix D

Table XV (cont.)

Run No.	H_2 Volume($ft.^3$)	Time (min)	Rate x 10^2	Remarks
F19 (cont.)	17	17.96		
			1.5	
	18	20.32		
			1.6	
	19	22.60		
			1.5	
	20	24.98		
			1.3	
	21	27.68		
			1.2	
	22	30.52		
			1.3	
	23	33.18		
			1.3	
	24	35.87		
			1.0	
	25	39.25		
			0.8	
	26	43.83		
			0.8	
	27	46.95		
			0.9	
	28	50.58		
			0.6	
	29	55.53		
			0.4	
	30	61.70		
			0.1	
	31	71.43		
			0	
	32	85.77		
			0	
	33	100.92		
F20	0	0		1500g bed
	6	1.00		Temp. = 1000±10°C
			5.7	
	7	1.75		
			4.8	

Appendix D

Table XV (cont.)

Run No.	H_2 Volume ($ft.^3$)	Time (min)	Rate x 10^2	Remarks
F20 (cont.)	8	2.65	3.4	Gas flow rate = 185 litre/min N.T.P. Amb. temp = 27°C
	9	3.90	2.5	
	10	5.60	2.0	
	11	7.74	1.9	
	12	10.02	1.9	
	13	12.32	2.2	
	14	14.27	2.2	
	15	16.25	2.2	
	16	18.20	2.2	
	17	20.17	2.2	
	18	22.05	2.0	
	19	24.15	1.7	
	20	26.53	1.6	
	21	29.25	1.5	
	22	31.78	1.6	
	23	34.47	1.6	
	24	37.25	1.3	
	25	40.50	1.1	
	26	44.33	0.9	
	27	49.33	0.6	
	28	56.33	0.2	
	29	76.00		

Appendix D

Table XV (cont.)

Run No.	H_2 Volume($ft.^3$)	Time (min)	Rate x 10^2	Remarks
F21	0	0		1500g bed
	6	0.82	6.1	Temp. = 1000±10°C
	7	1.53	4.6	Gas flow rate =
	8	2.45	3.5	220 litre/min
	9	3.68	3.2	N.T.P.
	10	5.00	3.1	Amb. temp. = 23°C
	11	6.37	3.5	
	12	7.60	3.4	
	13	8.85	3.6	
	14	10.03	3.4	
	15	11.28	3.6	
	16	12.45	3.3	
	17	13.73	3.4	
	18	14.97	3.4	
	19	16.22	3.5	
	20	17.45	3.4	
	21	18.70	3.3	
	22	20.00	2.8	
	23	21.50	2.6	
	24	23.28	1.8	

Appendix D

Table XV (cont.)

Run No.	H_2 Volume ($ft.^3$)	Time (min)	Rate x 10^2	Remarks
F21 (cont.)	25	25.60		
	26	28.50	1.4	
	27	32.70	0.9	
	28	39.25	0.6	
	29	61.00	0.1	
	30	98.00	0	
F22	0	0		750g bed
	6	0.95	5.2	Temp. = 1000±10°C
	7	2.60	3.5	Gas flow rate =
	8	4.97	3.6	185 litre/min
	9	7.27	4.4	Amb. temp. = 24°C
	10	9.17	4.1	
	11	11.20	3.6	
	12	13.53	3.4	
	13	15.98	3.2	
	14	18.50	2.7	
	15	21.55	1.8	
	16	25.91	0.8	
	17	35.25	0.2	
	18	61.33	0	
	18.5	83.00		

Appendix D

Table XV (cont.)

Run No.	H_2 Volume ($ft.^3$)	Time (min)	Rate x 10^2	Remarks
F23	0	0		750g bed
	6	0.82	4.2	Temp. = 990±15°C
	7	2.77	2.7	Gas flow rate =
	8	5.62	3.2	220 litre/min
	9	8.05	3.2	Amb. temp. = 35°C
	10	10.47	3.3	
	11	12.82	3.5	
	12	15.00	3.3	
	13	17.38	3.1	
	14	19.88	2.4	
	15	23.00	1.9	
	16	27.03	1.1	
	17	33.42	0.4	
	18	47.00	0	
	19	86.00		
F24	0	0		750g bed
	6	0.83	4.3	Temp. = 990±15°C
	7	2.70	3.1	Gas flow rate
	8	5.25	3.4	= 220 litre/min
	9	7.55	3.9	N.T.P.
	10	9.58	5.0	Amb. temp. = 26°C

Appendix D

Table XV (cont.)

Run No.	H_2 Volume ($ft.^3$)	Time (min)	Rate x 10^2	Remarks
F24 (cont.)	11	11.22		
			4.9	
	12	12.87		
			3.8	
	13	14.97		
			3.5	
	14	17.27		
			2.7	
	15	20.18		
			2.0	
	16	23.93		
			1.1	
	17	30.00		
			0.4	
	18	41.50		
			0.05	
	19	64.33		
			0	
	20	91.50		
F25	0	0		750g bed
	6	1.00		Temp. = 995±15°C
			3.6	
	7	3.22		Gas flow rate =
			3.4	
	8	5.60		185 litre/min
			4.0	
	9	7.64		N.T.P.
			4.1	
	10	9.62		Amb. temp. = 28°C
			4.7	
	11	11.38		
			4.6	
	12	13.15		
			3.8	
	13	15.28		
			3.2	
	14	17.75		
			2.5	

Appendix D

Table XV (cont.)

Run No.	H_2 Volume ($ft.^3$)	Time (min)	Rate x 10^2	Remarks
F25 (cont.)	15	20.90		
			1.9	
	16	25.02		
			0.7	
	17	35.20		
			0	
	18	78.20		
F26	0	0		1500g bed
	6	0.95		Temp. = 900±10°C
			1.0	
	7	4.95		Gas flow rate =
			0.6	
	8	11.17		185 litre/min
			0.45	
	9	18.93		N.T.P.
			0.75	
	10	24.02		Amb. temp. = 28°C
			0.55	
	11	30.47		
			0.60	
	12	36.80		
			0.55	
	13	43.22		
			0.60	
	14	49.30		
			0.60	
	15	55.30		
			0.65	
	16	61.13		
			0.60	
	17	67.23		
			0.60	
	18	73.32		
			0.60	
	19	79.60		
			0.60	
	20	85.60		
			0.60	

Appendix D

Table XV (cont.)

Run No.	H_2 Volume ($ft.^3$)	Time (min)	Rate x 10^2	Remarks
F26 (cont.)	21	91.60		
			0.55	
	22	98.18		
			0.50	
	23	105.40		
			0.50	
	24	112.72		
			0.45	
	25	120.75		
			0.40	
	26	129.17		
F27	0	0		750g bed
	6.0	0.93		Temp. = 900±10°C
			1.8	
	6.5	3.13		Gas flow rate =
			1.1	
	7.0	6.48		185 litre/min
			0.85	
	7.5	10.77		N.T.P.
			0.75	
	8.0	15.67		Amb. temp. = 35°C
			0.70	
	8.5	21.00		
			0.60	
	9.0	26.83		
	9.5	-	1.05	
	10.0	34.50		
			0.85	
	10.5	38.83		
			0.85	
	11.0	43.25		
			0.80	
	11.5	47.75		
			0.80	
	12.0	52.33		
			0.75	

Appendix D

Table XV (cont.)

Run No.	H_2 Volume($ft.^3$)	Time (min)	Rate x 10^2	Remarks
F27 (cont.)	12.5	57.25		
			0.80	
	13.0	61.83		
	13.5	-	0.80	
	14.0	70.83		
			0.65	
	14.5	76.17		
			0.70	
	15.0	81.33		
			0.65	
	15.5	86.67		
			0.60	
	16.0	92.33		
			0.50	
	16.5	99.17		
			0.55	
	17.0	105.50		
	17.5	-	0.45	
	18.0	120.50		
			0.25	
	18.5	132.83		
			0.20	
	19.0	144.00		
F28	0	0		1500g bed
	6	0.92		Temp. = 1110±10°C
			16.4	
	7	1.17		Gas flow rate
			17.9	
	8	1.40		= 150 litre/min
			17.9	
	9	1.63		N.T.P. of a H_2-N_2
			18.6	
	10	1.85		mixture containing
			16.4	
	11	2.10		10% by volume of N_2
			15.2	

Appendix D

Table XV (cont.)

Run No.	H_2 Volume ($ft.^3$)	Time (min)	Rate x 10^2	Remarks
F28 (cont.)	12	2.37		Amb. temp. = 35°C
	13	2.53	17.8	
	14	2.75	16.4	
	15	3.00	15.2	
	16	3.27	15.8	
	17	3.53	13.7	
	18	3.83	14.2	
	19	4.12	13.7	
	20	4.42	10.8	
	21	4.80	10.8	
	22	5.18	8.4	
	23	5.67	6.7	
	24	6.28	3.6	
	25	7.42	0.4	
	26	19.00	0.07	
	26.5	49.00		
F29	0	0		700g bed
	6	0.92	26	Temp. = 1100±20°C
	7	1.25	28	Gas flow rate =
	8	1.57	26	185 litre/min
				N.T.P.

Appendix D

Table XV (cont.)

Run No.	H_2 Volume($ft.^3$)	Time (min)	Rate x 10^2	Remarks
F29 (cont.)	9	1.57	30	
	10	2.20	28	
	11	2.52	20	
	12	2.95	17	
	13	3.47	14	
	14	4.18	5	
	15	5.95	1	
	16	24.17		
F30	0	0		750g bed
	6.0	0.90		Temp. = 985±15°C
	7.0	2.68	3.6	Gas flow rate =
	7.5	3.87		185 litre/min
	8.0	5.60	2.0	N.T.P. of a H_2-H_2S
	8.5	7.75		mixture containing
	9.0	10.18	1.7	2% by volume of H_2S
	9.5	12.66	1.8	Amb. temp. = 31°C
	10.0	15.12	2.1	
	10.5	17.18		
	11.0	19.68	1.9	
	11.5	21.90	1.9	

Appendix D

Table XV (cont.)

Run No.	H_2 Volume ($ft.^3$)	Time (min)	Rate x 10^2	Remarks
F30 (cont.)	12.0	24.15		
	12.5	26.50	1.8	
	13.0	28,92	1.8	
	13.5	31.70	1.6	
	14.0	-	1.4	
	14.5	37.83	1.1	
	15.0	41.75		
	15.5	44.0	0.8	
	16.0	49.50	0.6	
	16.5	56.75		
	17.0	61.50		
F31	0	0		780g bed of +65-48# barytes.
	2.0	6.17	1.3	Temperature
	2.5	9.27	1.1	900±10°C from 0-60 min
	3.0	13.00	1.0	1000±10°C from 66 to 120 min
	3.5	17.08	0.7	Gas flow rates
	4.0	22.33	0.6	26 litre/min - 0 to 39 min
	4.5	29.17	0.6	37 " " 39 " 71 "
	5.0	35.75	0.6	19 " " 71 " 120 "
	5.5	42.17	0.6	

Appendix D

Table XV (cont.)

Run No.	H_2 Volume ($ft.^3$)	Time (min)	Rate x 10^2	Remarks
F31 (cont.)	6.0	48.83		Amb. temp. = 36°C
	6.5	56.00	0.5	
	7.0	61.50	0.7	
	7.5	63.67	1.8	
	8.0	65.08	2.8	
	8.5	-	2.8	
	9.0	67.50		
	9.5	68.67	3.4	
	10.0	69.75	3.6	
	10.5	70.92	3.4	
	11.0	72.58	2.4	
	11.5	74.42	2.1	
	12.0	76.25	2.1	
	12.5	80.30	2.0	
	13.0	82.42	1.8	
	13.5	84.67	1.9	
	14.0	87.25	1.7	
	14.5	95.00	1.5	
	15.0	115.00	0.6	
	15.5		0.1	

Appendix D

Table XV (cont.)

Run No.	H_2 Volume ($ft.^3$)	Time (min)	Rate x 10^2	Remarks
F32	0	0		1500g bed
	6	0.95	26	Temp. = 1110±10°C
	7	1.05	26	Gas flow rate =
	8	1.30	25	185 litre/min
	9	1.47	26	N.T.P.
	10	1.63	27	Amb. temp. = 30°C
	11	1.85	20	
	12	2.05	22	
	13	2.27	20	
	14	2.45	24	
	15	2.70	18	
	16	2.93	19	
	17	3.18	18	
	18	3.45	16	
	19	3.75	15	
	20	4.08	13	
	21	4.48	11	
	22	4.97	9	
	23	5.75	6	
	24	7.48	3	
			0.6	

Appendix D

Table XV (cont.)

Run No.	H_2 Volume ($ft.^3$)	Time (min)	Rate x 10^2	Remarks
F32 (cont.)	24.5	10.92	0.05	
	25	30.00		
F33	0	0		1500g bed
	10	2.0	8.3	Temp. = 1120±20°C
	11	2.53	8.6	Gas flow rates =
	12	3.05	9.2	130 litre/min for
	13	3.53	8.8	the first 2 min
	14	4.03	9.0	then 60 litre/min
	15	4.52	8.8	N.T.P.
	16	5.02	8.8	Amb. temp. = 16°C
	17	5.52	6.6	
	18	6.18	3.8	
	19	7.32	1.9	
	20	9.58	0.3	
	20.5	16.00	0	
	20.75	24.00		

APPENDIX E

Design calculations for the fluidizing unit*

* This section has been included, primarily, to assist those who may be called upon to operate the fluidizing unit at a later date.

Appendix E

Design calculations for fluidizer

The basic specifications which the fluidizing unit will be required to meet are set out in Section E:1 while Sections E:2 to E:10, inclusive, deal with the design calculations and layout of the unit. Section E:11 is devoted to a discussion of the instrumentation required and an outline of the operating technique to be used is given in Section E:12.

E:1 Basic specifications for experimental unit

E:1:1 Bed diameter and height

Since most of the published work on gas mixing in fluidized systems relates to beds of 1" to 4" diameter, and this information may be required to correlate the data obtained for the reduction of barytes, a bed diameter of 3" has been selected for the present work.

In general, commercial processes utilizing fluidization techniques use beds with a depth less than four times the bed diameter, and, since the results of this work should have practical application, the maximum bed depth has been restricted to 12".

E:1:2 Maximum particle diameter

The finest material used in the work on static beds (see Section 4) was in the size range +14-10# (Tyler); further, it was found that the rate of reaction was sensitive to changes in the surface area of the material being reduced, accordingly, to minimise determinations of

Appendix E

surface area in the present work, +14-10# material has been adopted for use in the fluidized reactor.

E:1:3 Furnace requirements

Preliminary experiments with barytes in the selected size range - +14-10# (Tyler) - have indicated that for such coarse, heavy, close-sized material conditions of slugging fluidization prevail at gas velocities exceeding 150% of the gas velocity (V_{mf}) corresponding to incipient fluidization. While it is essential to avoid conditions where material will be thrown out of the bed it is also important to limit the magnitude of the temperature gradients in the bed consequent upon the reduced agitation of the bed material which results from the adoption of low gas velocities. Reconciliation of these conditions calls for preheating of the low-velocity inlet gas to a temperature approaching the selected bed temperature, therefore, adequate capacity must be provided in the gas preheating furnaces.

E:1:4 Rate measurements and flow sheet

Since reduction of barytes takes place according to the reaction,

$$BaSO_4 + 4H_2 = BaS + 4H_2O \quad \ldots\ldots\ldots\ldots\ldots\ldots (3)$$

the rate of reduction may be followed by measuring the rate of consumption of either of the reactants or, alternatively, by measuring the rate of production of either barium sulphate or water. In this case, the high temperatures (approximately 1000°C) to be used preclude direct determination of the quantities of either the $BaSO_4$

or the BaS present in the bed and, consequently, consideration must be confined to measurement of one or other of the gaseous components in the system. The simplest approach is to measure the rate at which hydrogen is consumed since laborious gravimetric methods would be needed to measure accurately the rate of production of water. With this in mind, the flow sheet shown in Fig. 41 has been adopted.

E:2 Selection of operating velocity and heating furnaces

It will be recalled from Section E:1:3 that the fluidized beds are to be operated at a gas velocity 1.5 times the gas velocity corresponding to the point of incipient fluidization to minimize the undesirable phenomena, temperature gradients in the bed and slugging fluidization. The first step is, therefore, to estimate the gas velocity which will be required to produce incipient fluidization in a bed of +14-10# barytes.

E:2:1 Minimum gas velocity for fluidization

Van Heerden, Nobel, and van Krevelen[49] give an equation which will enable calculation of the gas velocity corresponding to the point of incipient fluidization, for a bed of granular material. The proposed equation is,

$$G_{mf} = \frac{0.00123}{B_e} \quad \frac{\rho \rho_{bm} g d_e^2}{\eta}$$

Where G_{mf} = the superficial mass velocity at the point of incipient fluidization

B_e = a generalized shape factor = 1 for crushed material

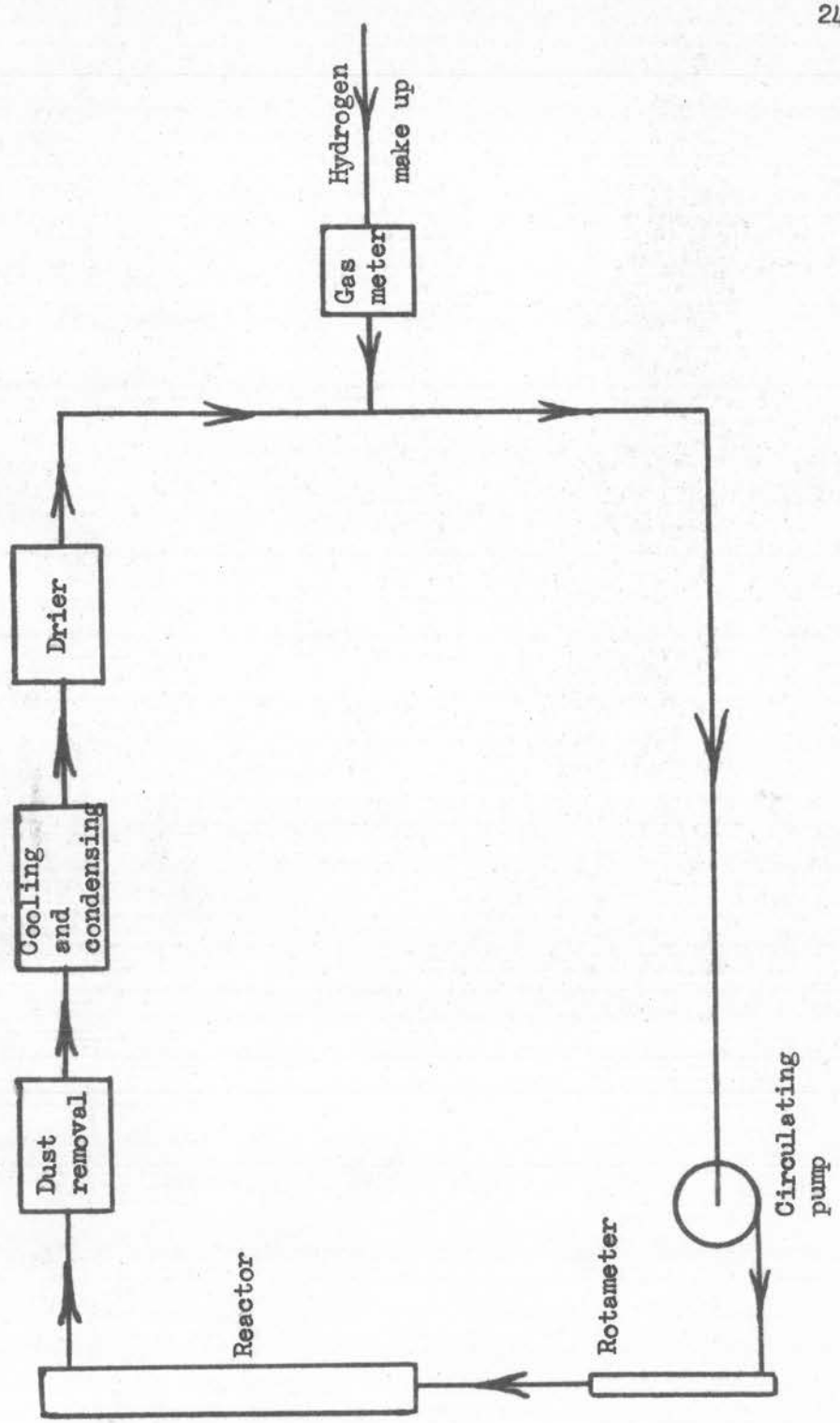

Fig. 41. Block flow sheet for fluidizing apparatus

Appendix E

ρ = the fluid density

η = the fluid viscosity

ρ_{bm} = the bed density at loosest stable packing

d_e = equivalent diameter = $1.043/n_m^{0.33}$

n_m = the number of particles in a unit volume of the bed at loosest stable packing.

Van Heerden, Nobel, and van Krevelen point out that the state of loosest stable packing can be approximated by pouring the crushed material into a measuring cylinder. The bed density for the material can then be easily estimated.

Examination of a sample of +14-10# barytes shows that

$\rho_{bm} = 2.4$ g/cm^3

and $n_m = 355$ particles per cm^3.

Hence, $d_e = 1.043/(355)^{0.33} = 0.147$ cm.

The fluidized bed will be operating at 1000°C under a pressure of approximately one atmosphere.

Hence ρ_{H_2} = 0.0192 g/litre at 1000°C (Perry p.176, Table 49)*

η_{H_2} = 0.023 cP at 1000°C and 1 atm. (Perry p.371).

Therefore

$$G_{mf} = 0.00123 \times 1.92 \times 10^{-5} \times 2.4 \times (0.147)^2 \times 980 / 2.3 \times 10^{-4}$$

$$= 5.45 \times 10^{-3} \text{ g/cm}^2\text{,sec.}$$

For a 3" diameter tube (7.6 cm dia.)

V_{mf} = the gas flow rate at incipient fluidization

* The general reference used throughout this design is, Perry, J. (Editor). (1950). "Chemical Engineers Handbook", 3rd. ed. New York:McGraw-Hill.

Appendix E

$$= 5.45 \times 10^{-3} \times \pi (7.6)^2 / 4 \times 0.898$$

$$= 2.76 \text{ litre/sec N.T.P.}.$$

Which is equivalent to 5.85 $ft.^3$/min N.T.P..

E:2:2 Furnaces and maximum gas rate

There are available in the Department, two cylindrical furnaces, each twenty inches long and having a four inch bore, rated at 4.5 kW and one similar furnace, twelve inches long, which is rated at 2 kW. It is desirable, in the interests of economy, to use these furnaces for gas preheating and for heating the bed and top of the reactor. The reactor must, therefore, be placed directly above the preheater and, it is proposed, that both components should be fabricated from heat resistant stainless steel, welded together to form a continuous 3" diameter tube as shown in Fig. 42, page 251; the bottom section of the tube serving to preheat the incoming gas, and the top section holding the fluidized bed.

If the 4.5 kW and 2 kW furnaces are to be used for gas preheating and the remaining 4.5 kW furnace is to be used to heat the bed and top of the reactor tube the preheating section of the preheater-reactor tube will be 32" long.

The preheating furnaces will have a capacity of 6.5 kW and it is necessary to calculate the maximum hydrogen flow which can be used if the gas is to be heated from room temperature to 1000°C, in order to find out if these furnaces will have sufficient capacity to meet all needs.

Appendix E

Heat will be lost to the surroundings by radiation and convection from the outside surface of the furnaces.

The area from which heat will be dissipated

$= \pi \times 20 \times 32/144 = 13.1\ ft^2$.

The temperature of this surface will be estimated as being 80°C and the temperature of the surroundings as 25°C.

Consider convection from the outside surface of the preheating furnaces to the surroundings. The coefficient of heat transfer,

$$h_c = 0.27(\Delta t_s)^{0.25} \qquad \text{(Perry p.474)}$$

$$= 0.27(100)^{0.25}$$

$$= 0.86\ B.Th.U./ft^2.,h,{}^\circ F$$

Consider heat loss by radiation. The coefficient of heat transfer,

$$h_r = 1.2\ B.Th.U./ft^2., \qquad \text{(Perry p.473)}.$$

Total heat loss

$$= (0.9 + 1.2)13.1 \times 100 = 2750\ B.Th.U./h.$$

Which is equivalent to 0.8 kW/sec.

Therefore, the power available for gas heating

$= (6.5 - 0.8) = 5.7$ kW. Say 5.5 kW since radiation losses from the bottom surface of the furnaces have been neglected.

It is required to heat the incoming gas from 20°C to 1000°C.

The mean specific heat of hydrogen in the range 20°C to 1000°C.

$= (3.5 + 3.7)/2 = 3.6\ P.C.U./lb.,{}^\circ C$ (Perry p.229).

Therefore, the maximum gas rate which can be handled

$= 5.5 \times 0.95/1.8 \times 3.6 \times 980 = 8.3 \times 10^{-4}$ lb./sec.

Appendix E

Which is equivalent to a flow of 8.9 ft.^{3}/min N.T.P. or a flow of 4.2 litre/sec N.T.P.. This is 152% of V_{mf} and consequently the preheating furnaces will have sufficient capacity to handle the largest gas flow (150% V_{mf}) to be used.

An attempt was made to calculate the maximum wall temperature which would be encountered in the preheating tube but there appear to be no heat transfer data available for the low rates of gas flow and high values of heat flux being used.

E:3 Reactor

The form of the reactor and constriction plate were decided upon after consultation with Mr. R.W. Urie, of the C.S.I.R.O. at Fishermans Bend, who has had considerable experience in high temperature work with fluidized beds. The details of the reactor are shown in Fig. 42. Comsteel heat resistant 25-20 stainless steel will be used to fabricate the unit and asbestos gaskets will be used between the flanges of the joints at the top of the reactor.

E:4 Gas cooler - atmospheric

The gases leaving the fluidized bed will be at a temperature of approximately 1000°C, therefore, it is proposed to pass these gases through a length of bare stainless steel pipe (see Fig. 43, page 263) so that the temperature will be reduced to about 500°C before the gases enter a dust removal cyclone. Operation at this temperature

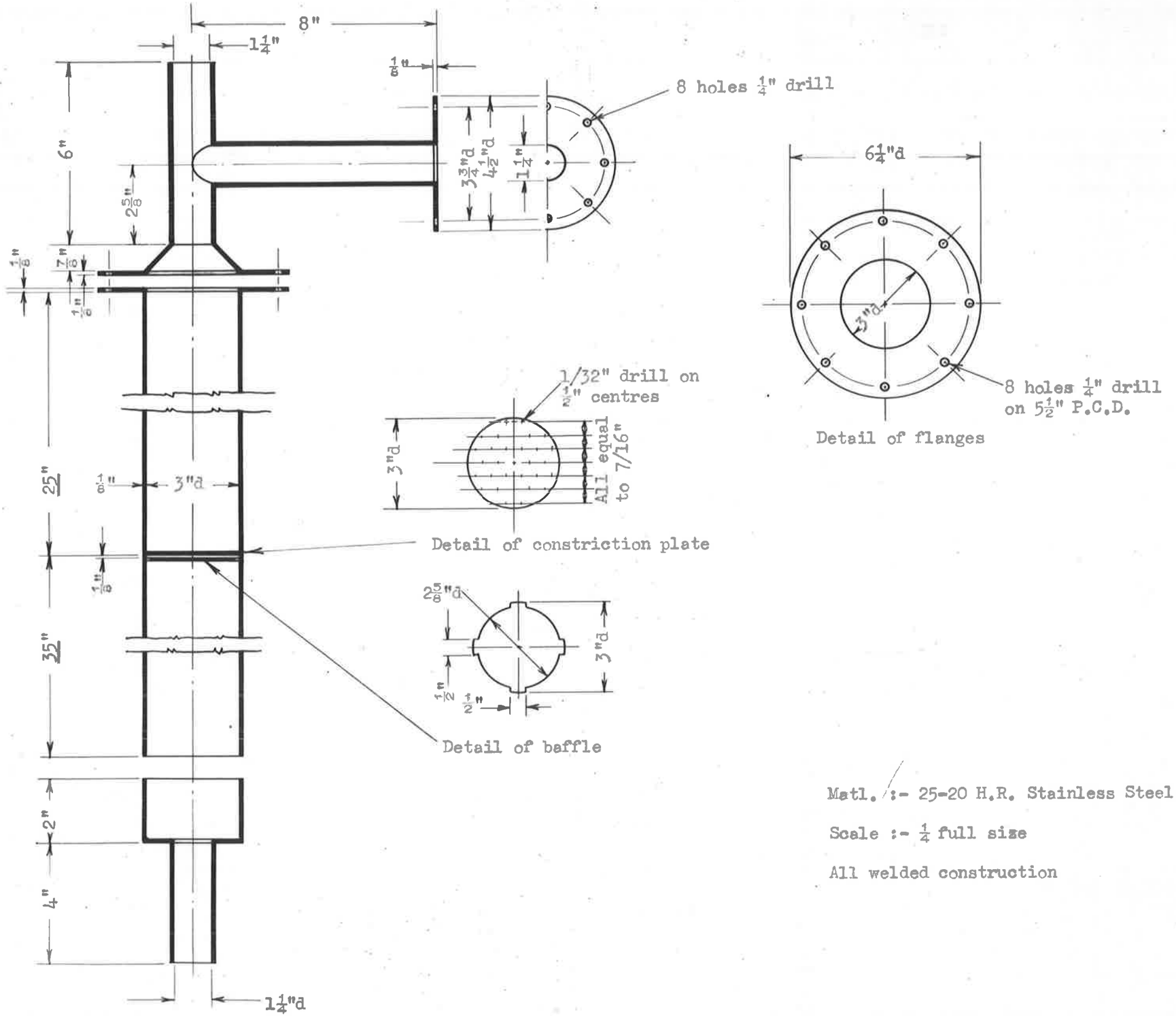

Matl. :- 25-20 H.R. Stainless Steel plate

Scale :- ¼ full size

All welded construction

Fig. 42. Detail of reactor-preheater tube

will permit the cyclone to be constructed, relatively inexpensively, from 18-8 stainless steel sheet which has an upper operating temperature of about 600°C.

Although the cooler proper consists of six feet of 1½" diameter stainless steel pipe some heat will also be dissipated from the top of the reactor tube so it will be necessary to consider both sections in order to estimate the temperature of the gas entering the cyclone. The exit gases from the bed will be cooled in two sections of bare pipe, (1) one foot of 3" diameter vertical pipe (the top of the reactor tube), and (2) six feet of 1½" diameter vertical pipe.

Since the exit gases may vary in composition from pure hydrogen to steam, both these cases will be considered. The greatest heat load on the cooling system will occur at the maximum gas rate which is 4.2 litre/sec, measured at N.T.P..

E:4:1 Pure hydrogen

(1) Three inch diameter pipe

It is necessary to calculate the value of Reynolds Number (N_{Re}) for the flowing gas so that the appropriate heat transfer coefficients can be selected.

$N_{Re} = \rho vd/\eta$

$\rho = 0.0056 \times 492/2290 = 1.2 \times 10^{-3}$ lb./ft.^{3} at 1000°C (Perry p.176)

$v = 4.2 \times 4 \times 144 \times 1273/28.3 \times 9 \times 273 \times \pi = 14.1$ ft./sec

$d = 0.25$ ft.

$\eta = 2.3 \times 10^{-2}/1488 = 1.55 \times 10^{-5}$ lb./ft.,sec (Perry p.371).

Appendix E

Hence N_{Re} = 273 for the flowing gas and since this is less than 2000 the gas must be flowing viscously.

Consider transfer of heat from the flowing gas to the pipe. The heat transfer coefficient,

h_g = 2 B.Th.U./ft.^{2},h,$^\circ$F (nomograph, Perry p.472)

(The nomograph was extrapolated to a film temperature of approximately 600°C since h_g appears to be almost independent of the film temperature.) Hydrogen does not show radiation bands (Perry p.490) so it is not necessary to assume a mean pipe temperature and then check to see if the rate of heat transfer from gas to pipe for this pipe temperature is equal to the rate of heat loss from the pipe to the surroundings. In the event of a discrepancy a new mean pipe temperature must be chosen and the calculation repeated.

Try a mean pipe temperature of 600°F. Then heat transfer from gas to pipe = (1800 - 600)2 = 2400 B.Th.U./ft.^{2},h.

Now consider heat transfer from the pipe to the surroundings by both radiation and convection. If the ambient temperature is assumed to be 100°F then the coefficient of radient heat transfer,

$h_r = 4e$ (Perry p.473)

Where e = the emissivity = 0.8 for an oxidized surface (Perry p.485).

Hence h_r = 3.2 B.Th.U./ft.^{2},h,$^\circ$F.

The coefficient for heat transfer by convection is given by,

$h_c = 0.5(t_s/D'_o)^{0.25}$ (Perry p.474)

Appendix E

$$= 0.5x(500/3)^{0.25} = 1.8 \text{ B.Th.U./ft.}^2\text{,h,}^\circ\text{F.}$$

Then

$$h_r + h_c = 3.2 + 1.8 = 5.0 \text{ B.Th.U./ft.}^2\text{,h,}^\circ\text{F.}$$

Total heat loss from the pipe to surroundings

$$= (600 - 100)5 = 2500 \text{ B.Th.U./ft.}^2\text{,h.}$$

If the mean pipe temperature chosen had been correct the rate of heat transfer from the gas to the pipe would have been equal to the rate of heat loss from the pipe to its surroundings. These two calculated figures differ only slightly so the pipe temperature chosen may be assumed to be correct. Therefore, the rate of heat loss from one foot of three inch diameter pipe = $2500\pi\ 3/12x3600$

$$= 0.55 \text{ B.Th.U./sec.}$$

It follows that the drop in gas temperature on passing through the three inch diameter pipe will be

$$= 0.55/(\text{specific heat of } H_2)(\text{wt. of } H_2 \text{ per sec})$$

$$= 0.55x453/3.6x4.2x0.09 = 180^\circ\text{F.}$$

Consequently the gas temperature at the end of the three inch diameter pipe will be = $(1800 - 180) = 1620^\circ$F.

(2) One and a half inch diameter pipe

The value of Reynolds Number for the flowing gas is given by,

$$N_{Re} = \rho\, vd/\eta$$

Where

$\rho = 5.6x10^{-3}x492/2080 = 1.32x10^{-3}$ lb./ft.^{3} (Perry p.176)

$v = 4.2x4x144x2090/28.3x\ \pi\ x2.25x492 = 51$ ft./sec

$d = 0.125$ ft.

$\eta = 2.1x10^{-2}/1488 = 1.42x10^{-5}$ lb./ft.,sec (Perry p.371).

Appendix E

Therefore, N_{Re} = 643 and, since this is less than the critical value of 2000, the gas flow must be viscous.

Consider the first two feet of one and a half inch diameter pipe, through which the gas will pass. If it is assumed that the mean pipe temperature is 550°F then the heat transfer coefficient between the flowing gas and the pipe,

$$h_c = 2.0 \text{ B.Th.U./ft.}^2\text{,h,}^\circ\text{F} \qquad \text{(Perry p.472)}$$

Consequently the rate of heat transfer from the gas to the pipe

$$= (1620 - 550)2 = 2140 \text{ B.Th.U./ft.}^2\text{,h.}$$

Consider now heat loss from the outside of the pipe to the surroundings by radiation and convection. The coefficient for heat transfer by ratiation from pipe to surroundings,

$$h_r = 4e \qquad \text{(Perry p.473)}$$

$$= 4 \times 0.8 \qquad \text{(Perry p.485)}$$

$$= 3.2 \text{ B.Th.U./ft.}^2\text{,h,}^\circ\text{F.}$$

The coefficient for heat transfer by convection is given by,

$$h_c = 0.5(\Delta t_s/D'_o)^{0.25} \qquad \text{(Perry p.474)}$$

$$= 0.5(450/1.5)^{0.25} = 2.1 \text{ B.Th.U./ft.}^2\text{,h,}^\circ\text{F.}$$

$$h_r + h_c = 3.2 + 2.1 = 5.3 \text{ B.Th.U./ft.}^2\text{,h,}^\circ\text{F.}$$

Therefore, the total heat loss from the pipe to surroundings

$$= (550 - 100)5.3 = 2400 \text{ B.Th.U./ft.}^2\text{,h.}$$

Compare this with 2140 B.Th.U./ft.^{2},h, the calculated rate of heat loss from the gas to the pipe. Agreement is within the limits of accuracy of the method and hence the pipe temperature chosen was

Appendix E

substantially correct. The rate of heat loss from the gas will be taken as 2300 B.Th.U./ft.^{2},h.

The rate of heat loss from the first two feet of 1½" diameter pipe

= 2300x xl.5x2/12x3600 = 0.50 B.Th.U./sec.

The specific heat of hydrogen at 1600°F = 3.6 B.Th.U./lb., °F (Perry p.229).

Hydrogen flow rate = 4.2x0.09/453 = 8.4×10^{-4} lb./sec.

Temperature drop = $0.50/3.6 \times 8.4 \times 10^{-4}$ = 165°F. Say 160°F.

Therefore the gas temperature at the end of two feet

= (1620 - 160) = 1420°F

Consider the last four feet of the 1½" diameter pipe. Try a mean pipe temperature = 500°F.

The heat transfer coefficient from gas to pipe,

h_c = 2.0 B.Th.U./ft.^{2},h,°F (Perry p.472).

Then the rate of heat transfer from gas to pipe

= (1400 - 500)2 = 1800 B.Th.U./ft.^{2},h.

The coefficient for heat transfer by radiation from the pipe to the surroundings,

h_r = 3e (Perry p.473)

= 3x0.8 (Perry p.485)

= 2.4 B.Th.U./ft.^{2},h,°F.

The coefficient for heat loss by convection is given by,

$h_c = 0.5(\Delta t_s/D'_o)^{0.25}$ (Perry p.474)

$= 0.5(400/1.5)^{0.25}$ = 2.0 B.Th.U./ft.^{2},h,°F.

$h_r + h_c$ = 2.4 + 2.0 = 4.4 B.Th.U./ft.^{2},h,°F.

Appendix E

Therefore, the total heat loss from the pipe

$= (500 - 100)4.4 = 1760$ B.Th.U./ft.^{2},h.

Compare this with 1800 B.Th.U./ft.^{2},h for the rate of heat transfer from gas to pipe. This means that the mean pipe temperature chosen was correct.

Heat losses from four feet of $1\frac{1}{2}$" diameter pipe

$= 1800 \times 1.5 \times 4\pi / 12 \times 3600$

$= 0.78$ B.Th.U./sec.

The specific heat of hydrogen = 3.5 B.Th.U./lb., $^\circ$F (Perry p.229).

Hydrogen flow rate = 8.4×10^{-4} lb./sec,

Therefore, drop in gas temperature $= 0.78/3.6 \times 8.4 \times 10^{-4} = 260^\circ$F.

Gas temperature at the end of the cooler

$= (1420 - 260) = 1160^\circ$F.

E:4:2 Pure steam

(1) Three inch diameter pipe

It is necessary to determine if the gas flow in the pipe is viscous or turbulent so that the appropriate heat transfer coefficients can be selected.

$N_{Re} = \rho vd/\eta$

$\rho = 1460/2290 \times 59 = 1.1 \times 10^{-2}$ lb./ft.^{3} (Perry p.279)

$v = 14.1$ ft./sec.

$d = 0.25$ ft.

$\eta = 4.5 \times 10^{-2}/1488 = 3.03 \times 10^{-5}$ lb./ft.,sec (Perry p.371)

Hence $N_{Re} = 1280$ which is less than 2000 and therefore viscous flow prevails.

Appendix E

Try a mean pipe temperature of 700°F and a mean gas temperature of 1700°F. The heat transfer coefficient for heat loss from the flowing gas by convection,

$$h_c = 1.0 \text{ B.Th.U./ft.}^2\text{,h,}^\circ\text{F} \qquad \text{(Perry p.472).}$$

Therefore, the rate of heat loss from the gas by convection

$$= (1700 - 700)1 = 1000 \text{ B.Th.U./ft.}^2\text{,h.}$$

Consider now radiation from the gas to the pipe, assuming the pipe is a black body. The rate of heat transfer is given by,

$$q = 0.173[\ \epsilon_g(T_g/100)^4 - \alpha_g(T_s/100)^4] \qquad \text{(Perry p.491)}$$

The beam length,

$$PL = 1x0.25x0.9 = 0.225 \text{ ft.,atm.} \quad \text{(Perry p.491, Table 2).}$$

Therefore,

$$\epsilon_g = 0.08x1.5 \qquad \text{(Perry p.491, Fig. 23)}$$

$$\alpha_g = 0.14x1.5 \qquad \text{(Perry p.491, Fig. 23)}$$

Hence,

$$q = 0.173x1.5[0.08(2160/100)^4 - 0.14(1160/100)^4]$$

$$= 3860 \text{ B.Th.U./ft.}^2\text{,h.}$$

It follows that the total heat transferred from the gas to the pipe

$$= (1000 + 3860) = 4860 \text{ B.Th.U./ft.}^2\text{,h.}$$

Consider heat loss from the pipe by radiation to its surroundings. The coefficient of radiant heat transfer is given by,

$$h_r = 5.5e \qquad \text{(Perry p.473)}$$

$$= 5.5x0.8 \qquad \text{(Perry, p.485)}$$

$$= 4.4 \text{ B.Th.U./ft}^2\text{,h,}^\circ\text{F.}$$

Appendix E

The coefficient for heat loss from the pipe by convection is given by,

$$h_c = 0.5(\Delta t_s/D_o')^{0.25} \qquad \text{(Perry p.474)}$$

$$= 0.5(600/3)^{0.25}$$

$$= 1.9 \text{ B.Th.U./ft.}^2\text{,h,}^\circ\text{F.}$$

$\therefore$ $h_r + h_c = 4.4 + 1.9 = 6.3$ B.Th.U./ft.^{2},h,$^\circ$F

The total heat loss from pipe to surroundings

$$= (700 - 100)6.3 = 3800 \text{ B.Th.U./ft}^2\text{.,h.}$$

This is lower than the figure obtained for the rate of heat transfer from gas to pipe but the accuracy of the method is not good, therefore, the rate of heat loss from the gas will be taken as 4000 B.Th.U./ft.^{2},h. The heat loss for the one foot of 3" diameter pipe will be

$$= 4000\text{x } x3/12x3600 = 0.87 \text{ B.Th.U./sec.}$$

The specific heat of steam = 0.6 B.Th.U./lb.,$^\circ$F (Perry p.229)

The steam flow rate = $4.2x18/22.4x453 = 7.5x10^{-3}$ lb./sec.

Therefore, the drop in gas temperature

$$= 0.87/0.6x7.5x10^{-3} = 190^\circ\text{F.}$$

Compare this with a temperature drop of 180°F for the corresponding case when the gas was 100% H_2. It appears that there is little difference between the case for pure H_2 and the case for pure H_2O, therefore, both gases may be assumed to leave the cooling section at the same temperature, viz. 1150°F.

E:5 Dust removal

In order to select the most suitable dust collection equipment it is necessary to find out the size of the largest dust particles

Appendix E

likely to be carried off from the bed.

E:5:1 Largest dust particle

If it is assumed that Stoke's Law will apply to particles in the flowing gas stream above the bed then the largest particle likely to be carried out of the reactor can be easily calculated. It will be necessary to consider the two extreme cases, where the gas is pure hydrogen, and where the gas is pure steam. However, in both of these cases the gas velocity in the open reactor tube above the bed will be = 4.2x1273x144x4/273x28.3x π = 14.1 ft./sec. Which is equivalent to 430 cm/sec.

(1) Gas is 100% hydrogen

The diameter of the largest particle likely to be carried out of the bed by a gas velocity of 430 cm/sec can be calculated from Stoke's Formula,

$$d_p^2 = 18\eta\, v_t / g(\rho_s - \rho) \qquad \text{(Perry p.937)}$$

Where η = 0.023 cP at 1000°C (Perry p.371)

v_t = 430 cm/sec

g = 980 cm/sec,sec

ρ_s = 4.2 g/cm^3 (for barium sulphide) (Perry p.113)

ρ = 0

Hence, $d_p^2 = 4.34 \times 10^{-4}$

and $d_p = 2.08 \times 10^{-2}$ cm

Checking to see if Stoke's Equation is valid, i.e. if Reynolds Number is less than 10.

Appendix E

$N_{Re} = \rho vd/\eta$

ρ = 0.019 g/litre = 1.9×10^{-5} g/cm^3 (see Section E:2:1, page 247)

v = 430 cm/sec

d = 0.02 cm

$\eta = 2.3 \times 10^{-4}$ P.

Hence, N_{Re} = 0.71 which is less than 10 so that the assumption of the validity of Stoke's Equation for this case was correct.

(2) Gas is 100% steam

Applying Stoke's Formula as above.

η = 0.046 cP at 1000°C (Perry p.371)

v_t = 430 cm/sec

g = 980 cm/sec, sec

ρ_s = 4.2 g/cm^3.

Hence, $d_p^2 = 8.7 \times 10^{-4}$

and $d_p = 2.95 \times 10^{-2}$ cm.

Checking on the validity of Stoke's Equation.

$\rho = 0.019 \times 9/1000 = 1.71 \times 10^{-4}$ g/cm^3 (see above)

v = 430 cm/sec

d = 0.03 cm

η = 0.046 cP.

Hence N_{Re} = 4.8 which is less than 10 so Stoke's Equation can be validly used.

It follows that the largest particles will be carried out of the bed when the gas is pure steam and that the largest particle likely to

Appendix E

be blown out of the reactor will have a diameter of 0.3 mm. This material is rather large to feed to a cyclone but the sharp change of direction at the bottom of the gas cooler (see Fig. 43) will knock most of the coarse particles out of the gas stream. A dust reservoir has, therefore, been provided below this change of direction (see Fig. 43) in the gas flow so that the device will act as a dust trap.

E:5:2 Dust trap

According to Lapple[72] the efficiency of a dust trap such as this will be greater than 50% for material having a terminal velocity (v_t) such that,

$$(v_t\, v_o)/(g\, d_b) = 1$$

In this case,

$$g = 32 \text{ ft./sec,sec}$$

$$d_b = 0.125 \text{ ft.}$$

$$v_o = 8.9x903x4/60x273x(0.125)^2\,\pi = 41 \text{ ft./sec.}$$

Solving for v_t gives,

$$v_t = 32x0.125/41 = 0.098 \text{ ft./sec.}$$

Which is equivalent to 3 cm/sec. The diameter of a particle having this settling velocity is given by Stoke's Formula,

$$d_p^2 = 18\,\eta\, v_t/g(\rho_s - \rho) \qquad \text{(Perry p.937).}$$

It will be assumed that the gas is pure steam since it was found, above, that this case gives the largest value of d_p and hence the coarsest material will be carried into the cyclone when the gas

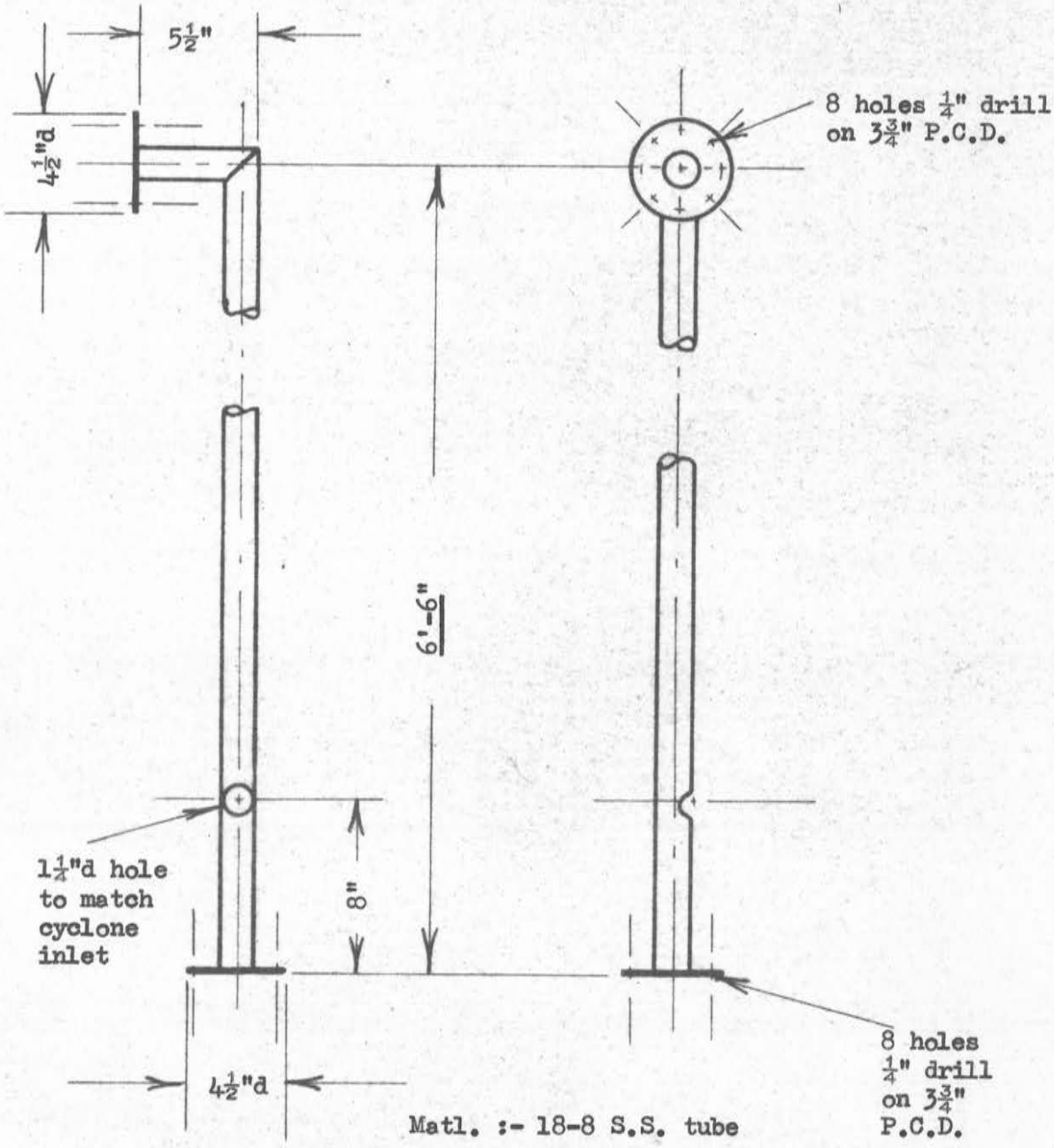

Fig. 43. Detail of gas cooler and dust trap

Appendix E

leaving the cooler is 100% steam.

Therefore, $\eta = 0.035$ cP (Perry p.371)

$v_t = 3$ cm/sec

$g = 980$ cm/sec,sec

$\rho_s = 4.2$ g/cm^3

$\rho \neq 0$

Hence, $d_p^2 = 4.6 \times 10^{-6}$

and $d_p = 2.1 \times 10^{-3}$ cm $= 21\mu$

That is 50%, or more of all material having a diameter greater than 21μ will be removed from the gas stream by the dust trap. Under these conditions it should then be possible to pass the gas to a cyclone to remove most of the remaining suspended material.

E:5:3 Cyclone

It is proposed to use a high efficiency cyclone of the type designed and tested by Stairmand[73]. The cyclone will be designed for a linear inlet gas velocity of 100 ft./sec which is the maximum allowable[73] since it will also be required to operate efficiently when beds finer than +14-10 are used. Under these conditions the gas rate will be smaller than the maximum rate of 4.2 litre/min, measured at N.T.P..

The inlet gas velocity = (gas rate)/(inlet area). The gas rate = $4.2 \times 903/28.3 \times 273 = 0.49$ ft.^{3}/sec at 630°C.

The inlet area = $0.5 \times 0.2D^2$ (from Fig.13)[73]

Hence, $D^2 = 0.049$

Appendix E

and $D = 0.221$ ft.. Therefore, take $D = 2\frac{1}{2}$". This will give a cyclone of the dimensions shown in Fig. 44. The cyclone must be lagged to prevent condensation of water on the inside of the walls with consequent clogging of the cyclone with dust.

The pressure drop across this cyclone may be calculated from Stairmand's equation[73],

$$P.D. = \frac{\rho}{2182}\left[V_I^2 \left\{ 1 + 2^{2(2R_I/R_E - 1)} \right\} + 2V_E^2 \right] \text{ (equation no.1)}^{73)}.$$

Where, V_I = inlet velocity = 100 ft./sec

V_E = exit velocity = 100x4/2.5 = 51 ft./sec (Fig.14)[73]

ϕ is the ratio of spinning speed to inlet velocity at the inlet. ϕ is obtained from Fig. 22[73]. In order to enter Fig. 22 GA/a and R_I/R_E must be known.

$G = 1/200$ (Stairmand[93])

$A/a = 5D^2/0.1D = 157$ (Fig.14)[73]

Hence, $GA/a = 0.78$

$R_I/R_E = (D - 0.2D)/0.5D = 1.6$ (Fig.14)[73]

Hence, from Fig. 22[73] get $\phi = 0.85$

$\rho = 16.02/59.1 = 0.27$ kg/m^3 (Perry p.279)

Hence,

$$P.D. = (0.27/2182)\left[10000 \left\{ 1 + 1.45(3.2 - 1) \right\} + 5200 \right]$$

= 6.85 milli-atmospheres. Which is equivalent to 4.4 inches of water.

Fig. 44. Detail of cyclone

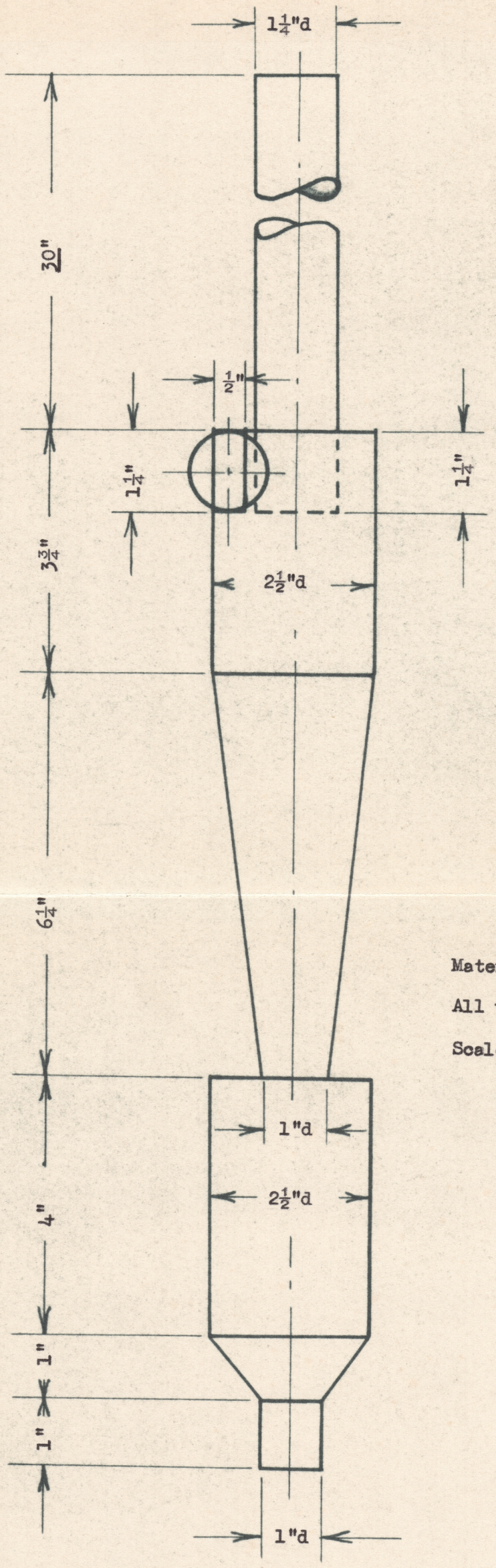

Material :- 18-8 Stainless Steel 18#

All welded construction

Scale :- half size

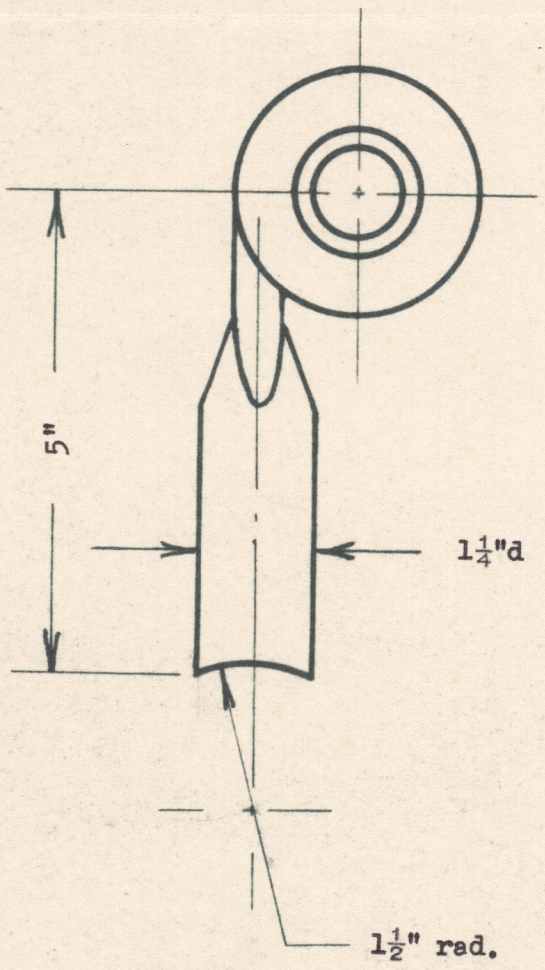

Appendix E

E:6 Design of a cooler-condenser

The greatest heat load on the condenser will occur when the entering gas is all steam but the heat transfer coefficient for this case is relatively high. A small quantity of non-condensable gas markedly lowers the heat transfer coefficient so that the worst case - high heat load and small coefficient - may occur when the gas composition is about 90% steam and 10% hydrogen (by volume). It is necessary, therefore, to examine this case as well as the cases where the gas entering the condenser is 100% hydrogen and 100% steam.

E:6:1 Diameter of water jacket

A single pipe with concentric cooling jacket affords the simplest construction so it is proposed to use a 1" diameter stainless steel pipe with concentric water jacket.

The greatest heat load will occur when the gas is pure steam.
The steam flow rate = $4.5 \times 18/22.4 \times 453 = 7.9 \times 10^{-3}$ lb./sec.
(The worst case in this instance may occur with a bed temperature of 900°C where the gas flow rate will be greater than the 4.2 litre/sec N.T.P. calculated on page 256).
The enthalpy of the steam = 1533/1.8 = 850 P.C.U./lb. (Perry p.279).
Heat given out = $7.9 \times 10^{-3} \times 850$ = 6.8 P.C.U./sec.

Tests show that the maximum water flow available is approximately 3 gallons per minute. This is equivalent to 0.5 lb./sec. Assuming that the water enters at 20°C, the exit temperature

$$= (20 + 6.8/0.5) = 33.5^{\circ}C.$$

Appendix E

This should be low enough to prevent formation of scale on the "water side" surfaces.

A $\frac{1}{4}$ inch thick water jacket will be tried. Reynold's Number for the water side is given by,

$$N_{Re} = Gd/\eta$$

Where, $G = 0.5 \times 4 \times 144 / \pi (1.5^2 - 1) = 73.5$ lb./ft.^{2}, sec

$d = 0.0208$ ft.

$\eta = 0.7/1488 = 4.7 \times 10^{-4}$ lb./ft.,sec (Perry p.373).

Hence $N_{Re} = 3250$, i.e. turbulent flow. This will give a desirably high coefficient for heat transfer on the water side so the jacket thickness chosen was suitable. The water jacket will have an internal diameter of $1\frac{1}{2}$".

E:6:2 Area of cooler-condenser for water-hydrogen mixture

The approximate method of Colburn[94] will be used to calculate the area of the cooler-condenser in this case since the temperature and flow rate of the gas leaving the cyclone are not known with any great accuracy. It has also been shown[95] that this method usually gives an area greater than that actually required.

The gas entering the cooler condenser will be 4.5 litre/sec N.T.P. of a 90%$H_2$0-10%H_2 mixture at a temperature of 550°C. The gas leaving the cooler-condenser will be 0.45 litre/sec N.T.P. of hydrogen (dry basis) saturated with water vapour at 50°C.

The cooler-condenser will be considered in two parts, (1) cooling

Appendix E

from 550°C to 100°C (cooling only), and (2) cooling from 100°C to 50°C (cooling and condensing). This treatment is very conservative since there will be condensation in the cooling section as soon as the wall temperature falls below 100°C and this will give heat transfer coefficients larger than the calculated values.

(1) Cooling section

Consider first the gas side of the cooling section. The gas flow rate = $4.5 \times 3600(2 \times 0.1 + 18 \times 0.9)/22.4 \times 453 = 26.1$ lb./h.

The specific heat of hydrogen = 3.5 P.C.U./lb., °C (Perry p.229)

Hydrogen flow rate = $0.45 \times 0.0898 = 4.05 \times 10^{-2}$ g/sec (Perry p.176)

Heat loss from hydrogen = $4.05 \times 10^{-2} \times 3.5(550 - 100)/453 = 0.14$ P.C.U./sec.

Super-heat of steam = (1533 - 1150) = 383 B.Th.U./lb. (Perry p.279)

which is equivalent to 213 P.C.U./lb.

Steam flow rate = $4.5 \times 0.9 \times 18/22.4 \times 453 = 7.15 \times 10^{-3}$ lb./sec.

Therefore, heat loss from steam = $213 \times 7.15 \times 10^{-3} = 1.53$ P.C.U./sec.

The total heat load on the cooling section = $(1.53 + 0.14)3600$

$= 6000$ P.C.U./h.

The temperature of the cooling water when the gas temperature is 100°C, i.e. at the end of the cooling section

$= 32.5 - (1.53 + 0.14)/0.5$ 29.2°C (see page 269)

(This assumes countercurrent flow of water and gas)

The heat transfer coefficient between gas and wall is required. Fig. 8 on page 468 of Perry will be used. The value of Reynolds Number or the gas is needed to enter Fig. 8.

Appendix E

$$N_{Re} = Gd/\eta$$

Where, $G = 26.1x4x144/\pi = 4780$ lb./ft.^{2},h

$d = 0.083$ ft.

$= (0.1x0.012 + 0.9x0.02)2.42 = 0.0465$ lb./ft.,h (Perry p.371.

Hence, $N_{Re} = 8600$ and entering Fig. 8 get $j = 0.004$ (curve ABC).

$j = (C_p\eta/k)^{0.6}(h_g/C_pG)$ (Perry p.468)

Take $C_p\eta/k = 0.78$ (Perry p.467)

$C_p = 3.5x0.1 + 0.48x0.9 = 0.78$ P.C.U./lb.,°C (Perry p.229)

Hence,

$$h_g = 0.004x0.78x4780/0.78^{0.6} = 17.4 \text{ P.C.U./ft.}^2\text{,h,°C.}$$

Consider now the water side of the cooling section. The heat transfer coefficient between the water and the inner wall is required. Fig. 8 on page 468 of Perry will be used. Reynolds Number for the water side = 3250 (see page 270) so entering Fig. 8 and using curve ABC the corresponding value of j is found to be 0.005.

$j = (C_p\eta/k)^{0.6}(h_w/C_pG)$ (Perry p.468)

$G = 73.5x3600 = 2.64x10^4$ lb./ft.^{2},h (see page 268)

$= 0.7x2.42 = 1.7$ lb./ft.,h (Perry p.373)

$k = 0.363$ P.C.U./ft.^{2},h,(°C/ft.) (Perry p.459)

Hence,

$$(C_p\eta/k)^{0.6} = 4.66^{0.6} = 2.52$$

Therefore,

$$h_w = 2.64x10^4x0.005/2.52 = 525 \text{ P.C.U./ft.}^2\text{,h,°C.}$$

Allowance is made for the possible formation of scale on the cooling

Appendix E

surface by the use of an additional coefficient (h_d). (Perry p.464)

The scaling coefficient for city water,

$$h_d = 500 \text{ P.C.U./ft.}^2\text{,h,}^\circ\text{C} \qquad \text{(Perry p.464)}$$

The overall heat transfer coefficient (U) for the cooling section is given by,

$$1/U = 1/h_g + 1/h_w + 1/h_d \qquad \text{(Perry p.464)}$$

$$= 1/17.4 + 1/525 + 1/500 = 0.061$$

Hence, $U = 16.4$ P.C.U./ft.^{2},h,$^\circ$C.

The area of the cooling section is given by,

$$A = q/U\ \Delta t_{lm} \qquad \text{(Perry p.464)}$$

Where,

$q = 6000$ P.C.U./h (see page 269)

$U = 16.4$ P.C.U./ft.^{2},h,$^\circ$C

$$\Delta t_{lm} = [(550 - 32.5) - (100 - 29.2)] / \ln [(550 - 32.5)/(100 - 29.2)]$$

$$= 219^\circ\text{C}$$

Hence,

$A = 1.67$ ft.^{2}.

(2) Condensing section

The basic equation for determining the area of the condensing section is,

$$A = q/(U_s/c_s)_{am}(i_v - i^*_w)_{lm} \qquad \text{(Colburn p.455)}^{94)}$$

Where

q = heat load in P.C.U./h

$$c_s/U_s = c_s/h_s + m/h_o$$

Appendix E

c_s = the heat capacity of one pound of dry gas plus vapour in P.C.U./lb., °C.

h_s = the coefficient of sensible heat transfer in P.C.U./ft.^{2},h,°C

h_o = the coefficient of heat transfer representing all resistances except gas-condensate

m = the slope of the curve of i_w^* vs temperature at the condensate temperature

i_w^* = the enthalpy of the saturated gas at the cooling water temperature in P.C.U./lb. of dry gas

i_v = the enthalpy of the vapour-gas mixture in P.C.U./lb. of dry gas

am signifies the arithmetic mean

lm signifies the logarithmic mean.

The gas side of the condensing section will be considered first.

(a) Hot end (gas inlet)

The gas temperature at this point = 100°C and the water temperature = 29°C (see page 271). In order to use Colburn's equation iv, i_w^*, U_s, and c_s must be evaluated.

i_v = the enthalpy of the vapour-gas mixture

= 3.5x100 + 9x0.9x1150/0.1x1.8 = 52100 P.C.U./lb. (dry) (Perry p.278)

The water vapour pressure at 29°C = 30 mm Hg (Perry p.149).

Therefore, the percentage of water vapour in gas saturated at 29°C

= 30x100/730 = 4.1% which is equivalent to 0.385 lb./lb. (dry).

i_w^* = the enthalpy of the saturated gas at the cooling water temperature

= 3.5x29 + 0.385x1100/1.8 = 335 P.C.U./lb. (dry).

Appendix E

The temperature of the condensate is not known so it is not possible to find the slope (m) of the plot of i_w^* vs temperature at the condensate temperature. Instead, m will be taken as the slope of the i_w^* vs temperature curve between 29° and 35°C, i.e. at the temperature of the cooling water. The value of i_w^* at 35°C is, therefore, required.

The water vapour pressure at 35°C = 42 mm Hg (Perry p.149)

The percentage of water in the saturated gas = 42x100/718 = 5.86%

which is equivalent to 0.56 lb./lb. of dry gas.

Hence,

$i_w^* = 3.5x35 + 0.56x1103/1.8 = 465$ P.C.U./lb. (dry).

Therefore, $m = (465 - 335)/(35 - 29) = 22$

c_s = the heat capacity of one pound of dry gas plus vapour

$= 3.5 + 9x0.9x0.46/0.1 = 40.7$ P.C.U./lb.,°C (dry) (Perry p.229).

$h_s = h_g = 17.4$ P.C.U./ft.^{2},h,°C (see page 270)

h_o = the coefficient of heat transfer representing all resistances except gas-condensate and is given by,

$1/h_o = 1/h_w + 1/h_d + 1/h_c$

$h_w = 525$ P.C.U./ft.^{2},h,°C (see page 270)

$h_d = 500$ P.C.U./ft.^{2},h,°C (see page 271)

$h_c = 800$ P.C.U./ft.^{2},h,°C (extrapolating Fig. 9^{94}) to G_{am} = 2000 lb./ft.^{2},h)

Hence $1/h_o = 0.005$

Now

$c_s/U_s = c_s/h_s + m/h_o = 40.7/17.4 + 22x0.005 = 2.44$

Hence, $U_s/c_s = 0.406$

Appendix E

(b) Cold end (gas outlet)

At this point the gas temperature = 50°C and the water temperature = 20°C. The water vapour pressure at 50°C = 92.5 mm Hg (Perry p.149). Therefore, the percentage of water vapour in the saturated gas = 92.5x100/667.5 = 13.85% which is equivalent to 1.45 lb./lb. of dry gas. Hence,

i_v = 3.5x50 + 1.45x1114/1.8 = 1075 P.C.U./lb. (dry) (Perry p.277)

The water vapour pressure at 20°C = 17 mm Hg (Perry p.149)

Therefore, the percentage of water in the saturated gas = 17x100/763 = 2.29% which is equivalent to 0.212 lb./lb. of dry gas. Hence,

i_w^* = 3.5x20 + 0.212x1092/1.8 = 199 P.C.U./lb. (dry).

Take m as the average slope of the i_w^* vs temperature curve between 20°C and 25°C. At 20°C the vapour pressure of water = 23.7 mm Hg. Therefore the percentage of water in the saturated gas = 23.7x100/736.3 = 3.21% which is equivalent to 0.299 lb./lb. of dry gas. Therefore,

i_w^* = 3.5x25 + 0.299x1096/1.8 = 269 P.C.U./lb. (dry). Hence,

m = (269 - 199)/(25 - 20) = 14

The coefficient of sensible heat transfer (h_s) is given by,

$h_s = jC_pG/(C_p\eta/k)^{0.6}$ (Perry p.422).

Where, C_p = 3.5x0.86 + 0.47x0.14 = 3.07 P.C.U./lb.,°C (Perry p229)

$(C_p\eta/k)$ = 0.75 (Perry p.467).

The flow rate of hydrogen at the inlet to the cooler = 4.5x3600x2x0.1/22.4x453 = 0.318 lb./h. Therefore,

Appendix E

the flow rate of gas at the outlet = 0.318(1 + 1.45)

= 0.78 lb./h. Consequently G = 0.78x4x144/π = 143 lb./ft.^{2},h.

η = (0.016x0.86 + 0.028x0.14)2.42

= 0.0426 lb./ft.,h (Perry p.372)

Hence N_{Re} = Gd/η = 280 and entering Fig. 422 in Brown[96] it is found that j = 0.01. Hence,

$h_s = 0.01x3.07x143/0.75^{0.6} = 5.2$ P.C.U./ft.^{2},h,$^\circ$C

c_s = the heat capacity of one pound of dry gas plus vapour

= 3.5 + 1.45x0.47 = 4.2 P.C.U./lb.,$^\circ$C (dry) (Perry p.229)

Take $1/h_o$ = 0.005 (same as at gas inlet). Since,

$c_s/U_s = c_s/h_s + m/h_o$

$= 4.2/5.2 + 14x^{0}.005 = {}^{0}.878$ then,

U_s/c_s = 1.14

It will be recalled that $A = q/(U_s/c_s)_{am}(i_v - i^*_w)_{lm}$

$q = (i_{v(hot)} - i_{v(cold)})$ x (hydrogen rate)

= (52100 - 1075)0.318 = 16200 P.C.U./h

$(U_s/c_s)_{am}$ = (1.14 + 0.406)/2 = 0.77

$(i_v - i^*_w)_{lm}$ = [(52100 - 335) - (1075 - 199)]/ln(51800/876

= 12450

Hence, A = 1.69 ft.^{2}.

Total area required = area for cooling plus the area for condensing

= 1.67 + 1.69 = 3.36 ft.^{2}.

Say 3.4 ft.^{2}.

Appendix E

E:6:3 Area of cooler-condenser for pure hydrogen

It is necessary to find the value of Reynolds Number (N_{Re}) for the flowing gas so that the coefficient of heat transfer between gas and wall can be found.

$N_{Re} = Gd/\eta$

$G = 4.5 \times 3600 \times 2 \times 4 \times 144 / 22.4 \times 453 \times \pi = 585$ lb./ft.^{2},h

$\eta = 0.012 \times 2.42 = 0.029$ lb./ft.,h (Perry p.371)

(Mean for 550°C - 50°C)

$d = 0.083$ ft.

Hence $N_{Re} = 1690$ which is less than 2000 so the gas must be flowing viscously. Entering Fig. 10a on page 471 of Perry at $N_{Re} = 1690$ it is found that $j = 0.0025$

$j = (h_g/C_p G)(C_p \eta/k)^{0.6} (\eta_g/\eta)^{0.14}$ (Perry p.471)

$(C_p \eta/k) = 0.75$ (Perry p.467)

For simplicity η_g/η will be taken as unity.

$C_p = 3.5$ P.C.U./lb.,°C (Perry p.229)

Therefore,

$h_g = 0.0025 \times 3.5 \times 585 / 0.75^{0.6} = 6.15$ P.C.U./ft.^{2},h,°C

Consider now the overall coefficient of heat transfer (U) which is given by

$$1/U = 1/h_g + 1/h_w + 1/h_d$$
$$= 1/6.15 + 1/525 + 1/500 = 0.167$$

Hence,

$U = 6.0$ P.C.U./ft.^{2},h,°C.

Appendix E

The heat load on the cooler-condenser in this case

$= 4.5 \times 3.5(550 - 50) = 1.55$ P.C.U./sec. (see page 267)

Hence the outlet temperature of the cooling water

$= 20 + 1.5/0.5 = 23^{\circ}C$ (see page 267)

The cooling area required is given by the equation,

$A = q/U\ \Delta t_{lm}$ (Perry p.468)

$\Delta t_{lm} = [(550 - 30) - (50 - 20)]/\ln(527/30) = 172^{\circ}C$

Consequently

$A = 1.55 \times 3600/6 \times 172 = 5.45\ ft^2$.

E:6:4 Area of cooler-condenser for pure steam

The cooler condenser will again be considered in two sections, viz. cooling from $550^{\circ}C$ to $100^{\circ}C$ and cooling and condensing from $100^{\circ}C$ to $50^{\circ}C$. This is a conservative approach as was pointed out on page 268.

Consider first the removal of superheat, i.e. cooling from $550^{\circ}C$ to $100^{\circ}C$. The enthalpy of steam at $550^{\circ}C$

$= 1533$ B.Th.U./lb. (Perry p.279)

The enthalpy of saturated steam at the same pressure

$= 1150$ B.Th.U./lb. (Perry p.277)

Therefore, super-heat $= (1633 - 1150) = 383$ B.Th.U./lb..

The value of Reynolds Number is needed so that the heat transfer coefficient can be found. Reynolds Number is given by,

$N_{Re} = Gd/\eta$

Where the steam flow rate $= 4.5 \times 3600 \times 18/22.4 \times 453 = 28.8$ lb./h and

$G = 28.8 \times 4 \times 144/\pi = 5300$ lb./ft.^{2},h

Appendix E

$\eta = 0.02 \times 2.42 = 0.048$ lb./ft.,h (Perry p.371)

(Mean value for 550°C to 100°C)

d = 0.083 ft..

Hence N_{Re} = 9200 and entering Fig. 8 on page 468 of Perry at this value of N_{Re} and using curve ABC it is found that j = 0.004.

The constant j is related to the heat transfer coefficient (h_g) by the equation,

$$j = h_g / C_p G \, (C_p \eta / k)^{0.6}$$ (Perry p.468).

In this case,

$(C_p \eta / k) = 0.78$ (Perry p.467)

C_p = 0.48 P.C.U./lb.,°C (Perry p.229)

Consequently,

$h_g = 0.004 \times 0.48 \times 5300 / 0.78^{0.6} = 11.9$ P.C.U./ft.^{2},h,°C.

The overall coefficient of heat transfer (U) is given by,

$$1/U = 1/h_g + 1/h_w + 1/h_d$$

$$= 1/11.9 + 1/525 + 1/500 = 0.088$$

Hence, U = 11.4 P.C.U./ft.^{2},h,°C.

The water temperature rise caused by the removal of latent heat = 28.8x1150/3600x1.8x0.5 = 10.2°C. The water temperature rise caused by the removal of latent and super-heats

= 28.8x1533/3600x1.8x0.5 = 13.6°C

Therefore the temperature of the water when the gas temperature is 100°C = 20 + 10.2 = 30.2°C and the water temperature when the gas temperature is 550°C = 20 + 13.6 = 33.6°C.

Appendix E

The area of the cooling section is given by the equation,

$$A = q/U\ \Delta t_{lm} \qquad \text{(Perry p.468)}$$

In this case

$$q = 28.8 \times 383 = 11000 \text{ B.Th.U./h}$$

$$\Delta t_{lm} = [(550 - 34) - (100 - 30)]/\ln(516/70)$$

$$= 223^{\circ}C$$

Hence,

$$A = 2.41 \text{ ft}^2.$$

Consider now the removal of latent and sensible heat, i.e. cooling from 100°C to 50°C. The nomograph on page 477 of Perry will be used to obtain the heat transfer coefficient between steam and tube. Values of Δt_m, t_f, and L are needed to enter the nomograph.

$t_m = [(100 - 30) + (50 - 20)]/2 = 50^{\circ}C$ or $90^{\circ}F$.

The film temperature (t_f) is given by,

$t_f = t_v - 0.75\ \Delta t_m$ (Perry p.476).

Assuming $t_v = 150^{\circ}F$, then,

$t_f = 150 - 68 = 82^{\circ}F$ or $28^{\circ}C$. The length (L) will be estimated at 10 ft. so that $L\Delta t = 900$. Entering the nomograph it is found that $h = 900$ B.Th.U./ft.^{2},h,°F, or 500 P.C.U./ft.^{2},h,°C.

The overall coefficient for heat transfer is given by,

$$1/U = 1/h + 1/h_w + 1/h_d$$

$$= 1/500 + 1/525 + 1/500 = 0.006$$

Therefore,

$$U = 170 \text{ P.C.U./ft.}^2\text{/h,}^{\circ}C$$

Appendix E

The area for condensing is given by,

$$A = q/U\ \Delta t_m \qquad \text{(Colburn}^{94}\text{)}_{p.450}.$$

In this case,

$q = 28.8 \times 1150/1.8 = 18400$ P.C.U./h

$\Delta t_m = 50^{\circ}C$

$U = 170$ P.C.U./ft.^{2},h,$^{\circ}$C.

Hence

$A = 2.16$ ft.^{2}.

The total area for cooling and condensing is equal to the area for cooling plus the area for condensing = 2.41 + 2.16 = 4.57 ft.^{2}.

E:6:5 Length of cooler-condenser

The largest area requirement is with pure hydrogen when A = 5.5 ft.^{2} (see page 277). Therefore, the length of 1" diameter pipe required = $5.5 \times 12/\pi$ = 21ft.. It is proposed that the cooler-condenser should take an "S" shape as shown in Fig. 26, page 145, to conserve space. A detail drawing of the cooler-condenser is shown in Fig. 45.

E:6:6 Pressure drop across the cooler-condenser

The nomograph on page 379 of Perry will be used to estimate the pressure drop which will be encountered. The largest pressure drop will occur when the gas entering the cooler condenser is pure hydrogen. The rate of hydrogen flow = 28.8/9 = 3.2 lb./h (see page 277). Entering the nomograph with this flow rate it is found that the pressure drop = 0.02 inches of water per foot of pipe.

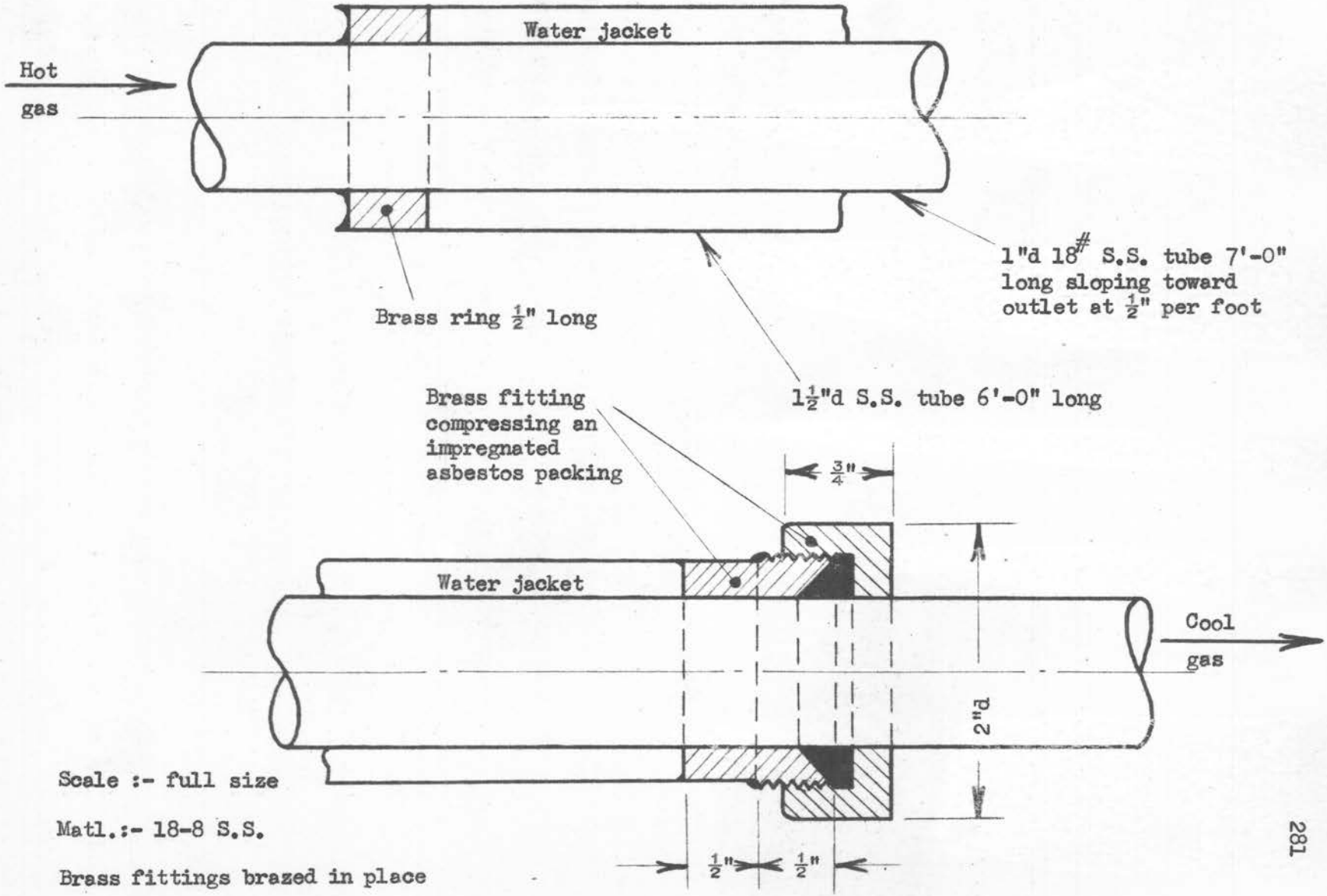

Fig. 45. Detail of cooler-condenser tube showing water jacket seals

Scale :- full size

Matl.:- 18-8 S.S.

Brass fittings brazed in place

Appendix E

Hence the pressure drop across the cooler-condenser = 0.02x21 = 0.42 inches of water. Say 0.5 inches of water.

E:7 Silica gel gas drier

Under the most severe operating conditions the drier would be required to handle 4.5 litre/sec N.T.P. of hydrogen saturated with water vapour at 50°C. The water vapour present under these conditions is 1.45 lb./lb. of dry hydrogen (see page 276).

A bed of +8-6# silica gel having a cross sectional area of one square foot will be used. It is proposed to use the method set out in Perry on page 882 to find the depth of bed needed to give a satisfactory period of efficient operation.

It is necessary to calculate the value of the constant b which is defined by the equation,

$$b = Gc/\rho_s H_d \qquad \text{(Perry p.483)}$$

Where

G = the superficial mass velocity of the dry gas

= 4.5x0.86x3600x2/22.4x453x1 = 2.75 lb./ft.^{2},h

ρ_s = 40 lb./ft.^{3} (Perry p.880)

H_d = the height of the mass transfer unit for the gas film.

c = the slope of the equilibrium line for silica gel (lb. silica gel/lb. dry air)

The height of the mass transfer unit (H_d) is given by the equation,

$$H_d = (0.55/a_v)(d_p G/\eta)^{0.51}(\eta/\rho D_v)^{0.67} \qquad \text{(Perry p.883)}$$

Appendix E

$a_v = 284$ ft.^{2}/ft.^{3} (Perry p.883, Table 35)

$d_p = 0.0091$ ft. (" " " ")

$G = 2.75$ lb./ft.^{2},h

$= (0.86 \times 0.0085 + 0.14 \times 0.01) 2.42 = 0.021$ lb./ft.,h (Perry p.371)

The diffusivity (D_v) may be calculated from the equation,

$$D_v = 0.0166 \left[T^{1.5}/P(V_A^{1/3})^2\right] (1/M_1 + 1/M_2)^{0.5}$$ (Perry p.538)

Where,

$T = 323^{\circ}K$

$P = 1$ atm.

V_A = atomic volume of $H_2O = 18.8$ (Perry p.538)

V_B = " " " $H_2 = 7.15$ (" " ")

$M_1 = 18$

$M_2 = 2$

Hence,

$D_v = 3.46$ ft.^{2}./h.

Initially, there is 13.8% by volume of water vapour in the gas (see page 274) so that the average percentage of water vapour in the gas flowing through the bed will be taken as the arithmetic mean = 7%.

Hence,

$\rho = (2 \times 0.93 + 18 \times 0.07) 273 \times 0.0624/22.4 \times 323 = 7.34 \times 10^{-3}$ lb./ft.^{3}

(Perry p. 40 for density equivalents)

Therefore,

$d_p G/\eta = 1.19$

and $\eta/\rho D_v = 0.825$

Appendix E

It follows that,

$H_d = (0.55/284)(1.19)^{0.51}(0.825)^{0.67} = 1.93 \times 10^{-3}$ ft..

In order to find c, the slope of the equilibrium line, it is necessary to use the treatment given by Hougen and Marshal[97]. They give the equation,

$p^* = 1.82 w p_s$ (Hougen and Marshal, equation 27)

Where

p^* = the partial pressure of water vapour in the gas in equilibrium with the vapour pressure of the water adsorbed by the gel

w = adsorbate content of the solid (lb./lb.)

p_s = the vapour pressure of water at the temperature of the gas

However p^* is also defined by the equation,

$p^* = y^* P M_g / M_s$

Where,

y^* = the adsorbate content of the fluid stream in equilibrium with the solid

P = the total pressure

M_g = the molecular weight of the adsorbate free gas

M_s = the molecular weight of water vapour

In this particular case,

$p^* = y^*/9$

and, therefore,

$y^* = 9 \times 1.82 p_s w$

Appendix E

But, $y^* = cw$ and, consequently,

$$c = 9x1.82p_s$$

In this case the water vapour pressure is 92.5 mm Hg, therefore,

$$p_s = 92.5/760 = 0.122 \text{ atm}..$$

Hence,

$$c = 2$$

The value of the constant (b) may now be found,

$$b = cG/\rho_s H_d = 2x2.75/40x1.93x10^{-3} = 108\ h^{-1}$$

The value of the constant (a) is also required.

$$a = 1/H_d \qquad \text{(Perry p.883)}$$

$$= 1/1.93x10^{-3} = 518\ ft.^{-1}$$

A bed 1 ft. thick will be tried to see if the operating time for which efficient operation can be obtained is sufficiently long. The thickness modulus = ax = 518x1 = 518. For efficient operation it will be necessary to remove 99% of the moisture in the entering gas and, therefore, the fraction of water remaining in the gas stream = Y/Y_o = 0.01. Entering Fig. 74 on page 882 of Perry at Y/Y_o = 0.01 and ax = 518 it is found that b = 420. Hence,

= 420/b = 420/108 = 3.9 h. However, the straight line relationship between y* and w only holds up to w = 0.2 (Perry p.880) and this value of w will be exceeded if the bed is operated for 3.9 h so the maximum operating time will occur when w = 0.2. The rate at which water enters the bed = 2.75x1.45 = 4.0 lb./h. The maximum capacity of the bed = $40x1x0.2$ = 8.0 lb.. Therefore, the operating time for

Appendix E

a 1 ft. thick bed = $8.0/4.0^{0}$ = 2.0 h. This should be adequate for most work so a bed of +8-6 silica gel, 1 ft. deep and 1'-1½" in diameter, has been adopted. A detail drawing of this gas drier is shown in Fig. 46.

The pressure drop through this drying bed will be needed to estimate the total pressure drop in the circulating system. It is necessary to calculate the value of Reynolds Number for the gas flowing through the bed so that the appropriate pressure drop equation can be selected.

$N_{Re} = Gd/\eta$

Where,

$G = 2.75$ lb./ft.^{2},h (see page 283)

$d = 0.0091$ ft. (" " 283)

$\eta = 0.021$ lb./ft.,h (" " 283)

Hence $N_{Re} = 1.19$ which is less than 10 so the flow is viscous and the appropriate equation for calculating the pressure drop is,

$\Delta p = 53\eta LV_{o}A_{f}/D_{p}^{2}$ (Perry p.393)

$\eta = 0.021/3600 = 5.85 \times 10^{-5}$ lb./ft.,sec

$L = 1$ ft.

$V_{o} = 4.5 \times {}^{0}.9 \times 323/273 \times 28.3 = {}^{0}.169$ ft./sec

$D_{p} = {}^{0}.009$ ft.

Hence $\Delta p = {}^{0}.645$ lb./ft.^{2} which is equivalent to 0.125 inches of water.

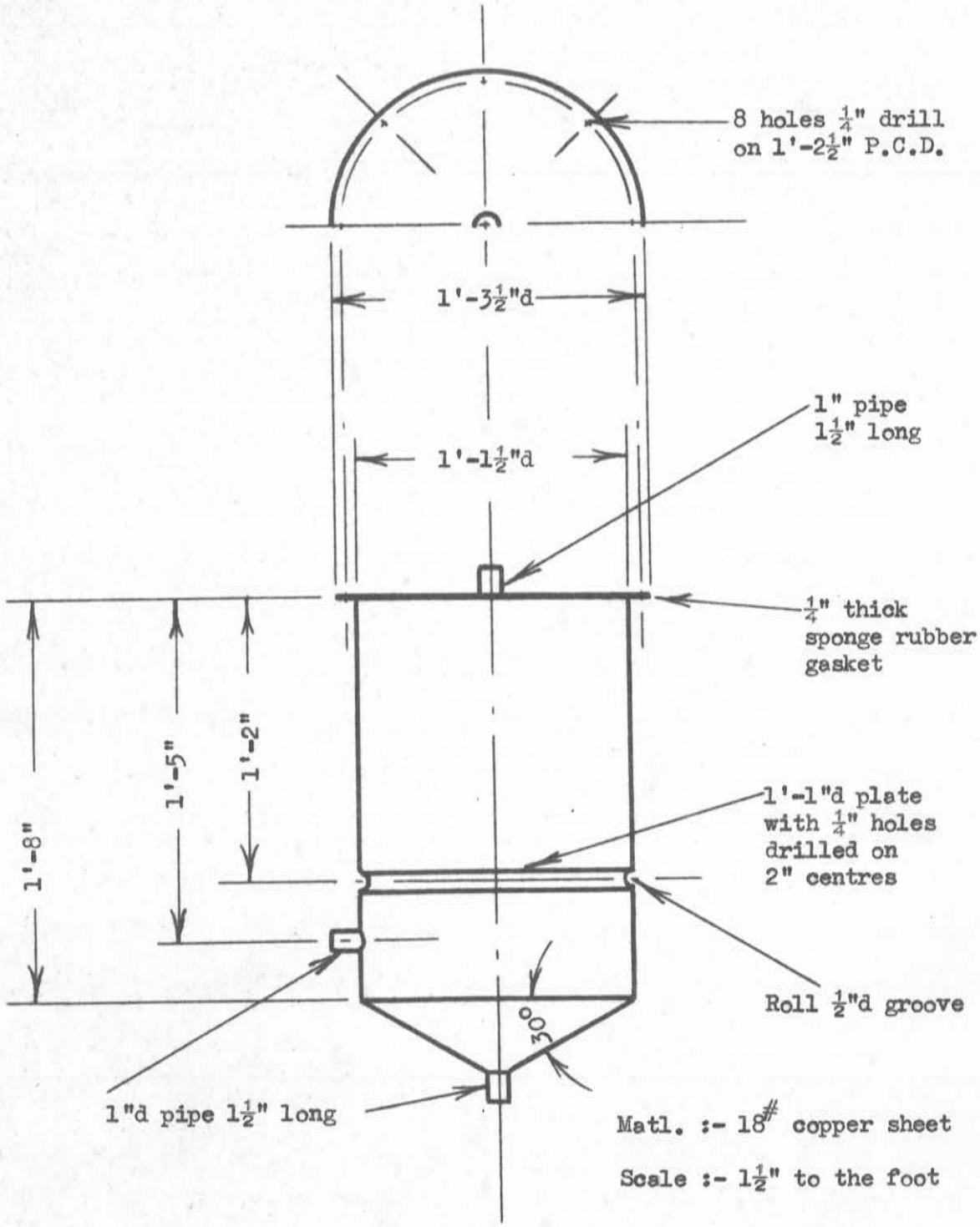

Fig. 46. Detail of silica gel gas drier

Appendix E

E:8 Selection of gas circulating fan

The type of circulating fan or pump will be determined by the pressure at which the required volume of gas must be delivered. This pressure will be equal to the sum of all the individual pressure drops in the circulating system.

The deepest fluidized bed of barytes which will be encountered will have a depth of twelve inches. The bed density = 2.4 g/cm^3, therefore, the weight of the bed = 2.4x12x2.54 = 73 g/cm^2. It follows that the pressure drop across the fluidized bed will be 73 g/cm^2. This is equivalent to 28.8 inches of water.

The pressure drop across the constriction plate will be of the order of 1 $lb./in.^2$ at a flow of 10 $ft.^3/min$ N.T.P.. This is equivalent to 28 inches of water.

The total pressure drop may now be calculated.

Pressure drop across the cyclone	= 4.4	inches of water	
" " " " condenser	= 0.5	" " "	
" " " " drier	= 0.1	" " "	
" " " " bed	= 29	" " "	
" " " " plate	= 28	" " "	
Total pressure drop	= 62	" " "	

A turbo blower or rotary blower will be needed to deliver gas against a pressure of the order of 62 inches of water. Wide variations in flow rate may be required so this eliminates the turbo blower which can only be throttled to 50% of rated volume. The blower will need

Appendix E

to have a maximum capacity of 4.5 litre/sec N.T.P. (6 ft.^{3}/min) so a Reavell R 2½x2¾ rotary compressor having a capacity of 8 ft.^{3}/min, when run at 2100 R.P.M., has been selected as being suitable for this purpose. It is proposed to drive the compressor with a Ward-Leonard variable speed drive.

E:9 Hydrogen consumption and storage

The maximum weight of any barytes bed likely to be reduced = 73xπ x9x6.46/4 = 3340 g (see page 247) so the volume of hydrogen required may be calculated as follows.

The equation for the reduction of barium sulphate by hydrogen is, $BaSO_4 + 4H_2 = BaS + 4H_2O$

Barium sulphate present in the bed = 3340/233 = 14.3 g mol, assuming that the barytes is 100% $BaSO_4$. Therefore, the hydrogen required = 4x14.3 = 57.2 g mol.

The volume of hydrogen which will be consumed = 57.2x22.4 = 1280 litre N.T.P.. This is equivalent to 45 ft.^{3} N.T.P..

A 50 ft.^{3} gas holder is available so this should be satisfactory for the storage of hydrogen. If necessary additional hydrogen may be fed into the holder from cylinders during the course of a run to augment the supply.

Appendix E

E:10 General Layout of the fluidizer

The shape of the available floor space makes it necessary to adopt the layout of components shown in the general arrangement drawing presented in Fig. 26, page 145.

E:11 Instrumentation

The points at which pressure and temperature measurements will be made are indicated on the flow sheet given in Fig. 25 on page 143. The temperature at each thermocouple will be measured by a Cambridge temperature indicator used in conjunction with a multi-position switch; simple manometers will be used for pressure measurements.

It is proposed to control the power input to the furnaces manually and the control circuit shown in Fig. 47 has been chosen for this purpose. During the warm up period the input to the furnaces will be controlled by Sunvic Type TYB Energy Regulators. However, these Regulators having a cycling period of over one minute at 80% of full power input and it seems possible that the bed temperature could fall during the part of the cycle when the power input to the furnaces was interrupted. Therefore, a cycling unit giving a controlled power input at a cycling rate of one cycle per second will be incorporated in the furnace control circuit to minimise such temperature variations. During runs the Energy Regulators will be turned fully on and the cycling units will be used to control the power input to the furnaces. The circuit for these cycling units is given in Appendix H.

Fig. 47. Furnace control circuit

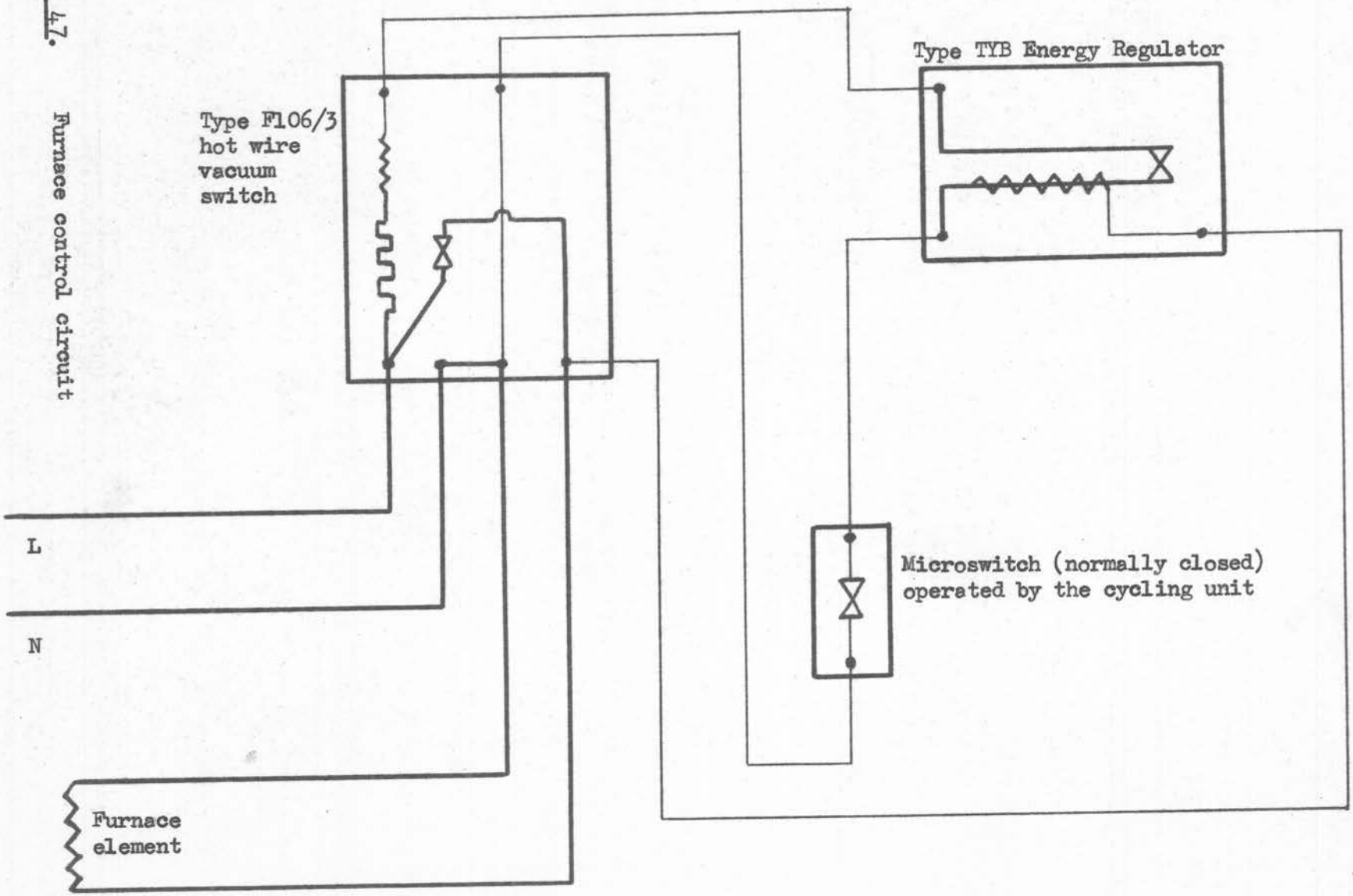

Appendix E

It is proposed that all instruments and controls should be mounted on a single board in front of the cooler-condenser as shown in Fig. 26 on page 145.

E:12 Operating notes

It is proposed that the bed of crushed barytes should be fluidized with nitrogen while the furnaces are heating up. When the bed has reached the set temperature valves A and B (see Fig. 25, page 143) will be set to vent the exit gases from the silica gel gas drier to atmosphere and then valves C and D will be manipulated to change the feed from nitrogen to hydrogen. When the nitrogen in the apparatus has been replaced by hydrogen, valves A and B will be set so that the gas from the drier will be fed to the circulating pump and only make up will be supplied from the hydrogen gas holder.

Both hydrogen and nitrogen gas holders will be counterbalanced so that a positive pressure of one or two inches of water will be maintained at the inlet of the circulating pump. This will ensure that there will be no leakage of air into the system and should avoid any risks of explosion.

APPENDIX F

Comparison between the design and actual performances of the fluidizer

Appendix F

Comparison between the design and actual performances of the fluidizer

It is proposed to discuss each section of the design in turn, beginning with the preheater and continuing around the apparatus along the path followed by the gas stream.

F:1 Gas preheater

The design calculations (see page 248) showed that, using the full preheating furnace capacity, it should have been possible to heat 250 litre/min N.T.P. of hydrogen to a temperature of 1000°C. However, in operation, it was found that the largest hydrogen flow which could be heated to this temperature was 190 litre/min N.T.P.. It seems likely that the estimate made of the heat losses from the furnace surfaces to the surroundings was in error. A simple heat balance shows that the heat losses must have been almost double the estimated loss of 0.8 kW/sec in order to reduce the capacity of the preheater to 190 litre/min N.T.P. of hydrogen.

A notable deficiency in the design of the preheater was the inability to find heat transfer data which would enable an estimate to be made of the maximum wall temperature likely to be encountered in the preheating tube. In actual operation, it was found that the highest wall temperature, 1160°C, occurred near the top of the preheater when a bed of barytes at 1100°C was being fluidized with nitrogen at a rate of 100 litre/min N.T.P. prior to the commencement of a run. During the run when hydrogen at a flow rate of 185 litre/min N.T.P.

was being used for the corresponding wall temperature was 1120°C.

The material used to fabricate the preheater-reactor tube, viz. Comsteel 25-20 heat resistant stainless steel, showed little sign of deterioration at these temperatures and there was no serious scaling from either the inside or outside surfaces of the tube. The high temperature strength of the metal appeared to be quite good and the tube showed no tendency to elongate under its own weight, however, care had to be taken to ensure that there were no bending moments acting otherwise such serious distortion was produced that the tube could not be lifted out from the surrounding furnaces.

F:2 Reactor

Estimation of the hydrogen velocity which would be needed to produce incipient fluidization in a bed of +14-10# barytes at 1000°C was an important step in the design of the unit (see page 246). The validity of the equation,

$$G_{mf} = \frac{0.00123}{B_e} \frac{\rho_{bm}\, g\, d_e^2}{\eta} \qquad \text{.....(a)}$$

due to van Heerden, Nobel, and van Krevelen[49], which was used to calculate this velocity, was checked by observation of beds at 1000°C. A clear silica window was inserted in the reactor in place of the top thermocouple sheath (see Fig. 28, page 147) so that an observer could see the top of the bed. The bed was fluidized with hydrogen

Appendix F

and the flow rate slowly decreased until the top surface of the bed was observed to be at rest; this was taken as the point of incipient fluidization and the flow rate at this point (V_{mf}) was noted. It was found that at 1000°C, for a 1500g bed of +14-10# barytes being fluidized and reduced with hydrogen, V_{mf} was 130 litre/min N.T.P.. This was lower than the corresponding flow rate of 165 litre/min N.T.P. predicted from equation (a) but the discrepancy was probably due to the presence of water vapour produced by the reaction taking place in the bed. At 1000°C, the viscosity of water vapour is twice the viscosity of hydrogen and consequently a smaller volume of gas is needed to produce incipient fluidization when water vapour is present.

In the case where there was a large change in composition as the gas passed up through the bed, the value of V_{mf} for the bottom of the bed was probably larger than the value for the top, i.e. the bottom part could act as a fixed bed while the top part was fluidized. Consequently, V_{mf} for 1100°C was taken at the point where the top surface of the bed was level but small bubbles were still breaking through. The value of V_{mf} for a 750g bed of +14-10# barytes being reduced at 1100°C was found to be 110 litre/min N.T.P.. Later observations through the transparent end of a thermocouple sheath buried in a similar bed showed the bottom of the bed to be quiescent when hydrogen was being pumped in at this rate confirming that 110 litre/min

Appendix F

N.T.P. represented a mean value for V_{mf} under these conditions.

The application of equation (a) was also checked by fluidizing samples of barytes with air at room temperature in a perspex replica of the stainless steel reactor. Values of V_{mf} obtained in this way are compared with the values predicted from equation (a) in Table XVI. It can be seen that the predicted rates were only 10% higher than the rates obtained in practice.

Visual observation of fluidized beds in the perspex replica of the reactor showed that the combination of baffle and perforated plate, used to support the bed, gave a uniform gas distribution. This design of constriction plate gave no trouble in the stainless steel reactor since the use of inert or reducing atmospheres eliminated the possibility of the small holes in the perforated plate becoming clogged by oxidation of the metal.

TABLE XVI.

Comparison of calculated and measured values of V_{mf} for barytes beds fluidized with air at room temperatures

Barytes size fraction (Tyler)	V_{mf} (litre/min N.T.P.)	
	Measured	Calculated
+65-48	35	39
+48-35	55	63
+28-14	102	123

Appendix F

F:3 Gas cooler

The gas cooler proved to be much more efficient in actual operation than the design calculations (see page 250) had suggested. It was necessary to lag the full length of the 1½" diameter pipe with 1" of magnesia to ensure that the temperature of the cyclone walls remained above 100°C thus preventing condensation of water on the cyclone walls. Even with the gas cooler lagged, the wall temperature at the cyclone exit was only 240°C with a hydrogen flow rate of 220 litre/min N.T.P. and reactor temperature of 1000°C. This is much lower than the temperature of 600°C at which it had been calculated (see page 259) the gas would leave the unlagged cooler under similar conditions. It appears, therefore, that the heat transfer coefficients used in the design calculations were too small.

F:4 Dust removal

The dust removal system appeared to operate efficiently at all times. About 90% of the dust blown out of the reactor was collected in the dust trap at the bottom of the gas cooler and the remainder appeared to be completely removed by the cyclone.

F:5 Cooler-condenser

The temperature of the gas entering the cooler-condenser was considerably lower than the temperature of 550°C used for design

purposes and, consequently, the unit had a much larger area than actually required. A cooler-condenser length of 14 ft. appeared to be quite sufficient to give an exit gas temperature of less than 50°C under all circumstances. The length of 21ft. which was actually installed gave a gas temperature at the exit close to that of the cooling water and hence decreased the amount of water vapour in the gas entering the silica gel gas drier.

F:6 Silica gel gas drier

The silica gel gas drier operated satisfactorily at all times. It was found that the bed could be operated for about three hours before the indicator in the top layers of the bed began to change colour, showing that the drying efficiency was beginning to decrease. As pointed out above, the load on the drier was less than the design load and consequently it might be expected that the actual operating time would be greater than the calculated time of two hours (see page 286).

APPENDIX G

Rate data for +14-10# barytes reduced at 1100°C and 900°C

Appendix G

Rate data for +14-10# barytes reduced at 1100°C and 900°C

G:1 At 1100°C

The equation which was developed to correlate the experimental data at 1100°C was (see page 110),

$$R/s = K(1 - f)/100 \quad \ldots\ldots\ldots\ldots\ldots\ldots\ldots\ldots (a)$$

Where R = the reaction rate (g_{H_2O}/min, g_{sample})

s = the specific surface of the sample (cm^2/g)

K = a constant depending upon the composition

f = the fraction of the barytes sample reduced at time t.

In order to apply this equation to +14-10# barytes it is necessary to estimate the specific surface (s) of such a sample.

Microscopic examination of a number of particles, taken at random, from the +14-10# sample of barytes used indicated that the specific surface of the material was approximately 10 cm^2/g. Fig. 21, page 111, shows that, for barytes such as this, where $SiO_2 + Fe_2O_3$ = 3.6% (see page 149), K = 2.2. Consequently equation (a) becomes,

$$R = 22(1 - f)/100 \quad \ldots\ldots\ldots\ldots\ldots\ldots\ldots\ldots (b)$$

If R is expressed as g_{BaSO_4}/min, g_{sample} equation (b) may be rewritten as,

$$R = 70(1 - f)/100 \quad \ldots\ldots\ldots\ldots\ldots\ldots\ldots\ldots (c)$$

The rate vs time data given in Table VIII, page 127, were obtained

Appendix G

from equation (c) as follows.

When f = 0.2, then R = 56×10^{-2} $g_{BaSO_4}/min, g_{sample}$.

The average rate for the period f = 0 to f = 0.2.

= $(70 + 56)10^{-2}/2 = 63 \times 10^{-2}$ $g_{BaSO_4}/min, g_{sample}$.

Therefore, the time corresponding to f = 0.2 is given by,

$t = 0.2/63 \times 10^{-2} = 0.32$ min.

The same treatment may then be applied for the period f = 0.2 to f = 0.4 and etc. to obtain the rest of the data in Table VIII.

G:2 <u>At 900°C</u>

Tests were not carried out at 900°C on material of known surface area, however, it will be assumed that the initial rate of reaction, at this temperature, is proportional to the surface area of the barytes sample as was the case at 1000°C and 1100°C (see Section 4:4:1, page 94).

The initial reaction rate obtained for Run No. E88, carried out on +10-8# material was 2.1×10^{-3} $g_{H_2O}/min, g_{sample}$ (see Appendix C, page 222). The specific surface of a similar sample of +10-8# material was estimated, after close examination on a sheet of graph paper, to be 6 cm^2/g. Consequently, the initial rate per unit area at 900°C is 3.5×10^{-4} $g_{H_2O}/min, cm^2$. Since the specific surface of +14-10# barytes is 10 cm^2/g (see Section G:1 above) the initial rate of reaction for such material will be 3.5×10^{-3} $g_{H_2O}/min, g_{sample}$. This is equivalent

Appendix G

to a reaction rate of 1.2×10^{-2} $g_{BaSO_4}/min, g_{sample}$.

APPENDIX H

Electrical Circuits

Appendix H

Electrical circuits

H:1 Photo-cell relay temperature controller

The circuit (see Fig. 48) for the photo-cell relay was based on a similar circuit described by Gadsby, Hinshelwood, and Sykes[39]. The thermocouple E.M.F. was bucked against a D.C. voltage, which was stabilised by an 85A2 voltage reference tube, in a potentiometer circuit. The galvanometer G (see Fig. 48) was used to detect the out of balance current in this potentiometer circuit. A small diameter hole was drilled in the face of the galvo and a torch globe L placed behind it. An opaque disk attached to the galvanometer needle then interrupted the light beam which fell on the 58CG, gas filled, photo-cell, thus controlling the relay R_o which switched the furnace input. This construction led to a very compact instrument (6"x8"x10").

It was found that a change of less than 2°C in the temperature of the control thermocouple would cause the relay to operate. The instrument was not compensated for variations in ambient temperature but, where runs lasted less than half an hour, cold junction compensation was considered an unnecessary refinement. The small changes encountered in the ambient temperature were measured by a thermometer placed near the cold junction of the control thermocouple and, if necessary, the potentiometer setting was altered to compensate for the change.

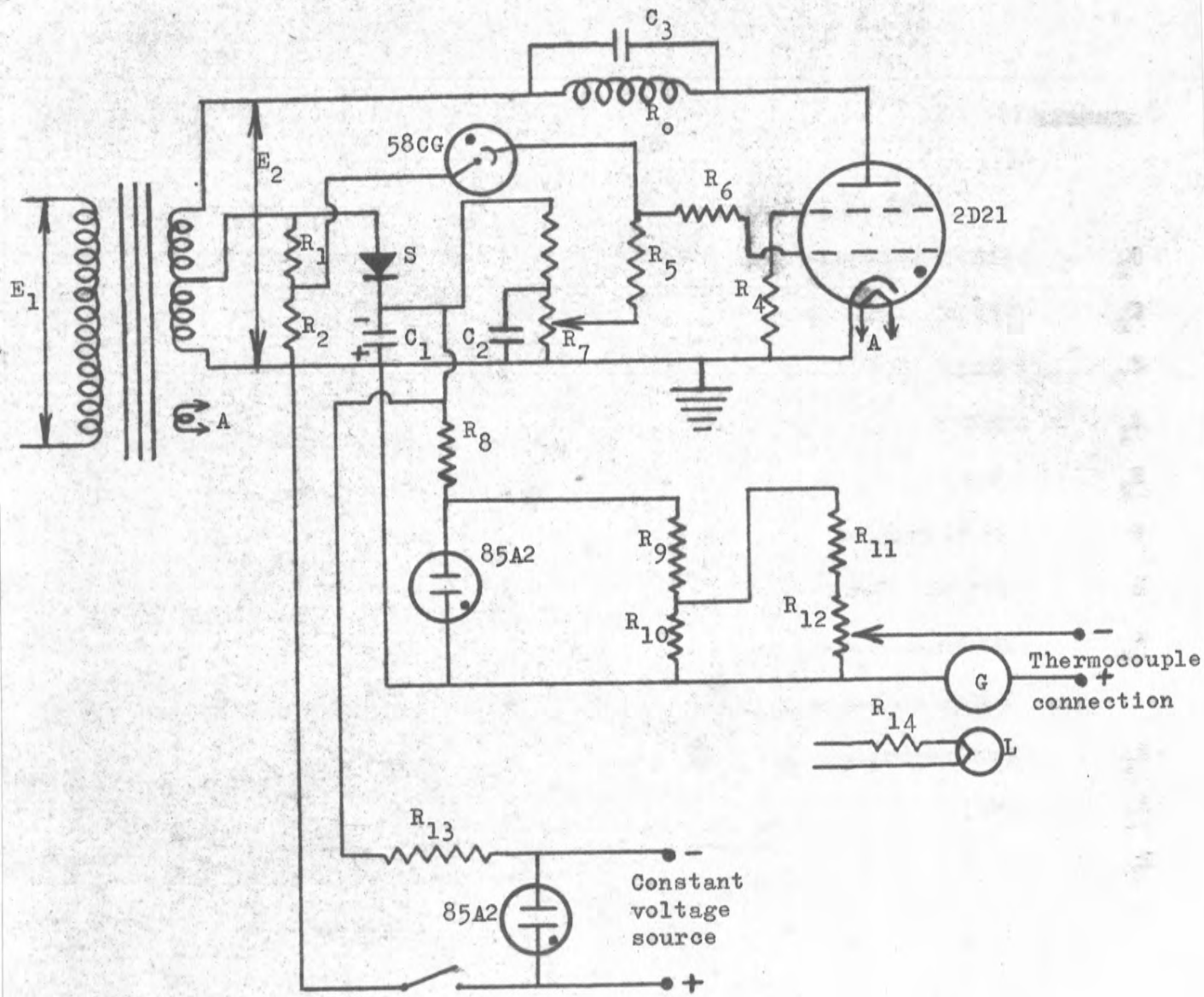

Fig. 48. Circuit diagram for photo-cell temperature controller

Fig. 48. Circuit diagram for photo-cell temperature controller

Appendix H

Key to Fig. 48

C_1	16 mf condenser	R_4	1 M resistor
C_2	25 mf "	R_5	5 M "
C_3	8 mf "	R_6	220 K "
E_1	250 V	R_7	250 K potentiometer
E_2	300 V	R_8	15 K resistor
G	40 pot galvo	R_9	25 K "
L	2.2 lens type globe	R_{10}	2 K "
R_o	20 K relay operating a 10 amp. mercury switch	R_{11}	25 K "
		R_{12}	20 K "
R_1	100 K resistor	R_{13}	200 W.W. pot.
R_2	80 K "	R_{14}	17 5 watt resistor
R_3	1 M "	S	300 V 80 ma selenium rectifier

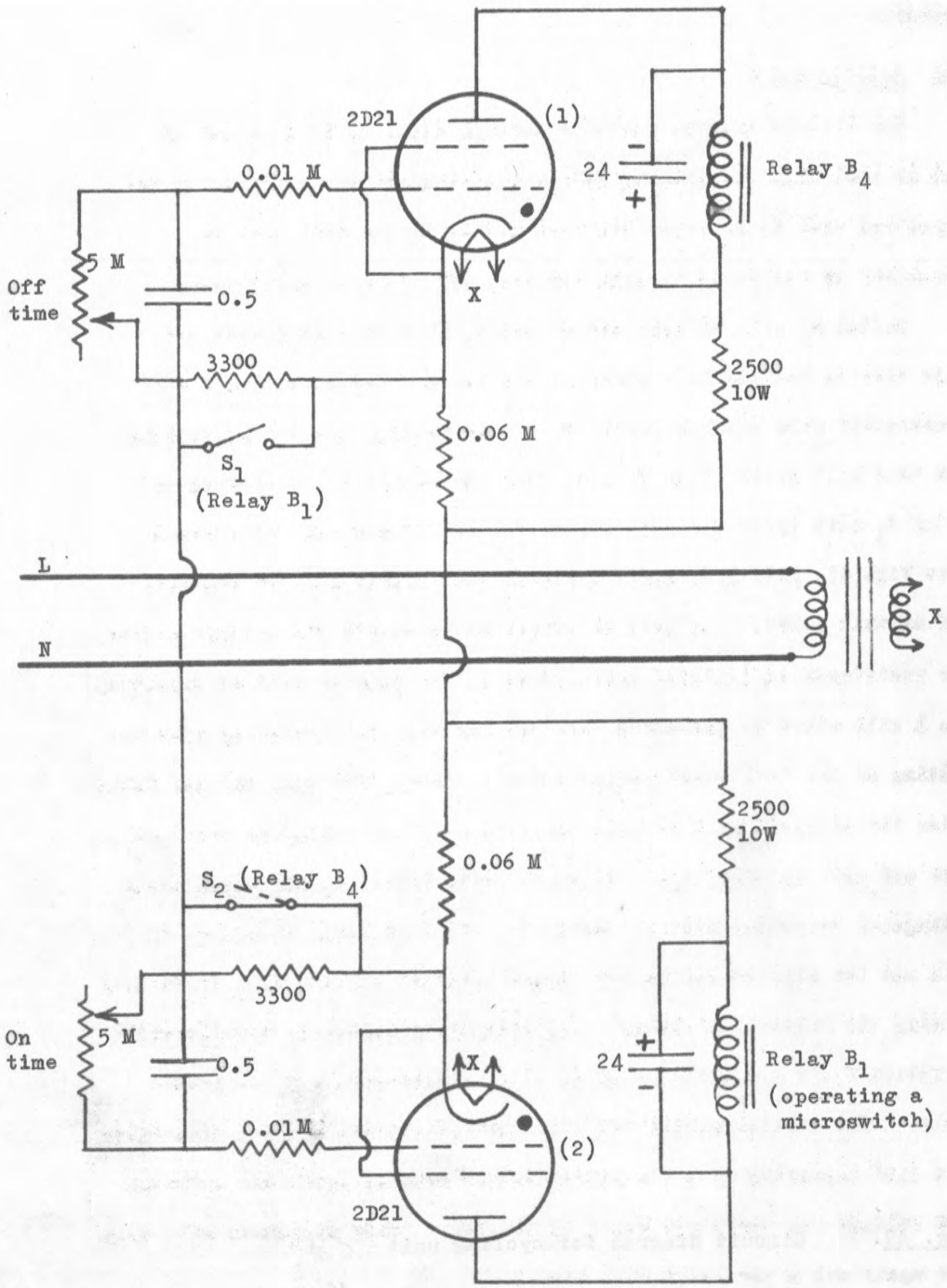
2D21
(1)
0.01 M
24
Relay B_4
5 M
Off time
0.5
X
3300
2500 10W
0.06 M
S_1 (Relay B_1)
L
N
X
2500 10W
0.06 M
S_2 (Relay B_4)
3300
5 M
On time
0.5
X
24
Relay B_1 (operating a microswitch)
0.01M
(2)
2D21

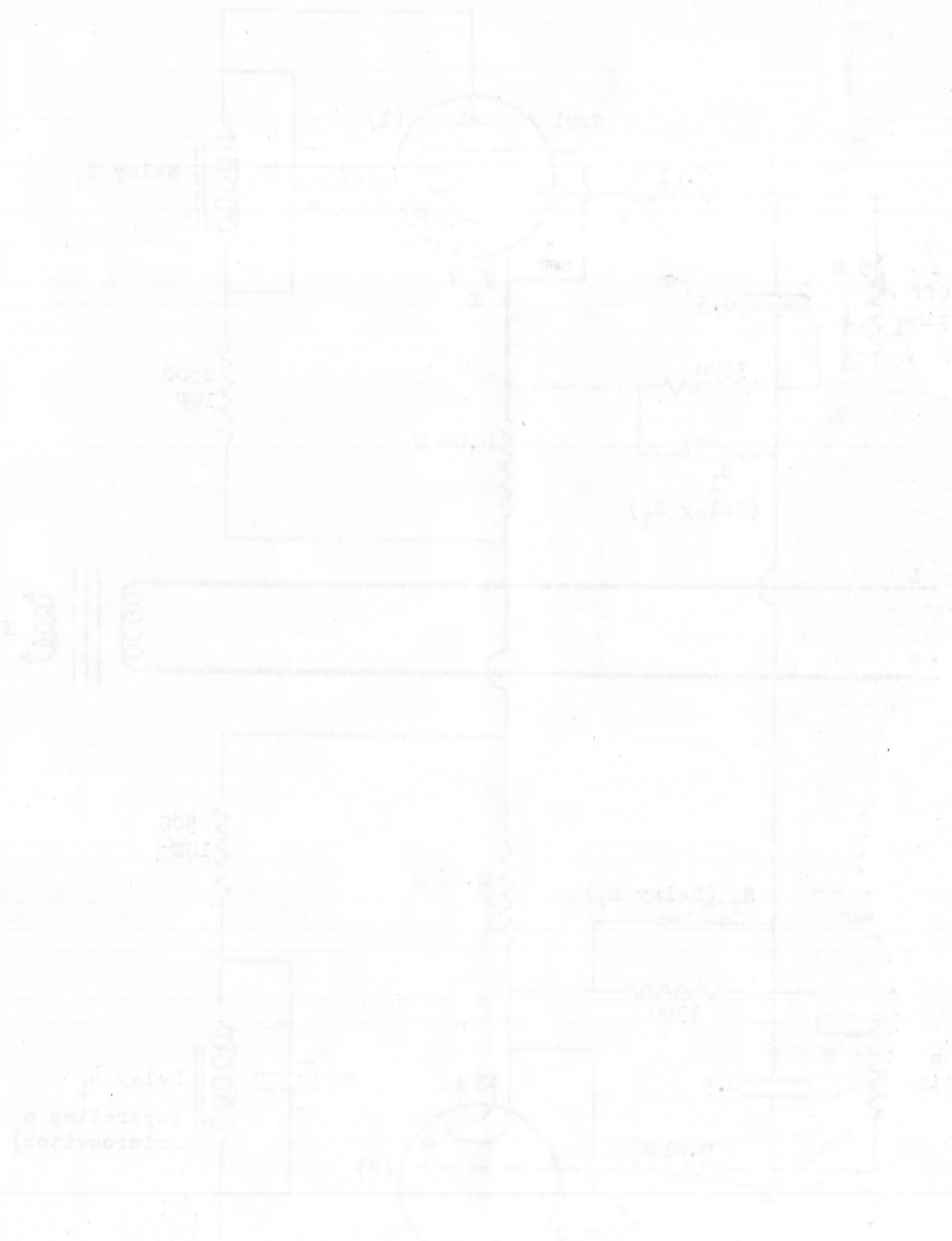

Fig. 49. Circuit diagram for cycling unit

Appendix H

H:2 Cycling unit

The circuit diagram for this unit is shown in Fig. 49 and it can be seen that the cycling action was obtained by interlocking two thyratron time delay circuits. The action of the unit will be explained by following through one complete cycle of operation.

Switch S_1 will be open and switch S_2 will be closed when the high tension voltage is applied to the unit. Thyratron No. 2 will immediately fire because there is no bias voltage applied to its grid and this will close relay B_1 and, with it, switch S_1. Closing of relay B_1 also opens the microswitch in the furnace control circuit (see Fig. 47, page 294) and therefore, the furnace will be switched off at this point. As soon as switch S_1 is closed the voltage across the resistance capacitance combination in the grid circuit of thyratron No. 1 will start to decrease; the rate of decrease depending upon the setting of the "off time" potentiometer. When this grid voltage falls below the critical grid voltage (approx. 4 volts) thyratron No. 1 will fire and pull in relay B_4. This will open switch S_2 and immediately extinguish thyratron No. 2. Relay B_1 will then open, switch S_1 will open and the microswitch in the furnace control circuit will close thus turning the furnace on again. The opening of switch S_1 extinguishes thyratron No. 1 and opens relay B_4 which allows switch S_2 to close again. The voltage across the "on time" potentiometer will then decay at a rate depending upon the potentiometer setting until the critical grid voltage for thyratron No. 2 is reached. This thyratron will then fire again and a new cycle will begin.

Appendix H

The maximum on and off times obtainable were about one minute and either of these times could be decreased to zero by turning the appropriate potentiometer to give zero resistance across its condenser.

BIBLIOGRAPHY

1. Okuno, T. (1935). J. Chem. Ind. Japan (Supp. binding) 38, 421.
2. Welles, A. (1916). Ind. Eng. Chem. 8,770.
3. Neric, M (1938). J. App. Chem. U.S.S.R. 11, 893.
4. Chaborski, G., & Pirtea, D. (1934). Bull. Chim. Soc. Romane Chim. 37, 129.
5. Eastman, E., & Evans, R. (1924). J. Am. Chem. Soc. 46, 888.
6. Emmett, P., & Shultz, J. (1929). J. Am. Chem. Soc. 51, 3249.
7. Emmett, P., & Shultz, J. (1938). J. Am. Chem. Soc. 55, 1376.
8. Gillespie, L. (1939). J. Chem. Phys. 7, 530.
9. Whalley, E. (1951). Trans. Farad. Soc. 47, 815.
10. Kubaschewski, O., & Evans, E. (1951). "Metallurgical Thermochemistry", Vol. 1, page 149. London:Butterworth.
11. Kitchener, J., & Ignatowicz, S. (1951). Trans. Farad. Soc. 47, 1278.
12. Pease, R., & Cook, R. (1926). J. Am. Chem. Soc. 48, 1199.
13. Darken, L., & Gurry, R. (1945). J. Am. Chem. Soc. 67, 1938.
14. Chipman, J., & Marshal, S. (1940). J. Am. Chem. Soc. 62, 299.
15. Rosenqvist, T. (1951). J. of Metals 535.
16. Langmuir, I. (1916). J. Am. Chem. Soc. 38, 2263.
17. Bircumshaw, L., & Riddiford, A. (1952). Quart. Rev. (Lond.) Vol. 6, No. 2, 157.
18. Van Name, R., & Hill, D. (1916). Am. J. of Science 42, 301.
19. Parravano, G. (1952). J. Am. Chem. Soc. 74, 1194.

20. Bircumshaw, L., & Everdell, M. (1942). J. Chem. Soc. 598.

21. Zimmerman, J. (1949). J. Phys. Chem. 53, 562.

22. Hougen, O., & Watson, K. (1949). "Chemical Process Principles", Vol. 3, Chap. 19. New York: Wiley.

23. Corrigan, T. (1955). Chem. Eng. No. 4, 199.

24. Olson, R., Schuler, R., & Smith, J. (1950). Chem. Eng. Prog. 46, 614.

25. Tu, C., Davis, H., & Hottel, H. (1934). Ind. Eng. Chem. 26, 749.

26. Riddiford, A. (1952). J. Phys. Chem. 56, 745.

27. Wilhelm, R. (1949). Chem. Eng. Prog. 45, 208.

28. Hougen, O., & Watson, K. (1943). Ind. Eng. Chem. 35, 529.

29. Hurt, D. (1943). Ind. Eng. Chem. 35, 522.

30. Perry, J. (Editor). (1950) "Chemical Engineers Handbook", 3rd. ed., Chap. 10. New York: McGraw-Hill.

31. Johnstone, H., Batchelor, J., & Shen, C. (1955). J. Am. Inst. Chem. Eng. 1, 318.

32. Shen, C., & Johnstone, H. (1955). J. Am. Inst. Chem. Eng. 1, 349.

33. Toomey, R., & Johnstone, H. (1952). Chem. Eng. Prog. 48, 220.

34. Taylor, G., & Starkweather, H. (1930). J. Am. Chem. Soc. 52, 2314.

35. Benton, A., & Emmett, P. (1924). J. Am. Chem. Soc. 46, 2728.

36. Pease, R., & Taylor, H. (1921). J. Am. Chem. Soc. 43, 2179.

37. Wetherill, W., & Furnas, C.(1934). Ind. Eng. Chem. 26, 983.

38. Woods, S. (1948). Disc. Farad. Soc. 4, 184.

39. Gadsby, J., Hinshelwood, C., & Sykes, K. (1946). Proc. R. Soc. (Lond.) 187A, 129.

40. Gadsby, J., Long, F., Sleightholm, P., & Sykes, K. (1948). Proc. R. Soc. (Lond.) 193A, 357.

41. Kivnick, A., & Hixson, A. (1952). Chem. Eng. Prog. 48, 394.

42. Lewis, W., Gilliland, E., & Sweeney, M. (1951). Chem. Eng. Prog. 47, 251.

43. Lewis, W., Gilliland, E., & McBride, G. (1949). Ind. Eng. Chem. 41, 1213.

44. Lewis, W., Gilliland, E., & Reed, W. (1949). Ind. Eng. Chem 41, 1227.

45. Gilliland, E., & Mason, E. (1953). Ind. Eng. Chem. 45, 1177.

46. Carman, P. (1937). Trans. Inst. Chem. Eng. 15, 150.

47. Leva, M., Grummer, M., Weintraub, M., & Polchick, M. (1948). Chem. Eng. Prog. 44, 619.

48. Miller, C., & Logwinuk, A. (1951). Ind. Eng. Chem. 43, 1220.

49. van Heerden, C., Nobel, A., & van Krevelen, D. (1952). Chem. Eng. Science 1, 37.

50. Cathala, J. (1953). Chem. Eng. Science 2, 273.

51. Leva, M., & Grummer, M. (1952). Chem. Eng. Prog. 48, 307.

52. Lewis, W., Gilliland, E., & Bauer, W. (1949). Ind. Eng. Chem. 41, 1104.

53. Jottrand, R. (1952). J. App. Chem. 2, Supp. Issue No. 1, S17.

54. Shuster, W., & Kisliak, P. (1952). Chem. Eng. Prog. 48, 455.

55. Gilliland, E., & Mason, E. (1949). Ind. Eng. Chem. 41, 1191.

56. Thompson, R. (1953). Chem. Eng. Prog. 49, 253.

57. Sittig, M. (1953). Chem. Eng. 60, No. 5, 219.

58. Kite, R., & Roberts, E. (1947). Chem. Eng. 54, No. 12, 112.

59. Danckwerts, P., Jenkins, J., & Place, G. (1954). Chem. Eng. Science 3, 26.

60. Askins, J., Hinds, G., & Kunrenther, F. (1951). Chem. Eng. Prog. 47, 401.

61. Heertjes, P., deBoer, H., & de Haas van Dorssor, A. (1953). Chem. Eng. Science 2, 97.

62. Osberg, G., & Charlesworth, D. (1951). Chem. Eng. Prog. 47, 566.

63. Leva, M. (1951). Chem. Eng. Prog. 47, 39.

64. Hall, C., & Crumley, P. (1952). J. App. Chem. 2, Supp. Issue No. 1, S47.

65. Evans, P., & Kepper, H. (1952). J. App. Chem. 2, Supp. Issue No. 1, S33.

66. Chu, J., Kalil, J., & Wetteroth, W. (1953). Chem. Eng. Prog. 49, 141.

67. Dow, W., & Jakob, M. (1951). Chem. Eng. Prog. 47, 637.

68. Bartholomew, R., & Katz, D. (1952). Chem. Eng. Prog. Symposium Series 48, No. 4, 3.

69. van Heerden, C., Nobel, A., & van Krevelen, D. (1953). Ind. Eng. Chem. 45, 1237.

70. Wamsley, W., & Johanson, L. (1954). Chem. Eng. Prog. 50, 347.

71. Gregory, S. (1952). J. App. Chem. 2, Supp. Issue No. 1, S1.

72. Lapple, C. (1951). Chem. Eng. 58, No. 5, 144.

73. Stairmand, C. (1951). Trans. Inst. Chem. Eng. 29, 356.

74. Barr, G. (1934). J. of Scientific Inst. 11, 321.

75. Terres, B., & Bruckner, K. (1920). Z. Electrochem. 26, 1.

76. U.S. Bureau of Standards. (1950). "Selected Values of Chemical Thermodynamic Properties".

77. Kelley, K. (1950). Bull. U.S. Bur. Mines No. 477.

78. Kireev, V. (1946). J. Gen. Chem. (Moscow) 16, 1569.

79. Kelley, K. (1949). Bull. U.S. Bur. Mines No. 476.

80. Perry, J. (Editor). (1950). "Chemical Engineers Handbook", 3rd. ed., p. 882. New York:McGraw-Hill.

81. Hobson, M., & Thodos, G. (1951). Chem. Eng. Prog. 47, 370.

82. Scott, W., & Furman, N. (1939). "Standard Methods of Chemical Analyses", Vol. 1, p. 130. London:Tech. Press..

83. Pavlyuchenko, M. (1951). J. App. Chem. U.S.S.R. 24, 666 Via Chem Abstract 47, 390a.

84. Chufarov, G., Averbukh, B., Tatievskaya, E., & Antonov, V. (1952). Zur. Fiz. Khim. 26, 31. Via Chem. Abstract 47, 4713g.

85. Shushunov, V., & Baryshnikow, Y. (1953). Zur. Fiz. Khim. 27, 703. Via Chem. Abstract 48, 2454d.

86. Gregg, S., & Razouk, R. (1949). J. Chem. Soc. S36.

87. Prout, E., & Tompkins, F. (1944). Trans Farad. Soc. 40, 488.

88. Brown, G., & associates. (1950). "Unit Operations," p. 546. New York: Wiley.

89. Perry, J. (Editor). (1950). "Chemical Engineers Handbook", 3rd. ed., p. 113. New York: McGraw-Hill.

90. Hougen, O., & Watson, K. (1949). "Chemical Process Principles", Vol. 3, p. 1066. New York: Wiley.

91. Roberts, L., & Anderson, J. (1952). Rev. of Pure and App. Chem. 2, 1.

92. Hougen, O., & Watson, K. (1949). "Chemical Process Principles", Vol. 2, p. 696. New York:Wiley.

93. Stairmand, C. (1949). Engineering 168, 409.

94. Colburn, A. (1951). Proc. Inst. Mech. Eng. 164, 448.

95. Cairns, R. (1954). Ph.D. Thesis, N.S.W. University of Technology.

96. Brown, G., & associates. (1950). "Unit Operations", p. 443. New York:Wiley.

97. Hougen, O., & Marshal, W. (1947). Chem. Eng. Prog. 43, 197.

98. Kelley, K. (1949). Bull. U.S. Bur. Mines No. 406.

Culver, R. V., & Hamdorf, C. J. (1955). Equilibria in the reduction of barium sulphate by hydrogen. *Journal of Applied Chemistry, 5*(8), 383-389.

NOTE:
This publication is included in the print copy
of the thesis held in the University of Adelaide Library.

It is also available online to authorised users at:
https://doi.org/10.1002/jctb.5010050806